School of Earth and Planetary Sciences

Functional diversity of active microbial mat communities inferred from lipid biomarkers and metatranscriptomics

Matthew Arthur Campbell

This thesis is presented for the Degree of

Doctor of Philosophy

of

Curtin University

July 2020

Declaration

To the best of my knowledge and belief this thesis contains no material previously published by any other person except where due acknowledgment has been made.

This thesis contains no material which has been accepted for the award of any other degree or diploma in any university.

Signature:

Date: 24/07/2020

Abstract

A unique study of microbial mats from common niches of elevated salinity environments (regions of Shark Bay, Western Australia: WA) and a freshwater wetland environment (Giblin River, Tasmania) are presented in this thesis. Microbial mat communities possess extensive taxonomic and functional diversity, which drive high metabolic rates and rapid cycling of major elements. Modern microbial mats occurring in hypersaline environments are considered as analogues to extinct geobiological formations dating back to ~ 3.5 Gyr ago. Despite efforts to understand the diversity and metabolic potential of hypersaline microbial mats in Shark Bay (WA), there has yet to be molecular analyses done at the transcriptional level in such microbial communities. In **chapter 3**, metatranscriptomes were generated and compared from actively growing mat types (albeit different in morphology) for the first time. Further, the influence of diel and seasonal cycles of the mats were also compared by metatranscriptomics. We observed that the overall gene transcription is largely influenced by microbial community structure and seasonality. The most transcribed genes were associated with tackling the low nutrient conditions by the uptake of fatty acids, phosphorus, iron, and nickel from the environment. A range of pathways involved in carbon, nitrogen and sulfur cycles were identified in mat metatranscriptomes, with anoxygenic photosynthesis and chemoautotrophy using the Arnon-Buchanan cycle inferred as major pathways involved in the carbon cycle. Furthermore, enrichment of active anaerobic pathways (e.g., sulfate reduction, methanogenesis, Wood–Ljungdahl) in smooth mats corroborates previous metagenomic studies and further advocates the potential of these communities as modern analogues of ancient microbialites.

Shark Bay, WA is also episodically impacted by tropical cyclones. During 2015, the region was hit by a category 3 cyclone, “severe tropical cyclone Olywn”, leading to the formation of a black sludge in an intertidal zone harbouring microbial mats and microbialites. Upon returning to the impacted site 12 months later, the black sludge deposit was still recognisable between the microbialite columns and as mucilaginous cobbles near to the shoreline in the impacted area. In **chapter 4**, metatranscriptomic and organic geochemical analyses were carried out on the black sludge derived materials and impacted microbial mat communities to unravel the

structure, function and potential preservation of these deposits following a tropical cyclone. It was found that samples which derived from the black sludge contained low relative abundances of cyanobacteria but had higher proportions of heterotrophic and anaerobic microorganisms (e.g. methanogens and sulfate-reducing bacteria). Increased metabolic activity by these microorganisms (e.g. sulfate reduction and organic matter degradation) is thought to drive calcium carbonate precipitation and helps in mat preservation. Comparison of the aliphatic biomarker by gas chromatography-mass spectrometry (GC-MS) analyses showed that C_{25} highly branched isoprenoid (HBI) alkenes were significantly higher in the black sludge derived materials attributed to the relocation of subtidal sediments containing HBI-producing diatom communities by the tropical cyclone. Raney nickel desulfurisation of the polar fraction extracted from a mucilaginous cobble revealed sulfur-bound hopanoids and a series of benzohopanes. The presence of these compounds could be indicative of microbial matter that has been influenced by the tropical cyclone which may have caused water column anoxia promoting increased sulfurisation of the organic matter to occur.

Chapter 5 focuses on heterocytous cyanophytes occurring in both elevated salinity and freshwater environments. Currently, enhanced salinity conditions are thought to greatly reduce the diversity of heterocytous cyanophytes. This study examined sixteen microbial mats living under different salinities for their heterocyte glycolipid (HG) contents and active cyanobacterial populations. Ten hypersaline mats and three metahaline mats were sampled from Shark Bay, WA, and three freshwater mats from Giblin River, Tasmania. We tentatively identified three novel long-chain pentose $HG_{32\text{-}36}$ triols occurring in all the mats from Shark Bay. A large variety of active heterocytous cyanophytes were discovered in the marine setting of Shark Bay showing that diversity of these cyanobacteria is much higher at elevated salinity than previously thought. Although, their overall abundance was relatively low in the saline mats it was higher in freshwater mats which corroborated previous findings. Metatranscriptomic analysis revealed that even though heterocytous cyanophytes make up a small portion of the active microbial community, they transcribed large portions of genes involved in biofilm formation and nitrogen fixation, indicating that they are essential builders and nutrient providers of these microbial mats. Our results extend the knowledge of HG and heterocytous cyanophyte distributions within microbial mats from elevated saline and freshwater environments, and illustrates the

potential use of HGs as chemotaxomic markers in both ecological and paleoenvironmental studies.

Acknowledgements

This project has been a fascinating, whilst challenging journey into the world of geomicrobiology.

Firstly, I would like to thank my supervisors Kliti and Marco for giving me the opportunity to do such a great PhD project and always supporting me with their scientific knowledge and enthusiasm in the fields of organic geochemistry and microbiology. A special thanks to Pieter and Therese for the help they provided during the first field trip to Shark Bay. Their extensive knowledge of the region and the microbial ecosystems was essential for sampling and later interpretation and discussion of results. A big thanks to Hon Lun, Brendan and Rick for introducing me to the world of bioinformatics and how to apply it to complex microbial ecosystems, without your help this project would not have been possible. I'd like to also thank Marco from the Pawsey Supercomputing Centre, I'll be forever grateful for time you spent teaching me to set up and run bioinformatic packages on the Nimbus virtual machine. I'd like to thank Bernadette and Rolan for giving me the opportunity to come to Tasmania and sample the interesting freshwater mats, the helicopter ride was also a big bonus. I'd like to thank Lorenz and Throsten for giving me to opportunity to analyse heterocyte glycolipids, their vast knowledge of these compounds was essential for this project.

I would also like to extend my thanks to the Western Australia Organic Isotope Geochemistry Centre group: Calum, Bettina, Sureyya, Jaime, Mattia, Darren, Kuldeep, Yali, Alex, Seb, Hendrik, Nannan Alan, Chloe, Pete, Gemma, Cornelia, Maddi, Danlei, Takashi, Ekram, and Sohaib.

Many thanks to my family and friends, in Perth as well as Margaret River, for supporting me throughout my entire university career. And a final and very special thanks to Chiara for always being there for me and helping me in any way she could.

This research is supported by an Australian Government Research Training Program (RTP) Scholarship, the Australian Research Council awarded to Kliti Grice (DP15010223) and The Institute for Geoscience Research (TIGeR).

Contributions of others

The work presented in this thesis was primarily designed, experimentally executed, interpreted, and written by the first author of the individual chapters (Matthew A. Campbell). Contributions by colleagues are described in the following.

Chapter 3 - Functional gene expression in Shark Bay hypersaline microbial mats: Adaptive Responses

Matthew A. Campbell, Kliti Grice, Pieter T. Visscher, Therese Morris, Hon Lun Wong, Richard Allen White III, Brendan P. Burns, Marco J.L. Coolen

Field sampling of microbial mats was conducted by MAC, KG, PTV, TM and MJLC. Laboratory sample processing was done by MAC and MJLC. Statistical and computational analysis was performed by MAC, RAW and HLW. Chapter was reviewed and edited by all authors.

Chapter 4 - Structure and function of Shark Bay microbial communities following tropical cyclone Olwyn: a metatranscriptomic and organic geochemical perspective

Matthew A. Campbell, Marco J.L. Coolen, Pieter T. Visscher, Therese Morris, Kliti Grice

Field sampling of microbial mats was conducted by MAC, KG, PTV and TM. Laboratory sample processing was done by MAC. Statistical and computational analysis was performed by MAC. Chapter was reviewed and edited by all authors.

Chapter 5 - Prevalence of heterocytous cyanophytes in elevated salinity environments

Matthew A. Campbell, Thorsten Bauersachs, Lorenz Schwark, Bernadette C. Proemse, Rolan S. Eberhard, Marco J.L. Coolen, Kliti Grice

Field sampling of microbial mats was conducted by MAC, KG, MJLC, BCP and RSE. Laboratory sample processing was done by MAC. Analysis of heterocyte glycolipids was done by TB and LS. Statistical and computational analysis was performed by MAC. Chapter was reviewed and edited by all authors.

Table of contents

Abbreviations

3'-phosphoadenylyl sulfate……... PAPS

Adenylyl sulfate……. APS

Black Sludge……. BS

Compound Specific Isotope Analysis……... CSIA

Dichloromethane……... DCM

Garden Point……. GP

Gas chromatography-mass spectrometry…….. GC-MS

Giblin River……. GR

Heterocyte glycolipids…… HGs

High performance liquid chromatography coupled to electrospray ionization tandem mass spectrometry…….….. HPLC–ESI/MS^2

Inner black section……. CI

Linke Lake…… LL

Magnesium sulfate…… $MgSO_4$

Methanol……. MeOH

Nilemah…… Nil

Outer cobble section……. CO

Principle component analysis……. PCA

Pustular mat…….. PM

Ron's Running Beach South…… RRBS

Sludge between columns…… SBC

Smooth mat…….. SM

Total lipid extraction…….. TLE

Tropical cyclone…….. TC

Tufted mat…… TM

Two-dimensional GC with time of flight mass spectrometry…… GC×GC-TOFMS

Chapter 1

Introduction

1.1 Geomicrobiology and microbial geochemistry

Through metabolic activity and growth requirements, microbes have the ability to shape their surrounding geochemical and mineralogical environments, but geochemical conditions dictate what kind of metabolic processes are possible (Thullner and Regnier, 2019). This means that the evolution of microbes has coincided with both changing geological conditions and microbial activity that has driven major shifts in ocean, continental and atmospheric chemistry (Cavalier-Smith et al., 2006). Geomicrobiology and microbial geochemistry is the combination of chemical, biological, and geological analyses to characterise the role of microbes in environmental and geological processes (Druschel and Kappler, 2015). Such analyses combine microbial diversity and activities (e.g. molecular ecology) and geochemical processes (e.g. isotope geochemistry) to address the complex interactions between microbes and their surroundings (Dwivedi et al., 2019). As seen in Figure 1.1, Earth history is interwoven with the evolution of microbes such as changes in iron and sulfur chemistry in ancient seas and the Great Oxidation Event of the Paleoproterozoic (Pufahl and Hiatt, 2012). In a more recent context, microbes are critical for the many processes that affect water quality, agriculture and changing climate (Dutta and Dutta, 2016).

"Microbes" is a common term applied to Bacteria, Archaea and unicellular Eukaryotes. It is estimated that they possibly represent more than 50 % of the biomass carbon on the planet and can be found in a whole range of locations that would be hostile to most other forms of life, such as glaciers (Garcia-Lopez et al., 2019), deep undersea thermal vents (Sogin et al., 2006) and acidic waters with high metal concentrations (Aguinaga et al., 2018). Microbial cells consist mostly of water (~85 %), the remaining biomass is made up of a combination of amino acids, nucleotides, fatty acids, and sugars which combine to produce the proteins, nucleic acids, lipids, and polysaccharides, respectively (Cooper, 2000). Deoxyribonucleic acid (DNA) contains the instructions for protein construction that are carried to ribosomes by a specific type of ribonucleic acid (RNA) called messenger RNA (mRNA) (Lodish et

al., 2000). Metabolic function is centered on the production of specific proteins known as enzymes that catalyze reactions; these proteins are complexly structured chains of amino acids that are synthesised in the ribosomes through the translation of mRNA (Serganov and Patel, 2009). Enzymes often have a metal centre and catalyze redox reactions by a "lock-and-key" mechanism, where a specific enzyme only interacts with specific reactants (Koshland, 1995).

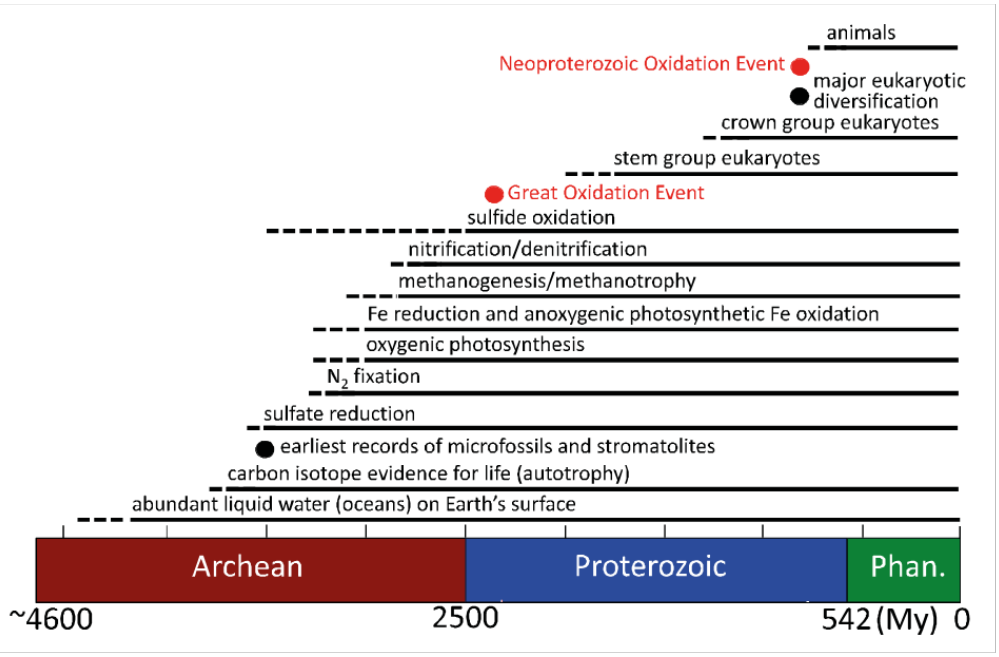

Figure 1.1 A fossil-based and isotopic, elemental, and organic geochemical perspective on the distributions of microbial metabolisms and other (environmental) milestones over Earth's history (modified from Druschel and Kappler, 2015)

In general, microbial DNA contains the possible instructions for what a specific microbe is capable of (i.e. its metabolic potential), whereas the extremely labile mRNA can elucidate what the cell is actually doing at any given time (Alberts et al., 2002). Microbes can perform a variety of metabolic and cellular functions, however these processes might not be expressed at any one time rather they become expressed in response to environmental variables such as nutrient availability (Brooks et al., 2011). In microbial communities, gene expression is typically correlated to the number of cells present and is regulated by cell–cell communication *via* the secretion of signaling molecules through a process known as quorum sensing (Papenfort and Bassler, 2016).

Microbes that enzymatically interact with their geochemical surroundings to generate energy use out-of-equilibrium redox compounds (Thullner and Regnier, 2019). These processes can lead to the acquisition of elements required for growth and reproduction such as, carbon, oxygen, nitrogen, phosphorus, and sulfur required for cellular materials, as well as metals including iron, manganese, cobalt, nickel, zinc, and molybdenum that are needed to form cofactors for specific enzymes and proteins (Kaim et al., 2013). Other microbes can build molecules from the carbon dioxide termed "autotrophy", or from more complex molecules that the organism sources from the external environment termed "heterotrophy" (Druschel and Kappler, 2015).

Now with the omics revolution, genomic DNA (metagenomics), mRNA (metatranscriptomics), and protein (metaproteomics) based techniques can advance our ability to characterize and identify microbes and gain new insights into their function in diverse environments (Dubey et al., 2020). Furthermore, membrane derived lipids and pigments, commonly referred to as "biomarkers", can be used as indicators of microbial presence and taxonomic assignment (Willers et al., 2015). The carbon "skeleton" of lipids are quite resistant to change and therefore serve as molecular fossils long after the organism dies (Whiteside and Grice, 2016). Studying the role of microbes involved in specific elemental cycles and the use of biomarker evidence in modern systems provides context to decipher the record of microbial processes throughout the geological record (Javaux and Lepot, 2018).

The geological record provides us the opportunity to see how microbial processes affect large-scale element cycling over time as other environmental conditions, such as climate, have changed (Brocks and Pearson, 2005). Geochemical and isotopic data provides evidence for biotic and abiotic processes being linked to the evolution of life (Mojzsis et al., 1996). It has been found that life on Earth was already flourishing by the time that the oldest known sedimentary rocks had formed some 3.5 Ga (Allwood et al., 2007) and that ancient microbes are most similar to microbes found in anoxic environments today (Wong et al., 2018). Microbes capable of oxygenic photosynthesis, such as cyanobacterial species, evolved relatively quickly thereafter leading to an increase in atmospheric oxygen (Shevela et al., 2013). This led to the Great Oxidation Event that gave rise to multicellularity and the evolution of Eukaryotes (Schirrmeister et al., 2013). Modern microbial assemblages, such as microbial mats, provide a basis for investigating microbial and geochemical

parameters with spatial and temporal factors, helping unravel the role that microbes play in both ecological and paleoenvironmental studies.

1.2 Microbial mats

Microbial mats represent complex communities of microorganisms bound within an organic matrix of extracellular polymeric substances (EPSs) along with sediment and minerals (Des Marais, 1995) (Figure 1.2). Microbial mats have persisted for ~85% of the geological history of the Earth and have had major impacts on past global biogeochemical cycles, particularly oxygen, nitrogen, hydrogen, and sulfur (Visscher and Stolz, 2005). Modern microbial mats are considered as analogues to extinct geobiological formations with the oldest known fossils found in Western Australia (WA), dating back ~ 3.5 Gyr ago (Allwood et al., 2006; Van Kranendonk et al., 2008; Noffke et al., 2013). Today, microbial mats are found in a diverse range of environments around the world, including hypersaline lagoons (Dupraz and Visscher, 2005), geothermal hot springs (Kato et al., 2004), tidal flats (Jahnert and Collins, 2013), freshwater lakes (White et al., 2016), remnant asbestos mines (White et al., 2015), and freshwater karstic wetlands (Proemse et al., 2017). Microbial mats represent complex communities of microorganisms bound within an organic matrix of extracellular polymeric substances (EPSs) along with sediment and minerals (Des Marais, 1995; Wong et al., 2016). Their combined metabolic activities result in steep geochemical gradients that allows for the efficient cycling of nutrients (van Gemerden, 1993; Wimpenny et al., 2000). Furthermore, this metabolic activity in combination with certain environmental factors may lead to the preservation of microbial mats through carbonate precipitation, resulting in the formation of lithified mats, or microbialites. It has been proposed this microbially induced mineralization is driven by two key components, the “alkalinity” engine (microbial metabolism and environmental conditions impacting the calcium carbonate saturation index) and an organic matrix comprised of EPS, which may provide a template for carbonate nucleation (Dupraz et al., 2009).

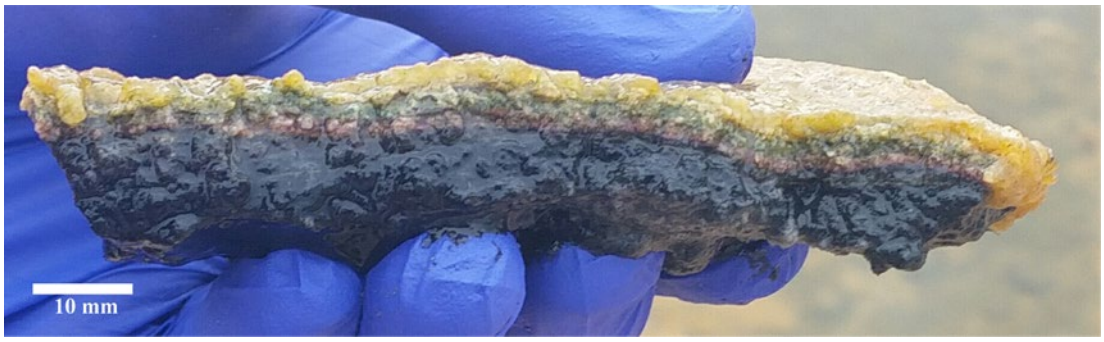

Figure 1.2 Image of a stratified gelatinous microbial mat sampled from Link Lake, Shark Bay Western Australia. Scale bar 10 mm (photograph by Yalimay Jiménez).

1.3 Biogeochemical cycling in microbial mats

Physiochemical gradients have a significant influence over the biological processes of microorganisms inhabiting microbial mats (Figure 1.3). These include the presence of oxygen, pH, redox potential, saline concentration, and the diversity of chemical species, with important physical parameters such as temperature and light (Prieto-Barajas et al., 2018). Microbial mats typically consist of a wide range of bifunctional Prokaryotic groups such as Cyanobacteria, anoxygenic photosynthetic bacteria (*e.g.* green non-sulfur bacteria known as Chloroflexi), green sulfur bacteria (Chlorobi) and purple bacteria (Chromatiaceae; Gammaproteobacteria), aerobic heterotrophs and anaerobes, sulfate-reducing bacteria (SRB), sulfur oxidizing bacteria and methanogenic archaea. These organisms take part in processes such as photosynthesis, nitrogen fixation, sulfate reduction, and methanogenesis that are vital to the overall performance of mats.

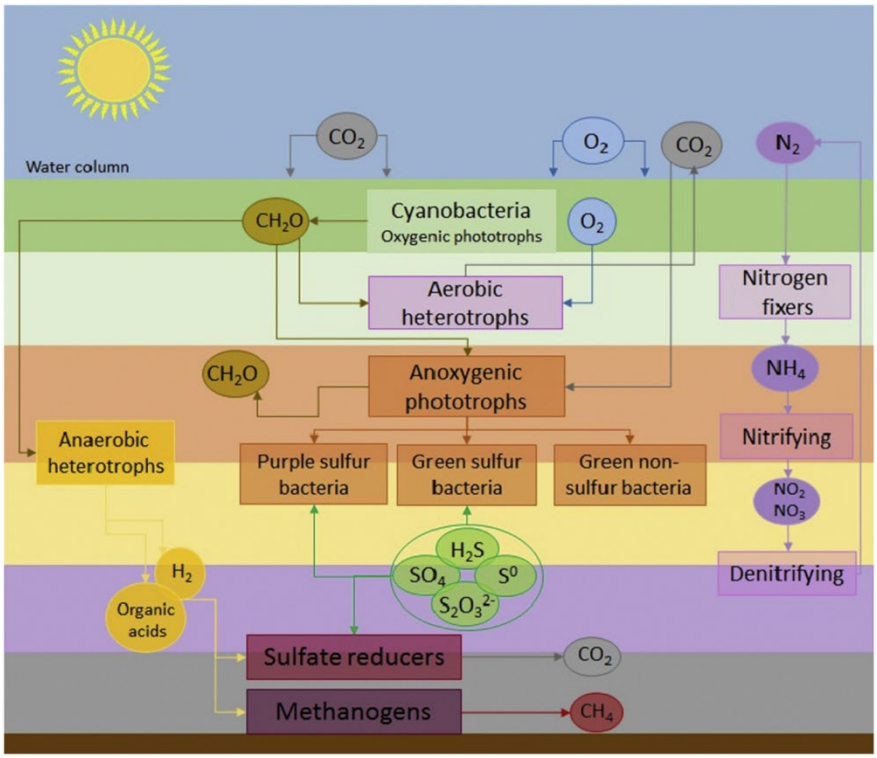

Figure 1.3 Structure and metabolism overview of photosynthetic mats (Prieto-Barajas et al., 2018).

Cyanobacteria, typically distributed in the aerobic zone of the microbial mat communities (top 2-3 mm), are considered as key primary producers in microbial mats (Prieto-Barajas et al., 2018). They are mainly involved in nitrogen and carbon fixation, as well as being major producers of EPS, providing nutrients (e.g. carbon and nitrogen) and structure to the other members of microbial mat communities (Stuart et al., 2016). Proteobacteria, Firmicutes, Spirochaetes, Chloroflexi and Bacteroidetes have been recognised as potentially dominant members of the heterotrophic microbial consortium that release nutrients from the degradation of EPS-rich cyanobacterial mats (Cole et al., 2014a; Decho and Gutierrez, 2017) and dominate below the cyanobacterial layer where low light and anaerobic conditions prevail (Wong et al., 2015). Anoxygenic phototrophic bacteria (Proteobacteria and Chlorobi, chemoheterotrophic bacteria (Spirochaetes), as well as other photoheterotrophic bacteria (Chloroflexi and Firmicutes) are known to have key roles in cycling carbon within microbial mats through respiration of organic compounds (i.e. carbohydrates), fermentation, carbon fixation, and acetogenesis (Ley et al., 2006; Abed et al., 2007; Stephens et al., 2008). Other prominent taxa include Deltaproteobacteria involved in sulfur cycling and

Planctomycetes involved in nitrogen cycling (Wasmund et al., 2017; Alcamán-Arias et al., 2018).

1.3.1 Carbon cycling

Carbon is the backbone of all organic molecules and is the most prevalent element in cellular (organic) material (Yannarell and Paerl, 2007). Among prokaryotes, cyanobacteria, lithotrophs and methanogens are a formidable biomass of autotrophs that account for a corresponding amount of CO_2 fixation in the global carbon cycle (Bertrand et al., 2019) (Figure 1.4). In most microbial mats, carbon enters *via* photosynthetic bacteria and protists (e.g. diatoms), which are able to synthesise their own food directly from CO_2 and water using energy from light. There are two main types of photosynthesis found in microbial ecosystems, oxygenic and anoxygenic. Anoxygenic photosynthesis is distinguished from oxygenic photosynthesis by the terminal reductant (e.g. hydrogen sulfide) and in the by-product generated (e.g. zero-valent sulfur) (Visscher et al., 1992; van Gemerden, 1993; Soontharapirakkul et al., 2011). However, not all organisms use CO_2 as a source of carbon atoms to carry out photosynthesis; photoheterotrophs use organic compounds, rather than carbon dioxide, as a source of carbon (Ingram et al., 1973).

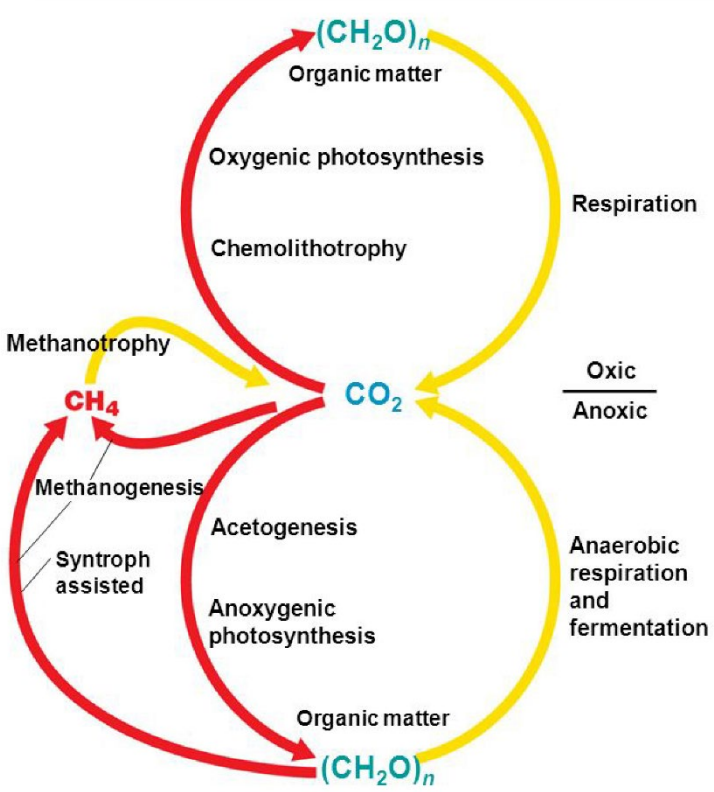

Figure 1.4 Major transformations in the carbon cycle (Madigan et al., 2008).

Photosynthesis utilizes light-dependent reactions that take place in protein complexes known as Photosystem II (PSII) and Photosystem I (PSI) (Caffarri et al., 2014). The main aim of these processes is to produce chemical energy that will be used in light independent pathways (i.e. carbon fixation) (Hügler and Sievert, 2011). PSI, found in chloroplasts and green-sulfur bacteria, uses ferredoxin-like iron-sulfur cluster proteins as terminal electron acceptors, while PSII in chloroplasts and purple non-sulfur bacteria (i.e. Rhodospirillaceae), shuttles electrons to a quinone terminal electron acceptor (Nelson, 2011). The best-known carbon fixation pathway is the Calvin–Bassham–Benson cycle, which is present in plants, algae, cyanobacteria and proteobacteria (Jones, 2008). However, there are several other carbon fixation pathways known to exist in autotrophic bacteria and archaea, which differ in reducing compounds, energy source, and oxygen sensitivity of enzymes (Berg, 2011). Such pathways include: the Arnon–Buchanan cycle uses a reductive citric acid cycle and is found in anaerobic or microaerophilic bacteria and archaea (Buchanan et al., 2017); the Wood–Ljungdahl pathway uses a reductive acetyl-CoA pathway and is only found

in strictly anaerobic bacteria and archaea (Ragsdale, 2008); and the 3-hydroxypropionate cycle found in some green non-sulfur bacteria of the family Chloroflexaceae (Alber and Fuchs, 2002).

Primary produced carbon that is available in the form of carbohydrates and other biomolecules (*e.g.* lipids, proteins, and polysaccharides) can be further cycled by a series of heterotrophic carbon utilization pathways (Bauer and Bianchi, 2012). Heterotrophic microorganisms require organic carbon for growth, forming relationships with autotrophs wherein the fixed carbon by autotrophs is needed by heterotrophs, and CO_2 produced by the heterotrophs is used by the autotrophs (Cole et al., 2014). Heterotrophic bacteria are key degraders in microbial ecosystems and considered to be the major contributors the carbon cycle (Thompson et al., 1996). The breakdown of these molecules serves to supply energy in aerobic environments commonly referred to as respiration (Peter and Del Giorgio, 2007). In anaerobic environments, microorganisms can cycle the carbon compounds to yield energy *via* fermentation (Müller, 2001). CO_2 can also be converted to methane (CH_4), this occurs in anaerobic environments and is accomplished by methanogens (Whitman et al., 2014). To complete the recycling pattern methane oxidising methanotrophs can convert CH_4 to CO_2, this conversion is an aerobic process, also yields water and energy (Hanson and Hanson, 1996).

1.3.2 Sulfur cycling

The transformation and fate of sulfur in the environment is largely dependent upon microbial activities (Lomans et al., 2002) (Figure 1.5). Sulfur has a wide range of stable redox states that play important roles in biochemistry as structural components, redox centres, and carbon carriers. Redox reactions that involve the reduction and oxidation of inorganic sulfur compounds are used by microbes to generate and conserve biochemical energy (Klotz et al., 2011). Microbes also produces organosulfur compounds (OSCs) that play a significant role in cellular functions along with the formation and preservation of sedimentary organic matter during diagenesis (Werne et al., 2004).

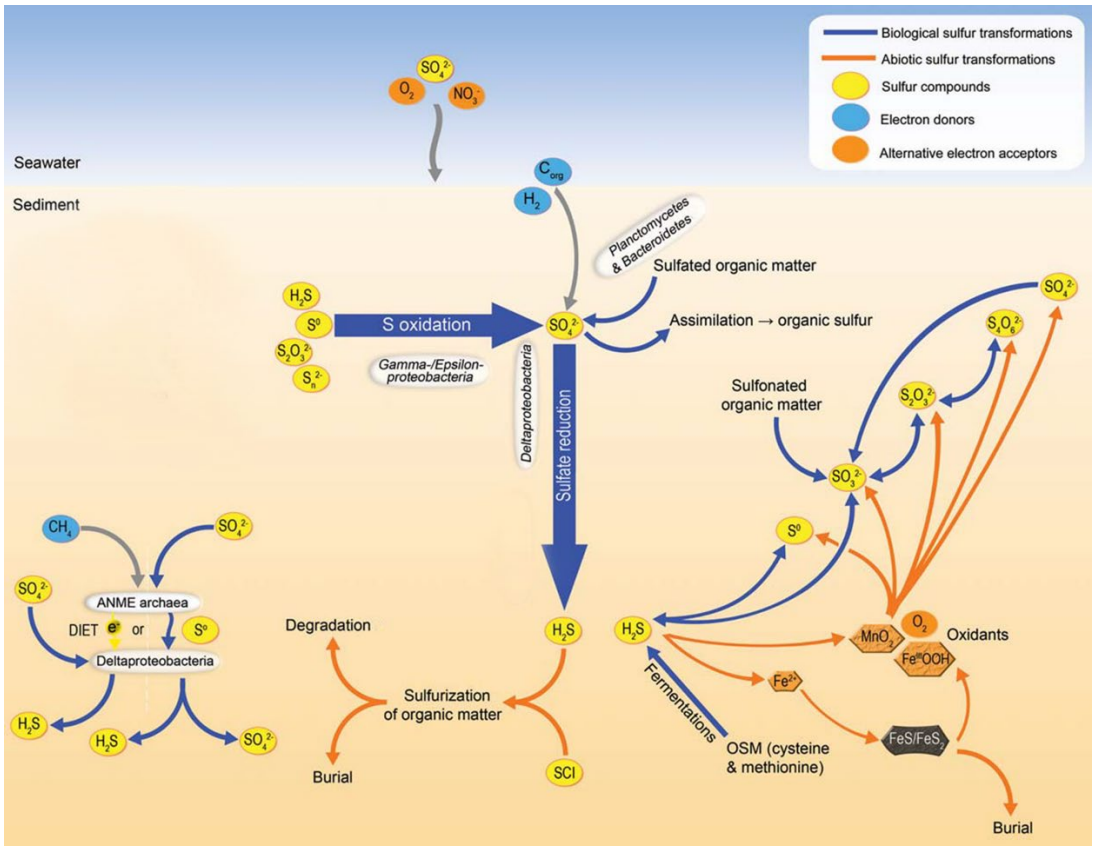

Figure 1.5 Conceptual depiction of the sulfur cycle in marine sediments, including main reactions of inorganic and organic sulfur compounds, selected taxa, sulfate-dependent anaerobic methane oxidation, and transformations of sulfur compounds of intermediate oxidation states (sulfur cycle intermediates, SCI). OSM = organo-sulfur molecules, Corg = organic matter. DIET = direct-interspecies electron transport. ANME = anaerobic methane-oxidising (modified from Wasmund et al., 2017).

The reduction of sulfate follows two major biosynthetic pathways: assimilatory incorporation of sulfur into cellular constituents and dissimilatory processes used by bacteria and archaea to reduce sulfate by using it as an electron acceptor for the oxidation of organic matter in oxygen-poor environments (Detmers et al., 2001). The assimilatory pathway, which is found in a wide range of organisms, produces reduced sulfur compounds for the biosynthesis of S-containing amino acids and does not lead to direct excretion of sulfide (Cooper, 1983). In the dissimilatory pathway, which is restricted to obligatory anaerobic bacterial and archaeal lineages, sulfate is the terminal electron acceptor of the respiratory chain producing large quantities of inorganic sulfide (Grein et al., 2013). Both pathways start from the activation of sulfate by reaction with adenosine triphosphate (ATP) to form adenylyl sulfate (APS). In the assimilatory pathway APS is converted to 3'-phosphoadenylyl sulfate (PAPS) and then

reduced to sulfite, and sulfite is further reduced to sulfide by the assimilatory sulfite reductase. In the dissimilatory pathway APS is directly reduced to sulfite, and sulfite is further reduced to sulfide by the dissimilatory sulfite reductase (Bick et al., 2000). Additionally, the oxidation of inorganic sulfur compounds by bacteria is a major part of the sulfur cycle. Oxidation of sulfur species provides reductants for use either in carbon dioxide fixation or for energy conservation through membrane-bound electron transport chains (Grabarczyk and Berks, 2017).

1.3.3 Nitrogen cycling

The nitrogen cycle involves several reduction and oxidation pathways (Figure 1.6), where nitrogen is found in various oxidation states ranging from nitrate (+5) to ammonium (-3) (Bothe et al., 2007; Thamdrup, 2012). Nitrogen commonly enters microbial ecosystems *via* the fixation of atmospheric nitrogen to which is reduced to ammonia, a biologically useful reduced form incorporated into amino acids and other vital compounds (Zehr and Kudela, 2011). The process is crucial for maintaining biological productivity in ecosystems, as it replenishes the pool of biologically available nitrogen that is lost via anaerobic ammonium oxidation and denitrification (Kraft et al., 2011). Nitrogen fixation is carried out by microorganisms termed diazotrophs, which are represented in both bacterial *(e.g.* cyanobacteria) and archaeal Domains (De Bruijn, 2015). Other reduction pathways include the assimilatory nitrate reduction, dissimilatory nitrate reduction to ammonia (DNRA), and denitrification that all utilise nitrate (Tiedje, 1981, 1988). The assimilatory nitrate reduction occurs under aerobic conditions when reduced nitrogen is limiting (Cole and Brown, 1980). Dissimilatory nitrate reduction and denitrification occur when oxygen is limiting, producing gaseous nitrogen compounds (N_2, NO and N_2O) (Korom, 1992). Oxidation pathways include nitrification and anaerobic ammonium oxidation (Anammox). Nitrification is the oxidation of ammonia (NH_3) with oxygen into nitrite followed by the oxidation of nitrite into nitrate (Hooper et al., 1997). The first step is performed by ammonia-oxidizing microorganisms and the second step by nitrite-oxidizing microorganisms. Anammox is a biochemical process of oxidizing ammonium (NH_4^+) into dinitrogen gas (N_2) using nitrite as an electron acceptor (Kuenen, 2008).

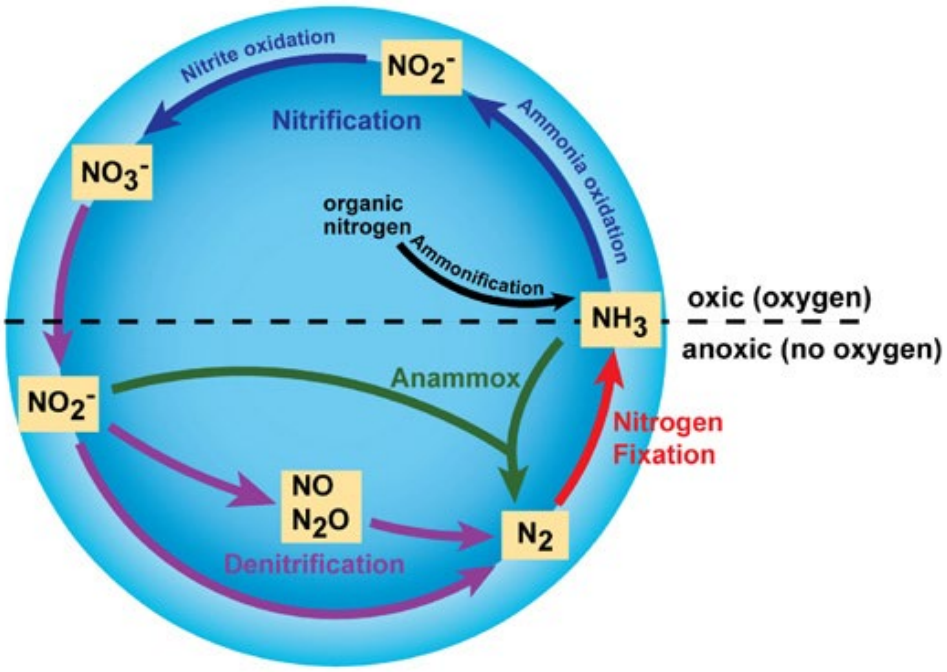

Figure 1.6 Major transformations in the nitrogen cycle (Bernhard, 2010).

1.4 Environmental Adaptation

Many microbial ecosystems are under a continuous state of change due to fluctuations in abiotic factors (e.g., nutrients, pH, light, temperature, heavy metals and salinity) caused by diel and seasonal cycles, as well as pressures from biotic influences (e.g., population density, parasites, predation and viral attack) (Bolhuis et al., 2014). Furthermore, many microbial ecosystems occur in extreme environments, which include physical extremes (e.g. temperature, radiation or pressure) and geochemical extremes (e.g. desiccation, salinity, pH, oxygen species or redox potential) (Merino et al., 2019). To maintain cellular functions, microorganisms have developed various pathways in order to adapt to environmental fluctuations and extreme environments. One common approach is to keep the hostile external environment out. For example bacteria found at pH 0.5 have been shown to produce acid-tolerant extracellular proteins, enabling them to keep near neutral cytoplasm conditions (Lund et al., 2014). Another approach is to remove the problem as fast as possible. For example, heavy metal-resistant bacteria use an efflux pump to remove zinc, copper and cobalt (Nies,

2003). A third option is to alter physiology or enhancing repair capabilities, which has been observed in many extremophilic microorganisms. For example, elevating the expression of enzymes that aid in repairing damaged cellular components and synthesis of molecules for relieving stresses (Haruta and Kanno, 2015). Chemotaxis, *i.e.* moving toward attractants and moving away from repellents, is an effective survival strategy in heterogeneous environments (Stocker and Seymour, 2012). Microorganisms dealing with elevated salinity and desiccation conditions respond by accumulating osmoprotectants in their cytosol, which protects them from cytoplasmic dehydration and desiccation, with glycine betaine being the most effective osmoprotectant found in most prokaryotes (Wood, 1999). Compatible solutes such as K^+, glutamate, glutamine, proline, glycine betaine and sucrose accumulate in cells and aid in the stabilization of cells and (dry) membranes *via* balancing the osmotic difference between the cell's surroundings and the cytosol (Welsh, 2000).

1.5 Genetic-based studies of microbial mats

Microbiologists have studied microbial mats for several decades. However, the initial studies were disadvantaged by the lack of appropriate methods and tools that would allow the investigation of microbial processes (Bolhuis et al., 2014). Until the application of molecular genetic techniques, information about the microorganisms in microbial mats was limited to cultivation and microscopy studies (Ward et al., 1998). The use of sequencing technologies revealed the extensive diversity of the microbial community and their metabolic pathways within microbial mats (Wong et al., 2016). The initial use of rRNA libraries in hypersaline mats showed distinct microbial signatures with average ratios of bacteria/archaea/eukaryote rRNA genes of 90%/9%/1% in Guerrero Negro and Shark Bay mats. This confirmed a bacterial dominance although with a significant archaeal contribution to the metabolic activities (Wong et al., 2016). rRNA based methods are now being replaced by meta-omics and high-throughput sequencing allowing for a greater understanding of the diversity, ecology, and evolution of microbial mats (Bolhuis et al., 2014). Metagenomics and metatranscriptomics have become powerful tools to study functional potentials (DNA-based) and activities (RNA-based) of microbial mat microbiomes. Metagenomics focuses on studying the genomic content and on identifying which microbes are

present within a whole community and their functional potential, whereas metatranscriptomics can be used to study the diversity of the actively expressed genes within such community (Aguiar-Pulido et al., 2016). Furthermore, coupling metatranscriptomic to metagenomics information can reveal the metabolic functions and gene expression patterns in complex microbial assemblages (Wang et al., 2020). This is achieved by mapping transcripts to assembled draft metagenome-assembled genomes (MAGs).

1.5.1 Metatranscriptomics

The advantage of metatranscriptomics is that it can provide information about differences in the active functions of microbial communities, which appear to be the same in terms of microbial composition (Bashiardes et al., 2016). While metagenomics addresses what the composition of a microbial community is under different conditions; metatranscriptomics addresses what genes are collectively being expressed under these different conditions. With the use of functional annotations of expressed genes, it is possible to infer the functional profile of a microbial community under specific conditions (Aguiar-Pulido et al., 2016). A typical metatranscriptomic analysis pipeline will either map reads to a reference genome or perform *de novo* assembly of the reads into transcript contigs (Anwar et al., 2019). Similar to the alignment-based methods, the first strategy map reads to reference databases, providing information to infer the relative expression of individual genes. Whereas, the second strategy infers the same but with assembled sequences (Aliyu Musa et al., 2018). The first strategy is limited by the information in the database of reference genomes, whereas the second strategy is limited by the ability of software programs to assemble contigs (transcripts) correctly from short reads data (Voshall and Moriyama, 2018). Using RNA sequencing (RNASeq) to record expressed transcripts within a microbiome at a given point in time under a set of environmental conditions provides a closer look at active members (Shakya et al., 2019). So far, this method has been used to focus on population and metabolic transcriptional activity over diel and seasonal cycles in thrombolite-forming mats from the Bahamas found that the most transcribed genes in all seasons were associated with photosynthesis. The study also showed that transcripts associated with nitrogen fixation, methanogenesis and dissimilatory sulfate reduction exhibited diel

cycling, and variability between seasons (Louyakis et al., 2018). Another metatranscriptomic study involving the analysis of Antarctic relic microbial mat communities revealed that the most abundant transcripts code for products involved in genetic information processing pathways, particularly translation, DNA replication, and DNA repair (Zaikova et al., 2019).

1.6 Lipid biomarkers used to study microbial ecosystems

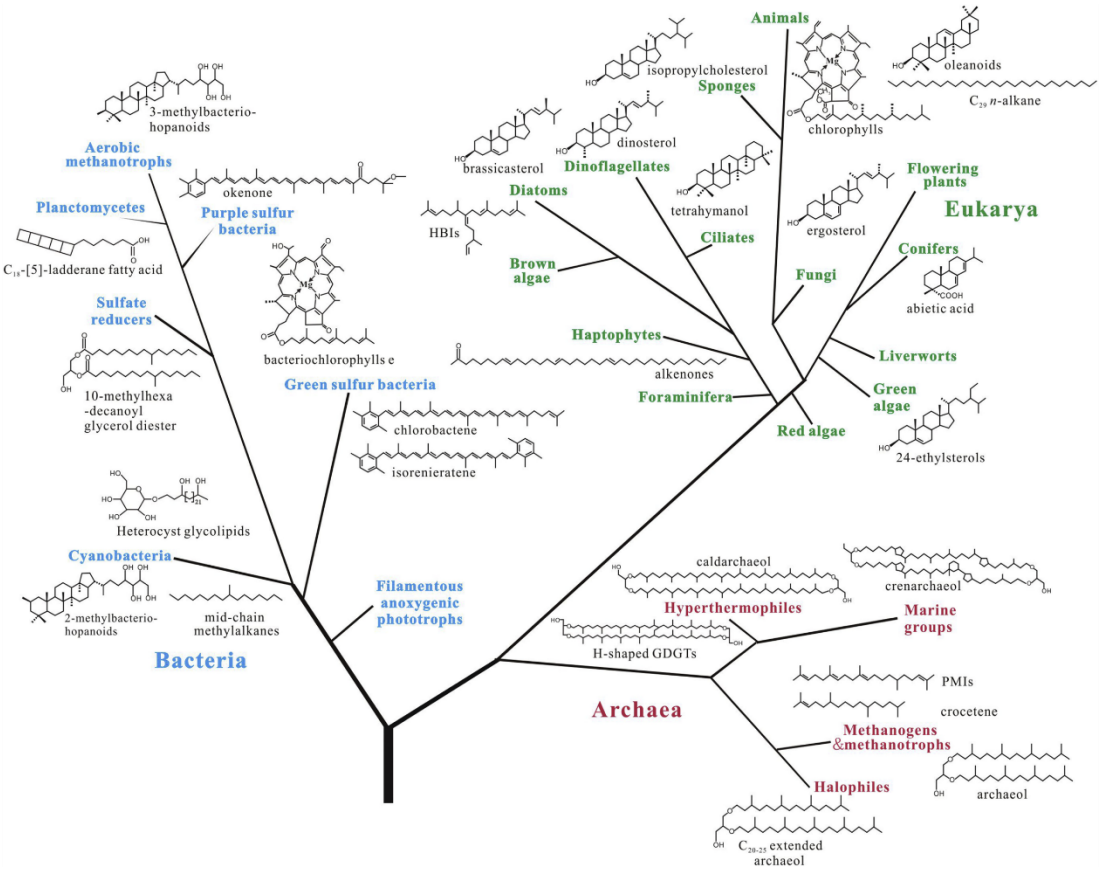

Figure 1.7 Characteristic lipids of Bacterial, Eukaryotic and Archaeal domains (Luo et al., 2019).

Lipid biomarkers originate from all three domains of life: Eukaryota, Bacteria, and Archaea (Figure 1.7) (Grice and Eiserbeck, 2013; Luo et al., 2019). Lipids function as the main constituents of cell membranes, act as carbon storage bodies and facilitate signal transduction (Spector and Yorek, 1985). The specific identity, isomeric and stable isotopic configurations of biomarkers have provided insights into the ecology of microbial communities (*e.g.* Pagès et al., 2015). Sterols are the main constituents of

the eukaryotic cell membrane, and bacteriohopanepolyols complemented by linear, branched and cyclic fatty acids are the main components of the bacterial cell membrane (*e.g.* Luo et al., 2019). In Eukaryotes and Bacteria, these compounds are generally linked to glycerol through an ester bond. In Archaea, isoprenoids connected to glycerol by an ether bond form the main components of the cell membrane (*e.g.* Briggs and Summons, 2014).

A variety of lipids have been extracted from microbial mat communities including fatty acids, hydrocarbons, wax esters, steroids and hopanoids (Allen et al., 2010). Fatty acids have been widely used to characterize individual microbial species and to provide a profile of microbe-dominated ecosystems (*e.g.* Agrawal et al., 2015). Cyclic isoprenoids such as hopanoids and steroids have been used extensively as biomarkers in organic geochemistry because of their ubiquity as membrane stabilising molecules in cells, the stability of their degradation products and the variety of modifications on the basic structure which allow identification of source organisms (Rohmer et al., 1984). Hopanoids are pentacyclic triterpenoids with a five-membered E-ring, and sterols are tetracyclic triterpenoids. This, along with the observation that hopanoids are mainly found in bacteria, whilst sterols are mainly found in eukaryotes, has led to their use as proxies for prokaryotic and eukaryotic input in sediments (e.g. Sohlenkamp and Geiger, 2015). Hydrocarbons and wax esters can also give valuable insight into the presence of specific groups of organisms. Certain monomethyl-branched hydrocarbons indicate contributions from cyanobacteria, and wax esters of varying length can indicate the presence of anoxygenic phototrophs or of higher eukaryotes (Cranwell and Volkman, 1981; Summons, 1987).

Certain lipid groups can be useful as chemotaxonomic markers within specific group's organisms. For instance, cyanobacteria contain two orders*, i.e.* Nostocales and Stigonematales, capable of differentiating vegetative cells into heterocytes under nitrogen-depleted conditions (Komárek et al., 2014). These specialised cells contain nitrogenase, the enzyme required for the conversion of dinitrogen (N_2) to ammonia (Kumar et al., 2010). As nitrogenase is readily inactivated by even low amounts of oxygen, the thick heterocyte cell wall limits gas diffusion into their cell and consists of distinct polysaccharide and glycolipid layers (Meeks and Elhai, 2002). The latter is known to contain a suite of unique glycolipid structures commonly referred to as heterocyte glycolipids (HGs), comprising either a hexose or pentose head group,

bound to long-chain diols, triols, or hydroxyketones (Bauersachs et al., 2009; Wörmer et al., 2012). Their distribution in heterocytous cyanobacteria suggests a chemotaxonomic relevance that might allow for identification between different genera (Bauersachs et al., 2009) and as biomarkers (molecular fossils) of N_2 fixation in both ecological and paleoenvironmental settings (Wörmer et al., 2012).

1.6.1 Compound specific stable isotope analysis (CSIA)

Carbon is the main component of organic matter and is strongly involved in biochemical, ecological, environmental and atmospheric processes (Bolan et al., 2011). CSIA allows the measurement of stable isotope ratios in individual compounds providing a highly detailed insight into biogeochemical processes (Ruess and Chamberlain, 2010). CSIA of lipids has been utilized to investigate biomarkers origins, variations in carbon cycle, paleoclimates and biogeochemical cycling (Grice and Brocks, 2011). The measurement of the abundance of naturally-occurring stable isotopes within biological samples has proven to be a powerful tool for a wide range of ecological and physiological studies (Pagès et al., 2014; Plet et al., 2018). The key premises of isotope ecology are that carbon isotope ($\delta^{13}C$) values vary among primary producers, and this variation persists in higher trophic-level consumers (Whiteman et al., 2019). Moreover, isotope values are also influenced by an organisms physiology, specifically the biochemical reactions that control the assimilation, synthesis, and degradation of macromolecules (protein, lipid, carbohydrate) required by producers and consumers for homeostasis (Whiteman et al., 2019).

1.6.2 Sulfurisation of lipids

As discussed in section 1.3.2, the cycling of sulfur can lead to biologically induced preservation of sulfur into biomolecules *via* dissimilatory processes that use sulfate as a terminal electron acceptor for the oxidation of organic matter by bacteria and archaea in oxygen-poor environments (Berner, 1982; Jørgensen, 1982). There are three major conditions required for sulfurisation of organic matter in microbial ecosystems. First, reactive reduced sulfur species must be present; second, the concentration of free metal ions, especially iron, must be low; and third, organic compounds (i.e. hopanepolyol)

with functional sites that are receptive to the addition of inorganic sulfur species must be present (Amrani, 2014). Chemical desulfurisation of sulfur-bound extracts from microbial material can be accomplished using the Raney-Nickel catalyst (Grice et al., 1998). Released hydrocarbons can provide information about the original carbon skeletons of the sulfurised lipids. Desulfurisation of polar fractions extracted from immature hypersaline sediments of Miocene/Pliocene age from the Sdom Formation, Dead Sea, Israel released high amounts of apolar components (Grice et al., 1998). These components have been credited to the major part of the macromolecular matrix being comprised of multiple sulfur-linked biomarkers derived from a limited number of highly functionalised lipids mainly from the planktonic alga *Botryococcus braunii*. In contemporary sediments, the metabolism of SRB generates H_2S providing a reducing agent for abiotic reduction of biolipids (Hebting et al., 2006). Desulfurisation of a extant smooth mat from Shark Bay, WA found high abundance of sulfur-bound hopanes (C_{27}–C_{31}) and a high proportion of C_{31} 17β,21β-homohopane (Pagès et al., 2015) confirming early diagenetic sulfurization of funtionalised hopanoids had occurred.

1.7 Study Sites

1.7.1 Shark Bay, Western Australia

Shark Bay is located 800 Km north of Perth, WA, harbours microbial mats and microbialites living in areas of high salinity (>60 ppt) (Figure 1.8). Hamelin Pool is considered to have some of the most extensive and diverse marine microbial systems that have been suggested to be modern-day analogues of Archean stromatolites (Jahnert et al., 2012). Based on surface morphology, several different types of extant microbial mat have been identified in Shark Bay that include gelatinous, smooth, tufted, pustular, colloform, film and blister mats (Logan et al., 1972). For example, the Nilemah tidal flat has three major types of microbial mat that occur along a littoral gradient. These include tufted mats occurring in upper intertidal zone, pustular mats in the intertidal zone and smooth mats in the subtidal zone. Tufted mats are composed of long filaments made by *Lingbya* sp. This type of mat normally thrives over shallow muddy substrates where sediments permanently retain moisture. Pustular mats contain coccoid cyanobacteria and exhibit an irregular clotted fabric characteristic of

thrombolitic deposits covered by brown mucilage produced from the organomineralisation of gelatinous mucilage. Laminated smooth mats are composed of "sub-horizontal millimetric laminae made of fine-grained carbonate sediments interbedded with laminae of microbial organic matter that had become lithified as micrite laminae".

Shark Bay has an unusually high abundance of Archaea relative to other marine microbial mat ecosystems. The predominant members of these mats are considered to be Euryarchaeota, known to possess high tolerance to hypersalinity (Wong et al., 2016). Current studies in Shark Bay have focused on understanding microbial diversity and function using cultures, sequencing of 16S rDNA, shotgun metagenome and lipid analyses (Burns et al., 2004; Papineau et al., 2005; Allen et al., 2009; Goh et al., 2009; Jungblut et al., 2009; Jahnert and Collins, 2013; Pagès et al., 2014; Ruvindy et al., 2016; Wong et al., 2018). These studies have indicated that Shark Bay microbial ecosystems are mainly dominated by Proteobacteria, Bacteroidetes, Cyanobacteria, Chloroflexi, and Haloarchaea with the particular novelty of Shark Bay appearing to have relatively higher abundances of Archaea compared with other microbial mat ecosystems found around the world. A 16S rDNA study utilizing high-throughput sequencing of prokaryotic populations at the millimeter scale in a Shark Bay mats proposed that there are tightly coupled cooperative niches regulated by microbial interactions between different microbial groups that include cyanobacteria, sulfate reducers/sulfate oxidizers, and hydrogenotrophic methanogens. Furthermore, this study found a considerable abundance of anaerobic Bacteria and Archaea coexisting at the surface of the mat along with the phototrophic consortia, suggesting metabolic specialization of these anaerobic organisms that is potentially being driven by the daily tidal and salinity fluctuations (Wong et al., 2015). However, 16S rDNA sequencing is limited as it cannot directly link function to phylogeny, a recent study utilizing shotgun metagenomics to annotate microbial functional capacity in Shark Bay microbial mats found alternative modes of carbon fixation (3-hydroxypropionate/4-hydroxybutyrate pathway), heavy metal resistance genes, and osmoadaptive pathways (Ruvindy et al., 2016). Another recent metagenomic study of the functional metagenomic potentials in Shark Bay mats *via* Illumina NextSeq sequencing found a range of pathways involved in carbon, nitrogen, sulfur, and phosphorus cycles. The most abundant genes being affiliated with sulfate assimilation, methanogenesis, Wood–Ljungdahl pathway,

phosphate transport, and copper efflux (Wong et al., 2018). Additionally, lipid biomarkers and stable isotopic analysis have provided insight into the complex relationship of microbial mats with their surrounding environment, the microbial communities present in microbial mats and can help to characterize how these microbial communities are regulating specific biomarker distributions. Previous lipid analysis revealed a predominance of photosynthetic cyanobacteria within the surface of the mat and an increased abundance in sulfate reducing bacteria with depth (Pagès et al., 2015).

However, these studies failed to inform about the activity of the various mat microbiomes in Shark Bay, and many of the previous genomic and lipid studies have mainly focused on microbial communities within Hamelin Pool (*i.e.* Nilemah, Carbla station). Therefore, the aims of my study were to analyse a diversity of active microbial communities (mat types) occurring in different salinities within Shark Bay area. Furthermore, Shark Bay is episodically impacted by tropical cyclones that generate strong storm surges capable of reworking, transporting and depositing marine sediments (Jahnert et al., 2012). There is yet to be an understanding of how microbial ecosystems respond and recover to these disturbances in Shark Bay, therefore this study aimed to assess the effect that a severe tropical cyclone had on a microbial assemblage. Additionally, this study focused on mucilaginous cobbles that formed due to cyclonic activity in Shark Bay. This study aimed to investigate if the reworking and deposition of mucilaginous sediments in microbial dominated ecosystems may lead to the potential archiving of unique geological and biological signatures.

Figure 1.8 Satellite images of the Shark Bay world heritage area: 1. Nilemah, 2. RRBS, 3. Garden Point and 4. Linke lake. Images were generated with ArcGIS Desktop: Release 10. Redlands, CA: Environmental Systems Research Institute.

Microbial mats were sampled from four locations in Shark Bay: 1. Nilemah, 2. RRBS, 3. Garden Point and 4. Linke lake (Figure 1.8). 1. Nilemah is an intertidal flat located in the southern area of Hamelin Pool (26°27'02.9"S 114°05'39.3"E). The tidal flat covers an area of about 16 km^2 within Hamelin Pool, a semi-enclosed shallow embayment (<10 m) that extends up to 1400 km^2 with a relatively small volume ~7 km^3 (Jahnert and Collins, 2013; Pages et al., 2014). High rates of evaporation and limited rainfall leads to the water in Hamelin Pool to be hypersaline (60 to 70 ppt) with pH ranges between 7.5-8. (2) The site referred to as 'RRBS' is a cyclone impacted located in a south eastern area of Hamelin Pool (26°37'60.3"S 114°20'50.9"E). RRBS is a indurated zone close to an enclosed river mouth and is described as an intertidal beach face unit with a steep the depositional gradient and intertidal processes that regularly affect the beach front (a more detailed description of RRBS can be found in Morris et al., 2019). Garden Point is a small re-entrant of about 11 km^2, located on the eastern area of Henry Freycinet embayment (26°36'45.8"S 113°88'08.5"E). This location is metahaline (40–56 ppt) with pH ranges between 7.8-8.7 (Jahnert and

Collins, 2013). Linke Lake is a gypsum lake located north of Denham in the Francois Peron national park (25°88'06.7"S 113°55'41.3"E). Also known as a “Birridas”, this lake is oval in shape, 1 km wide and contained a central, raised platform ringed by a moat-like depression (Bufarale and Collins, 2015).

1.7.2 Giblin River, Tasmania

Figure 1.9 Satellite images of the Giblin River UNESCO-listed Tasmanian Wilderness World Heritage Area. Images were generated with ArcGIS Desktop: Release 10. Redlands, CA: Environmental Systems Research Institute.

Giblin River lies within the United Nations Educational, Scientific and Cultural Organization (UNESCO) listed Tasmanian Wilderness World Heritage Area (Figure 1.9). Within the Giblin River catchment occur peat-bound karstic wetlands that are regionally distinctive due to the presence of prominent spring mounds. These mounds are up to 60 m in diameter with densely vegetated marshy tops, but only rise up to

approximately 0.5 m above surrounding wetlands. The freshwater karstic spring mounds are mildly alkaline with pH ranges between 7.0-7.9. Recently, freshwater microbial mat communities were discovered in the Giblin River catchment, located in south-west Tasmania, Australia (−42°56′S, 145°45′E) in December of 2015 and was revisited in August 2016 to collect samples for this study. A previous 16 S rRNA gene analysis of the mats revealed that the bacterial community is dominated by Cyanobacteria, Alphaproteobacteria with an unusually high proportion of Chloroflexi, followed by Armatimonadetes and Planctomycetes, therefore making then unique compared to other living examples (detailed descriptions of this location and microbial mats can be found in Proemse et al., 2017).

However, still little is known about the metabolic activity and lipid biomarker signatures of these freshwater microbial ecosystems, the aim of this study was to investigate the active role and lipid biomarker profiles of cyanobacteria occurring within these mats, as well as compare their composition to the elevated salinity environment of Shark bay.

1.8 Aims of the thesis

The main goals of the thesis were to use metatranscriptomic and organic geochemical approaches to further characterise microbial communities forming the microbial mats in Shark Bay, Western Australia and Giblin River, Tasmania. This study employed metatranscriptomics to understand how the microbiome in the microbial mats respond to the environment and to better understand the role that specific communities play in elemental cycling and carbonate precipitation.

The purpose of the research presented in **Chapter 3** was to investigate the metatranscriptomes in Shark Bay microbial mats to unravel how the active microbial communities, transcript abundances, and photosynthetic and chemosynthetic capacities change in accordance to mat type, diel cycle, and sampling season.

Chapter 4 had three specific objectives: 1) to understand the ecological functioning and stability of hypersaline microbial communities after a cyclonic event by contrasting the active and resident microbial communities, biogeochemical cycles (e.g. sulfur and nitrogen), and stress and defence mechanisms; 2) to obtain hydrocarbon

biomarker distributions, together with their stable carbon isotopic compositions, to provide insight into the organic matter source and relation of the samples to each another; 3) evaluate if the microbial activity occurring within the cobble formation will lead to carbonate precipitation and biomarker preservation.

In **Chapter 5**, the main intention was to explore the diversity and ecological role (e.g. nitrogen and carbon fixation) of heterocytous cyanobacteria along with HGs distributions in microbial mats occurring in freshwater environment of Giblin River, and metahaline and hypersaline environments of Shark Bay.

1.9 References

Abed, R.M.M., Zein, B., Al-Thukair, A., de Beer, D., 2007. Phylogenetic diversity and activity of aerobic heterotrophic bacteria from a hypersaline oil-polluted microbial mat. Syst. Appl. Microbiol. 30, 319–330.

Agrawal, P.K., Agrawal, S., Shrivastava, R., 2015. Modern molecular approaches for analyzing microbial diversity from mushroom compost ecosystem. 3 Biotech.

Aguiar-Pulido, V., Huang, W., Suarez-Ulloa, V., Cickovski, T., Mathee, K., Narasimhan, G., 2016. Metagenomics, Metatranscriptomics, and Metabolomics Approaches for Microbiome Analysis. Evol. Bioinform. Online 12, 5–16.

Aguinaga, O.E., McMahon, A., White, K.N., Dean, A.P., Pittman, J.K., 2018. Microbial community shifts in response to acid mine drainage pollution within a natural wetland ecosystem. Front. Microbiol. 9.

Alber, B.E., Fuchs, G., 2002. Propionyl-coenzyme a synthase from Chloroflexus aurantiacus, a key enzyme of the 3-hydroxypropionate cycle for autotrophic CO2 fixation. J. Biol. Chem. 277, 12137–12143.

Alberts, B., Johnson, A., Lewis, J., Raff, M., Roberts, K., Walter, P., 2002. Studying Gene Expression and Function.

Alcamán-Arias, M.E., Pedrós-Alió, C., Tamames, J., Fernández, C., Pérez-Pantoja, D., Vásquez, M., Díez, B., 2018. Diurnal Changes in Active Carbon and Nitrogen Pathways Along the Temperature Gradient in Porcelana Hot Spring Microbial Mat. Front. Microbiol. 9, 2353.

Aliyu Musa, Laleh Soltan Ghoraie, Shu-Dong Zhang, Galina Glazko, Olli Yli-Harja, Matthias Dehmer, Benjamin Haibe-Kains, Frank Emmert-Streib, 2018. A review of connectivity map and computational approaches in pharmacogenomics. Brief. Bioinform. 19, 506–523.

Allen, M.A., Goh, F., Burns, B.P., Neilan, B.A., 2009. Bacterial, archaeal and eukaryotic diversity of smooth and pustular microbial mat communities in the hypersaline lagoon of Shark Bay. Geobiology 7, 82–96.

Allen, M.A., Neilan, B.A., Burns, B.P., Jahnke, L.L., Summons, R.E., 2010. Lipid biomarkers in Hamelin Pool microbial mats and stromatolites. Org. Geochem.

41, 1207–1218.

Allwood, A.C., Walter, M.R., Burch, I.W., Kamber, B.S., 2007. 3.43 billion-year-old stromatolite reef from the Pilbara Craton of Western Australia: Ecosystem-scale insights to early life on Earth. Precambrian Res. 158, 198–227.

Allwood, A.C., Walter, M.R., Kamber, B.S., Marshall, C.P., Burch, I.W., 2006. Stromatolite reef from the Early Archaean era of Australia. Nature 441, 714–718.

Amrani, A., 2014. Organosulfur Compounds: Molecular and Isotopic Evolution from Biota to Oil and Gas. Annu. Rev. Earth Planet. Sci. 42, 733–768.

Anwar, M.Z., Lanzen, A., Bang-Andreasen, T., Jacobsen, C.S., 2019. To assemble or not to resemble-A validated Comparative Metatranscriptomics Workflow (CoMW). Gigascience 8, 1–10.

Bashiardes, S., Zilberman-Schapira, G., Elinav, E., 2016. Use of metatranscriptomics in microbiome research. Bioinform. Biol. Insights 10, 19–25.

Bauer, J.E., Bianchi, T.S., 2012. Dissolved Organic Carbon Cycling and Transformation, in: Treatise on Estuarine and Coastal Science. Academic Press, pp. 7–67.

Bauersachs, T., Compaoré, J., Hopmans, E.C., Stal, L.J., Schouten, S., Sinninghe Damsté, J.S., 2009. Distribution of heterocyst glycolipids in cyanobacteria. Phytochemistry 70, 2034–2039.

Berg, I.A., 2011. Ecological aspects of the distribution of different autotrophic CO2 fixation pathways. Appl. Environ. Microbiol.

Berner, R.A., 1982. Burial of organic carbon and pyrite sulfur in the modern ocean: Its geochemical and environmental significance. Am. J. Sci. 282, 451–473.

Bernhard, A., 2010. The Nitrogen Cycle: Processes, Players, and Human Impact. Nature Education Knowledge 3 (10), 25.

Bertrand, J.C., Bonin, P., Ollivier, B., Alain, K., Godfroy, A., Pradel, N., Normand, P., 2019. Evolutionary success of prokaryotes, in: Prokaryotes and Evolution. Springer International Publishing, pp. 131–240.

Bick, J.A., Dennis, J.J., Zylstra, G.J., Nowack, J., Leustek, T., 2000. Identification of a new class of 5'-adenylylsulfate (APS) reductases from sulfate-assimilating bacteria. J. Bacteriol. 182, 135–142.

Bolan, N.S., Adriano, D.C., Kunhikrishnan, A., James, T., McDowell, R., Senesi, N., 2011. Dissolved Organic Matter. Biogeochemistry, Dynamics, and Environmental Significance in Soils., Advances in Agronomy. Academic Press.

Bolhuis, H., Cretoiu, M.S., Stal, L.J., 2014. Molecular ecology of microbial mats. FEMS Microbiol. Ecol.

Bothe, H., Ferguson, S., Newton, W.E., 2007. Biology of the Nitrogen Cycle, Biology of the Nitrogen Cycle.

Briggs, D.E.G., Summons, R.E., 2014. Ancient biomolecules: Their origins, fossilization, and role in revealing the history of life. BioEssays 36, 482–490.

Brocks, J.J., Pearson, A., 2005. Brocks, J. J. & PEarson, A.-2005_Building the Biomarker Tree of Life. Rev. Mineral. Geochemistry 59, 233–258.

Brooks, A.N., Turkarslan, S., Beer, K.D., Yin Lo, F., Baliga, N.S., 2011. Adaptation of cells to new environments. Wiley Interdiscip. Rev. Syst. Biol. Med.

Buchanan, B.B., Sirevåg, R., Fuchs, G., Ivanovsky, R.N., Igarashi, Y., Ishii, M., Tabita, F.R., Berg, I.A., 2017. The Arnon–Buchanan cycle: a retrospective, 1966–2016. Photosynth. Res. 134, 117–131.

Bufarale, G., Collins, L.B., 2015. Stratigraphic architecture and evolution of a barrier seagrass bank in the mid-late Holocene, Shark Bay, Australia. Mar. Geol. 359, 1–21.

Burns, B.P., Goh, F., Allen, M., Neilan, B.A., 2004. Microbial diversity of extant stromatolites in the hypersaline marine environment of Shark Bay, Australia. Environ. Microbiol. 6, 1096–1101.

Caffarri, S., Tibiletti, T., Jennings, R., Santabarbara, S., 2014. A Comparison Between Plant Photosystem I and Photosystem II Architecture and Functioning. Curr. Protein Pept. Sci. 15, 296–331.

Cavalier-Smith, T., Brasier, M., Embley, T.M., 2006. Introduction: How and when

did microbes change the world? Philos. Trans. R. Soc. B Biol. Sci.

Cole, J.A., Brown, C.M., 1980. Nitrite reduction to ammonia by fermentative bacteria: a short circuit in the biological nitrogen cycle. FEMS Microbiol. Lett. 7, 65–72.

Cole, J.K., Hutchison, J.R., Renslow, R.S., Kim, Y.M., Chrisler, W.B., Engelmann, H.E., Dohnalkova, A.C., Hu, D., Metz, T.O., Fredrickson, J.K., Lindemann, S.R., 2014a. Phototrophic biofilm assembly in microbial-mat-derived unicyanobacterial consortia: Model systems for the study of autotroph-heterotroph interactions. Front. Microbiol. 5.

Cole, J.K., Hutchison, J.R., Renslow, R.S., Kim, Y.M., Chrisler, W.B., Engelmann, H.E., Dohnalkova, A.C., Hu, D., Metz, T.O., Fredrickson, J.K., Lindemann, S.R., 2014b. Phototrophic biofilm assembly in microbial-mat-derived unicyanobacterial consortia: Model systems for the study of autotroph-heterotroph interactions. Front. Microbiol. 5, 109.

Cooper, A.J.L., 1983. Biochemistry of Sulfur-Containing Amino Acids. Annu. Rev. Biochem. 52, 187–222.

Cooper, G.M., 2000. The Molecular Composition of Cells.

Cranwell, P.A., Volkman, J.K., 1981. Alkyl and steryl esters in a recent lacustrine sediment. Chem. Geol. 32, 29–43.

De Bruijn, F.J., 2015. Biological nitrogen fixation, in: Principles of Plant-Microbe Interactions: Microbes for Sustainable Agriculture. Springer International Publishing, pp. 215–224.

Decho, A.W., Gutierrez, T., 2017. Microbial Extracellular Polymeric Substances (EPSs) in Ocean Systems. Front. Microbiol. 8, 922.

Des Marais, D.J., 1995. The biogeochemistry of hypersaline microbial mats. Adv. Microb. Ecol.

Detmers, J., Brüchert, V., Habicht, K.S., Kuever, J., 2001. Diversity of sulfur isotope fractionations by sulfate-reducing prokaryotes. Appl. Environ. Microbiol. 67, 888–894.

Druschel, G.K., Kappler, A., 2015. Geomicrobiology and Microbial Geochemistry. Elements 11, 389–394.

Dubey, R.K., Tripathi, V., Prabha, R., Chaurasia, R., Singh, D.P., Rao, C.S., El-Keblawy, A., Abhilash, P.C., 2020. Metatranscriptomics and Metaproteomics for Microbial Communities Profiling. pp. 51–60.

Dupraz, C., Reid, R.P., Braissant, O., Decho, A.W., Norman, R.S., Visscher, P.T., 2009. Processes of carbonate precipitation in modern microbial mats. Earth-Science Rev.

Dupraz, C., Visscher, P.T., 2005. Microbial lithification in marine stromatolites and hypersaline mats. Trends Microbiol.

Dutta, H., Dutta, A., 2016. The microbial aspect of climate change. Energy, Ecol. Environ.

Dwivedi, D., Tang, J., Bouskill, N., Georgiou, K., Chacon, S.S., Riley, W.J., 2019. Abiotic and Biotic Controls on Soil Organo–Mineral Interactions: Developing Model Structures to Analyze Why Soil Organic Matter Persists. Rev. Mineral. Geochemistry 85, 329–348.

Garcia-Lopez, E., Rodriguez-Lorente, I., Alcazar, P., Cid, C., 2019. Microbial Communities in Coastal Glaciers and Tidewater Tongues of Svalbard Archipelago, Norway. Front. Mar. Sci. 5.

Goh, F., Allen, M.A., Leuko, S., Kawaguchi, T., Decho, A.W., Burns, B.P., Neilan, B.A., 2009. Determining the specific microbial populations and their spatial distribution within the stromatolite ecosystem of Shark Bay. ISME J. 3, 383–396.

Grabarczyk, D.B., Berks, B.C., 2017. Intermediates in the Sox sulfur oxidation pathway are bound to a sulfane conjugate of the carrier protein SoxYZ. PLoS One 12, e0173395.

Grein, F., Ramos, A.R., Venceslau, S.S., Pereira, I.A.C., 2013. Unifying concepts in anaerobic respiration: Insights from dissimilatory sulfur metabolism. Biochim. Biophys. Acta - Bioenerg.

Grice, K., Brocks, J.J., 2011. Biomarkers (Organic, Compound-Specific Isotopes),

in: Encyclopedia of Earth Sciences Series. Springer Netherlands, pp. 167–182.

Grice, K., Eiserbeck, C., 2013. The Analysis and Application of Biomarkers, in: Treatise on Geochemistry: Second Edition. Elsevier Inc., pp. 47–78.

Grice, K., Schouten, S., Nissenbaum, A., Charrach, J., Sinninghe Damsté, J.S., 1998. A remarkable paradox: Sulfurised freshwater algal (Botryococcus braunii) lipids in an ancient hypersaline euxinic ecosystem. Org. Geochem. 28, 195–216.

Hanson, R.S., Hanson, T.E., 1996. Methanotrophic bacteria. Microbiol. Mol. Biol. Rev. 60.

Haruta, S., Kanno, N., 2015. Survivability of microbes in natural environments and their ecological impacts. Microbes Environ. 30, 123–125.

Hebting, Y., Schaeffer, P., Behrens, A., Adam, P., Schmitt, G., Schneckenburger, P., Bernasconi, S.M., Albrecht, P., 2006. Biomarker evidence for a major preservation pathway of sedimentary organic carbon. Science (80-.). 312, 1627–1631.

Hooper, A.B., Vannelli, T., Bergmann, D.J., Arciero, D.M., 1997. Enzymology of the oxidation of ammonia to nitrite by bacteria, in: Antonie van Leeuwenhoek, International Journal of General and Molecular Microbiology. Kluwer Academic Publishers, pp. 59–67.

Hügler, M., Sievert, S.M., 2011. Beyond the Calvin Cycle: Autotrophic Carbon Fixation in the Ocean. Ann. Rev. Mar. Sci. 3, 261–289.

Ingram, L.O., Calder, J.A., Van Baalen, C., Plucker, F.E., Parker, P.L., 1973. Role of Reduced Exogenous Organic Compounds in the Physiology of the Blue-Green Bacteria (Algae): Photoheterotrophic Growth of a “Heterotrophic” Blue-Green Bacterium. J. Bacteriol. 114.

Jahnert, R., de Paula, O., Collins, L., Strobach, E., Pevzner, R., 2012. Evolution of a coquina barrier in Shark Bay, Australia by GPR imaging: Architecture of a Holocene reservoir analog. Sediment. Geol. 281, 59–74.

Jahnert, R.J., Collins, L.B., 2013. Controls on microbial activity and tidal flat evolution in Shark Bay, Western Australia. Sedimentology 60, 1071–1099.

Javaux, E.J., Lepot, K., 2018. The Paleoproterozoic fossil record: Implications for the evolution of the biosphere during Earth's middle-age. Earth-Science Rev.

Jones, S., 2008. Microbial physiology: Five ways to cycle carbon. Nat. Rev. Microbiol. 6, 94.

Jørgensen, B.B., 1982. Mineralization of organic matter in the sea bed - The role of sulphate reduction. Nature 296, 643–645.

Jungblut, A.D., Allen, M.A., Burns, B.P., Neilan, B.A., 2009. Lipid biomarker analysis of cyanobacteria-dominated microbial mats in meltwater ponds on the McMurdo Ice Shelf, Antarctica. Org. Geochem. 40, 258–269.

Kaim, W., Schwederski, B., Klein, A., 2013. Bioinorganic Chemistry--Inorganic Elements in the Chemistry of Life: An Introduction and Guide.

Kato, K., Kobayashi, T., Yamamoto, H., Nakagawa, T., Maki, Y., Hoaki, T., 2004. Microbial mat boundaries between chemolithotrophs and phototrophs in geothermal hot spring effluents. Geomicrobiol. J. 21, 91–98.

Klotz, M.G., Bryant, D.A., Hanson, T.E., 2011. The Microbial Sulfur Cycle. Front. Microbiol. 2, 241.

Komárek, J., Kaštovský, J., Mareš, J., Johansen, J.R., 2014. Taxonomic classification of cyanoprokaryotes (cyanobacterial genera) 2014, using a polyphasic approach, Preslia.

Korom, S.F., 1992. Natural denitrification in the saturated zone: A review. Water Resour. Res. 28, 1657–1668.

Koshland, D.E., 1995. The Key–Lock Theory and the Induced Fit Theory. Angew. Chemie Int. Ed. English 33, 2375–2378.

Kraft, B., Strous, M., Tegetmeyer, H.E., 2011. Microbial nitrate respiration - Genes, enzymes and environmental distribution. J. Biotechnol. 155, 104–117.

Kuenen, J.G., 2008. Anammox bacteria: From discovery to application. Nat. Rev. Microbiol. 6, 320–326.

Kumar, K., Mella-Herrera, R.A., Golden, J.W., 2010. Cyanobacterial heterocysts. Cold Spring Harb. Perspect. Biol. 2.

Ley, R.E., Harris, J.K., Wilcox, J., Spear, J.R., Miller, S.R., Bebout, B.M., Maresca, J.A., Bryant, D.A., Sogin, M.L., Pace, N.R., 2006. Unexpected diversity and complexity of the Guerrero Negro hypersaline microbial mat. Appl. Environ. Microbiol. 72, 3685–3695.

Lodish, H., Berk, A., Zipursky, S.L., Matsudaira, P., Baltimore, D., Darnell, J., 2000. The Three Roles of RNA in Protein Synthesis.

Lomans, B.P., Van der Drift, C., Pol, A., Op den Camp, H.J.M., 2002. Microbial cycling of volatile organic sulfur compounds. Cell. Mol. Life Sci.

Louyakis, A.S., Gourlé, H., Casaburi, G., Bonjawo, R.M.E., Duscher, A.A., Foster, J.S., 2018. A year in the life of a thrombolite: comparative metatranscriptomics reveals dynamic metabolic changes over diel and seasonal cycles. Environ. Microbiol. 20, 842–861.

Lund, P., Tramonti, A., De Biase, D., 2014. Coping with low pH: Molecular strategies in neutralophilic bacteria. FEMS Microbiol. Rev.

Luo, G., Yang, H., Algeo, T.J., Hallmann, C., Xie, S., 2019. Lipid biomarkers for the reconstruction of deep-time environmental conditions. Earth-Science Rev.

Madigan, M.T., Martinko, J.M., Dunlap, P. V, Clark, D.P., Benjamin Cummings, P., 2008. Brock Biology of microorganisms 12th edn. B. Rev. Int. Microbiol. 11, 65–73.

Meeks, J.C., Elhai, J., 2002. Regulation of Cellular Differentiation in Filamentous Cyanobacteria in Free-Living and Plant-Associated Symbiotic Growth States. Microbiol. Mol. Biol. Rev. 66, 94–121.

Merino, N., Aronson, H.S., Bojanova, D.P., Feyhl-Buska, J., Wong, M.L., Zhang, S., Giovannelli, D., 2019. Living at the extremes: Extremophiles and the limits of life in a planetary context. Front. Microbiol. 10.

Mojzsis, S.J., Arrhenius, G., McKeegan, K.D., Harrison, T.M., Nutman, A.P., Friend, C.R.L., 1996. Evidence for life on Earth before 3,800 million years ago. Nature 384, 55–59.

Morris, T.E., Visscher, P.T., O'Leary, M.J., Fearns, P.R.C.S., Collins, L.B., 2019. The biogeomorphology of Shark Bay's microbialite coasts. Earth-Science Rev.

102921.

Müller, V., 2001. Bacterial Fermentation, in: ELS. Wiley.

Nelson, N., 2011. Photosystems and global effects of oxygenic photosynthesis. Biochim. Biophys. Acta - Bioenerg.

Nies, D.H., 2003. Efflux-mediated heavy metal resistance in prokaryotes. FEMS Microbiol. Rev.

Noffke, N., Christian, D., Wacey, D., Hazen, R.M., 2013. Microbially induced sedimentary structures recording an ancient ecosystem in the ca. 3.48 Billion-year-old dresser formation, pilbara, Western Australia. Astrobiology 13, 1103–1124.

Pagès, A., Grice, K., Ertefai, T., Skrzypek, G., Jahnert, R., Greenwood, P., 2014. Organic geochemical studies of modern microbial mats from Shark Bay: Part I: Influence of depth and salinity on lipid biomarkers and their isotopic signatures. Geobiology 12, 469–487.

Pagès, A., Grice, K., Welsh, D.T., Teasdale, P.T., Van Kranendonk, M.J., Greenwood, P., 2015. Lipid Biomarker and Isotopic Study of Community Distribution and Biomarker Preservation in a Laminated Microbial Mat from Shark Bay, Western Australia. Microb. Ecol. 70, 459–472.

Pages, A., Welsh, D.T., Teasdale, P.R., Grice, K., Vacher, M., Bennett, W.W., Visscher, P.T., 2014. Diel fluctuations in solute distributions and biogeochemical cycling in a hypersaline microbial mat from Shark Bay, WA. Mar. Chem. 167, 102–112.

Papenfort, K., Bassler, B.L., 2016. Quorum sensing signal-response systems in Gram-negative bacteria. Nat. Rev. Microbiol.

Papineau, D., Walker, J.J., Mojzsis, S.J., Pace, N.R., 2005. Composition and structure of microbial communities from stromatolites of Hamelin Pool in Shark Bay, Western Australia. Appl. Environ. Microbiol. 71, 4822–32.

Peter, P.J., Del Giorgio, P.A., 2007. Respiration in aquatic ecosystems: History and background, in: Respiration in Aquatic Ecosystems.

Plet, C., Pagès, A., Holman, A.I., Madden, R.H.C., Grice, K., 2018. From supratidal to subtidal, an integrated characterisation of Carbla Beach shallow microbial mats (Hamelin Pool, Shark Bay, WA): Lipid biomarkers, stable carbon isotopes and microfabrics. Chem. Geol. 493, 338–352.

Prieto-Barajas, C.M., Valencia-Cantero, E., Santoyo, G., 2018. Microbial mat ecosystems: Structure types, functional diversity, and biotechnological application. Electron. J. Biotechnol. 31, 48–56.

Proemse, B.C., Eberhard, R.S., Sharples, C., Bowman, J.P., Richards, K., Comfort, M., Barmuta, L.A., 2017. Stromatolites on the rise in peat-bound karstic wetlands. Sci. Rep. 7, 15384.

Pufahl, P.K., Hiatt, E.E., 2012. Oxygenation of the Earth's atmosphere-ocean system: A review of physical and chemical sedimentologic responses. Mar. Pet. Geol.

Ragsdale, S.W., 2008. Enzymology of the Wood-Ljungdahl pathway of acetogenesis, in: Annals of the New York Academy of Sciences. Blackwell Publishing Inc., pp. 129–136.

Rohmer, M., Bouvier-Nave, P., Ourisson, G., 1984. Distribution of hopanoid triterpenes in prokaryotes. J. Gen. Microbiol. 130, 1137–1150.

Ruess, L., Chamberlain, P.M., 2010. The fat that matters: Soil food web analysis using fatty acids and their carbon stable isotope signature. Soil Biol. Biochem.

Ruvindy, R., White, R.A., Neilan, B.A., Burns, B.P., 2016. Unravelling core microbial metabolisms in the hypersaline microbial mats of Shark Bay using high-throughput metagenomics. ISME J. 10, 183–196.

Schirrmeister, B.E., De Vos, J.M., Antonelli, A., Bagheri, H.C., 2013. Evolution of multicellularity coincided with increased diversification of cyanobacteria and the Great Oxidation Event. Proc. Natl. Acad. Sci. U. S. A. 110, 1791–1796.

Serganov, A., Patel, D.J., 2009. Amino acid recognition and gene regulation by riboswitches. Biochim. Biophys. Acta - Gene Regul. Mech.

Shakya, M., Lo, C.C., Chain, P.S.G., 2019. Advances and challenges in metatranscriptomic analysis. Front. Genet.

Shevela, D., Pishchalnikov, R., Eichacker, L., 2013. Oxygenic photosynthesis in cyanobacteria.

Sogin, M.L., Morrison, H.G., Huber, J.A., Welch, D.M., Huse, S.M., Neal, P.R., Arrieta, J.M., Herndl, G.J., 2006. Microbial diversity in the deep sea and the underexplored "rare biosphere." Proc. Natl. Acad. Sci. U. S. A. 103, 12115–12120.

Sohlenkamp, C., Geiger, O., 2015. Bacterial membrane lipids: Diversity in structures and pathways. FEMS Microbiol. Rev.

Soontharapirakkul, K., Promden, W., Yamada, N., Kageyama, H., Incharoensakdi, A., Iwamoto-Kihara, A., Takabe, T., 2011. Halotolerant cyanobacterium Aphanothece halophytica contains an Na +-dependent F1F0-ATP synthase with a potential role in salt-stress tolerance. J. Biol. Chem. 286, 10169–10176.

Spector, A.A., Yorek, M.A., 1985. Membrane lipid composition and cellular function, Journal of Lipid Research.

Stephens, E.A., Braissant, O., Visscher, P.T., 2008. Spirochetes and salt marsh microbial mat geochemistry: Implications for the fossil record. Carnets géologie (Notebooks Geol.

Stocker, R., Seymour, J.R., 2012. Ecology and Physics of Bacterial Chemotaxis in the Ocean. Microbiol. Mol. Biol. Rev. 76, 792–812.

Stuart, R.K., Mayali, X., Lee, J.Z., Craig Everroad, R., Hwang, M., Bebout, B.M., Weber, P.K., Pett-Ridge, J., Thelen, M.P., 2016. Cyanobacterial reuse of extracellular organic carbon in microbial mats. ISME J. 10, 1240–1251.

Summons, R.E., 1987. Branched alkanes from ancient and modern sediments: Isomer discrimination by GC/MS with multiple reaction monitoring. Org. Geochem. 11, 281–289.

Thamdrup, B., 2012. New Pathways and Processes in the Global Nitrogen Cycle. Annu. Rev. Ecol. Evol. Syst. 43, 407–428.

Thompson, M. V., Randerson, J.T., Malmström, C.M., Field, C.B., 1996. Change in net primary production and heterotrophic respiration: How much is necessary to sustain the terrestrial carbon sink? Global Biogeochem. Cycles 10, 711–726.

Thullner, M., Regnier, P., 2019. Microbial Controls on the Biogeochemical Dynamics in the Subsurface. Rev. Mineral. Geochemistry 85, 265–302.

Tiedje, J.M., 1981. ASSIMILATORY AND DISSIMILATORY NITRATE REDUCTION: PERSPECTIVES AND METHODOLOGY FOR SIMULTANEOUS MEASUREMENT OF SEVERAL NITROGEN CYCLE PROCESSES. Ecol. Bull. 33, 324–331.

Tiedje, J.M., 1988. Ecology of denitrification and dissimilatory nitrate reduction to ammonium. Environ. Microbiol. Anaerobes 179–244.

van Gemerden, H., 1993. Microbial mats: A joint venture. Mar. Geol. 113, 3–25.

Van Kranendonk, M.J., Philippot, P., Lepot, K., Bodorkos, S., Pirajno, F., 2008. Geological setting of Earth's oldest fossils in the ca. 3.5 Ga Dresser Formation, Pilbara Craton, Western Australia. Precambrian Res. 167, 93–124.

Visscher, P.T., Stolz, J.F., 2005. Microbial mats as bioreactors: Populations, processes, and products, in: Geobiology: Objectives, Concepts, Perspectives. Elsevier B.V., pp. 87–100.

Visscher, P.T., van den Ende, F.P., Schaub, B.E.M., van Gemerden, H., 1992. Competition between anoxygenic phototrophic bacteria and colorless sulfur bacteria in a microbial mat. FEMS Microbiol. Lett. 101, 51–58.

Voshall, A., Moriyama, E.N., 2018. Next-Generation Transcriptome Assembly: Strategies and Performance Analaysis, in: Bioinformatics in the Era of Post Genomics and Big Data. InTech.

Wang, D., Zheng, Q., Huang, K., Springael, D., Zhang, X.X., 2020. Metagenomic and metatranscriptomic insights into the complex nitrogen metabolic pathways in a single-stage bioreactor coupling partial denitrification with anammox. Chem. Eng. J. 398, 125653.

Ward, D.M., Ferris, M.J., Nold, S.C., Bateson, M.M., 1998. A Natural View of Microbial Biodiversity within Hot Spring Cyanobacterial Mat Communities. Microbiol. Mol. Biol. Rev. 62, 1353.

Wasmund, K., Mußmann, M., Loy, A., 2017. The life sulfuric: microbial ecology of sulfur cycling in marine sediments. Environ. Microbiol. Rep. 9, 323–344.

Welsh, D.T., 2000. Ecological significance of compatible solute accumulation by micro-organisms: from single cells to global climate. FEMS Microbiol. Rev. 24, 263–290.

Werne, J.P., Hollander, D.J., Lyons, T.W., Sinninghe Damsté, J.S., 2004. Organic sulfur biogeochemistry: Recent advances and future research directions, in: Special Paper of the Geological Society of America. Geological Society of America, pp. 135–150.

White, R.A., Chan, A.M., Gavelis, G.S., Leander, B.S., Brady, A.L., Slater, G.F., Lim, D.S.S., Suttle, C.A., 2016. Metagenomic analysis suggests modern freshwater microbialites harbor a distinct core microbial community. Front. Microbiol. 6, 1531.

White, R.A., Power, I.M., Dipple, G.M., Southam, G., Suttle, C.A., 2015. Metagenomic analysis reveals that modern microbialites and polar microbial mats have similar taxonomic and functional potential. Front. Microbiol. 6, 966.

Whiteman, J., Elliott Smith, E., Besser, A., Newsome, S., 2019. A Guide to Using Compound-Specific Stable Isotope Analysis to Study the Fates of Molecules in Organisms and Ecosystems. Diversity 11, 8.

Whiteside, J.H., Grice, K., 2016. Biomarker Records Associated with Mass Extinction Events. Annu. Rev. Earth Planet. Sci. 44, 581–612.

Whitman, W.B., Bowen, T.L., Boone, D.R., 2014. The methanogenic bacteria, in: The Prokaryotes: Other Major Lineages of Bacteria and The Archaea. pp. 123–163.

Willers, C., Jansen van Rensburg, P.J., Claassens, S., 2015. Phospholipid fatty acid profiling of microbial communities-a review of interpretations and recent applications. J. Appl. Microbiol.

Wimpenny, J., Manz, W., Szewzyk, U., 2000. Heterogeneity in biofilms: Table 1. FEMS Microbiol. Rev. 24, 661–671.

Wong, H., Ahmed-Cox, A., Burns, B., 2016. Molecular Ecology of Hypersaline Microbial Mats: Current Insights and New Directions. Microorganisms 4, 6.

Wong, H.L., Smith, D.L., Visscher, P.T., Burns, B.P., 2015. Niche differentiation of

bacterial communities at a millimeter scale in Shark Bay microbial mats. Sci. Rep. 5, 15607.

Wong, H.L., White, R.A., Visscher, P.T., Charlesworth, J.C., Vázquez-Campos, X., Burns, B.P., 2018. Disentangling the drivers of functional complexity at the metagenomic level in Shark Bay microbial mat microbiomes. ISME J. 12, 2619–2639.

Wood, J.M., 1999. Osmosensing by Bacteria: Signals and Membrane-Based Sensors. Microbiol. Mol. Biol. Rev. 63, 230–262.

Wörmer, L., CirÉs, S., VelÁzquez, D., Quesada, A., Hinrichs, K.-U., 2012. Cyanobacterial heterocyst glycolipids in cultures and environmental samples: Diversity and biomarker potential. Limnol. Oceanogr. 57, 1775–1788.

Yannarell, A.C., Paerl, H.W., 2007. Effects of salinity and light on organic carbon and nitrogen uptake in a hypersaline microbial mat. FEMS Microbiol. Ecol. 62, 345–353.

Zaikova, E., Goerlitz, D.S., Tighe, S.W., Wagner, N.Y., Bai, Y., Hall, B.L., Bevilacqua, J.G., Weng, M.M., Samuels-Fair, M.D., Johnson, S.S., 2019. Antarctic relic microbial mat community revealed by metagenomics and metatranscriptomics. Front. Ecol. Evol. 7, 1.

Zehr, J.P., Kudela, R.M., 2011. Nitrogen Cycle of the Open Ocean: From Genes to Ecosystems. Ann. Rev. Mar. Sci. 3, 197–225.

Chapter 2

Materials and Methods

2.1 Field sampling

Microbial mats from Shark Bay were sampled in the field using aluminium push cores (20 cm x 10 cm), whereas Giblin River mats were sampled with a sterilized spatula and then wrapped in aluminium foil. Both the aluminium foil and push cores were annealed at 550°C prior to field sampling. All mats were sampled during daylight hours with additional sampling of smooth and pustular mats during the night from Nilemah tidal flat. The top 20 mm of the 'active' mats were immediately subsampled in triplicate for genomic analysis using UV sterilized open-ended single-use 5 mL syringes. The subsampled microbial mat material was then placed into a sterile tube containing RNAlater (Thermo Fischer Scientific, MA, U.S.A). Cores and samples were wrapped in aluminium foil were frozen at -20°C for transport together with the genomic samples. All samples were kept frozen until the lipid biomarker extraction was performed, whereas the subsampled genomic samples were stored at -80°C until nucleic acid extraction. Physiochemical parameters of the surrounding water at each site (e.g. pH, salinity, temperature) was recorded using a multi-probe system (HI 9829 Multiparameter, Hanna® Instruments), refractometer and pH meter. A summary of the mat types collected with sampling dates and times, as well as field measurements are given in Supplementary Table 2.1.

2.2 Metatranscriptomics

2.2.1 RNA isolation, library preparation and sequencing

Laboratory fume cupboard, spatulas and other molecular related equipment was sterilized with RNase AWAY^{TM} and flame or UV sterilized where necessary. The RNeasy PowerSoil Total RNA Kit (Qiagen, Hilden, Germany) was used to extract total RNA (in triplicate) from 50-100 mg of sample per reaction. An additional DNAse treatment with the Turbo DNA-free Kit (Qiagen), was used to remove residual DNA and the DNA-free RNA extracts were purified using the MEGAclear kit (Thermo Fischer Scientific, MA, U.S.A). RNA concentrations were measured with a NanoDrop

3300 (Thermo Fisher Scientific), using the Quant-iT^{TM} RiboGreen^{TM} RNA Assay Kit (Thermo Fisher Scientific), and a SYBR green based quantitative PCR targeted bacterial 16S rDNA (V4 region) was used to test if the DNase-treated RNA samples were completely free of DNA. Equimolar amounts of the triplicate DNA-free RNA samples were pooled for the synthesis of cDNA using the Ovation RNAseq System V2 kit and subsequent library preparation using the Ovation Ultralow Library System V2 kit (NuGEN technologies, CA, U.S.A) following manufacturers protocol. cDNA libraries were analysed for quality and quantity with a 2100 bioanalyzer (Agilent, CA, U.S.A). Barcoded libraries were diluted in 10 mM Tris-HCl at pH 8.5 (25 uL) and sent to the Australian Genomic Research Facility (AGRF). At AGRF, the Illumina HiSeq 2500 platform was used to generate 2 × 125-bp pair-end sequencing reads. The HiSeq Control Software (HCS) v2.2.68 and Real Time Analysis (RTA) v1.18.66.3 software performed real-time image analysis and base calling on the HiSeq instrument computer. The AGRF Illumina bcl2fastq 2.20.0.422 pipeline was used to generate the sequence data.

2.2.2 Bioinformatics

Taxonomic analysis of the microbiota was based on assembled 16S rRNA transcripts, followed by functional and taxonomic annotation of transcripts derived from the mRNA fraction. As outlined in Figure 2.1, raw paired-end Illumina sequenced reads were trimmed with BBDuk. BBDuk was ran twice; (1) to trim adapters with parameters ktrim=r, k=21, mink=11, hdist=2, tpe, tbo and (2) for quality trimming with parameters qtrim=r, trimq=25, maq=25, minlen=50, k=31, qhdist=1 (Bushnell, 2014). Bowtie2 was used to map rRNA and phiX sequences then Samtools was used to separate and convert sequences into mapped and unmapped fastq files (Li et al., 2009; Langmead and Salzberg, 2012). Fastq-pair was used to match the pair-end mapped and unmapped reads, to ensure that all reads were paired and to separate out singletons (Edwards and Edwards, 2019).

For taxonomic analysis of the mapped reads (rRNA sequences), the pair-end mapped reads were analysed using the Phyloflash pipeline (v.3.3). Reconstructed 16S and 18S rRNA gene sequences were aligned to sequences from the SILVA SSU132

NR99 database with BBmap, with minimum identity of 85% and read limit of <5000000 (Gruber-Vodicka et al., 2019).

For functional and taxonomic analysis of unmapped reads (mRNA sequences), the unmapped pair-end reads were checked again for presence of rRNA and phiX sequences using Bowtie2, then assembled into transcripts using rnaSPAdes (v.3.13.0) with the default k-mer size of k = 55 (Bushmanova et al., 2019). Protein sequences predicted with Prodigal (v.2.6.1) were then annotated using eggnog-mapper (v.1.0.3) in 'diamond' run mode with the eggNOG database (v.4.5.1) for functional analysis (Hyatt et al., 2010; Huerta-Cepas et al., 2017). Kegg orthologs (KOs), enzymes, pathways and modules were inferred from the eggnog-mapper output using the Kegg brite hierarchy information (Kanehisa et al., 2008). Additional functional assignments were made using the DIAMOND blastp aligner (Buchfink et al., 2014) with the default settings in more sensitive against the SEED subsystems (Overbeek et al., 2014) and CAZy databases (Lombard et al., 2014). Taxonomic assignments were achieved by mapping the predicted proteins using DIAMOND blastp aligner with the default settings in more sensitive mode; reads were mapped against NCBI's most recent RefSeq non-redundant protein release (O'Leary et al., 2016).

To decipher Phylum/Class/Order level functionality, transcripts were submitted to the MG-RAST server 4.0.3 for automated annotation of the NCBI RefSeq database against either the SEED subsystems or KEGG databases. Only hits to reference proteins with at least 70% amino acid similarity over an alignment length of more than 50 amino acids were considered to be homologs and used for downstream analysis (More et al., 2019).

Illumina HiSeq 2500 pair-end sequencing read output with percentage summaries of trimmed and aligned sequences, number of assembled transcripts and number of annotations for Phyloflash, DIAMOND and eggnog-mapper can be found in Supplementary Table 2.1.

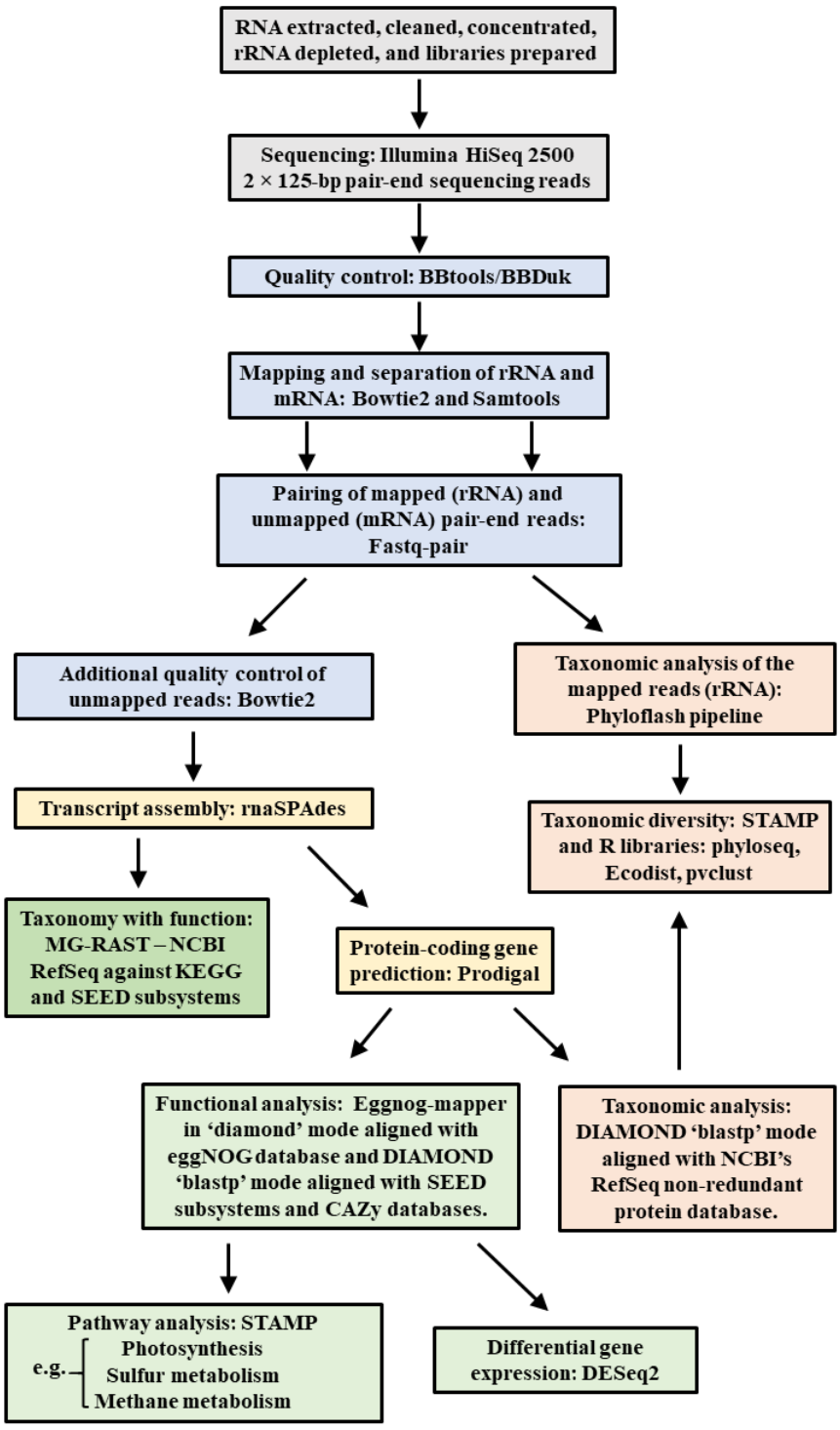

Figure 2.1 Flowchart outlining the bioinformatics tools used in the analysis of the metatranscriptomic and rRNA data.

2.3 Lipid biomarker and organic geochemical analysis

2.3.1 Preparation of materials

All glassware, Pasteur pipettes, mortar and pestles and aluminium foil were combusted at 550°C prior to laboratory work up to remove any traces of contaminants (e.g. aliphatic hydrocarbons, fatty acids, etc.). All spatulas, measuring cylinders, cotton wool and syringes were washed nine times (3x in methanol (MeOH), 3x in dichloromethane (DCM), 3x in *n*-hexane). MilliQ water and hydrochloric acid was washed 6 times with DCM in a separating funnel to ensure removal of contaminants. All solvents the were analytical grade. All experiments were carried out in a fume hood while wearing nitrile gloves, lab coat and safety goggles. Additional safety measures were implemented as required for individual reagents and procedures.

2.3.2 Lipid extraction and fractionation of neutral lipids

Total lipid extraction (TLE) from the top ~10 mm of the core or biomass containing the 'living' mat section was performed using a modification of the Bligh-Dyer procedure (Bligh and Dyer, 1959; Hallmann et al., 2008; Allen et al., 2010). Freeze-dried microbial mats were ground in a solvent-cleaned mortar and pestle and ~5 g aliquots were weighed into glass centrifuge tubes. The mat material was extracted 4 times; extractions 1 and 2 were performed with phosphate buffer (dipotassium phosphate ($K_2HPO_4^-$) 50 mmol L^{-1}, pH 7.4), methanol (MeOH) and dichloromethane (DCM; 20 mL 1:2:1, v:v:v); and extractions 3 and 4 with trichloroacetic acid buffer (50 g L^{-1}, pH 2), MeOH and DCM (20 mL 1:2:1, v:v:v). Centrifuge tubes were sealed with a layer of aluminium foil, sonicated for 20 minutes in an ice bath and then centrifuged at 450 x g for 5 minutes. Solvent phases from each extraction were transferred into 100 mL glass centrifuge tubes. Solvent phases were then separated by adding DCM and MilliQ water (20 mL 1:1, v:v) and centrifuged at 200 x g for 5 minutes to break the emulsion. The organic (bottom) layer was transferred to a clean collection tube containing freshly activated copper turnings and stirred at room temperature for 72 hours to remove elemental sulfur. Sulfur-free TLE was filtered over anhydrous magnesium sulfate ($MgSO_4$) and dried gently under a nitrogen purge. Activated silica gel column chromatography (5.5 cm × 0.5 cm i.d.) was performed to separate TLEs (≥ 10 mg) into neutral and polar lipid fractions. The neutral lipid

fractions were eluted with DCM (7 mL) and the polar fractions with MeOH (14 mL) as described by Heinzelmann et al. (2014). The neutral lipid fraction was separated into an aliphatic hydrocarbon fraction with n-hexane (2 mL); wax ester fraction with a 1:3 v/v mixture of DCM/*n*-hexane (2 mL), free fatty acid/sterol fraction with DCM/MeOH (2 mL 1:1 v/v) and residual intact-polar lipids were eluted back into the polar lipid fraction with MeOH (4 mL). The aliphatic hydrocarbon fractions were analysed by gas chromatography-mass spectroscopy (GC-MS) and isotope ratio mass spectroscopy (GC-IRMS). Remaining neutral lipid fractions were stored at -20 °C for future analysis and a portion of the polar fraction was used for either Raney nickel desulfurization or analysis for HGs.

2.3.4 Raney nickel desulfurisation, hydrogenation and fractionation

Raney nickel desulfurisation was performed using a modified procedure described in Grice et al., 1998. An aliquot of the polar fraction (~5 mg) was dissolved in a small amount of toluene (4 mL) then transferred to a round bottom flask. A mixture of EtOH:toluene (2 mL 1:1 v/v) followed by a suspension of Raney nickel (0.25 g in 0.5 mL of EtOH) was added to the reaction mixture. Internal standard (D2-C22 thiophene, 10 µg/mL) was added and then heated at reflux under a nitrogen stream for 3 hours. The desulfurisation product was obtained by subsequent extraction with DCM (5 mL, 3 times). The organic phase was passed through a 'large' column (20 cm x 0.9 cm i.d.) of anhydrous $MgSO_4$ to ensure H_2O removal. The desulfurised extract was separated on an activated silica gel column (5.5 cm × 0.5 cm i.d.) into apolar and polar sub-fractions with a 1:3 v/v mixture of DCM/*n*-hexane (4 mL) and DCM/MeOH (4 mL 1:1 v/v), respectively. The apolar fraction was then hydrogenated in a hydrogen atmosphere in the presence of PtO_2 and acetic acid (4 mL) and stirred with a magnetic stirrer at room temperature for 24 hours. Acetic acid was neutralised with a saturated solution of sodium bicarbonate ($NaHCO_3$), extracted with DCM, filtered through anhydrous $MgSO_4$ and then prepared for GC-MS and two-dimensional GC with time of flight mass spectrometry (GCxGC-TOFMS).

2.3.5 Gas chromatography-mass spectrometry (GC-MS)

GC-MS analysis was carried out using a Hewlett Packard 6890 gas chromatograph equipped with a 6890 autosampler, interfaced to a Hewlett Packard 5973 mass selective detector (MSD) and split/splitless injector, operating in pulsed splitless mode at 320°C. The gas chromatograph was fitted with a 60 m DB1-MS column (0.25 mm internal diameter, 0.25 µm film thickness). Helium was used as a carrier gas at a constant flow rate of 1.1 mL/minute. The extract (1 µL) was injected, the oven temperature was raised from 50 °C to 320 °C at a rate of 6 °C/min and held at 320 °C for 24 minutes. The transfer line was maintained at 290 °C with the MSD operating with a solvent delay of 4.9 minutes in full scan mode for a mass range of 50 to 700 Daltons and held isothermally at 320 °C. Ion identification in the mass spectra, relative retention time and peak integration was achieved using both Chemstation software (Agilent Technologies 2005 Version D.02.00.275) and PARAFAC2 based Deconvolution and Identification System (PARADISe) (Johnsen et al., 2017). Mass spectra were compared with National Institute of Standards & Technology (NIST, Gaithersburg, MD, USA) libraries.

2.3.6 Two-dimensional GC with time of flight mass spectrometry (GC×GC-TOFMS)

GCxGC-TOFMS analyses were performed using a Leco Pegasus IV system equipped with dual stage cryogenic modulator (Leco, Saint Joseph, MI, USA). The primary column was a 60 m × 0.25 mm × 0.25 µm Rxi 5Sil MS (Restek, Bellefonte, PA, USA) coupled to a secondary column 1.4 m × 0.25 mm × 0.25 µm DB-17 ms (Agilent). The carrier gas was ultrahigh purity helium with constant flow of 2 mL min^{-1}. The inlet temperature was 310 °C with 2 µL injection. Fractions were analysed with temperature program: 50 °C (1 min isothermal), then 3.6 °C min^{-1} to 320 °C (isothermal 20 min), and a modulation period of 4 s, with 2 °C oven and modulator offset 15 °C. The mass spectrometer was operated in positive ion electron ionisation mode at 70 eV with ion source at 250 °C and transfer line 320 °C. The scan speed was 100 Hz with a range of 45–580 Da. ChromaTOF (LECO) software package was used for instrument control and data analysis. Mass spectra were compared with National Institute of Standards & Technology (NIST, Gaithersburg, MD, USA) libraries plus in-house TOFMS libraries.

2.3.7 Compound Specific Isotope Analysis (CSIA)

Compound-specific $\delta^{13}C$ measurements were carried out using a Thermo Trace GC Ultra fitted with a Thermo GC IsoLink, connected to a Thermo Delta V Advantage mass spectrometer via a Conflo IV interface. Samples were injected into a split/splitless injector operating in splitless mode, held at 300 °C. The GC column was an Agilent DB1-MS ultra-inert column (60 m long, 0.25 mm internal diameter, 0.25 µm film thickness). The GC oven was held at 50 °C for 1 minute after injection, heated at 6 °C / min to a final temperature of 320 °C, and held for 24 minutes. Helium was used as the carrier gas at a constant flow of 1.1 mL/min. The flow from the GC column passed through the combustion reactor of the GC IsoLink, consisting of a ceramic tube filled with CuO and NiO heated to 1000 °C, which completely combusts hydrocarbons to CO_2 and H_2O. The flow from the reactor passed through a Nafion membrane to remove water, then through the Conflo interface into the mass spectrometer. The mass spectrometer monitored the ions m/z 44, 45 and 46. The mass ratios 45/44 and 46/44 were calculated for each peak using Isodat 3.0 software. These ratios were converted into $\delta^{13}C$ by comparison with CO_2 reference gas, using the Santrock Studley Hayes (SSH) correction equation (Santrock et al., 1985). The δ13C values were calibrated to the Vienna Pee Dee Belemnite (VPDB) scale by comparison with n-alkane standards of known isotopic composition (Werner and Brand, 2001).

2.3.8 High performance liquid chromatography coupled to electrospray ionization tandem mass spectrometry (HPLC–ESI/MS^2)

Polar fractions containing HGs were analysed using HPLC–ESI/MS^2. Separation of the target analytes was achieved on a Waters Alliance 2690 HPLC system fitted with a Phenomenex Luna NH_2 column (2 x 150 mm; 3 µm particle size) and a guard column of the same material. Separation was accomplished at 30 °C and using the following gradient profile: 95% A/5% B to 85% A/15% B in 10 min (held 7 min) at a constant flow of 0.5 mL min^{-1}, followed by back-flushing with 30% A/70% B for 20 min at 0.2 mL min^{-1} and re-equilibrating the column with 95% A/5% B for 15 min. Solvent mixture A was *n*-hexane/2-propanol/HCO_2H/14.8M NH_3 aq. (79:20:0.12:0.04, v:v:v:v) and solvent mixture B was 2-propanol/water/HCO_2H/14.8M NH_3 aq. (88:10:0.12:0.04, v:v:v:v). Detection of HGs was achieved using a Micromass Quattro

LC triple quadrupole mass spectrometer equipped with electrospray ionization (ESI) interface operated in positive ion mode. MS conditions were identical to those provided by Bauersachs et al. (2015). HGs were monitored following the transitions specified in Schaefer et al. (2020) and quantified by integrating peak areas using the QuanLynx application software.

2.4 Statistical analysis and visualisation

Statistical analysis was completed using R (R Core Team, 2017) and Statistical Analysis of Metagenomic Profiles (STAMP) (Parks et al., 2014), any other software used are mentioned herein. Alpha diversity indices (Chao1 richness and Shannon diversity) of the SSU SILVA (rRNA) and RefSeq classifications (mRNA) were evaluated with the R library phyloseq. A STAMP two-way analysis of variance (ANOVA) followed by Tukey's t-test (P-value > 0.05) of the taxonomic distributions (phyla level, as well as class level for Proteobacteria). Analysis of similarity (ANOSIM) using the vegan package with 999 permutations was conducted to determine whether the dissimilarity of lipid and taxonomic classifications between locations was significant (Dixon, 2003). Dotplots of the normalised transcript, SSU rRNA and lipid classifications were completed using Reshape2 with the melt function then plotted using ggplot2 showing the relative abundance as a percentage (Wickham and Chang, 2009). Principle component analysis (PCA) of the normalised lipid and taxonomic classifications used Ecodist (dissimilarity-based functions for ecological analysis), and pvclust (hierarchical clustering with P-values *via* Multiscale Bootstrap Resampling) using ward clustering and Bray-Curtis distance metrics at a thousand replicates (Suzuki and Shimodaira, 2006; Goslee and Urban, 2007). *k*-means cluster analysis using the ggplot2 and ggfortify packages (Tang et al., 2016), and multilevel pattern analysis using the indicspecies package (De Cáceres and Jansen, 2016) were applied to further assess groupings of sampling caused by particular HGs or cyanobacterial genera. To investigate correlations between cyanobacterial and HG distributions, a regularized canonical correlation analysis (rCCA) was performed using the package mixOmics (Rohart et al., 2017). To evaluate the transcription of genes in nostocalean cyanobacteria, differential analysis of transcribed genes was calculated from the variance stabilising transformation of SEED subsystems count data using the DESeq2 package and visualised using pheatmap (Love et al., 2014). Transcribed gene

counts lower than 10 were excluded from analysis. Relative abundance of compound groups and isotopic distributions were visualised with scatter or bar plots in OriginPro (Seifert, 2014)

2.5 References

Allen, M.A., Neilan, B.A., Burns, B.P., Jahnke, L.L., Summons, R.E., 2010. Lipid biomarkers in Hamelin Pool microbial mats and stromatolites. Org. Geochem. 41, 1207–1218.

Bauersachs, T., Rochelmeier, J., Schwark, L., 2015. Seasonal lake surface water temperature trends reflected by heterocyst glycolipid Seasonal lake surface water temperature trends reflected by heterocyst glycolipid based molecular thermometers Seasonal lake surface water temperature trends reflected by heterocyst glycolipid. Biogeosciences Discuss 12, 751–778.

Bligh, E.G., Dyer, W.J., 1959. A rapid method of total lipid extraction and purification. Can. J. Biochem. Physiol. 37, 911–917.

Buchfink, B., Xie, C., Huson, D.H., 2014. Fast and sensitive protein alignment using DIAMOND. Nat. Methods.

Bushmanova, E., Antipov, D., Lapidus, A., Prjibelski, A.D., 2019. RnaSPAdes: A de novo transcriptome assembler and its application to RNA-Seq data. Gigascience 8.

Bushnell, B., 2014. BBMap: a fast, accurate, splice-aware aligner.

De Cáceres, M., Jansen, F., 2016. 'indicspecies' R Package - Functions to assess the strength and significance of relationship of species site group associations.

Dixon, P., 2003. VEGAN, a package of R functions for community ecology. J. Veg. Sci.

Edwards, R., Edwards, J.A., 2019. fastq-pair: efficient synchronization of paired-end fastq files. bioRxiv 552885.

Goslee, S.C., Urban, D.L., 2007. The ecodist package for dissimilarity-based analysis of ecological data. J. Stat. Softw. 22, 1–19.

Grice, K., Schouten, S., Nissenbaum, A., Charrach, J., Sinninghe Damsté, J.S., 1998. A remarkable paradox: Sulfurised freshwater algal (Botryococcus braunii) lipids in an ancient hypersaline euxinic ecosystem. Org. Geochem. 28, 195–216.

Gruber-Vodicka, H.R., Seah, B.K., Pruesse, E., 2019. phyloFlash — Rapid SSU

rRNA profiling and targeted assembly from metagenomes. bioRxiv 521922.

Hallmann, C., Schwark, L., Grice, K., 2008. Community dynamics of anaerobic bacteria in deep petroleum reservoirs. Nat. Geosci. 1, 588–591.

Heinzelmann, S.M., Bale, N.J., Hopmans, E.C., Sinninghe Damsté, J.S., Schouten, S., van der Meer, M.T.J., 2014. Critical assessment of glyco- and phospholipid separation by using silica chromatography. Appl. Environ. Microbiol. 80, 360–5.

Huerta-Cepas, J., Forslund, K., Coelho, L.P., Szklarczyk, D., Jensen, L.J., Von Mering, C., Bork, P., 2017. Fast genome-wide functional annotation through orthology assignment by eggNOG-mapper. Mol. Biol. Evol. 34, 2115–2122.

Hyatt, D., Chen, G.L., LoCascio, P.F., Land, M.L., Larimer, F.W., Hauser, L.J., 2010. Prodigal: Prokaryotic gene recognition and translation initiation site identification. BMC Bioinformatics 11, 119.

Johnsen, L.G., Skou, P.B., Khakimov, B., Bro, R., 2017. Gas chromatography – mass spectrometry data processing made easy. J. Chromatogr. A 1503, 57–64.

Kanehisa, M., Araki, M., Goto, S., Hattori, M., Hirakawa, M., Itoh, M., Katayama, T., Kawashima, S., Okuda, S., Tokimatsu, T., Yamanishi, Y., 2008. KEGG for linking genomes to life and the environment. Nucleic Acids Res. 36, D480–D484.

Langmead, B., Salzberg, S.L., 2012. Fast gapped-read alignment with Bowtie 2. Nat. Methods 9, 357–359.

Li, H., Handsaker, B., Wysoker, A., Fennell, T., Ruan, J., Homer, N., Marth, G., Abecasis, G., Durbin, R., 2009. The Sequence Alignment/Map format and SAMtools. Bioinformatics 25, 2078–2079.

Lombard, V., Golaconda Ramulu, H., Drula, E., Coutinho, P.M., Henrissat, B., 2014. The carbohydrate-active enzymes database (CAZy) in 2013. Nucleic Acids Res. 42, D490–D495.

Love, M.I., Huber, W., Anders, S., 2014. Moderated estimation of fold change and dispersion for RNA-seq data with DESeq2. Genome Biol. 15, 550.

More, K.D., Giosan, L., Grice, K., Coolen, M.J.L., 2019. Holocene paleodepositional changes reflected in the sedimentary microbiome of the Black Sea. Geobiology 17, 436–448.

O'Leary, N.A., Wright, M.W., Brister, J.R., Ciufo, S., Haddad, D., McVeigh, R., Rajput, B., Robbertse, B., Smith-White, B., Ako-Adjei, D., Astashyn, A., Badretdin, A., Bao, Y., Blinkova, O., Brover, V., Chetvernin, V., Choi, J., Cox, E., Ermolaeva, O., Farrell, C.M., Goldfarb, T., Gupta, T., Haft, D., Hatcher, E., Hlavina, W., Joardar, V.S., Kodali, V.K., Li, W., Maglott, D., Masterson, P., McGarvey, K.M., Murphy, M.R., O'Neill, K., Pujar, S., Rangwala, S.H., Rausch, D., Riddick, L.D., Schoch, C., Shkeda, A., Storz, S.S., Sun, H., Thibaud-Nissen, F., Tolstoy, I., Tully, R.E., Vatsan, A.R., Wallin, C., Webb, D., Wu, W., Landrum, M.J., Kimchi, A., Tatusova, T., DiCuccio, M., Kitts, P., Murphy, T.D., Pruitt, K.D., 2016. Reference sequence (RefSeq) database at NCBI: current status, taxonomic expansion, and functional annotation. Nucleic Acids Res. 44, D733–D745.

Overbeek, R., Olson, R., Pusch, G.D., Olsen, G.J., Davis, J.J., Disz, T., Edwards, R.A., Gerdes, S., Parrello, B., Shukla, M., Vonstein, V., Wattam, A.R., Xia, F., Stevens, R., 2014. The SEED and the Rapid Annotation of microbial genomes using Subsystems Technology (RAST). Nucleic Acids Res. 42.

Parks, D.H., Tyson, G.W., Hugenholtz, P., Beiko, R.G., 2014. STAMP: Statistical analysis of taxonomic and functional profiles. Bioinformatics 30, 3123–3124.

R Core Team, 2017. R: A Language and Environment for Statistical Computing.

Rohart, F., Gautier, B., Singh, A., Lê Cao, K.-A., 2017. mixOmics: An R package for 'omics feature selection and multiple data integration. PLOS Comput. Biol. 13, e1005752.

Santrock, J., Studley, S.A., Hayes, J.M., 1985. Isotopic analyses based on the mass spectra of carbon dioxide. Anal. Chem. 57, 1444–1448.

Schaefer, B., Grice, K., Coolen, M.J.L., Summons, R.E., Cui, X., Bauersachs, T., Schwark, L., Böttcher, M.E., Bralower, T.J., Lyons, S.L., Freeman, K.H., Cockell, C.S., Gulick, S.P.S., Morgan, J. V., Whalen, M.T., Lowery, C.M., Vajda, V., 2020. Microbial life in the nascent Chicxulub crater. Geology 48,

328–332.

Seifert, E., 2014. OriginPro 9.1: Scientific Data Analysis and Graphing Software—Software Review. J. Chem. Inf. Model. 54, 1552–1552.

Suzuki, R., Shimodaira, H., 2006. Pvclust: An R package for assessing the uncertainty in hierarchical clustering. Bioinformatics 22, 1540–1542.

Tang, Y., Horikoshi, M., Li, W., 2016. Ggfortify: Unified interface to visualize statistical results of popular r packages. R J. 8, 478–489.

Werner, R.A., Brand, W.A., 2001. Referencing strategies and techniques in stable isotope ratio analysis. Rapid Commun. Mass Spectrom. 15, 501–519.

Wickham, H., Chang, W., 2009. ggplot2: An implementation of the Grammar of Graphics. R package version 0.8. 3.

2.6 Supplementary material

Supplementary table 2.1 Illumina HiSeq 2500 pair-end sequencing read output with percentage summaries of trimmed and aligned sequences, number of assembled transcripts and number of annotations for Phyloflash, DIAMOND and eggnog-mapper. *Indicating paired Day/Night samples in the 2016 sampling trip.

		Percentage of trimmed and aligned sequences					# annotations				
									DIAMOND		
Sample Name	**Paired Reads**	**Quality trimming**	**Remaing reads**	**aligned 0 times**	**aligned >1 times**	**# transcripts assembled**	**PhyloFlash (SSU rRNA SILVA)**	**eggNOG (KOs)**	**NCBI RefSeq**	**SEED subsystems**	**CAZy**
Nilemah Pustular Mat Day 1 2016	10737329	8.87	91.13	7.1	92.9	26890	1474649	10275	81411	50630	1522
Nilemah Smooth Mat Day 1 2016*	9621836	8.49	91.51	8.41	91.59	25348	1707460	10096	75294	46164	1444
Nilemah Smooth Mat Day 2 2016	9771353	9.38	90.62	15.57	84.43	63494	905558	18172	167058	99913	3705
Nilemah Pustular Mat Day 2 2016*	9066195	7.71	92.29	7.57	92.43	9393	1652757	2670	20637	12382	326
Nilemah Pustular Mat Night 2016*	8869056	11.8	88.2	63.11	36.89	29879	820936	7119	89388	35066	950
Nilemah Smooth Mat Night 2016*	9153948	9.39	90.61	16.8	83.2	57592	755780	22330	185322	118442	4103
Garden Point Smooth Mat Day 2016	8509997	8.39	91.61	10.1	89.9	27442	1850380	11550	77540	49967	1479
Garden Point Pustular Mat Day 2016	8966989	8.63	91.37	8.52	91.48	14554	1206356	5221	43248	25443	739
Garden Point Tufted Mat Day 2016	8890215	14.87	85.13	58.27	41.73	14284	751314	3932	41535	24811	1059
RRBS Sludge Between Columns Day 2016	9049876	9.95	90.05	7.98	92.02	14818	1613982	6634	37907	25330	694
RRBS Tufted Mat Day 2016	9189088	8.73	91.27	9.55	90.45	28538	778082	12696	96892	57792	1840
RRBS Smooth Mat Day 2016	8084891	16.74	83.26	31.44	68.56	48288	1040348	11431	139833	81072	3544
RRBS Ooze Over Sand Day 2016	9975457	8.47	91.53	7.12	92.88	19737	1683164	9249	58697	37566	1011
RRBS Inner Cobble Section Day 2016	10578934	8.74	91.26	7.43	92.57	18026	1579223	7098	49526	31211	874
RRBS Outer Cobble Section Day 2016	9978001	8.59	91.41	8.59	91.41	18981	1524945	10629	64260	43046	1108
Nilemah Pustular Mat Night 2017	9938032	8.59	91.41	8.59	91.41	29383	1690603	13261	94040	59883	1868
Nilemah Smooth Mat Night 2017	9956952	8.45	91.55	9.67	90.33	26087	1703240	12427	89531	57062	1827
Nilemah Pustular Mat Day 2017	9184291	9.86	90.14	9.39	90.61	29423	1827324	13866	94486	61629	1831
Nilemah Smooth Mat Day 2017	9214600	8.74	91.26	9.47	90.53	24822	1293097	12490	79939	49422	1239
Linke Lake Gelatenous Mat Day 2017	9810574	8.85	91.15	6.59	93.41	16412	1453025	8753	53715	34168	903
Giblin River Green Mat 1 Day 2016	8674558	9.39	90.61	7.19	92.81	8192	2322053	3083	27287	15496	484
Giblin River Yellow Mat Day 2016	9232190	10.9	89.1	95.29	4.71	447678	45821	212732	1613767	996550	31113
Giblin River Green Mat 2 Day 2016	8732656	9.14	90.86	4.66	95.34	13725	1595651	6045	40503	26450	720
Procedural Blank	9270213	12.58	87.42	44.11	55.89	5217	1216475	2727	23378	12486	230

Supplementary table 2.1 Illumina HiSeq 2500 pair-end sequencing read output with percentage summaries of trimmed and aligned sequences, number of assembled transcripts and number of annotations for Phyloflash, DIAMOND and eggnog-mapper. *Indicating paired Day/Night samples in the 2016 sampling trip.

Sample Name	# annotations		
	NCBI RefSeq	KEGG (KOs)	SEED subsystem
Nilemah Pustular Mat Day 1 2016	9309	3620	4236
Nilemah Smooth Mat Day 1 2016*	6994	3138	3189
Nilemah Smooth Mat Day 2 2016	11057	4689	4682
Nilemah Pustular Mat Day 2 2016*	2376	1009	1162
Nilemah Pustular Mat Night 2016*	7052	1915	2319
Nilemah Smooth Mat Night 2016*	12072	5386	5620
Garden Point Smooth Mat Day 2016	6275	3025	3051
Garden Point Pustular Mat Day 2016	4664	1669	1975
Garden Point Tufted Mat Day 2016	2588	803	956
RRBS Sludge Between Columns Day 2016	7331	3404	3373
RRBS Tufted Mat Day 2016	13121	4475	4918
RRBS Smooth Mat Day 2016	5882	2188	2593
RRBS Ooze Over Sand Day 2016	7411	3084	3444
RRBS Inner Cobble Section Day 2016	5749	2671	2680
RRBS Outer Cobble Section Day 2016	10670	4719	5199
Nilemah Pustular Mat Night 2017	8985	3849	4224
Nilemah Smooth Mat Night 2017	7387	3425	3454
Nilemah Pustular Mat Day 2017	10892	4914	5160
Nilemah Smooth Mat Day 2017	11875	5580	5424
Linke Lake Gelatenous Mat Day 2017	10351	4158	4380
Giblin River Green Mat 1 Day 2016	2774	921	1072
Giblin River Yellow Mat Day 2016	139254	55577	58176
Giblin River Green Mat 2 Day 2016	6373	2327	2985
Procedural Blank	2831	937	1153

Chapter 3

Functional gene expression in Shark Bay hypersaline microbial mats: Adaptive Responses

This chapter is published in Frontier in Microbiology: Extreme Microbiology (https://doi.org/10.3389/fmicb.2020.560336)

3.1 Background

Shark Bay in Western Australia has currently some of the most extensive extant microbial mat systems in the world occurring in meta- and hypersaline waters where they cover wide areas of intertidal and subtidal zones along ~100 km of shoreline (Jahnert et al., 2012). Daily tidal cycles and meteorologically driven water level changes cause fluctuations in salinity, pH, temperature, desiccation stress, and UV radiation at a local scale adding to the extreme conditions present (Wong et al., 2018). Several different types of microbial mats have been recognised to occur in Shark Bay due to their surface morphology, namely gelatinous, smooth, tufted, pustular, and blister mats (Logan et al., 1972). These microbial mats present opportunities to investigate biological and physicochemical factors that influence their composition, morphology, and functionality (Allen et al., 2009; Suosaari et al., 2016). Previous taxonomic studies of Shark Bay microbial communities (e.g. 16S rRNA) have indicated that are mainly dominated by Proteobacteria, Bacteroidetes, Cyanobacteria, Chloroflexi, and Euryarchaeota (Burns et al., 2004; Goh et al., 2009; Wong et al., 2015). Furthermore, Shark Bay has high archaea diversity dominated by Parvarchaeota with a methanogenic community containing hydrogenotrophic Methanomicrobiales, as well as methylotrophic Methanosarcinales, Methanococcales, Methanobacteriales and Methanomassiliicoccaceae (Wong et al., 2017). More recently, studies have examined the metagenomes of Shark Bay microbial mats. In these studies, the taxa and potential pathways associated with carbon, nitrogen, sulfur, and phosphorus cycles have been delineated, as well as environmental adaptations (e.g. low nutrients, hypersalinity, oxidative stress and heavy metal resistance) (Ruvindy et al., 2016; Wong

et al., 2018). However, it is currently unknown to what extent these pathways are actively expressed in these extreme environments.

Metatranscriptomic profiling of microbial mats provides an opportunity to define key active metabolic pathways and adaptation mechanisms under different environmental conditions, as well as comparing active microbial populations from rRNA and mRNA transcripts. In Shark Bay microbial mat communities, the degree of which certain metabolic pathways (e.g. carbon fixation, oxygenic/anoxygenic photosynthesis, sulfate reduction) contribute to overall biogeochemical cycling and taxa responsible is still not fully understood. Here, we analyzed metatranscriptomes in Shark Bay microbial mats to investigate how active microbial communities, abundant gene transcription, and photosynthetic and chemosynthetic capacities change in accordance to mat type, diel cycle, and sampling season.

3.2 Materials and methods

3.2.1 Sampling and site description

Microbial mats were sampled from the Nilemah tidal flat (26°27'02.9"S 114°05'39.3"E) located in the southern area of Hamelin Pool, Shark Bay, Western Australia (Figure 3.1). Restricted circulation in conjunction with high rates of evaporation and limited rainfall leads to the water in Hamelin Pool to be hypersaline (60 to 70 ppt) with pH ranges between 7.5 and 8 (Jahnert and Collins, 2013; Suosaari et al., 2016). The Nilemah tidal flat is shallow and characterized by a littoral gradient that varies from 20 to 150 cm km^{-1} restricting tidal influxes and causing laterally well-defined tidal zonation (Jahnert and Collins, 2013). Fluctuations in the water level within the intertidal and upper subtidal zone occur on both semidiurnal (astronomical tide) frequency but also at seasonal periodicity with highest water in March/April and lowest water levels in October/November. Recent studies of water elevation within Hamelin Pool found that up to 60% of the observed variation in surface elevation was attributable to meteorological drivers (Burne and Johnson, 2012; Suosaari et al., 2016). In addition, wind induced set down is particularly important in the Nilemah tidal flat since it can prevent the inundation of the mat platform by the tide for extended periods,

however this phenomenon is most likely to affect the setting during windy months and not during the time of sampling in this study (April and July) (Morris et al., 2020).

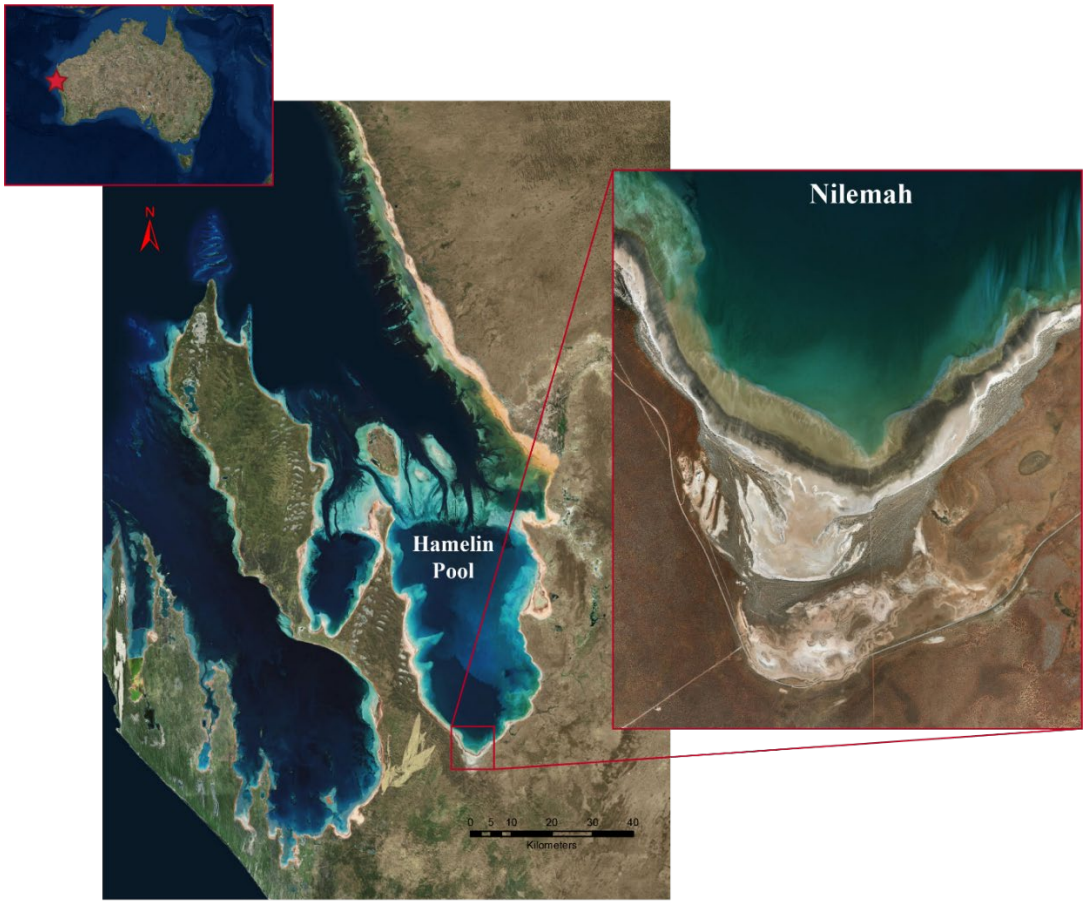

Figure 3.1 Satellite images of the Shark Bay world heritage area, Hamelin Pool and the Nilemah tidal flat. Images were generated with ArcGIS Desktop: Release 10. Redlands, CA: Environmental Systems Research Institute.

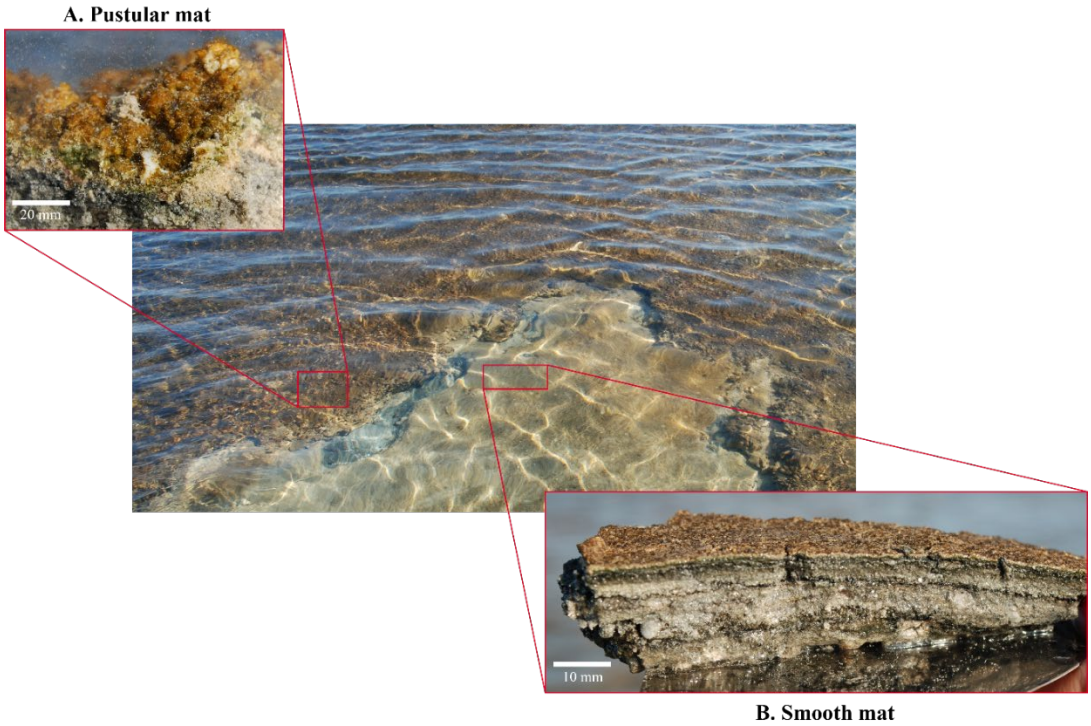

Figure 3.2 Smooth and pustular microbial mats sampled from the Nilemah tidal flat. A. Pustular mat (bar, 20 mm) and B. Smooth mat (bar, 10 mm) collected in April 2017 from Nilemah.

Smooth and pustular microbial mats were sampled from the intertidal and uppermost subtidal zone of the Nilemah tidal flat (Figure 2). These mat types were chosen for this study since they are the most common mat types for this area and parallel metagenomics datasets are available for comparison. Smooth mats are uniformly laminated with a pale brown-green surface overlaying a light to dark green second layer followed by a third purple layer and fourth black layer and were located in small depressions between mat covered microbialite ridges that remained submerged at low tide. In contrast, pustular mats are dark brown at the surface with jelly-like pustules composed of green, gold and purple mucilage. This mat type was located at on the crests of microbialite ridges between depressions in the shallow subtidal zone and as continuous sheets across the intertidal platform where it was exposed at low tide. Additional information on the sampling locations and descriptions of the mats can be found in Supplementary Table 1.

3.2.2 Metatranscriptomic analysis

Metatranscriptomic analysis is detailed in Section 2.2 – Chapter 2. RNA isolation, library preparation and sequencing (2.2.1), and bioinformatics (2.2.2). Illumina HiSeq 2500 pair-end sequencing read output with percentage summaries of trimmed and aligned sequences, number of assembled transcripts and number of annotations for Phyloflash and DIAMOND can be found in Table S2.1. Statistical analysis and visualisation are detailed in Section 2.4 – Chapter 2.

3.3 Results

3.3.1 Microbial community structure of smooth and pustular mats

The alpha diversity of microbial community structure between smooth and pustular mats was estimated for both rRNA and mRNA derived classifications with the Shannon diversity index and Choa1 species richness estimator. Shannon index of diversity for rRNA classifications ranged from 5.66 to 6.12 in pustular mats, averaging higher than smooth mats that ranged from 5.25 to 5.75 (Supplementary Figure 3.1A). Interestingly, the mRNA showed an opposite trend, ranging from 6.10 to 6.29 in smooth mats, averaging higher than pustular mats that ranged from 5.11 to 6.10 (Supplementary Figure 3.1B). The Chao1 species richness estimator revealed that richness for rRNA classifications varied from 2260 to 3800 in pustular mats and from 2020 to 3250 in smooth mats with the highest values found in pustular mats sampled in April 2017 (Supplementary Figure 3.1A). Coincidently, mRNA classifications revealed that smooth mats had an overall higher species richness varying from 1580 to 1800, whereas pustular mats varied from 1290 to 1690 (Supplementary Figure 3.1B).

Principle component analysis (PCA) of rRNA and mRNA classifications revealed that smooth mats are distinct from pustular mats, however the mRNA classification indicated a significant discrepancy with pustular mats sampled in 2016 during the night (Figures 3.3B and 3.4B). Based on both classification methods the community composition was primarily dominated by bacteria with a general proportion of 90:3:7 % of Bacteria, Archaea, and Eukaryotes, respectively. Smooth and pustular mats were

dominated by Proteobacteria, predominately the alpha, delta and gamma classes, as well as Bacteroidetes, Planctomycetes, Cyanobacteria, Spirochaetes, Firmicutes and Chloroflexi (Figures 3.3A and 3.4A). Furthermore, mRNA classifications indicated that Betaproteobacteriales were also abundant but are not shown in the rRNA classifications, since this former bacterial class has been included within Gammaproteobacteria as Betaproteobacteriales in the updated Silva 132 database. Lower abundant taxa can be seen in Supplementary Figures 3.2A and 3.3A.

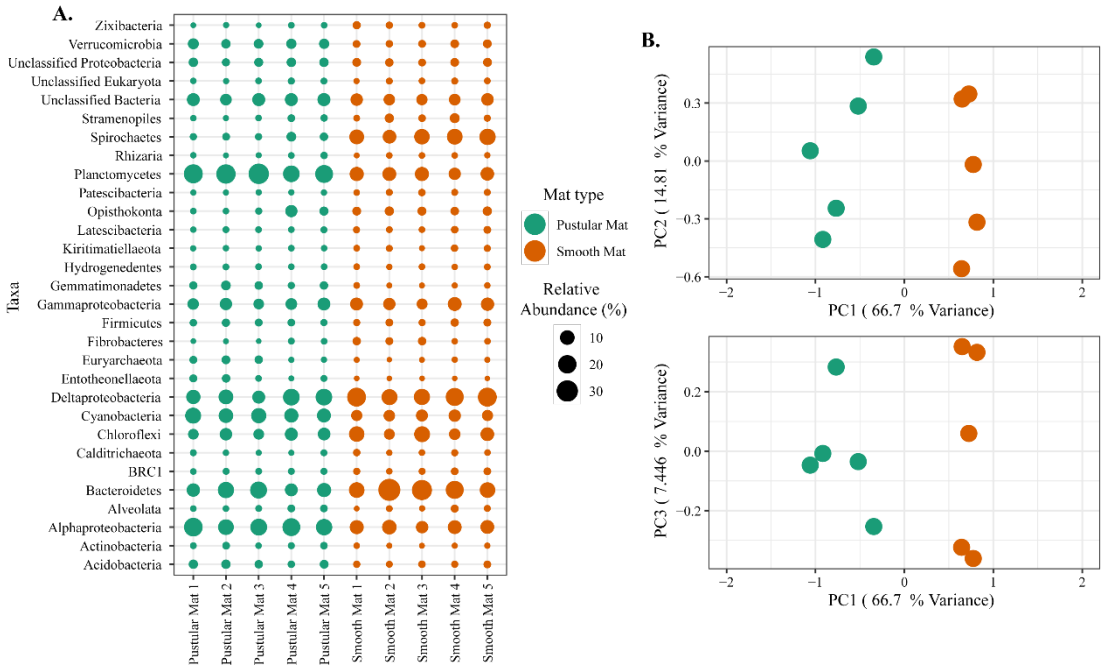

Figure 3.3 Composition of Archaea, Bacteria and Eukaryote taxa in Nilemah smooth and pustular mats based on SSU rRNA genes (SILVA Database). A. Dot plot displaying the composition and abundance of the top 30 most abundant taxa. B. PCA plots constructed from similarity matrices. Mats 1, 2 and 3 were sampled in July 2016; mats 4 and 5 were sampled in April 2017. Pustular and smooth mats 2 and 3 are the paired samples from July 2016.

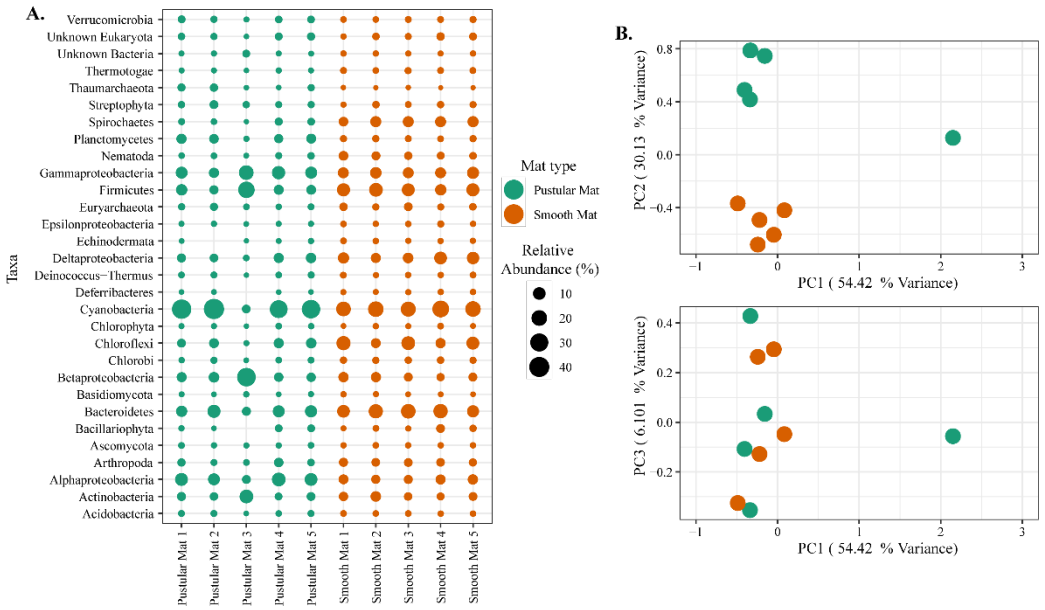

Figure 3.4 Composition of Bacteria, Archaea1 and Eukaryote2 taxa in Nilemah smooth and pustular mats based on transcripts (RefSeq Database). A. Dot plot displaying the composition and abundance of the top 30 most abundant taxa. B. PCA plots constructed from similarity matrices. Mats 1, 2 and 3 were sampled in July 2016; mats 4 and 5 were sampled in April 2017. Pustular and smooth mats 2 and 3 are the paired samples from July 2016.

The rRNA classifications indicated that Cyanobacteria, Planctomycetes, Verrucomicrobia, Amoebozoa, Alphaproteobacteria, Acidobacteria, Gemmatimonadetes, Thaumarchaeota, Nitrospirae, Omnitrophicaeota and Actinobacteria were significantly more represented in the pustular mats (P-value < 0.05), whereas, smooth mats contained significant proportions of Spirochaetes, Patescibacteria, Deltaproteobacteria, Dependentiae, Modulibacteria, Asgardeota and Nanoarcheaeota (Supplementary Figure 3.2B). The mRNA classifications indicated that Planctomycetes and Alphaproteobacteria were significantly higher in pustular mats (P-value < 0.05), whereas Spirochaetes, Thermotogae, Deferribacteres, Chrysiogenetes, Synergistetes, Aquificae, Chlorobi, Deltaproteobacteria, Dictyoglomi, Bacteroidetes, Fusobacteria, Choroflexi and Epsilonproteobacteria were more abundant in smooth mats (Supplementary Figure 3.3B). Both classifications indicated that Alphaproteobacteria and Planctomycetes were significantly more represented in pustular mats, whereas Deltaproteobacteria and Spirochaetes were more significant in smooth mats.

3.3.2 Key functional gene distribution in metatranscriptomes

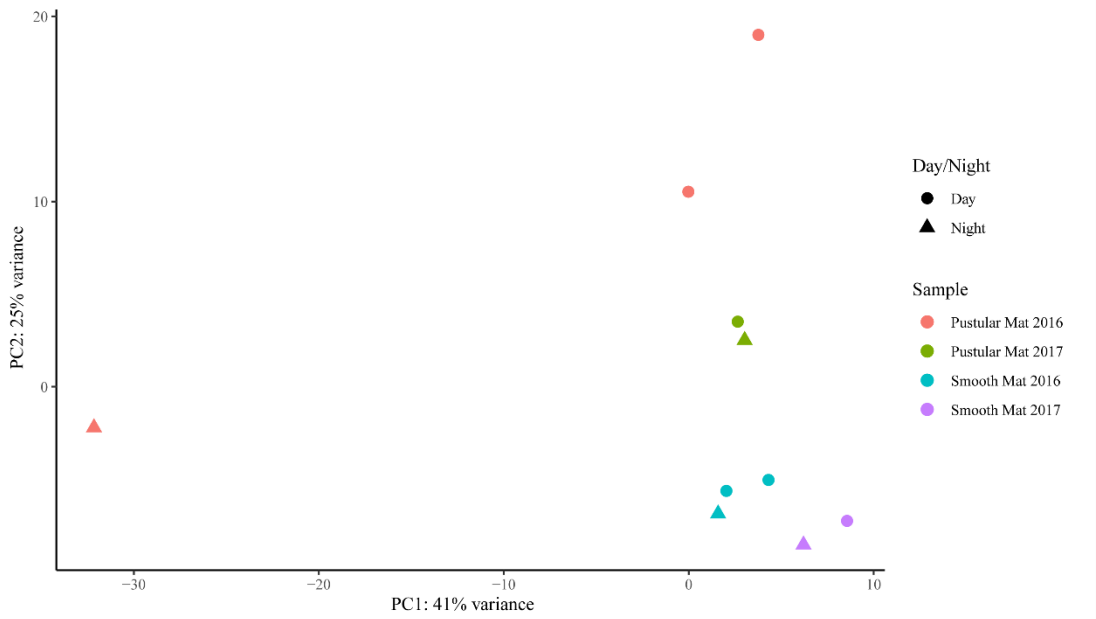

Figure 3.5 Principle component analysis showing relationships between mat types, day/night samples and sampling period. Differential analysis of the transcribed genes was calculated from the variance stabilising transformation of KO count data using the DESeq2 package in R.

Transcripts of genes for microbial functions only differed significantly between smooth and pustular mats (ANOSIM, R= 0.34; P=0.008), but not between diel cycles and sampling period (P>0.5). PCA of all transcribed genes indicated that there was no clustering observed between day and night samples. However, smooth mats clustered significantly more than pustular mats with the majority of the samples clustering within their sampling period (Figure 3.5). A large portion of most abundantly transcribed genes were associated with maintenance of basic cellular functions (e.g. chaperones, elongation factors, RNA polymerase) for both mat types. However, high levels of gene transcripts that encode quorum sensing (ABC.PE.S; ABC.MS.S; *opp*A, *mpp*A; *liv*K; ABC-2.A), motility/chemotaxis (*fli*C, *mcp*, *rbs*B), environmental adaptation (*clp*C, *pro*X), biofilm formation (*rpoS*), phosphorus uptake (*pst*S; *pho*ABX), iron uptake (TC.FEV.OM), terpene biosynthesis (*isp*H, *lyt*B) and fatty acid metabolism (ACSL, *fad*D) were observed (Figure 6). Furthermore, genes involved in photosynthesis (*puf*LM; *psa*A, *psb*A), as well as carbon metabolisms relating to carbon fixation and methane metabolism (*por*, *nif*J; *ppd*K; GAPDH, *gap*A; *hdr*A2; ACSS1_2; *pps*, *pps*A) were also highly abundant in both mat types. Additionally, both the PCA

and heatmap (Figures 3.5 and 3.6) confirmed the same discrepancy observed in mRNA classification of the 2016 pustular mats sampled during the night.

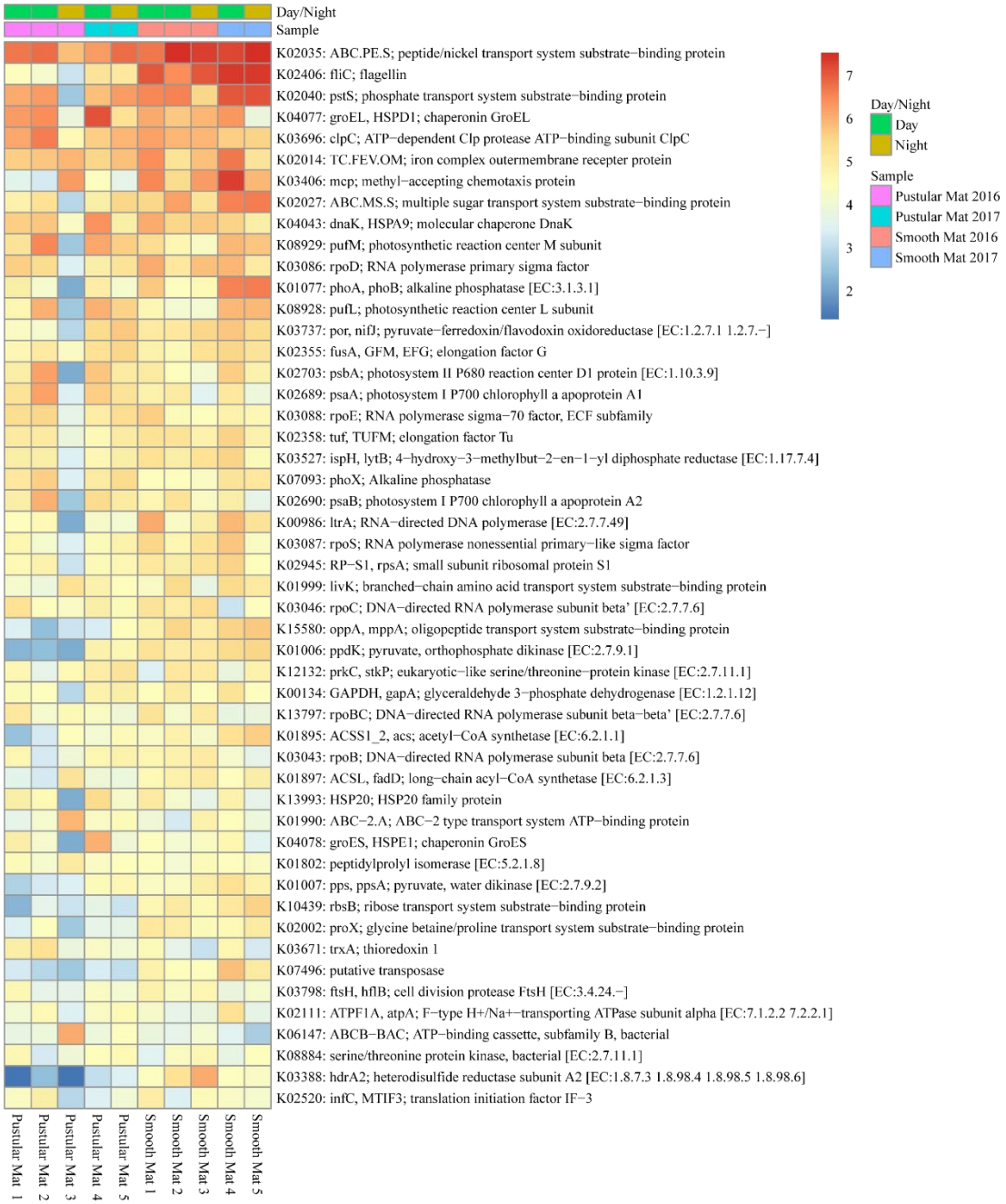

Figure 3.6 Heatmap showing the top 50 out of 2298 transcribed genes (>10) in Nilemah smooth and pustular mat metatranscriptomes. Differential analysis of the transcribed genes was calculated from the variance stabilising transformation of KO count data using the DESeq2 package in R. A gradient from red to blue indicates gene abundance across samples with red representing genes that are highly transcribed and blue indicating genes that have lower relative transcription. Pustular and smooth mats 2 and 3 are the paired samples from July 2016.

3.3.3 Key functional gene distribution in microbial metabolic pathways

3.3.3.1 Photosynthesis

An abundance of transcripts encoding photosystems I (*psa*ABCDEFL) and II (*psb*ABCDEFOTUV) were found in both mat types, however the most abundantly transcribed phototrophy-related genes were associated with anoxygenic photosystem II (*puf*BLM) (Figure 3.7). Other abundantly transcripts relating to phototrophy included the cytochrome b6/f complex (*pet*ABCD), F_1F_0-type ATPase (*atp*ABCDEFGH), and photosynthetic electron transport (*pet*CEH).

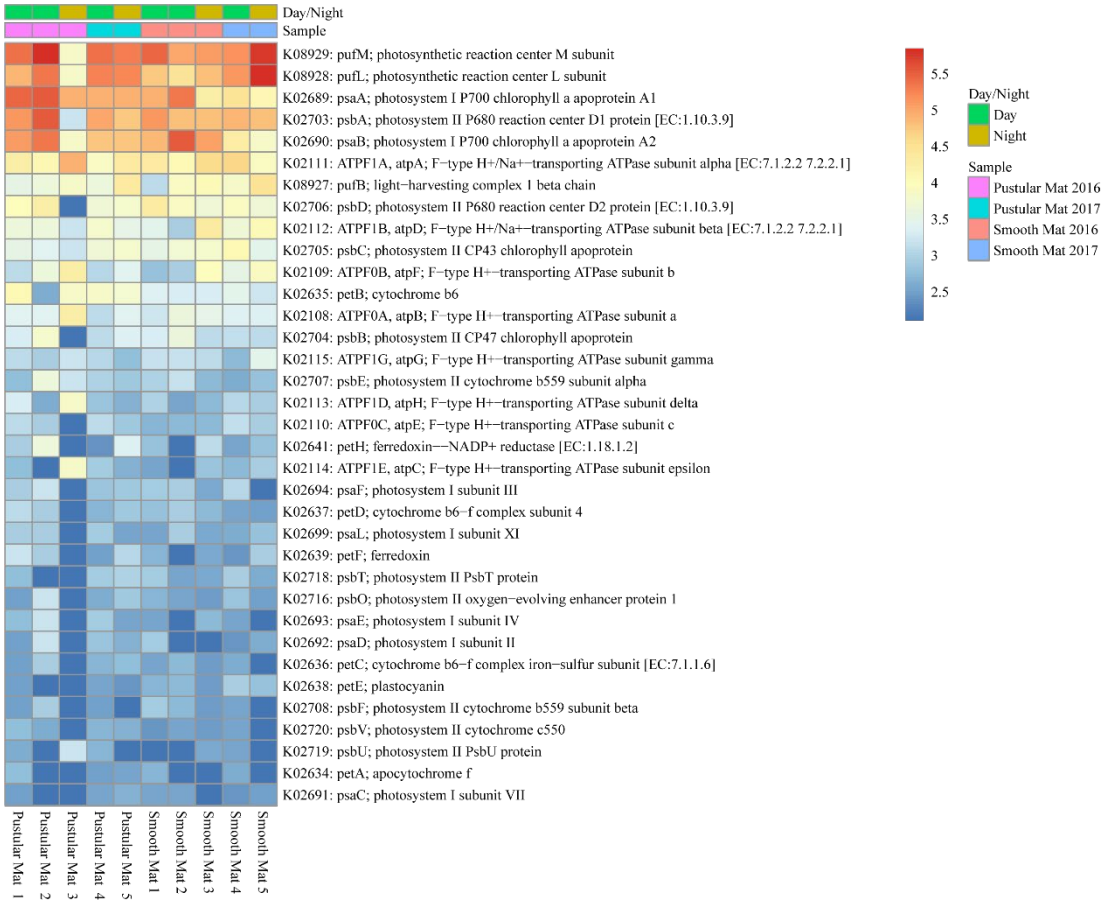

Figure 3.7 Heatmap showing 35 transcribed genes (>10) in Nilemah smooth and pustular mat metatranscriptomes related to photosynthesis. Differential analysis of the transcribed genes was calculated from the variance stabilising transformation of KO count data using the DESeq2 package in R. A gradient from red to blue indicates gene abundance across samples with red representing genes that are highly transcribed and blue indicating genes that have lower relative transcription. Pustular and smooth mats 2 and 3 are the paired samples from July 2016.

3.3.3.2 Carbon fixation

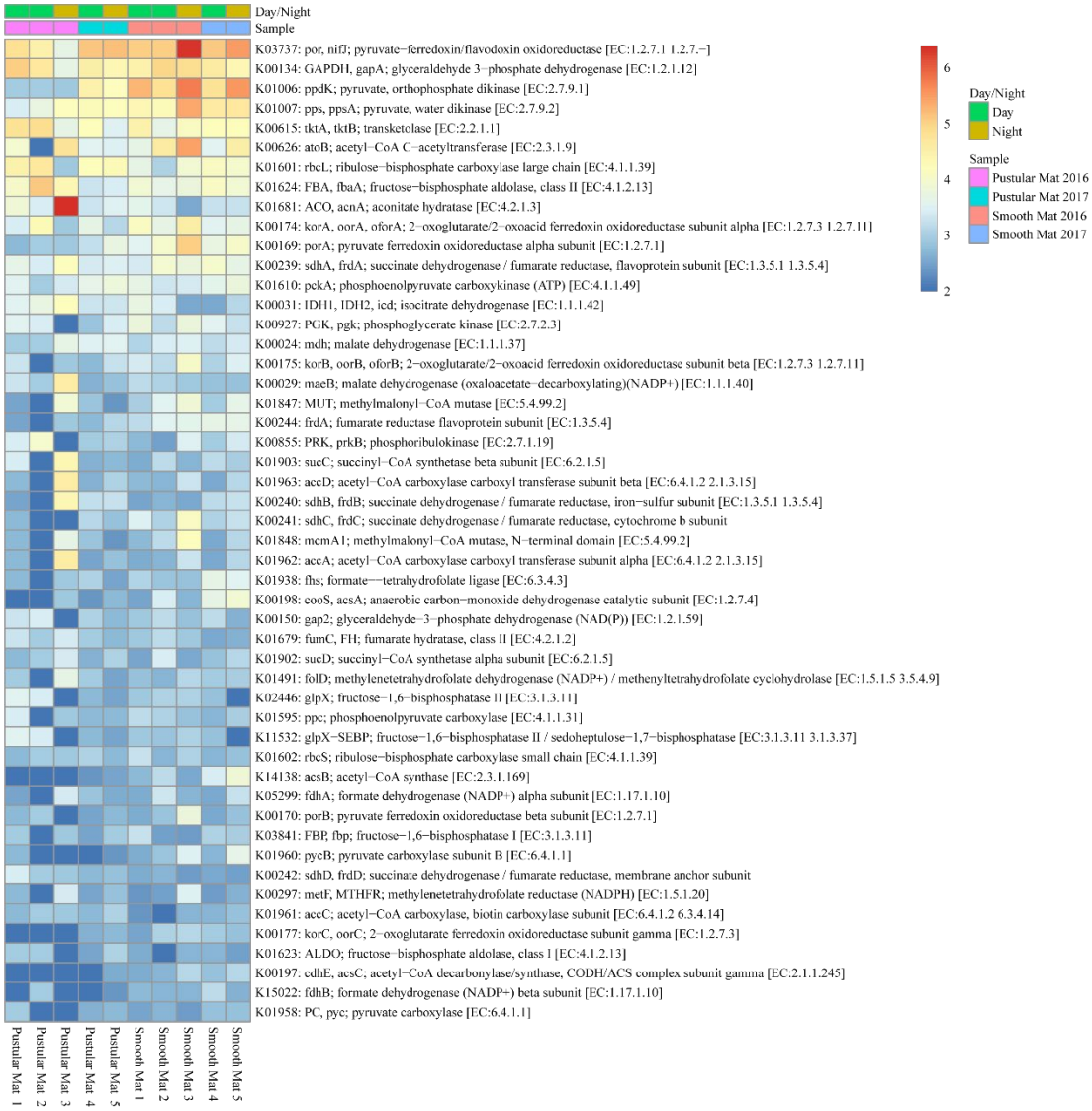

Figure 3.8 Heatmap showing the top 50 out of 67 transcribed genes (>10) in Nilemah smooth and pustular mat metatranscriptomes related to carbon fixation. Differential analysis of the transcribed genes was calculated from the variance stabilising transformation of KO count data using the DESeq2 package in R. A gradient from red to blue indicates gene abundance across samples with red representing genes that are highly transcribed and blue indicating genes that have lower relative transcription. Pustular and smooth mats 2 and 3 are the paired samples from July 2016.

The reductive citric acid cycle (Arnon-Buchanan cycle) had the highest abundance and proportion of transcripts related to carbon fixation across all metatranscriptomes (*por*, *nif*J; *ppd*K; *pps*, *pps*A; *por*A; *kor*ABC, *oor*ABC, *ofor*ABC; *sdh*ABCD, *frd*ABCD; ACO, *acn*A; *mdh*; IDH1, IDH2, *icd*; *suc*C; IDH1, IDH2, *icd*; *fum*C, FH; *suc*D; *por*B;

*pyc*B; PC, *pyc*) (Figure 3.8). The reductive pentose phosphate cycle (Calvin-Benson cycle) had the second highest abundance and proportion of transcripts (GAPDH, *gap*A; *tkt*A, *tkt*B; *rbc*L; FBA, *fba*A; PGK, *pgk*; PRK, *prk*B; *gap*2; *glp*X; *glp*X-SEBP; *rbc*S; FBP, *fbp*; ALDO). Genes involved in reductive acetyl-CoA pathway (Wood-Ljungdahl pathway) were abundantly transcribed in the smooth mat metatranscriptomes (*fhs*; *coo*S, *acs*A; *fol*D; *acs*BC; *fdh*AB; *met*F, MTHFR; *cdh*E). Transcripts of genes involved in 3-hydroxypropionate bi-cycle (*sdh*ABC, *frd*ABC; MUT; *mcm*A1; *fum*C, FH; *acc*ACD), as well as the hydroxypropionate-hydroxybutyrate cycle (*ato*B, *mcm*A1) were transcribed in both mat types.

3.3.3.3 Methane metabolism

Genes involved in methane metabolism were found to be abundantly transcribed within smooth mat metatranscriptomes (Figure 3.9), with the most abundant transcripts associated with the final reaction steps of the methanogenic pathway (*hdr*ABC2; *mvh*ADG, *vhu*ADG, *vhc*ADG). Two major types of methanogenic pathways were found to be expressed, CO_2 to methane (*fwd*ABF, *fmd*ABF) and acetate to methane (ACSS1_2, *acs*; *pta*; *ack*A; *cdh*E, *acs*C; *cdh*C; *cdh*D, *acs*D), as well as the less common trimethylamine to methane (*mtt*B). Moreover, transcriptiojn of genes involved in pathways that convert formaldehyde to C2 or C3 compounds were also highly expressed between mat types, these include the serine pathway (ENO, *eno*; *mdh*; *gly*A, SHMT; *ppc*; *mtk*AB; AGXT) and ribulose monophosphate pathway (FBA, *fba*A; *pfk*A, PFK; *hxl*A). Interestingly, methanotrophic oxidation of methane to formaldehyde was only observed in pustular mat metatranscriptomes (*pmo*A-*amo*A), however this gene is also associated with encoding nitrification. Furthermore, transcription of genes associated with the acetyl-CoA pathway (Wood-Ljungdahl pathway) were also observed (*cdh*ACDE; *acs*CD).

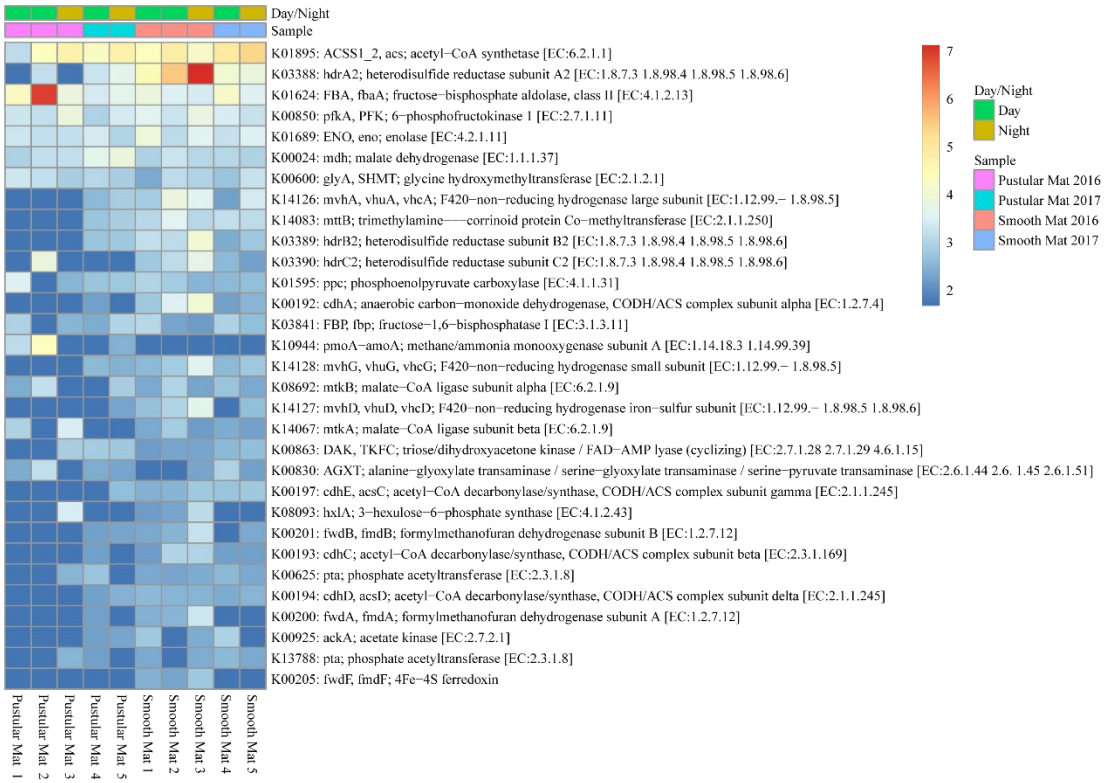

Figure 9 Heatmap showing 31 transcribed genes (>10) in Nilemah smooth and pustular mat metatranscriptomes related to methane metabolism. Differential analysis, gradient and sample descriptions are the same as figure 4.

3.3.3.4 Nitrogen metabolism

Transcription of genes that encode nitrogen metabolising pathways showed no clear pattern between mat types (Figure 3.10). Transcription of genes involved with the breakdown and biosynthesis of glutamate were heavily represented in all metatranscriptomes (*gdh*A; *glt*BD; GLU, *glt*S; GLUD1_2, *gdh*A; GLT1; *gud*B, *roc*G; GDH2), with glutamine synthetase (*gln*A, GLUL) being the most abundantly transcribed nitrogen metabolism related gene. Genes involved in nitrogen fixation were also abundantly transcribed (*nif*DHK) in both mat types, however they were found to be more abundantly transcribed in samples collected during the night in April 2017. Other reduction pathways found in the mats included assimilatory nitrate reduction (*nar*B, *nir*A, *nas*A), dissimilatory nitrate reduction (*nar*G, *nar*Z, *nxr*A; *nap*A; *nrf*A) and denitrification (*nar*G, *nar*Z, *nxr*A; *nos*Z; *nap*A; *nir*K). Additionally, genes encoding ammonia/bicarbonate cycling (*cyn*T, *can*; *arc*C; CPS1), hydroxylamine reduction to ammonia (*hcp*), nitroalkane assimilation (*ncd*2, *npd*),

nitrate assimilation (NRT, *nark*, *nrt*P, *nas*A), nitrile assimilation (E3.5.5.1) and formamide assimilation (E3.5.1.49) were transcribed across all samples studied.

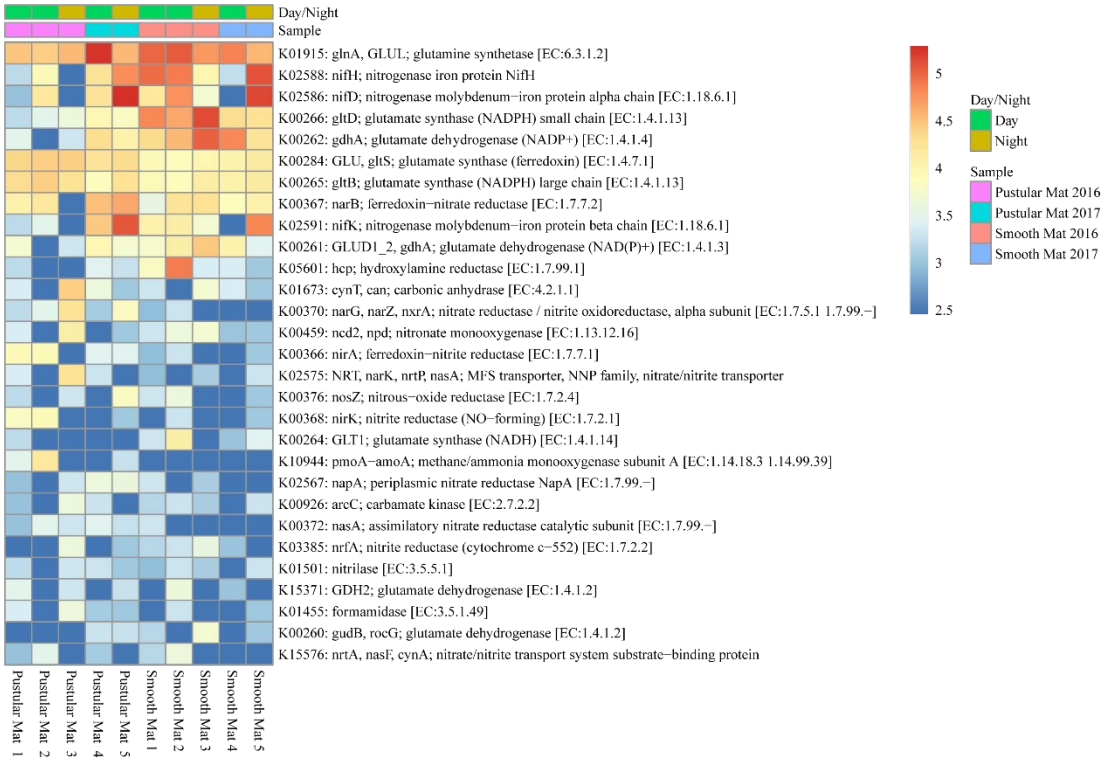

Figure 3.10 Heatmap showing 29 transcribed genes (>10) in Nilemah smooth and pustular mat metatranscriptomes related to nitrogen metabolism. Differential analysis of the transcribed genes was calculated from the variance stabilising transformation of KO count data using the DESeq2 package in R. A gradient from red to blue indicates gene abundance across samples with red representing genes that are highly transcribed and blue indicating genes that have lower relative transcription. Pustular and smooth mats 2 and 3 are the paired samples from July 2016.

3.3.5 Sulfur metabolism

Genes involved in sulfur metabolism were found to be abundantly transcribed within the smooth mat metatranscriptomes (Figure 3.11), with the most abundant genes being associated with the dissimilatory sulfate reduction pathway (*apr*AB; *dsr*AB; *sat*, *met*3) and assimilatory sulfate reduction pathway (*sat*, *met*3; *cysCD*HIJNQ; PAPSS; *sir*). Genes encoding polysulfide metabolism (*sqr* and *hyd*D), thiosulfate reduction (TST, MPST, *sse*A; *phs*A, *psr*A), cysteine and methionine metabolism (*cys*K, *cys*E, *met*B, *met*X), dimethyl sulfoxide reduction (*dms*A), taurine assimilation (*tau*C), thiosulfate oxidation (*sox*B), alkanesulfonate assimilation (*ssu*C), and assimilation of dimethylsulphoniopropionate (*dmd*C) were transcribed across all samples studied.

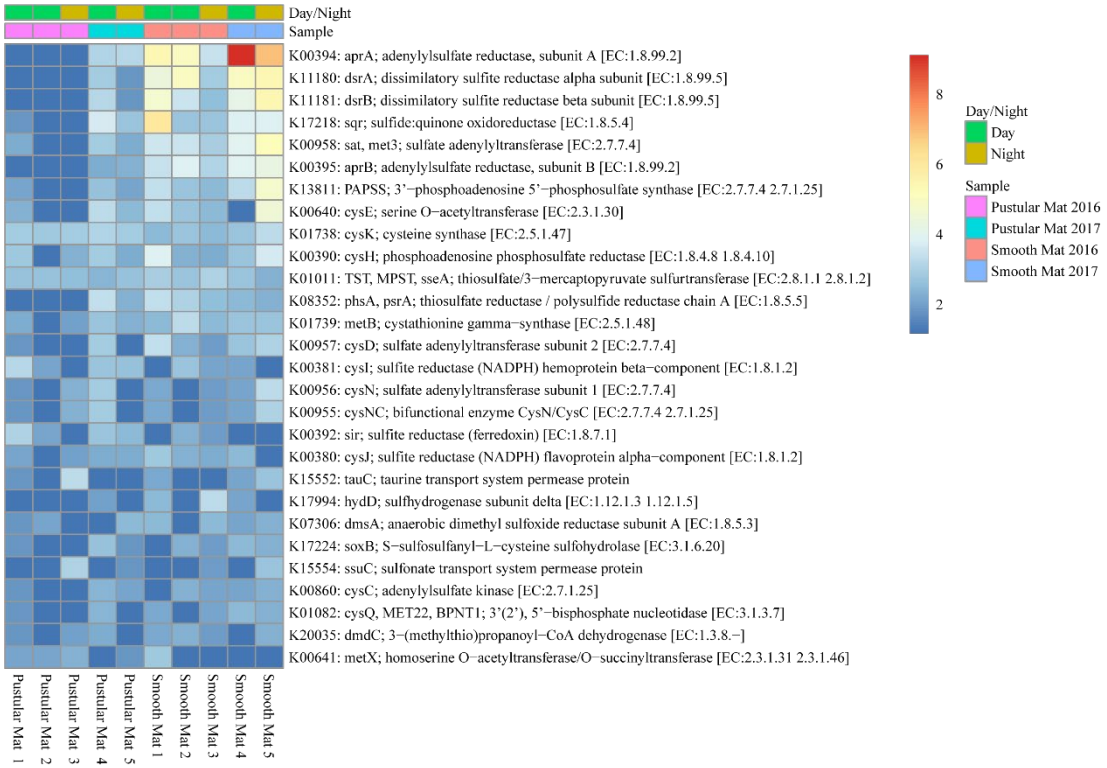

Figure 3.11 Heatmap showing 28 transcribed genes (>10) in Nilemah smooth and pustular mat metatranscriptomes related to sulfur metabolism. Differential analysis, gradient and sample descriptions are the same as figure 4.

3.3.4 Significant metabolic activity

Overall expression of metabolic pathways between mat types indicated that photorespiration, cysteine biosynthesis, nitrate assimilation, denitrification and the pentose phosphate pathway were significantly represented in pustular mats, whereas the metabolic activity in smooth mats was more represented by anaerobic pathways that included methanogenesis, non-phosphorylative Enter-Doudoroff pathway, acetyl-CoA pathway, dissimilatory sulfate reduction, and the Wood-Ljungdahl pathway (Figure 12A). Comparison of day and night samples indicated that transcription of genes involved in photosystems I and II, as well as the reductive pentose phosphate cycle (glyceraldehyde-3P) and reductive pentose phosphate cycle (Calvin cycle) were more abundant during the day time (Figure 12B).

A.

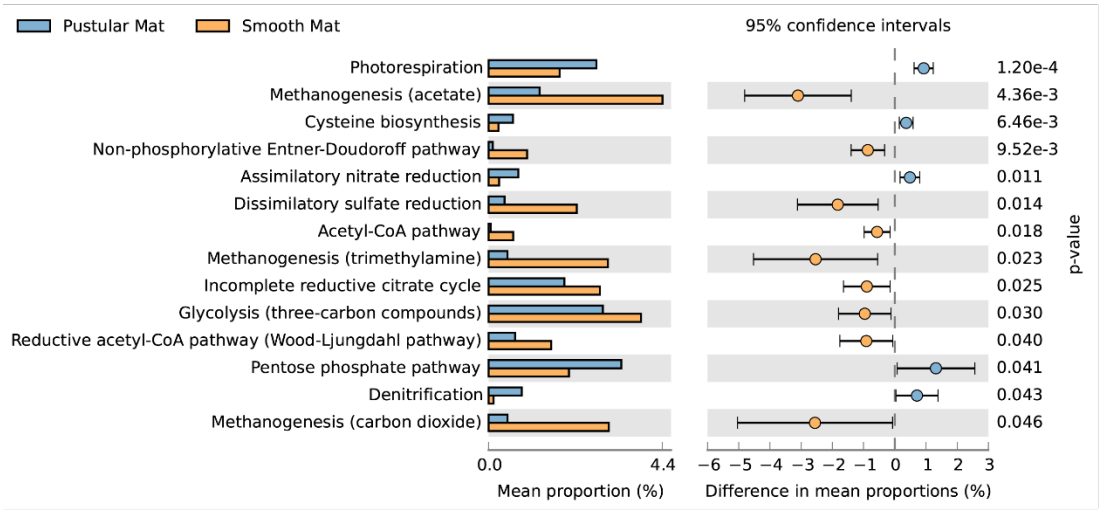

B.

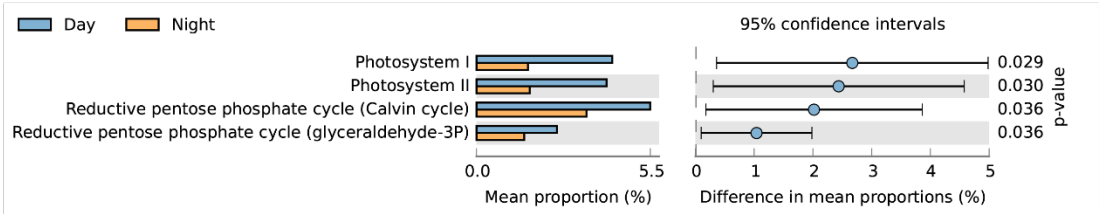

Figure 3.12 Extended error bar plot identifying significant differences ($p < 0.05$) between mean proportions of 56 metabolic pathways (KEGG level 3) in smooth and pustular mats (A.), and day and night samples (B.) (Welch's t-test)

3.4 Discussion

3.4.1 Active microbial mat communities

The overall microbial community composition of Nilemah smooth and pustular mats exhibited similar distributions to previous metagenomic and 16S rRNA/rDNA studies of Nilemah microbial mats and stromatolites (Burns et al., 2004; Allen et al., 2009; Ruvindy et al., 2016; Wong et al., 2016; Babilonia et al., 2018). This suggests that the microbial communities in the Nilemah tidal flat have been relatively stable for the last two decades, dominated by Proteobacteria, Bacteroidetes, Planctomycetes, Cyanobacteria, Spirochaetes, Firmicutes, and Chloroflexi occupying the mats. Comparison of active microbial communities derived from rRNA and mRNA transcripts in both mat types indicated that pustular mats had an overall higher species richness and diversity than smooth mats based on rRNA classifications, however an

opposite trend was observed with transcript derived mRNA classifications suggesting that the density of active microbes in smooth mats is relatively higher. This corroborates with previous depth profiles of oxygen and sulfide concentrations in Shark Bay microbial mats, which indicated that smooth mats had higher cell densities due to the increased metabolic activity of aerobes and intense cycling of carbon in their upper layers when compared to pustular mats (Wong et al., 2015). PCA of both classifications revealed that the microbial community compositions of smooth mats are distinct from pustular mats, however the mRNA classification indicated a significant discrepancy with a 2016 pustular mat sampled during the night. This discrepancy is not observed in the rRNA classification, therefore indicating that this particular sample is showing a possible shift in the active microbial community with Gammaproteobacteria, Firmicutes, Betaproteobacterials and Actinobacteria becoming more active during the night, and Cyanobacteria, Bacteroides and Alphaproteobacteria becoming less active.

3.4.2 Microbial mats surviving in a low nutrient, hypersaline environment

A large portion of most abundantly transcribed genes were associated with maintaining basic cellular functions. However, the metatranscriptomes exhibited elevated expressions of genes associated with combating hypersalinity and low nutrient conditions such as biofilm formation, nutrient uptake and osmoadaptation. Our study found an abundance of genes encoding sigma factor rpoS, ATP-binding subunit ClpC and transport systems associated with quorum sensing (QS), which are all linked with biofilm formation and are recognized as a key factors in the stationary phase of growth and survival of bacteria during exposure to stress conditions (i.e. starvation, UV radiation, salinity and oxidative stress) (Muñoz-Elías et al., 2008; Klauck et al., 2018; Lee et al., 2018). Moreover, the most transcribed gene found across all metatranscriptomes encodes a peptide/nickel ABC transporter associated with transcriptional regulators that serve as key components of QS pathways which utilize peptides as intercellular signalling molecules aiding in virulence and biofilm formation (Rutherford and Bassler, 2012; Papenfort and Bassler, 2016). However in bacteria, peptide/nickel ABC transporters are also linked with nickel uptake, and as soluble Ni_2^+ in natural environments usually exists in trace amounts, high-affinity uptake of nickel

is needed to ensure intracellular metalloenzyme activities (Hiron et al., 2010; Zhu et al., 2017). Previous analysis of the a Shark Bay smooth mats found the nickel concertation to be at 7 ppm, an adequate concentration for [NiFe] hydrogenase activity (Skyring et al., 1988). Additionally, sub-millimolar concentrations of nickel can inhibit biofilm formation in bacteria through the inhibition (at the transcriptional level) of QS (Vega et al., 2014). Therefore, high expression of this peptide/nickel ABC transporter suggests that microorganisms that utilise nickel in Shark Bay microbial mats need to highly regulate the intracellular concentrations of nickel to ensure adequate levels for metalloenzyme activities while not inhibiting QS.

Genes involved in the uptake and regulation of iron, phosphorus and long chain fatty acids were also abundantly transcribed in the metatranscriptomes. A variety of nutrients are known to be limited in Shark Bay microbial mats (i.e. phosphorus), with their distribution fluctuating in accordance to oxic and anoxic conditions (Pagès et al., 2014; Wong et al., 2018). The high abundance of an inorganic phosphate transport gene (*pst*S) is likely critical for inorganic phosphorus uptake, with its accumulation being enhanced under phosphate starvation conditions (Varin et al., 2010). Genes encoding alkaline phosphatase (*pho*ABX) were also abundant throughout the metatranscriptomes. Alkaline phosphatase is responsible for salvaging phosphorus from organic molecules in the community (Chróst, 1994). A gene regulating the iron complex outer membrane receptor protein (TC.FEV.OM) was also highly expressed; this protein regulates intracellular iron and prevents its over accumulation (Mackenzie et al., 2008). Another abundantly transcribed gene in the metatranscriptomes encodes long-chain acyl-CoA synthetase (ACSL, fadD) known for catalysing the activation of a long fatty acid chain to a fatty acyl CoA, and has key involvement in obtaining essential fatty acids from the environment to then be oxidized for energy production (Dirusso and Black, 2004).

Genes enhancing a microbe's ability to sense chemical gradients in their environment and then move towards more favourable conditions were also abundantly expressed in all samples studied, but were especially transcribed in smooth mat metatranscriptomes. These include the flagellin protein (*fli*C), the methyl-accepting chemotaxis protein (*mcp*) and the ribose transport system substrate-binding protein

(*rbs*B). Methyl-accepting chemotaxis proteins are the most common receptors in Bacteria and Archaea (Salah Ud-Din and Roujeinikova, 2017). The *rbs*B protein is associated with the methyl-accepting chemotaxis protein III, which is influenced by D-ribose, D-galactose, and certain structural analogues (Kondoh et al., 1979). The overexpression of the *fli*C gene has been associated with the enhancement of motile activity; however, deletion of the *fli*C gene has also been found to cause an inhibited in QS activity and biofilm formation. This suggests that the *fli*C gene may have a variety of functional properties (Morohoshi et al., 2009; Zhou et al., 2014). The higher abundance of these genes in the smooth mats is likely a result of the heterotrophic bacteria needing to adjust their position within these stratified systems during diel fluctuations that change the oxic and anoxic conditions. Furthermore, a previous study found evidence of an anoxic niche occurring in the upper photic-oxic zone of Shark Bay microbial mats with large portions of anaerobic bacteria, such as Spirochaetes, occurring in the oxygenated surface layer (Wong et al., 2015).

Previous functional annotations of Shark Bay metagenomes have identified clusters of osmoadaptive traits such as the uptake of the osmoprotectant glycine betaine (Wong et al., 2018). In this study genes encoding glutamine synthetase (*gnl*A, GLUL) and glutamate synthase (*glt*D) were highly represented in all metatranscriptomes. Glutamate is known to be a major anionic solute involved in osmoregulation (Kang and Hwang, 2018). However, in most photosynthetic organisms, ammonium assimilation takes place by the sequential action of glutamine synthetase and glutamate synthase, constituting a link between nitrogen and carbon metabolisms (Muro-Pastor et al., 2005). Cycling of glutamate could be critical in the Shark Bay systems as a protective mechanism against elevated salinity conditions as well as potential source of carbon and energy in times of stress. Furthermore, genes transcribing F_1F_0-type ATP synthase relating to H^+/Na^+ transport were abundantly expressed in both mat types. The F_1F_0-type ATP synthase plays vital functions in the energy-transducing membranes of bacteria by catalysing ATP synthesis and hydrolysis coupled with transmembrane proton or sodium ion (Na^+) transport (von Ballmoos et al., 2009). To survive at high salinity, organisms must prevent the excessive Na^+ accumulation in the cytoplasm (Assaha et al., 2017). Studies on halotolerant Cyanobacteria have indicated that they potentially utilise Na^+-dependent F_1F_0-type

synthase to tolerate salt-stress in conjunction with more common osmoprotectants such as glycine betaine (Soontharapirakkul et al., 2011). Therefore, the elevated expression of genes encoding H^+/Na^+ dependent F_1F_0-ATP synthase maybe a significant osmoadaptation for photosynthetic organisms living in the hypersaline mats of Shark Bay.

3.4.3 Carbon Cycling

Photosynthesis is (one of) the primary driving force(s) of various nutrient cycles in microbial mats (van Gemerden, 1993; Mobberley et al., 2013). The most abundantly expressed phototrophy-related genes found in both mat types were involved in anoxygenic photosystem II. Anoxygenic photosynthesis is distinguished from oxygenic photosynthesis by the terminal reductant (e.g. hydrogen sulfide) and in the by-product generated (e.g. zero-valent sulfur) (Visscher et al., 1992; van Gemerden, 1993; Soontharapirakkul et al., 2011). The abundant *puf*LM transcripts encode photosynthetic reaction centre L and M proteins involved in the Type II reaction centres which are known occur in bacteria such as Chloroflexi, Proteobacteria and Gemmatimonadetes (Masuda et al., 2000; Zeng et al., 2014). Cyanobacteria, when conducting oxygenic photosynthesis use photosystem II (PSII) and a Type I reaction centre known as photosystem I (PSI), which were also abundantly expressed within the metatranscriptomes. The reductive pentose phosphate cycle (Calvin Benson cycle) regarded quantitatively as the most important mechanism of autotrophic CO_2 fixation in nature, is a feature of oxygenic photosynthesis in Cyanobacteria, as well as anoxygenic photosynthesis in purple sulfur bacteria and chemolithotrophic (incl. sulfide/sulfur-oxidizing) bacteria (Lengeler et al., 1998; Berg, 2011). However, the Calvin Benson cycle had the second highest level of transcription in contrast to the reductive citrate cycle (Arnon-Buchanan cycle), which is typically found in anoxygenic photosynthetic green sulfur bacteria (Chlorobi), as well as in various anaerobic or microaerobic members of Aquificae, Proteobacteria, and Nitrospirae (Hügler and Sievert, 2011). Interestingly, green sulfur bacteria use anoxygenic photosystem I and the Arnon-Buchanan cycle, but no genes were transcribed for anoxygenic photosystem I in any of the metatranscriptomes studied, suggesting that this carbon fixation pathway is primarily used by chemosynthetic organisms residing

in Shark Bay microbial mats. The higher abundance of genes transcribing anoxygenic photosystem II could be ascribed to either Alphaproteobacteria that utilise the Calvin Benson cycle or to the significant presence of green non-sulfur bacteria (Chloroflexi) that utilise the 3-hydroxypropionate bi-cycle to which was another abundantly transcribed carbon fixation pathway found in both mat types. On a further note, the Calvin Benson cycle generally operates in situations of high light intensity, therefore the presence of this pathway is primarily associated with Cyanobacteria and Alphaproteobacteria occurring in the upper layers of the mats, whereas, under low light conditions, oligotrophic organisms use the more energetically favourable Arnon-Buchanan cycle (Berg, 2011).

Methanogenesis coupled to the reductive acetyl-CoA pathway (Wood–Ljungdahl pathway) is possibly one of the most ancient metabolisms for energy generation and carbon fixation (Borrel et al., 2016). Genes associated with the Wood–Ljungdahl pathway along with methanogenic pathways (i.e. CO_2 to methane and acetate to methane) were over-represented in smooth mat metatranscriptomes. This corroborates with a previous study of Shark Bay smooth mats which reported higher rates of methane production in the presence of H_2/CO_2 as the methanogenic substrates (Wong et al., 2017). The Wood–Ljungdahl pathway is found strictly in anaerobic bacteria and archaea, such as Proteobacteria, Planctomycetes, Spirochaetes, and Euryarchaeota, that utilise a bifunctional enzyme, carbon monoxide dehydrogenase/acetyl-CoA synthase, to catalyse reactions from CO_2 to CO and from CO_2 to a methyl group, to which then acetyl-CoA is generated (Ragsdale and Pierce, 2008). High expression of genes encoding heterodisulfide reductase (*hdr*ABC2) were observed in the smooth mats. This enzyme is required for the final reaction steps of methanogenic pathways and is found in most methanogens (i.e. Euryarchaeota). Interestingly, the primary gene for methane production, *mcr*A, encoding methyl-coenzyme M reductase, was absent in all of the metatranscriptomes. This has previously been observed in metagenomes from smooth mats from Shark Bay and has been attributed to the presence of other potentially novel genes responsible for methanogenesis (Wong et al., 2018). Furthermore, both mat types exhibited an abundance of genes expressed by microorganisms capable of surviving on methane which included methylotrophic pathways such as serine and ribulose monophosphate

pathways. These pathways have been characterised in Alpha-, Beta-, and Gammaproteobacteria, Actinobacteria, Firmicutes and Verrucomicrobia, and were actively abundant in both smooth and pustular mats (Chistoserdova, 2015). The abundance of active methane producing and consuming bacteria suggests the presence of symbiotic relationships and complete cycling of methane within Shark Bay microbial mats.

3.4.4 Sulfur cycling

Genes involved in sulfur metabolism were also found to be abundantly transcribed within smooth mat metatranscriptomes, with the most abundant gene transcripts being associated with the dissimilatory and assimilatory sulfate reduction pathways. Previous studies have shown higher rates of sulfate reduction in smooth mats when compared to pustular mats from Shark Bay using the silver foil technique (Pagès et al., 2014; Wong et al., 2015, 2018). The dissimilatory pathway is typically found in anaerobic bacterial and archaeal lineages (e.g. Deltaproteobacteria and Euryarchaeota), whereas the assimilatory pathway is found in a wider range of organisms (Pereira et al., 2011). It was recently reported that the majority of draft genomes constructed from Nilemah smooth mats encode partial and complete assimilatory sulfate-reduction pathways, indicating the potential importance of sulfur respiration in the Shark Bay ecosystems (Wong et al., 2018). In this study the elevated transcription of sulfur reduction pathways suggests that this is true for smooth mats, however, sulfur respiration does not appear to be a key active function in pustular mats investigated in our study. Additionally, genes encoding sulfide:quinone reductase (*sqr*) and sulfhydrogenase subunit gamma (*hyd*G) were also abundantly expressed in smooth mats, suggesting that sulfide is being converted to polysulfide and subsequently assimilated as has been reported for intertidal microbial mats and in cultures of purple sulfur bacteria (Visscher et al., 1990; Visscher and van Gemerden, 1993).

3.4.5 Nitrogen cycling

There was no clear distribution of genes that encode nitrogen metabolising pathways between both mat types. However, genes involved in nitrogen fixation were abundantly expressed as well as other reduction pathways such as assimilatory and dissimilatory nitrate reduction. Recent taxonomic studies of Shark Bay microbial mats suggest that there are few nitrifiers present, leading to a potential incomplete cycling of nitrogen (Wong et al., 2015, 2018; Ruvindy et al., 2016). Any build-up of ammonium produced by nitrate reducing microorganisms is hypothesized to be assimilated by other members of the mat community (Wong et al., 2018). The elevated expression of glutamine synthase and glutamate synthase genes throughout the metatranscriptomes corroborates this. Additionally, a gene encoding methane/ammonia monooxygenase subunit A (*pmo*A-*amo*A) was transcribed in pustular mat metatranscriptomes. Genes encoding methane monooxygenase and ammonia monooxygenase share high sequence identity and therefore can represent members in phylogenetic groups of both methanotrophs (Alpha- and Gamma-Proteobacteria) and ammonia-oxidizing nitrifying bacteria (Beta- and Gamma-Proteobacteria) (Holmes et al., 2006). Therefore, due to the significant abundance of active Alphaproteobacteria in pustular mats, as well as there being incomplete cycling of nitrogen suggests that the *pmo*A-*amo*A gene is likely encoding methane monooxygenase.

3.4.6 Functional differences between mat types, diel cycles and sampling periods

The overall expression of individual functional genes indicated that there were no significant differences in day and night mat samples, however the results showed that samples grouped within their mat type and sampling period. This was also observed with the active microbial community distributions, which indicates that physiochemical conditions that shape microbial community structures as well as seasonal variations are significant factors influencing functional gene expression in these ecosystems. However, the combination of functional genes into the respective pathways indicated that PSI and PSII, as well as the Calvin Benson cycle were transcribed more during the day time when peak oxygen production is known to occur

(Louyakis et al., 2018). A potential reason for not observing diel changes in individual functional genes might be due to their stability. PSII is made up of two core subunits D1 and D2 encoded by *psb*A and *psb*D, while the two core subunits of PSI (A1 and A2) are encoded by *psa*A and *psa*B. Genes, *psa*A and *psa*B (PSI), and *psb*A (PSII) were highly expressed in all the samples but indicated no significant diel variation. At night, PSII transcripts, such as *psb*A, have been shown to be more stable with a half-life of 7 hours and play a role in regulating D1 production in some diazotrophic coccoid cyanobacteria, as well as being transcribed at night to form non-functional D1 proteins thereby preventing oxygen evolution during the nitrogen fixation period (Wegener et al., 2015). Additionally, cultured cyanobacteria have indicated that under high light intensity almost all of the PSI genes are downregulated to lower the susceptibility of the cells to damage, giving the appearance of no diel rhythm (Hihara et al., 1998).

3.5 Conclusions

Extant microbial mats occurring in enhanced salinity environments are unique ecological niches representative of early life on Earth. Therefore, examining the underlying ecological drivers in active microbial mat communities is essential for gaining a more detailed understanding of ancient ecosystems. Our comparative analysis of smooth and pustular mat metatranscriptomes provided a new outlook on how these communities respond and adapt to an elevated salinity and nutrient depleted environment, as well as to diel and seasonal cycles. We conclude that: 1) similarities observed between mat types and sampling periods suggests that microbial community structure and seasonality have a greater influence on the overall transcription of genes in these systems. Whereas, diel cycling showed no significant effect on the transcription of genes, however a pustular mat sampled during the night showed a large shift in the gene transcription and taxonomy based on mRNA transcripts. Therefore, in order to decipher transcriptional changes during diel cycles within these mat communities, we suggest that future studies use greater sampling and sequencing depth; 2) comparing active communities derived from rRNA and mRNA classifications indicated that the type of RNA analysed affects the outcome of the microbial diversity analysis, showing a discrepancy between the organisms present in the microbial mats; 3) a large amount of the transcribed genes were associated with

combating the low nutrient conditions present in the Nilemah tidal flat such as the uptake of fatty acids, phosphorus, iron and potentially nickel from the environment; 4) cycling of glutamine and glutamate is likely to be critical in these systems as both protective mechanism against elevated salinity conditions and stopping any build-up of ammonium produced by nitrate reducing microorganisms; 5) both mat types indicated that anoxygenic photosynthesis and the chemoautotrophic Arnon-Buchanan cycle are potentially the most important pathways related to carbon cycling; 6) the enrichment of active anaerobic pathways (e.g., sulfate reduction, methanogenesis, Wood–Ljungdahl) in smooth mats corroborates previous metagenomic studies and further advocates the potential of these communities as modern analogues of ancient microbial ecosystems.

3.6 References

Allen, M. A., Goh, F., Burns, B. P., and Neilan, B. A. (2009). Bacterial, archaeal and eukaryotic diversity of smooth and pustular microbial mat communities in the hypersaline lagoon of Shark Bay. *Geobiology* 7, 82–96. doi:10.1111/j.1472-4669.2008.00187.x.

Allwood, A. C., Walter, M. R., Kamber, B. S., Marshall, C. P., and Burch, I. W. (2006). Stromatolite reef from the Early Archaean era of Australia. *Nature* 441, 714–718. doi:10.1038/nature04764.

Assaha, D. V. M., Ueda, A., Saneoka, H., Al-Yahyai, R., and Yaish, M. W. (2017). The role of Na+ and K+ transporters in salt stress adaptation in glycophytes. *Front. Physiol.* 8. doi:10.3389/fphys.2017.00509.

Babilonia, J., Conesa, A., Casaburi, G., Pereira, C., Louyakis, A. S., Reid, R. P., et al. (2018). Comparative metagenomics provides insight into the ecosystem functioning of the Shark Bay Stromatolites, Western Australia. *Front. Microbiol.* 9. doi:10.3389/fmicb.2018.01359.

Berg, I. A. (2011). Ecological aspects of the distribution of different autotrophic CO2 fixation pathways. *Appl. Environ. Microbiol.* 77, 1925–1936. doi:10.1128/AEM.02473-10.

Borrel, G., Adam, P. S., and Gribaldo, S. (2016). Methanogenesis and the wood–ljungdahl pathway: An ancient, versatile, and fragile association. *Genome Biol. Evol.* 8, 1706–1711. doi:10.1093/gbe/evw114.

Burne, R. V., and Johnson, K. (2012). Sea-level variation and the zonation of microbialites in Hamelin Pool, Shark Bay, Western Australia. *Mar. Freshw. Res.* 63, 994–1004. doi:10.1071/MF12184.

Burns, B. P., Goh, F., Allen, M., and Neilan, B. A. (2004). Microbial diversity of extant stromatolites in the hypersaline marine environment of Shark Bay, Australia. *Environ. Microbiol.* 6, 1096–1101. doi:10.1111/j.1462-2920.2004.00651.x.

Bushmanova, E., Antipov, D., Lapidus, A., and Prjibelski, A. D. (2019). RnaSPAdes: A de novo transcriptome assembler and its application to RNA-Seq data. *Gigascience* 8. doi:10.1093/gigascience/giz100.

Bushnell, B. (2018). BBTools: a suite of fast, multithreaded bioinformatics tools designed for analysis of DNA and RNA sequence data. *Jt. Genome Institute.*

https//jgi. doe. gov/data-and-tools/bbtools.

Chistoserdova, L. (2015). Methylotrophs in natural habitats: current insights through metagenomics. *Appl. Microbiol. Biotechnol.* 99, 5763–5779. doi:10.1007/s00253-015-6713-z.

Chróst, R. J. (1994). "Microbial Enzymatic Degradation and Utilization of Organic Matter," in (Springer, New York, NY), 118–174. doi:10.1007/978-1-4612-2606-2_6.

Clarke, K. R., and Gorley, R. N. (2006). Plymouth routines in multivariate ecological research. PRIMER v6: Use manual/Tutorial. *PRIMER-E:Plymouth*, 190.

Des Marais, D. J. (1995). The biogeochemistry of hypersaline microbial mats. *Adv. Microb. Ecol.* 14, 251–274. doi:10.1007/978-1-4684-7724-5_6.

Dirusso, C. C., and Black, P. N. (2004). Bacterial long chain fatty acid transport: Gateway to a fatty acid-responsive signaling system. *J. Biol. Chem.* 279, 49563–49566. doi:10.1074/jbc.R400026200.

Dupraz, C., and Visscher, P. T. (2005). Microbial lithification in marine stromatolites and hypersaline mats. *Trends Microbiol.* 13, 429–438. doi:10.1016/j.tim.2005.07.008.

Edwards, R., and Edwards, J. A. (2019). fastq-pair: efficient synchronization of paired-end fastq files. *bioRxiv*, 552885. doi:10.1101/552885.

Goh, F., Allen, M. A., Leuko, S., Kawaguchi, T., Decho, A. W., Burns, B. P., et al. (2009). Determining the specific microbial populations and their spatial distribution within the stromatolite ecosystem of Shark Bay. *ISME J.* 3, 383–396. doi:10.1038/ismej.2008.114.

Gruber-Vodicka, H. R., Seah, B. K., and Pruesse, E. (2019). phyloFlash — Rapid SSU rRNA profiling and targeted assembly from metagenomes. *bioRxiv*, 521922. doi:10.1101/521922.

Hihara, Y., Sonoike, K., and Ikeuchi, M. (1998). A novel gene, pmgA, specifically regulates photosystem stoichiometry in the cyanobacterium Synechocystis species PCC 6803 in response to high light. *Plant Physiol.* 117, 1205–1216. doi:10.1104/pp.117.4.1205.

Hiron, A., Posteraro, B., Carrière, M., Remy, L., Delporte, C., La Sorda, M., et al. (2010). A nickel ABC-transporter of Staphylococcus aureus is involved in urinary tract infection. *Mol. Microbiol.* 77, 1246–1260. doi:10.1111/j.1365-

2958.2010.07287.x.

Holmes, A. J., Costello, A., Lidstrom, M. E., and Murrell, J. C. (2006). Evidence that participate methane monooxygenase and ammonia monooxygenase may be evolutionarily related. *FEMS Microbiol. Lett.* 132, 203–208. doi:10.1111/j.1574-6968.1995.tb07834.x.

Huerta-Cepas, J., Forslund, K., Coelho, L. P., Szklarczyk, D., Jensen, L. J., Von Mering, C., et al. (2017). Fast genome-wide functional annotation through orthology assignment by eggNOG-mapper. *Mol. Biol. Evol.* 34, 2115–2122. doi:10.1093/molbev/msx148.

Hügler, M., and Sievert, S. M. (2011). Beyond the Calvin Cycle: Autotrophic Carbon Fixation in the Ocean. *Ann. Rev. Mar. Sci.* 3, 261–289. doi:10.1146/annurev-marine-120709-142712.

Hyatt, D., Chen, G. L., LoCascio, P. F., Land, M. L., Larimer, F. W., and Hauser, L. J. (2010). Prodigal: Prokaryotic gene recognition and translation initiation site identification. *BMC Bioinformatics* 11, 119. doi:10.1186/1471-2105-11-119.

Jahnert, R., de Paula, O., Collins, L., Strobach, E., and Pevzner, R. (2012). Evolution of a coquina barrier in Shark Bay, Australia by GPR imaging: Architecture of a Holocene reservoir analog. *Sediment. Geol.* 281, 59–74. doi:10.1016/j.sedgeo.2012.08.009.

Jahnert, R. J., and Collins, L. B. (2013). Controls on microbial activity and tidal flat evolution in Shark Bay, Western Australia. *Sedimentology* 60, 1071–1099. doi:10.1111/sed.12023.

Kanehisa, M., Araki, M., Goto, S., Hattori, M., Hirakawa, M., Itoh, M., et al. (2008). KEGG for linking genomes to life and the environment. *Nucleic Acids Res.* 36, D480–D484. doi:10.1093/nar/gkm882.

Kang, Y., and Hwang, I. (2018). Glutamate uptake is important for osmoregulation and survival in the rice pathogen Burkholderia glumae. *PLoS One* 13, e0190431. doi:10.1371/journal.pone.0190431.

Kato, K., Kobayashi, T., Yamamoto, H., Nakagawa, T., Maki, Y., and Hoaki, T. (2004). Microbial mat boundaries between chemolithotrophs and phototrophs in geothermal hot spring effluents. *Geomicrobiol. J.* 21, 91–98. doi:10.1080/01490450490266334.

Klauck, G., Serra, D. O., Possling, A., and Hengge, R. (2018). Spatial organization of

different sigma factor activities and c-di-GMP signalling within the three-dimensional landscape of a bacterial biofilm. *Open Biol.* 8. doi:10.1098/rsob.180066.

Kondoh, H., Ball, C. B., and Adler, J. (1979). Identification of a methyl-accepting chemotaxis protein for the ribose and galactose chemoreceptors of Escherichia coli. *Proc. Natl. Acad. Sci. U. S. A.* 76, 260–264. doi:10.1073/pnas.76.1.260.

Langmead, B., and Salzberg, S. L. (2012). Fast gapped-read alignment with Bowtie 2. *Nat. Methods* 9, 357–359. doi:10.1038/nmeth.1923.

Lee, Y., Song, S., Sheng, L., Zhu, L., Kim, J. S., and Wood, T. K. (2018). Substrate binding protein DppA1 of ABC transporter DppBCDF increases biofilm formation in Pseudomonas aeruginosa by inhibiting Pf5 prophage lysis. *Front. Microbiol.* 9. doi:10.3389/fmicb.2018.00030.

Lengeler, J. W., Drews, G., and Schlegel, H. G. (1998). *Biology of the Prokaryotes*. doi:10.1002/9781444313314.

Li, H., Handsaker, B., Wysoker, A., Fennell, T., Ruan, J., Homer, N., et al. (2009). The Sequence Alignment/Map format and SAMtools. *Bioinformatics* 25, 2078–2079. doi:10.1093/bioinformatics/btp352.

Louyakis, A. S., Gourlé, H., Casaburi, G., Bonjawo, R. M. E., Duscher, A. A., and Foster, J. S. (2018). A year in the life of a thrombolite: comparative metatranscriptomics reveals dynamic metabolic changes over diel and seasonal cycles. *Environ. Microbiol.* 20, 842–861. doi:10.1111/1462-2920.14029.

Mackenzie, E. L., Iwasaki, K., and Tsuji, Y. (2008). Intracellular iron transport and storage: From molecular mechanisms to health implications. *Antioxidants Redox Signal.* 10, 997–1030. doi:10.1089/ars.2007.1893.

Masuda, S., Nagashima, K. V. P., Shimada, K., and Matsuura, K. (2000). Transcriptional control of expression of genes for photosynthetic reaction center and light-harvesting proteins in the purple bacterium Rhodovulum sulfidophilum. *J. Bacteriol.* 182, 2778–2786. doi:10.1128/JB.182.10.2778-2786.2000.

Mobberley, J. M., Khodadad, C. L. M., and Foster, J. S. (2013). Metabolic potential of lithifying cyanobacteria-dominated thrombolitic mats. *Photosynth. Res.* 118, 125–140. doi:10.1007/s11120-013-9890-6.

Morohoshi, T., Yokoyama, Y., Ouchi, M., Kato, N., and Ikeda, T. (2009). Motility and the expression of the flagellin protein FliC are negatively regulated by quorum

sensing in Edwardsiella tarda. *J. Biosci. Bioeng.* 108, 314–318. doi:10.1016/j.jbiosc.2009.04.006.

Morris, T. E., Visscher, P. T., O'Leary, M. J., Fearns, P. R. C. S., and Collins, L. B. (2020). The biogeomorphology of Shark Bay's microbialite coasts. *Earth-Science Rev.*, 102921. doi:10.1016/j.earscirev.2019.102921.

Muñoz-Elías, E. J., Marcano, J., and Camilli, A. (2008). Isolation of Streptococcus pneumoniae biofilm mutants and their characterization during nasopharyngeal colonization. *Infect. Immun.* 76, 5049–5061. doi:10.1128/IAI.00425-08.

Muro-Pastor, M. I., Reyes, J. C., and Florencio, F. J. (2005). Ammonium assimilation in cyanobacteria. *Photosynth. Res.* 83, 135–150. doi:10.1007/s11120-004-2082-7.

Noffke, N., Christian, D., Wacey, D., and Hazen, R. M. (2013). Microbially induced sedimentary structures recording an ancient ecosystem in the ca. 3.48 Billion-year-old dresser formation, pilbara, Western Australia. *Astrobiology* 13, 1103–1124. doi:10.1089/ast.2013.1030.

P. Hoffman, B. W. Logan, C. D. Gebe (1972). Algal Mats, Cryptalgal Fabrics, and Structures, Hamelin Pool, Western Australia: ABSTRACT. *Am. Assoc. Pet. Geol. Bull.* 56, 628–628. doi:10.1306/819a3f6a-16c5-11d7-8645000102c1865d.

Pagès, A., Grice, K., Ertefai, T., Skrzypek, G., Jahnert, R., and Greenwood, P. (2014). Organic geochemical studies of modern microbial mats from Shark Bay: Part I: Influence of depth and salinity on lipid biomarkers and their isotopic signatures. *Geobiology* 12, 469–487. doi:10.1111/gbi.12094.

Papenfort, K., and Bassler, B. L. (2016). Quorum sensing signal-response systems in Gram-negative bacteria. *Nat. Rev. Microbiol.* 14, 576–588. doi:10.1038/nrmicro.2016.89.

Parks, D. H., Tyson, G. W., Hugenholtz, P., and Beiko, R. G. (2014). STAMP: Statistical analysis of taxonomic and functional profiles. *Bioinformatics* 30, 3123–3124. doi:10.1093/bioinformatics/btu494.

Pereira, I. A. C., Ramos, A. R., Grein, F., Marques, M. C., da Silva, S. M., and Venceslau, S. S. (2011). A comparative genomic analysis of energy metabolism in sulfate reducing bacteria and archaea. *Front. Microbiol.* 2. doi:10.3389/fmicb.2011.00069.

Proemse, B. C., Eberhard, R. S., Sharples, C., Bowman, J. P., Richards, K., Comfort,

M., et al. (2017). Stromatolites on the rise in peat-bound karstic wetlands. *Sci. Rep.* 7, 15384. doi:10.1038/s41598-017-15507-1.

Ragsdale, S. W., and Pierce, E. (2008). Acetogenesis and the Wood-Ljungdahl pathway of CO2 fixation. *Biochim. Biophys. Acta - Proteins Proteomics* 1784, 1873–1898. doi:10.1016/j.bbapap.2008.08.012.

Rutherford, S. T., and Bassler, B. L. (2012). Bacterial quorum sensing: Its role in virulence and possibilities for its control. *Cold Spring Harb. Perspect. Med.* 2. doi:10.1101/cshperspect.a012427.

Ruvindy, R., White, R. A., Neilan, B. A., and Burns, B. P. (2016). Unravelling core microbial metabolisms in the hypersaline microbial mats of Shark Bay using high-throughput metagenomics. *ISME J.* 10, 183–196. doi:10.1038/ismej.2015.87.

Salah Ud-Din, A. I. M., and Roujeinikova, A. (2017). Methyl-accepting chemotaxis proteins: a core sensing element in prokaryotes and archaea. *Cell. Mol. Life Sci.* 74, 3293–3303. doi:10.1007/s00018-017-2514-0.

Skyring, G. W., Lynch, R. M., and Smith, G. D. (1988). Acetylene reduction and hydrogen metabolism by a cyanobacterial/sulfate-reducing bacterial mat ecosystem. *Geomicrobiol. J.* 6, 25–31. doi:10.1080/01490458809377819.

Soontharapirakkul, K., Promden, W., Yamada, N., Kageyama, H., Incharoensakdi, A., Iwamoto-Kihara, A., et al. (2011). Halotolerant cyanobacterium Aphanothece halophytica contains an Na +-dependent F1F0-ATP synthase with a potential role in salt-stress tolerance. *J. Biol. Chem.* 286, 10169–10176. doi:10.1074/jbc.M110.208892.

Suosaari, E. P., Reid, R. P. R., Araujo, T. A. A., Playford, P. E., Holley, D. K., McNamara, K. J., et al. (2016). Environmental Pressures Influencing Living Stromatolites in Hamelin Pool, Shark Bay, Western Australia. *Palaios* 31, 483–496. doi:10.2110/palo.2016.023.

Team, R. C. (2018). R Development Core Team. R: A language and environment for statistical computing. R Foundation for Statistical Computing, Vienna, Austria; 2014. *Google Sch.*

van Gemerden, H. (1993). Microbial mats: A joint venture. *Mar. Geol.* 113, 3–25. doi:10.1016/0025-3227(93)90146-M.

Van Kranendonk, M. J., Philippot, P., Lepot, K., Bodorkos, S., and Pirajno, F. (2008).

Geological setting of Earth's oldest fossils in the ca. 3.5 Ga Dresser Formation, Pilbara Craton, Western Australia. *Precambrian Res.* 167, 93–124. doi:10.1016/j.precamres.2008.07.003.

Varin, T., Lovejoy, C., Jungblut, A. D., Vincent, W. F., and Corbeil, J. (2010). Metagenomic profiling of Arctic microbial mat communities as nutrient scavenging and recycling systems. *Limnol. Oceanogr.* 55, 1901–1911. doi:10.4319/lo.2010.55.5.1901.

Vega, L. M., Mathieu, J., Yang, Y., Pyle, B. H., McLean, R. J. C., and Alvarez, P. J. J. (2014). Nickel and cadmium ions inhibit quorum sensing and biofilm formation without affecting viability in Burkholderia multivorans. *Int. Biodeterior. Biodegrad.* 91, 82–87. doi:10.1016/j.ibiod.2014.03.013.

Visscher, P. T., Nijburg, J. W., and van Gemerden, H. (1990). Polysulfide utilization by Thiocapsa roseopersicina. *Arch. Microbiol.* 155, 75–81. doi:10.1007/BF00291278.

Visscher, P. T., and Stolz, J. F. (2005). "Microbial mats as bioreactors: Populations, processes, and products," in *Geobiology: Objectives, Concepts, Perspectives* (Elsevier B.V.), 87–100. doi:10.1016/B978-0-444-52019-7.50009-7.

Visscher, P. T., van den Ende, F. P., Schaub, B. E. M., and van Gemerden, H. (1992). Competition between anoxygenic phototrophic bacteria and colorless sulfur bacteria in a microbial mat. *FEMS Microbiol. Lett.* 101, 51–58. doi:10.1111/j.1574-6968.1992.tb05761.x.

Visscher, P. T., and van Gemerden, H. (1993). "Sulfur Cycling in Laminated Marine Microbial Ecosystems," in *Biogeochemistry of Global Change* (Springer US), 672–690. doi:10.1007/978-1-4615-2812-8_37.

von Ballmoos, C., Wiedenmann, A., and Dimroth, P. (2009). Essentials for ATP Synthesis by F 1 F 0 ATP Synthases. *Annu. Rev. Biochem.* 78, 649–672. doi:10.1146/annurev.biochem.78.081307.104803.

Wegener, K. M., Nagarajan, A., and Pakrasi, H. B. (2015). An atypical psbA gene encodes a sentinel D1 protein to form a physiologically relevant inactive photosystem II complex in cyanobacteria. *J. Biol. Chem.* 290, 3764–3774. doi:10.1074/jbc.M114.604124.

White, R. A., Chan, A. M., Gavelis, G. S., Leander, B. S., Brady, A. L., Slater, G. F., et al. (2016). Metagenomic analysis suggests modern freshwater microbialites

harbor a distinct core microbial community. *Front. Microbiol.* 6, 1531. doi:10.3389/fmicb.2015.01531.

White, R. A., Power, I. M., Dipple, G. M., Southam, G., and Suttle, C. A. (2015). Metagenomic analysis reveals that modern microbialites and polar microbial mats have similar taxonomic and functional potential. *Front. Microbiol.* 6, 966. doi:10.3389/fmicb.2015.00966.

Wimpenny, J., Manz, W., and Szewzyk, U. (2000). Heterogeneity in biofilms: Table 1. *FEMS Microbiol. Rev.* 24, 661–671. doi:10.1111/j.1574-6976.2000.tb00565.x.

Wong, H., Ahmed-Cox, A., and Burns, B. (2016). Molecular Ecology of Hypersaline Microbial Mats: Current Insights and New Directions. *Microorganisms* 4, 6. doi:10.3390/microorganisms4010006.

Wong, H. L., Smith, D. L., Visscher, P. T., and Burns, B. P. (2015). Niche differentiation of bacterial communities at a millimeter scale in Shark Bay microbial mats. *Sci. Rep.* 5, 15607. doi:10.1038/srep15607.

Wong, H. L., Visscher, P. T., White, R. A., Smith, D. L., Patterson, M. M., and Burns, B. P. (2017). Dynamics of archaea at fine spatial scales in Shark Bay mat microbiomes. *Sci. Rep.* 7, 1–12. doi:10.1038/srep46160.

Wong, H. L., White, R. A., Visscher, P. T., Charlesworth, J. C., Vázquez-Campos, X., and Burns, B. P. (2018). Disentangling the drivers of functional complexity at the metagenomic level in Shark Bay microbial mat microbiomes. *ISME J.* 12, 2619–2639. doi:10.1038/s41396-018-0208-8.

Zeng, Y., Feng, F., Medová, H., Dean, J., and Koblížek, M. (2014). Functional type 2 photosynthetic reaction centers found in the rare bacterial phylum Gemmatimonadetes. *Proc. Natl. Acad. Sci. U. S. A.* 111, 7795–7800. doi:10.1073/pnas.1400295111.

Zhou, M., Guo, Z., Yang, Y., Duan, Q., Zhang, Q., Yao, F., et al. (2014). Flagellin and F4 fimbriae have opposite effects on biofilm formation and quorum sensing in F4ac+ enterotoxigenic Escherichia coli. *Vet. Microbiol.* 168, 148–153. doi:10.1016/j.vetmic.2013.10.014.

Zhu, Y., Ma, N., Jin, W., Wu, S., and Sun, C. (2017). Genomic and transcriptomic insights into calcium carbonate biomineralization by marine actinobacterium Brevibacterium linens BS258. *Front. Microbiol.* 8. doi:10.3389/fmicb.2017.00602.

3.7 Supplementary material

Supplementary Table 3.1 Summary of the mat types collected with sampling dates and times, and field measurements of salinity, pH and water temperature. *Indicating paired Day/Night samples in the 2016 sampling trip. Elevation as measured by DGPS, approx. values derived from contoured LiDAR and hyperspectral bathymetry DTM's (see Morris et al in press for method (1)). Biogeomorphic Unit, TMMU = Transitional Microbilite Mosaic Unit, MPU = Mat Platform Unit (terminology after Morris et al in press). Geomorphic unit, terminology after Nordstrom and Jackson, 2012 (2). Note: Samples were collected under spring tide conditions.

Sample ID	Sampling date	UTM Coordinates (Zone 50)	Day/Night	Sampling time	Subsampling time	Salinity (‰)	pH	Water temp (°C)	Elevation (mAHD)	Biogeomorphic unit	Geomorphic setting	Morphological feature
Pustular Mat 1	7/5/2016	210428, 7071152	Day	12:40 PM	3:10 PM	67	7.94	13.2	-0.32	TMMU	inter-tidal terrace front	microbialite ridge crest
Pustular Mat 2*	7/5/2016	210386, 7071116	Day	12:10 PM	3:00 PM	66	8.06	13.2	0.01	MPU	mid-intertidal terrace	continuous mat sheet
Pustular Mat 3*	7/6/2016	210386, 7071116	Night	11:45 PM	5:00 AM	66	8.28	13.1	0.01	MPU	mid-intertidal terrace	continuous mat sheet
Pustular Mat 4	4/10/2017	210421, 7071167	Day	8:30 AM	11:45 PM	70	7.51	18	~ -0.25	TMMU	inter-tidal terrace front	microbialite ridge crest
Pustular Mat 5	4/11/2017	210421, 7071167	Night	10:00 PM	4:15 AM	70	8.12	16	~ -0.25	TMMU	inter-tidal terrace front	microbialite ridge crest
Smooth Mat 1	7/5/2016	210390, 7071195	Day	12:00 PM	2:45 PM	66	7.99	13.2	-0.42	TMMU	inter-tidal terrace front	swale between microbialite ridges
Smooth Mat 2*	7/5/2016	210387, 7071191	Day	12:30 PM	2:30 PM	67	7.93	13.2	-0.42	TMMU	inter-tidal terrace front	swale between microbialite ridges
Smooth Mat 3*	7/6/2016	210387, 7071191	Night	12:00 AM	5:10 AM	66	8.28	13.1	-0.42	TMMU	inter-tidal terrace front	swale between microbialite ridges
Smooth Mat 4	4/10/2017	210421, 7071167	Day	8:45 PM	12:00 PM	70	7.51	18	~ -0.4	TMMU	inter-tidal terrace front	swale between microbialite ridges
Smooth Mat 5	4/11/2017	210421, 7071167	Night	10:15 PM	4:20 PM	70	8.12	16	~ -0.4	TMMU	inter-tidal terrace front	swale between microbialite ridges

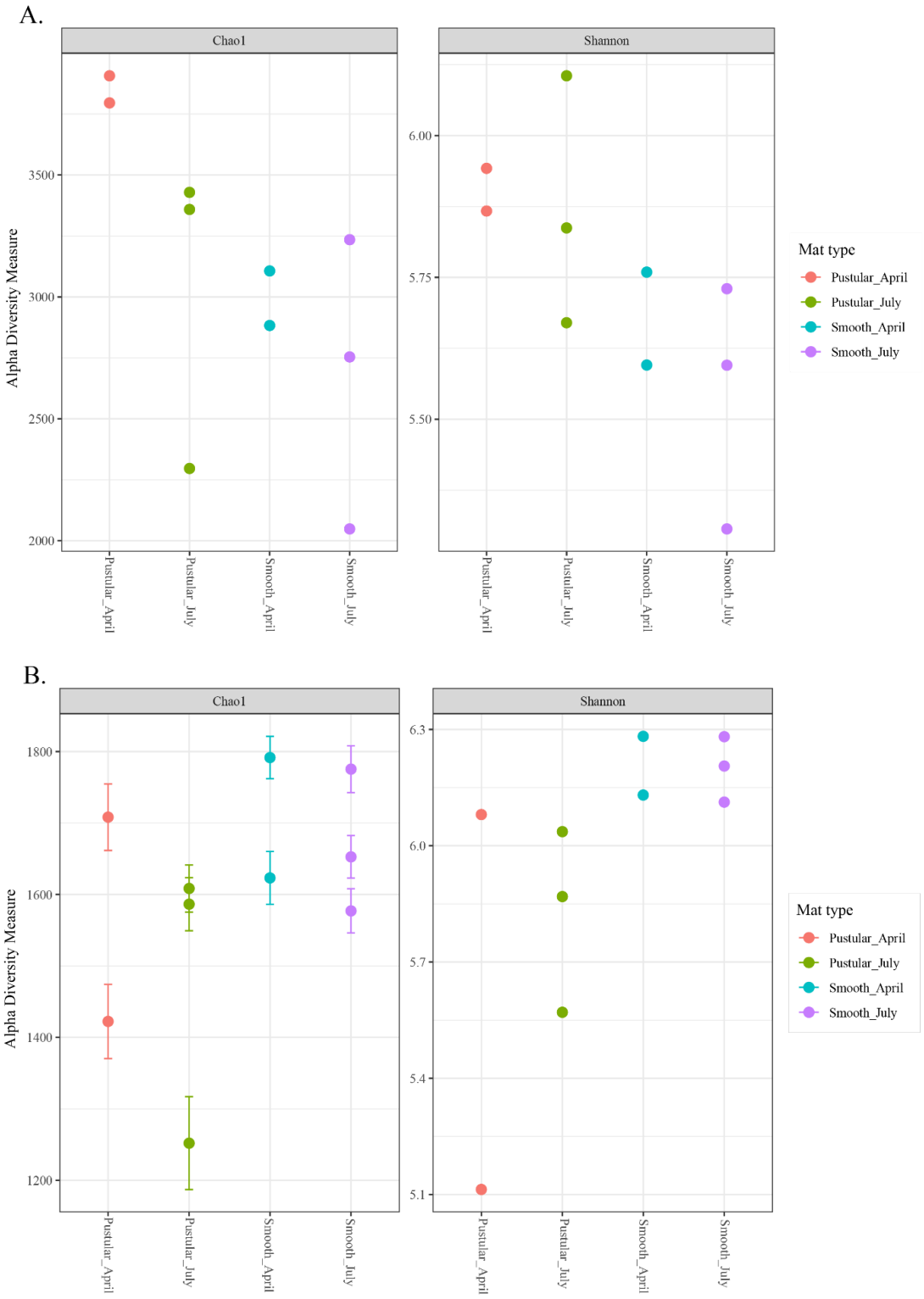

Supplementary Figure 3.1 Pustular and smooth mat alpha diversity represented by the Choa1 and Shannon's diversity indices. A. SSU rRNA (SILVA) and B. Transcripts (RefSeq).

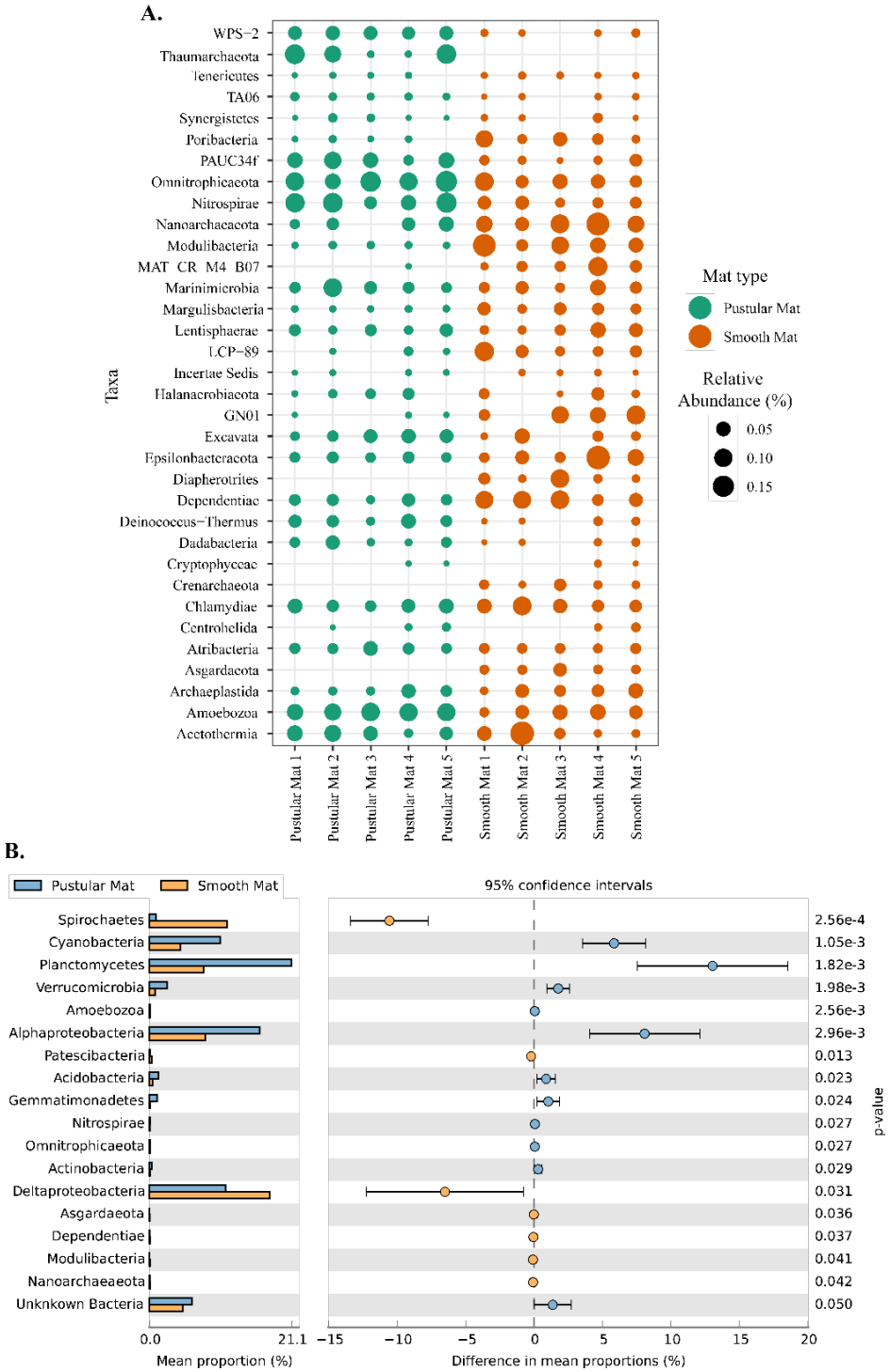

Supplementary Figure 3.2 Composition of Archaea, Bacteria and Eukaryote taxa in Nilemah smooth and pustular mats based on SSU rRNA genes (SILVA Database). A. Dot plot displaying the composition and abundance of the low abundant taxa. B. Extended error bar plot identifying significant differences ($p < 0.5$) between mean proportions of microbial taxa in smooth and pustular mats (ANOVA, Tukey's t-test). Mats 1, 2 and 3 were sample in July 2016; mats 4 and 5 were sampled in April 2017. Pustular and smooth mats 2 and 3 are the paired samples from July 2016.

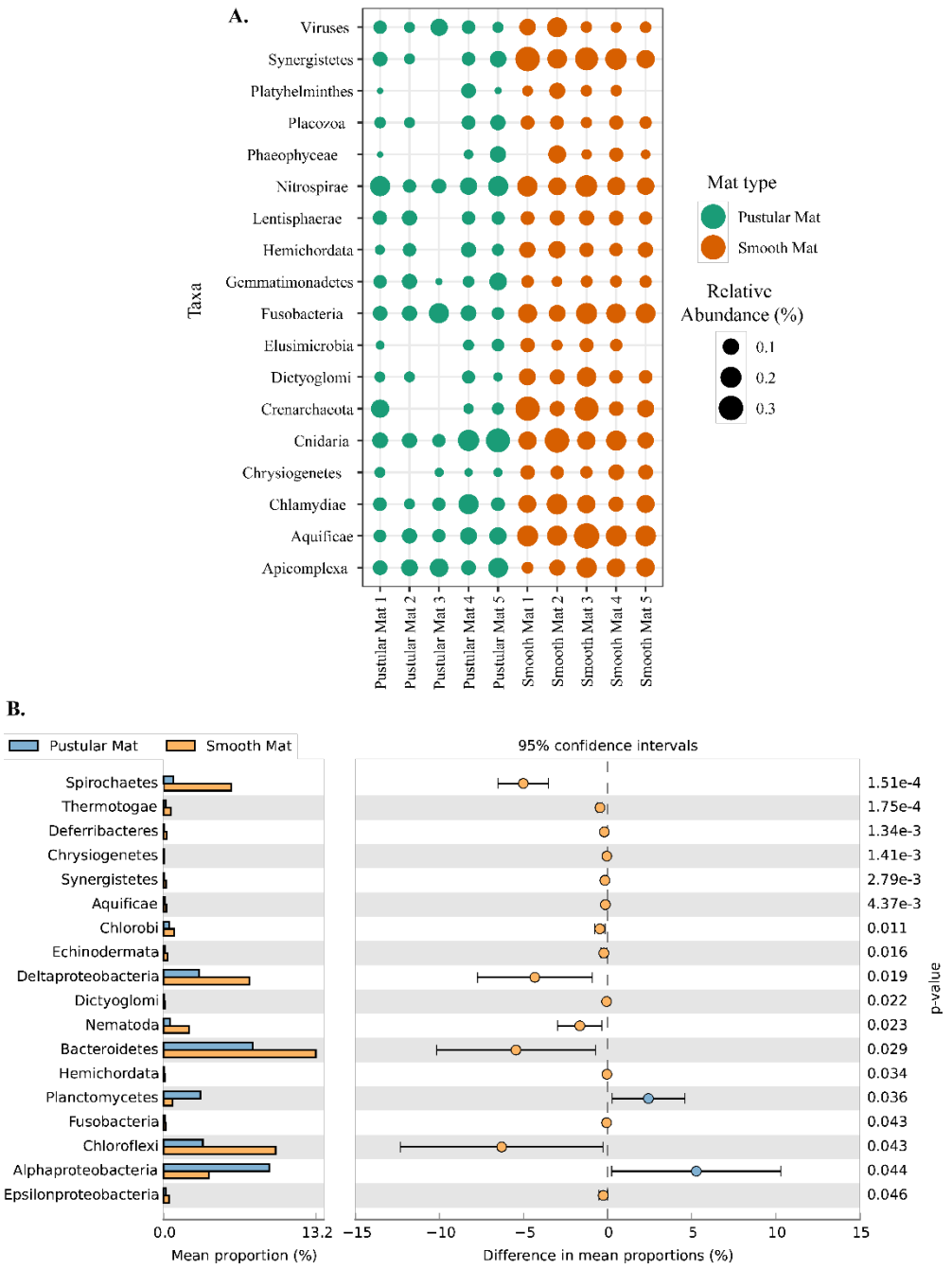

Supplementary Figure 3.3 Composition of Archaea, Bacteria and Eukaryote taxa in Nilemah smooth and pustular mats based on transcripts (RefSeq Database). A. Dot plot displaying the composition and abundance of the low abundant taxa. B. Extended error bar plot identifying significant differences ($p < 0.5$) between mean proportions of microbial taxa in smooth and pustular mats (ANOVA, Tukey's t-test). Mats 1, 2 and 3 were sample in July 2016; mats 4 and 5 were sampled in April 2017. Pustular and smooth mats 2 and 3 are the paired samples from July 2016.

Chapter 4

Structure and function of Shark Bay microbial communities following tropical cyclone Olwyn: a metatranscriptomic and organic geochemical perspective

This chapter is currently under review in Geobiology.

4.1. Background

Since the 1970s, sedimentologists have shifted their attention to episodic events, such as cyclic deposits caused by storm activities in both modern and ancient strata. Storm deposits, commonly referred to as 'tempestites', provide valuable tools in paleoenvironmental, stratigraphic and reservoir analysis as well as predicting cyclonic trends under global warming scenarios (Chuanmao et al., 1993). Tempestites are widespread in the rock record ranging from Precambrian to Holocene aged deposits, but their frequency varies from one geological period to another (Laajoki, 1996; Williams, 2011). Many well-preserved storm deposits associated with microbially derived structures (e.g. stromatolites) have been interpreted in Miocene limestones from Northern Bulgaria, Middle to Upper Cambrian strata from the North China Platform and Precambrian mixed carbonate-siliclastic sediments from East Greenland (Fairchild and Herrington, 1989; Chuanmao et al., 1993; Koleva-Rekalova and Dobrev, 2019). These deposits are interpreted in supra- to intertidal zones from lagoonal settings with the presence of carbonate conglomerates, stromatolites and wave-laminated micrite suggested as indicators for this depositional environment. Past cyclonic activity has been deciphered from reliable proxy techniques, including sedimentological, paleontological, and organic geochemical and stable isotopic indicators (Fan and Liu, 2008).

Shark Bay is episodically impacted by tropical cyclones that generate strong storm surges capable of reworking, transporting and depositing marine sediments (Jahnert et al., 2012). During March 2015, Shark Bay was hit by a category 3 cyclone, "severe tropical cyclone (TC) Olwyn", with destructive wind gusts of up to 140

kilometres per hour and a [record] total of 122 mm of rain fell in 24 hours measured at the Shark Bay airport. After the storm, the formation of black sludge was observed in a southern region of Hamelin Pool in Shark Bay covering parts of the intertidal zone (Morris et al in prep). The black sludge is suggested to consist of sloughed microbial mats, other eroded and released benthic mucilaginous materials, eroded algae and suspended material released from the sedimentary substrate and discharged into Hamelin Pool during the storm (Morris et al in prep). These [released] exopolymeric substances (EPS) were observed to form a mucilaginous floc within the water column in the days that the followed the storm. The material settled and underwent biological and physical consolidation processes forming deposits of various thicknesses (Morris et al in prep). Thick deposits occurred/were mapped between microbialitic structures within the mid-intertidal zone (TMMU of Morris et al., 2020) and in protected areas of the upper intertidal zone (MPU) (Morris et al in prep). In the Upper intertidal zone these were reworked into cobble sized mucilaginous clasts (mud balls) close to the base of the beach face (BFU/MPU boundary of Morris et al., 2020). Thin sheets of mucilaginous floc adhered to both mats and sediments (Morris et al., in prep). Mucilaginous mud balls formed following cycles of low tide exposure and desiccation and high tide inundation and wave reworking, in some sludge accumulations, most commonly at the base of the beach face (Morris et al., in prep). Upon returning to the impacted site in July 2016 (481 days after the cyclone), [it was found that] the black sludge deposits were still recognisable between microbialite columns and mucilaginous cobbles were still present closer to the shoreline in the impacted area. The reworking and deposition of mucilaginous sediments in microbial dominated ecosystems may lead to the potential archiving of unique geological and biological signatures. The storm generated materials in Shark Bay represent modern analogues of storm deposits found throughout the geological record providing insights into how microbialite-forming communities respond and recover after cyclonic events and potentially provide new biomarker indicators of episodic events in hypersaline lagoonal settings.

The ability of an ecosystem to adapt to significant changes under natural environmental conditions depends on the duration and intensity of these changes and the overall biological diversity of the system (Preisner et al., 2016). Many ecosystems are influenced by episodic events that cause fluctuations in abiotic factors (e.g.,

nutrients, pH, light, temperature, and salinity). Microbial communities often have significant biological diversity, which control the biogeochemical processes that form the foundation of these ecosystems (Azam and Malfatti, 2007). Here, we obtained gene expression profiles (metatranscriptomes) and organic geochemical compositions (lipid biomarkers) of cyclone derived materials and microbial mats from a cyclone impacted microbial ecosystem. This investigation had three specific objectives: 1) to understand the ecological functioning and stability of hypersaline microbial communities after a cyclonic event by contrasting the active and resident microbial communities, biogeochemical cycles (e.g. sulfur and nitrogen), and stress and defence mechanisms; 2) to obtain hydrocarbon biomarker distributions, together with their stable carbon isotopic compositions, to provide additional insight into the organic matter source and relation of the samples to one another; 3) evaluate if the microbial activity occurring within the cobble will lead to biomineralization and biomarker preservation.

4.2 Methodology

4.2.1 Site and sample descriptions

Microbial mats and cyclone derived materials were sampled from the RRBS monitoring site (Morris et al., 2020) on the south eastern coast/shore(line) of Hamelin Pool (Figure 4.1). The RRBS monitoring site lies at the southern end of a bight (sensu Logan and Cebulski, 1970), north of Flint Cliff, at the mouth of an outwash drainage channel that flows episodically during rare high rainfall events such as TC Olwyn. At this location the steep beach face abuts a more gently sloping intertidal terrace across which a number of distinct biogeomorphological units have been defined (Morris et al., 2020). Samples were collected from within the intertidal zone across a number of different biogeomorphological units both within the mouth of the channel and beyond. Summary of sampling times, biogeomorphic units, and physical properties can be found in Supplementary Table 4.1.

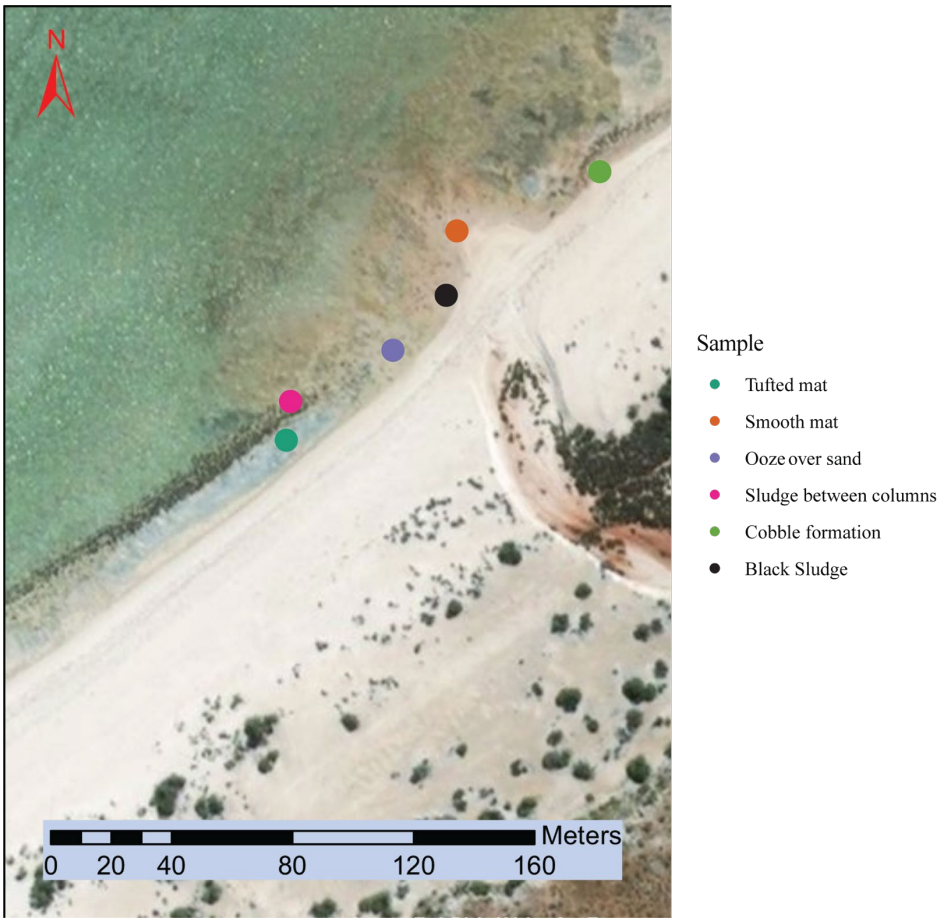

Figure 4.1 Sampling locations of microbial mats (smooth and tufted), ooze over sand (post cyclone formed deposit) and black sludge derived materials (black sludge, sludge between columns and cobble formation collected from RRBS. Satellite image was generated with ArcGIS Desktop: Release 10. Redlands, CA: Environmental Systems Research Institute (source: Maxar – 11/02/2019).

Sampling occurred twice, the initial sample of black sludge was collected in 2015 and all other samples were collected in 2016 (Figure 4.1). The cyclone derived black sludge deposits, sludge between columns (SBC) and cobble, were sampled within the transitional microbial mosaic and outer edge of the breccia platform unit, respectively. The outer light brown section (CO) and inner black section (CI) of the cobble were sampled (see Figure 4.9). The ooze over sand (OVS) was sampled within the outwash channel subunit within the mat platform unit and was also generated during the cyclonic event. The OVS is described as a thin mucilaginous sheet deposited as floc/ooze on a newly formed sand sheet that by 2016 was transitioning into a microbial mat (Morris et al in prep). The smooth mat (SM) was also sampled in the outwash channel subunit within the mat platform unit, this mat had formed over sand ripples and was uniformly laminated with a pale brown-green surface. The tufted mat

(TM) was sampled in the mat platform unit, this mat was dark green and had the distinctive laminated scalloped fabric (Logan et al., 1974).

4.2.2 Genomic and lipid biomarker analysis

Metatranscriptomic analysis is detailed in Section 2.2 – Chapter 2. RNA isolation, library preparation and sequencing (2.2.1), and bioinformatics (2.2.2). Illumina HiSeq 2500 pair-end sequencing read output with percentage summaries of trimmed and aligned sequences, number of assembled transcripts and number of annotations for Phyloflash, MG-RAST and DIAMOND can be found in Supplementary Table 2.1. Lipid biomarker analysis is detailed in Section 2.3 – Chapter 2. Lipid extraction and lipid fractionation (2.3.2), Raney-Nickel desulfurization (2.3.4), GC-MS (2.3.5), GCxGC-TOFMS (2.3.6) and irGC-MS (2.3.7). Statistical analysis and visualisation are detailed in Section 2.4 – Chapter 2.

4.3. Results

4.3.1 Microbial community structure

The alpha diversity was estimated for both SSU rRNA and transcript derived classifications with the Shannon diversity index and Choa1 species richness estimator. Shannon index of diversity for SSU rRNA classifications ranged from 5.41 to 6.05, averaging lower than the transcript classifications that ranged from 5.55 to 6.37 (Supplementary Figure 4.1). The SM had the highest diversity of active microbes, whereas the TM had the lowest. Chao1 species richness estimator revealed that richness for SSU rRNA classifications varied from 1950 to 4000 and from 1340 to 1570 in transcript classifications. Both classification methods indicated that Proteobacteria, predominately the Alpha, Delta and Gamma classes, as well as Bacteroidetes, Planctomycetes, Cyanobacteria and Chloroflexi were the prominent taxa among the samples (Figures 4.2A and 4.3A). Principle component analysis (PCA) of both classifications revealed two groupings of the samples; Group 1 containing the OVS, TM and SM, and Group 2 containing the SBC, CO and CI (Figures 4.2B and 4.3B). Based on these PCA groupings, Chloroflexi, Cyanobacteria and Deinococcus-Thermus were significantly (P-value < 0.1) more represented in Group 1 samples,

whereas Group 2 had significantly higher abundances of Acidobacteria, Bacteroidetes, Calditrichaeota, Deltaproteobacteria, Kiritimatiellaeota, Spirochaetes, Synergistetes and Zixibacteria (Supplementary Figures 4.2 A and B).

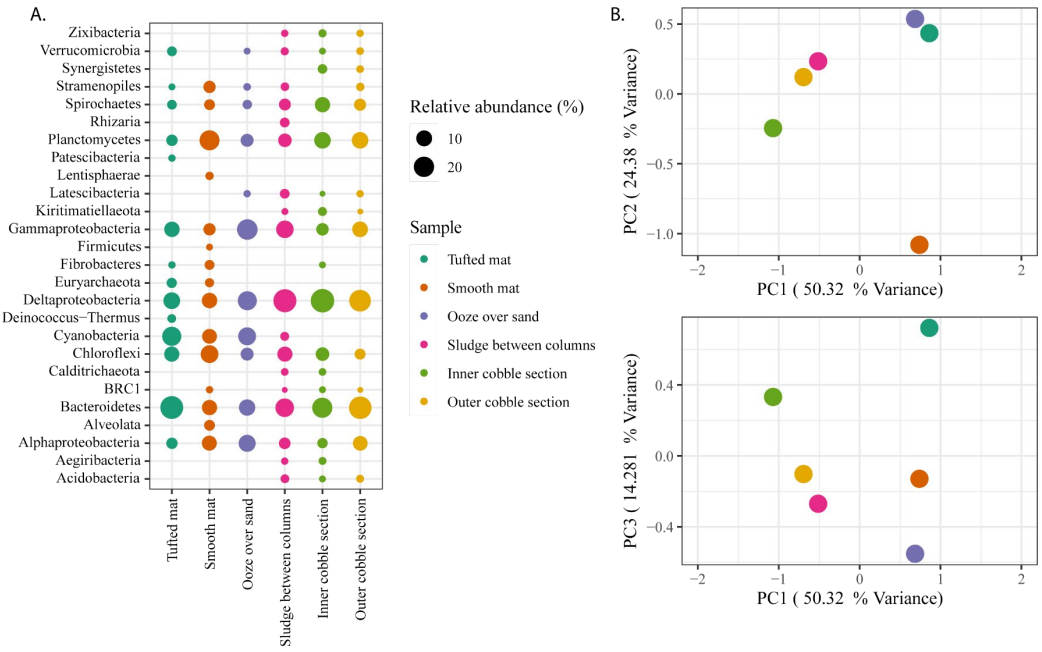

Figure 4.2 Composition of Archaea, Bacteria and Eukaryote taxa in RRBS samples based on SSU rRNA genes (SILVA Database). A. Dot plot displaying the composition and abundance of taxa (< 0.5 %). B. PCA plots constructed from similarity matrices.

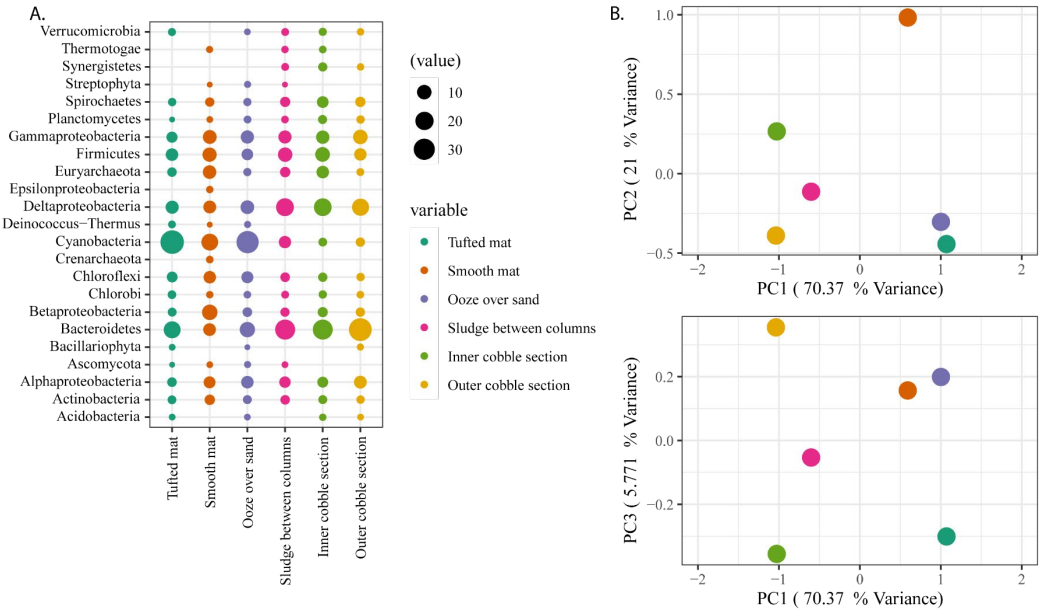

Figure 4.3 Composition of Archaea, Bacteria and Eukaryote taxa in RRBS samples based on transcripts (RefSeq Database). A. Dot plot displaying the composition and abundance of taxa (< 0.5 %). B. PCA plots constructed from similarity matrices.

4.3.2 Ecological functioning

PCA of the genes transcribing nitrogen and sulfur metabolisms, as well as stress response indicated similar groupings of the samples as the taxonomic analysis (Supplementary Figure 4.2). Particularly low amounts of variance were observed to occur between the TM and OVS, and SBC and CO samples, however CI and CO showed lower amounts of variance in expressed genes relating to stress response. Based on the PCA groupings, genes involved in nitrogen fixation, cyanate hydrolysis, ammonia assimilation, inorganic sulfur assimilation, sigmaB stress response regulation and copper homeostasis were significantly ($P < 0.1$) more expressed in Group 1 samples. Whereas, genes involved in sulfate reduction-associated complexes, thioredoxin-disulfide reductase, galactosylceramide and sulfatide metabolism, zinc resistance, periplasmic stress response, glutathione-dependent pathway of formaldehyde detoxification, oxidative stress, multidrug resistance efflux pumps and bacitracin stress response were were significantly ($P < 0.1$) more expressed in Group 2 samples (Figure 4.4).

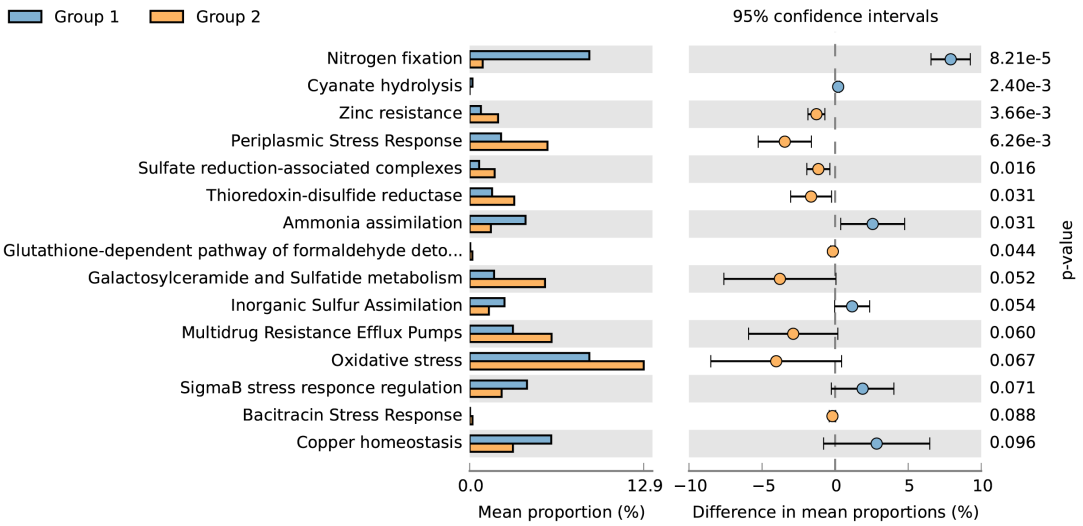

Supplementary Figure 4.4 Extended error bar plot identifying significant differences ($p < 0.1$) between mean proportions of SEED subsystems level 3 pathways involved in sulfur and nitrogen metabolisms, stress response, and virulence and defence in Groups 1 and 2 (ANOVA, Tukey's t-test).

4.3.2.1 Nitrogen metabolism

Transcription of genes involved in nitrogen fixation (e.g. nitrogenase - *nifD*, *nif*H, *nif*K) and ammonia assimilation (e.g. ammonia transporter and regulating proteins;

glutamine synthase - *gif*A, *gif*B) were highly expressed in Group 1 samples (Figure 4.5). Interestingly, the nitrogenase (molybdenum-iron)-specific transcriptional regulator (*nif*A) was found to be more abundantly expressed in the Group 2 samples. Furthermore, expression of genes involved in nitrosative stress (e.g. hydroxylamine reductase – *hcp*; nitric oxide-dependent regulator - *dnr*N), denitrification (e.g. nitrous-oxide reductase – *nos*Z, *nos*D), and nitrate and nitrite ammonification (e.g. nitrite reductase – *nas*A, *nar*B) were found across all metatranscriptomes studied. Cyanobacteria had the highest portion of genes associated with nitrogen metabolism in the Group 1 samples, but they were only detected in a low amount in the SBC from Group 2. Deltaproteobacteria were found to be expressing nitrogen metabolizing genes in all the samples, however they were most prominent in Group 2 samples (Supplementary Figure 4.4 A).

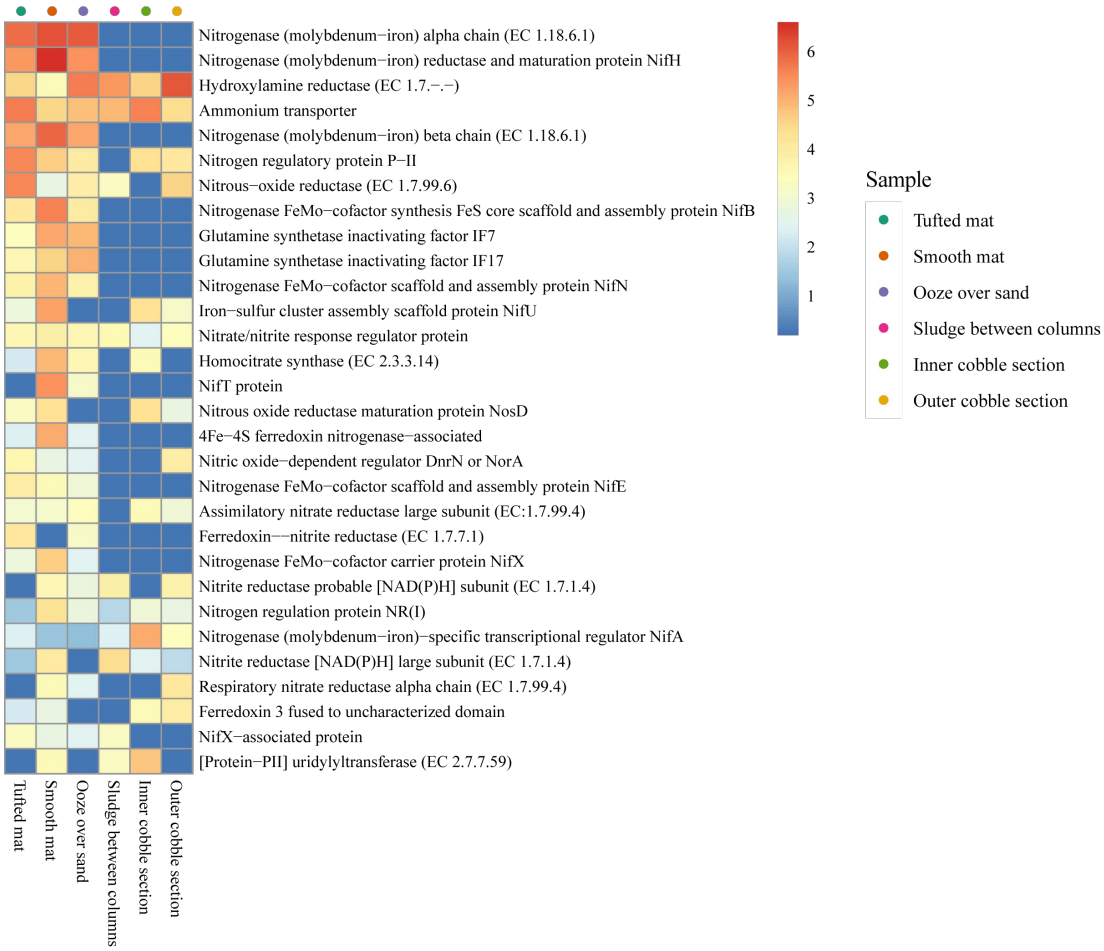

Figure 4.5 Heatmap showing the top 30 transcribed genes (>10) in RRBS metatranscriptomes related to nitrogen metabolism. Gradient from red to blue indicates gene abundance across samples with red representing genes that are highly transcribed and blue indicating genes that have lower relative

transcription. Differential analysis of the transcribed genes was calculated from the variance stabilising transformation of SEED subsystem count data using the DESeq2 package in R.

4.3.2.2 Sulfur metabolism

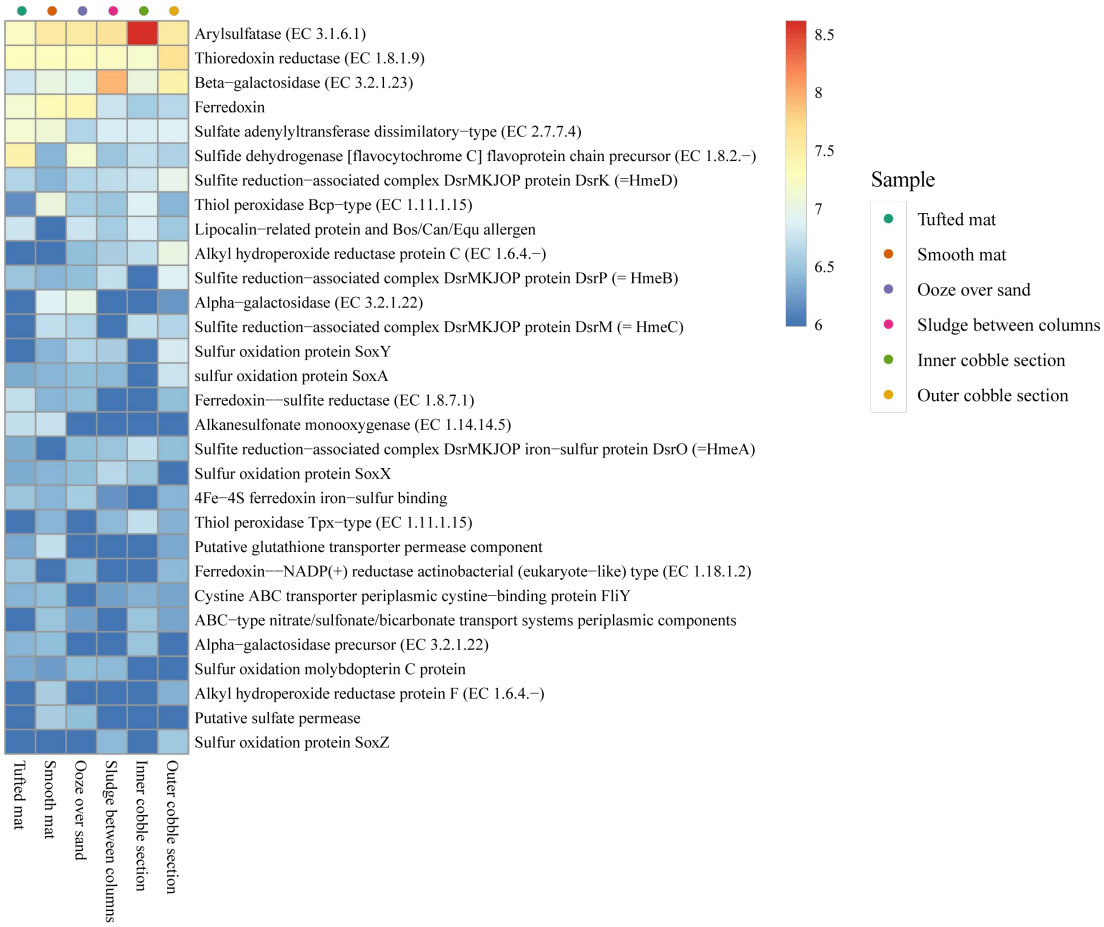

Figure 4.6 Heatmap showing the top 30 transcribed genes (>10) in RRBS metatranscriptomes related to sulfur metabolism. Differential analysis and gradient are the same as described in Figure 4.6.

Transcription of genes associated with thioredoxin-disulfide reductase (e.g. thioredoxin reductase - *trxB*, TRR; thiol peroxidase – *bcp*, *tpx*) and sulfur oxidation (e.g. sulfide dehydrogenase - *fcc*B; lipocalin-related protein; sulfur oxidation proteins – *sox*Y, *sox*A, *sox*X) were expressed across all metatranscriptomes (Figure 4.6). Genes expressing inorganic sulfur assimilation (e.g. ferredoxin; sulfate adenylyltransferase - *sat*, *met*3) were higher in Group 1 samples, whereas, genes associated with galactosylceramide and sulfatide metabolism (e.g. beta-galactosidase - *lac*Z) and sulfate reduction-associated complexes (e.g. sulfite reduction-associated complex *dsr*K, *dsr*P, *dsr*O) were expressed more in Group 2 samples. Arylsulfatase (*asl*A) associated with both alkanesulfonate assimilation, and galactosylceramide and

sulfatide metabolism was expressed in all samples, but predominantly in the CI sample. Deltaproteobacteria were found to have the highest relative proportion of genes associated with sulfur metabolism in all the samples, however cyanobacteria occurring in samples from Group 1 exhibited an increased expression of sulfur metabolizing genes related to anabolic processes (Supplementary Figure 4.4 B).

4.3.2.3 Stress response

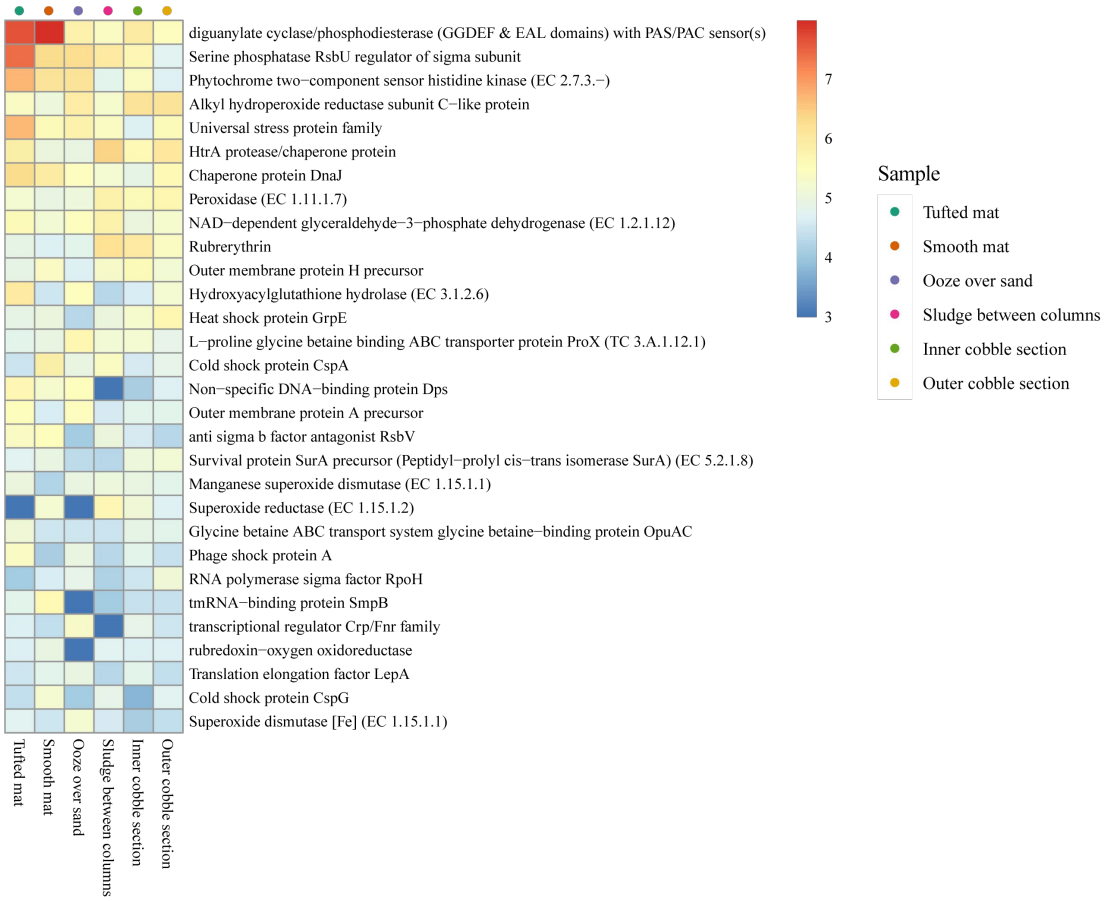

Figure 4.7 Heatmap showing the top 30 transcribed genes (>10) in RRBS metatranscriptomes related to stress response. Differential analysis, gradient and B. PCA are the same as Figure 4.6.

Genes involved in bacterial hemoglobins (e.g. diguanylate cyclase/phosphodiesterase) and SigmaB stress response regulation (e.g. serine phosphatase R*sb*U; anti sigmaB factor - R*sb*V) were the most abundantly expressed genes related to stress responses across all metatranscriptomes, however they were especially upregulated in Group 1 samples (Figure 4.7). Additionally, genes associated with periplasmic (e.g. protease/chaperone protein – H*tr*A) and osmotic stress (e.g. Glycine betaine ABC

transport system glycine betaine-binding protein - O*pu*AC) were found to be expressed in all metatranscriptomes (Figure 4.8). Genes involved in oxidative stress (e.g. Alkyl hydroperoxide reductase – *ahp*C; glyceraldehyde 3-phosphate dehydrogenase - *gapA*) were expressed in all the samples, however phytochrome two-component sensor histidine kinase (HK) was found to be more abundantly expressed in Group 1 samples, whereas rubrerythrin and superoxide reductase were more abundant in Group 2 samples.

4.3.2.4 Virulence and Defence

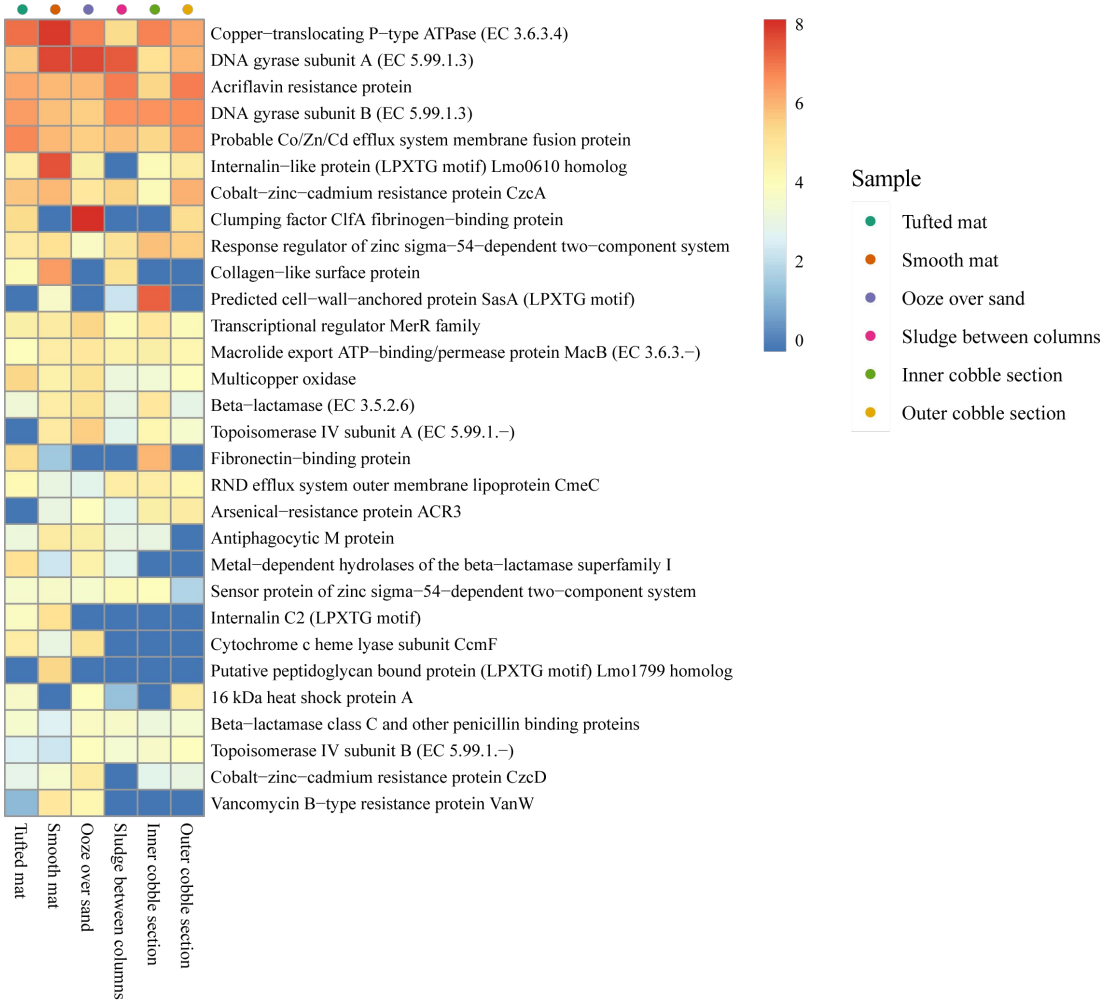

Figure 4.8 Heatmap showing the top 30 transcribed genes (>10) in RRBS metatranscriptomes related to virulence and defence. Differential analysis, gradient and B. PCA are the same as figure.

No distinct patterns were observed between samples for genes encoding virulence and defence pathways. Copper homeostasis (e.g. copper-translocating P-type ATPase – C*tp*A, multicopper oxidase - *mmc*O), resistance to fluoroquinolones (e.g. DNA gyrase

– *gyr*A, *gyr*B), multidrug resistance efflux pumps (e.g. acriflavin resistance protein – *arc*B; macrolide export ATP-binding protein - M*ac*B) were expressed across all samples (Figure 4.8). Additionally, genes associated with cobalt-zinc-cadmium (e.g. probable Co/Zn/Cd efflux system membrane fusion protein; cobalt-zinc-cadmium resistance protein - C*zc*A) and arsenic (e.g. Arsenical-resistance protein ACR3) resistance were expressed. Surface protein adhesions such as the clumping factor fibrinogen-binding protein (C*lf*A) was highly expressed in OVS and the predicted cell-wall-anchored protein (S*as*A) was highly expressed in CI. Resistance to Vancomycin (e.g. vancomycin B-type resistance protein - V*an*W) was abundantly expressed in Group 1 samples, especially SM and OVS.

4.3.3 Community and functional characteristics of the cobble

Dominant taxa in the cobble included Alteromonadales, Bacteroidales, Clostridiales, Cytophagales, Desulfobacterales, Desulfovibrionales, Flavobacteriales and Spirochaetales (Figure 4.9 A). The inner cobble section had higher relative abundances of Bacteroidales (17 %), Spirochaetales (9 %), and Clostridiales (6 %), whereas the outer cobble section had higher relative abundances of Flavobacteriales (28 %), Cytophagales (15 %) and Alteromonadales (6 %). Additionally, Methanosarcinales, comprising of methanogenic Euryarchaeota, was only found in the inner cobble section at a relative abundance of 6 %. Expressed pathways associated with capsular and extracellular polysaccharides indicated that sialic acid metabolism (~30 %) and aTMP-rhamnose synthesis (~15 %) were the two most abundantly expressed pathways in both sections of the cobble. However, the inner cobble section also showed relatively high levels of expression associated with Rhamnose containing glycans (27 %) and alginate metabolism (12 %) (Figure 4.9 B). Biosynthetic pathways associated with colanic acid, capsular polysaccharides and exopolysaccharides were only found to be expressed in the outer cobble section. Sulfur and methane metabolisms were the most expressed energy producing metabolic pathways within the cobble (Figure 4.9 C). Notably, methane metabolism was highly expressed in the inner cobble section at 58 %, whereas photosynthesis was only expressed in the outer cobble section.

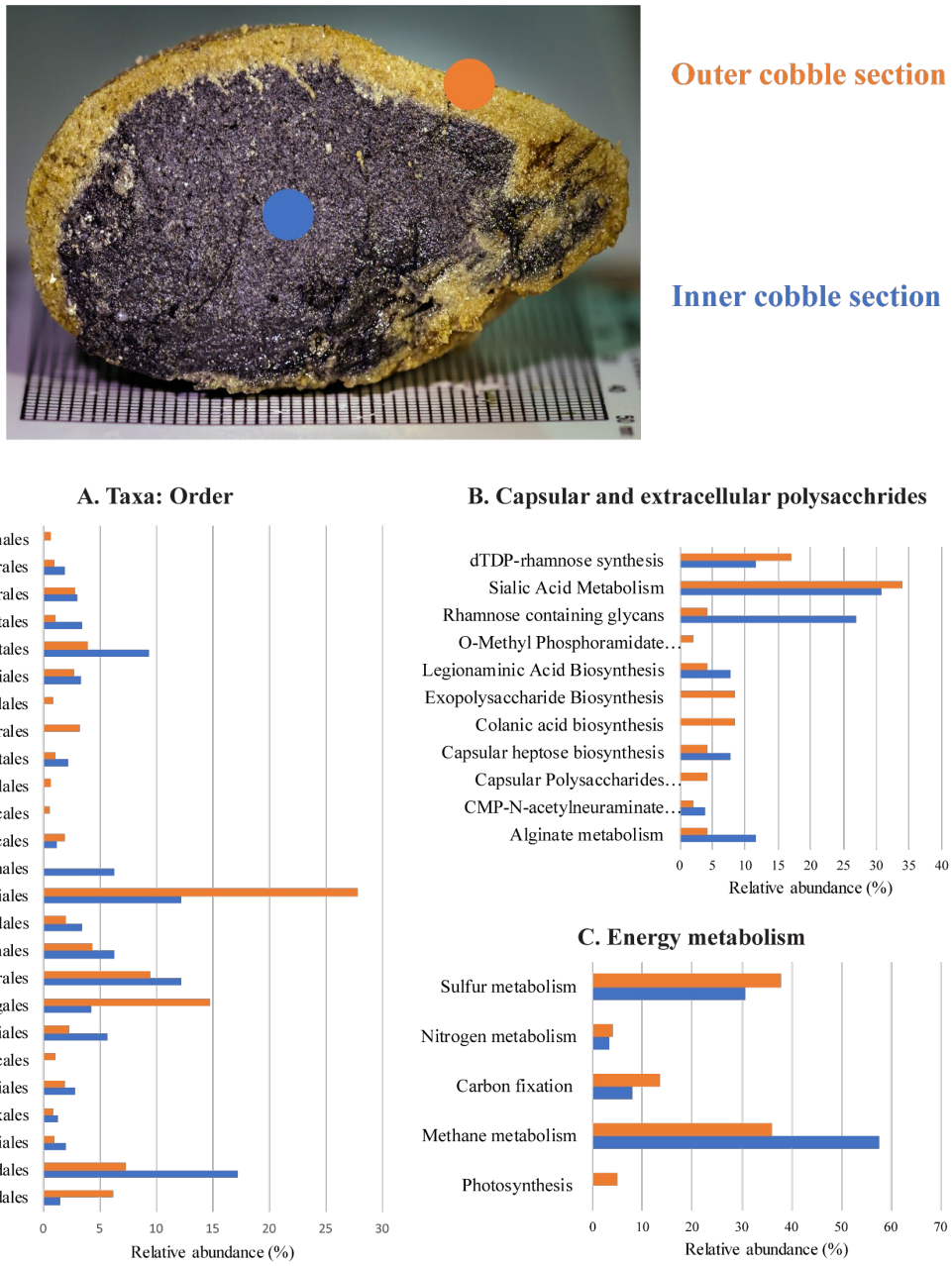

Figure 4.9 Bar charts displaying the relative abundances of active taxa and pathways associated with capsular and extracellular polysaccharides, and energy metabolisms in the outer and inner sections of the cobble. A. RefSeq classification (Order), B. and C. expression of pathways in capsular and extracellular polysaccharides (SEED subsystems, level 3), and energy metabolisms (KEGG, level 3), respectively.

4.3.4 Aliphatic Hydrocarbons—Molecular and $\delta^{13}C$ Distributions

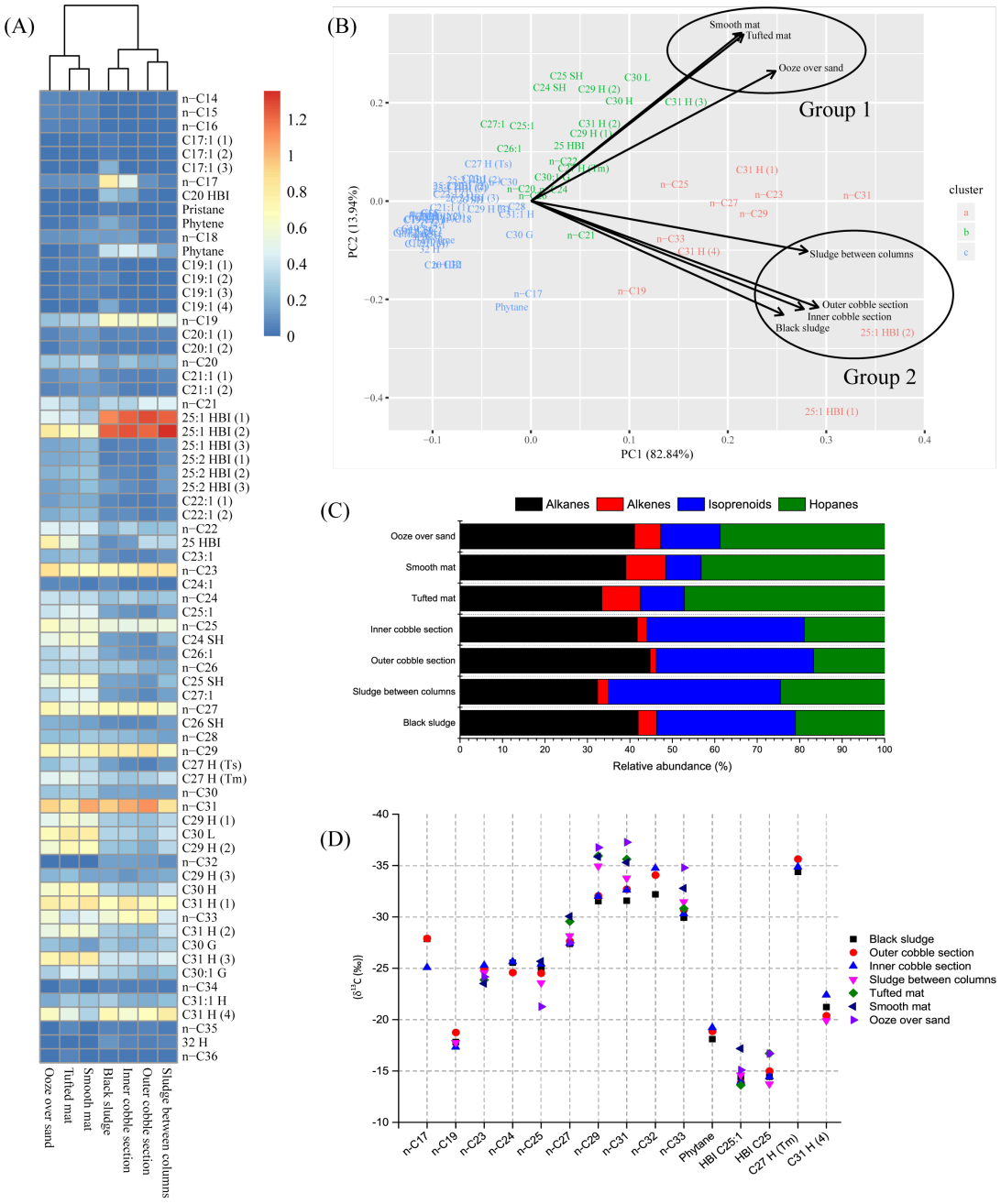

Figure 4.10 Molecular and $\delta^{13}C$ distributions of aliphatic hydrocarbons from microbial mats, a post cyclone deposit and black sludge derived materials from RRBS. A. Heatmap showing the distribution and abundance of aliphatic hydrocarbons. Gradient from red to blue indicates compound abundance across samples with red indicating high abundance and blue indicating low abundance. B. Principle component analysis of aliphatic hydrocarbons with eigen-vectors. C. Relative abundance of alkanes, alkenes, isoprenoids (regular and highly branched) and hopanes ($C_{24\text{-}26}$ *seco*hopanes and $C_{27\text{-}31}$ hopanes/hopenes). D. $\delta^{13}C$ distributions of aliphatic hydrocarbons (maximum standard deviation of the $\delta^{13}C$ values is ± 0.5‰.). Heatmap and PCA used values produced from normalised peak areas of each compound followed by a log (n+1) transformation. Numbers within brackets represent the elution order

of isomers to a specific compound. HBI = highly branched isoprenoid, SH = *seco*hopanes, H = hopane, Ts = t*risnorneo*hopane, Tm = *trisnor*hopane, L = *seco*lupane and G = gammacerane.

Hierarchal clustering and PCA of the aliphatic hydrocarbon distributions indicated the same two groupings of the samples as the metatranscriptomic analysis with Group 1 containing OVS, TM and SM, and Group 2 containing SBC, CO and CI with the addition of the black sludge (BS) (Figure 4.10 A, B and C). $C_{24\text{-}31}$ hopanes were more dominant in Group 1 samples whereas two isomers of the $C_{25:1}$ highly branched isoprenoid (HBI) were found to be the most dominant hydrocarbons in Group 2 samples. Compound specific carbon isotope analysis showed no significant variation between the compounds and samples (Figure 4.10 D).

4.3.4.1 Alkane and alkene distribution

The total relative abundance of *n*-alkanes varied from 30-45% with an odd-over-even carbon number preference in all the samples. The most abundant *n*-alkanes ranged from odd chain lengths of $C_{23\text{-}33}$. The $\delta^{13}C$ values of the long-chain n-alkanes ($C_{27\text{-}33}$) were more depleted in ^{13}C with $\delta^{13}C$ values ranging from -27.4 ‰ to -37.3 ‰, whereas the short to mid-chain n-alkanes ($C_{23\text{–}25}$) showed more enriched $\delta^{13}C$ values ranging from -21.3 ‰ to -25.7 ‰. Shorter chain *n*-C_{17} and *n*-C_{19} alkanes were also found to be in abundance, especially in Group 2 samples. The $\delta^{13}C$ values of the *n*-C_{17} and *n*-C_{19} alkanes ranged from -25.1 ‰ to -27.9 ‰ and -17.3 ‰ to -18.8 ‰, respectively. Alkenes varied from 1-10% with an odd-over-even carbon number preference. The most abundant alkenes were monoenes ranging from $C_{22:1}$-$C_{27:1}$ with generally higher abundances in Group 1 samples.

4.3.4.2 Isoprenoid distribution

The total relative abundance of isoprenoids varied from 8-40% within the samples, Group 1 containing lower abundances between 8-14%, whereas Group 2 contained a relatively high abundance between 32-40%. A mixture of C_{25} HBI alkene and alkadiene isomers, a C_{25} HBI alkane and a C_{20} HBI alkene were detected in all the samples. Group 1 contained higher amounts of the C_{25} HBI alkadienes and the C_{25} HBI alkane whereas Group 2 contained significantly higher amounts of the C_{25} HBI alkenes. The $\delta^{13}C$ values of the combined $C_{25:1}$ alkene and C_{25} HBI alkane had

relatively heavy $\delta^{13}C$ values compared to the other hydrocarbon products that ranged from -13.9 ‰ to -17.2 ‰ and -13.6 ‰ to -16.7 ‰, respectively. Phytane, phytene and pristane were present in all the samples with a higher percentage found in Group 2 samples. The $\delta^{13}C$ values of phytane had relatively heavy values compared to the other hydrocarbon products ranging from -18.1 ‰ to -19.2 ‰.

4.3.4.3 Hopane distribution

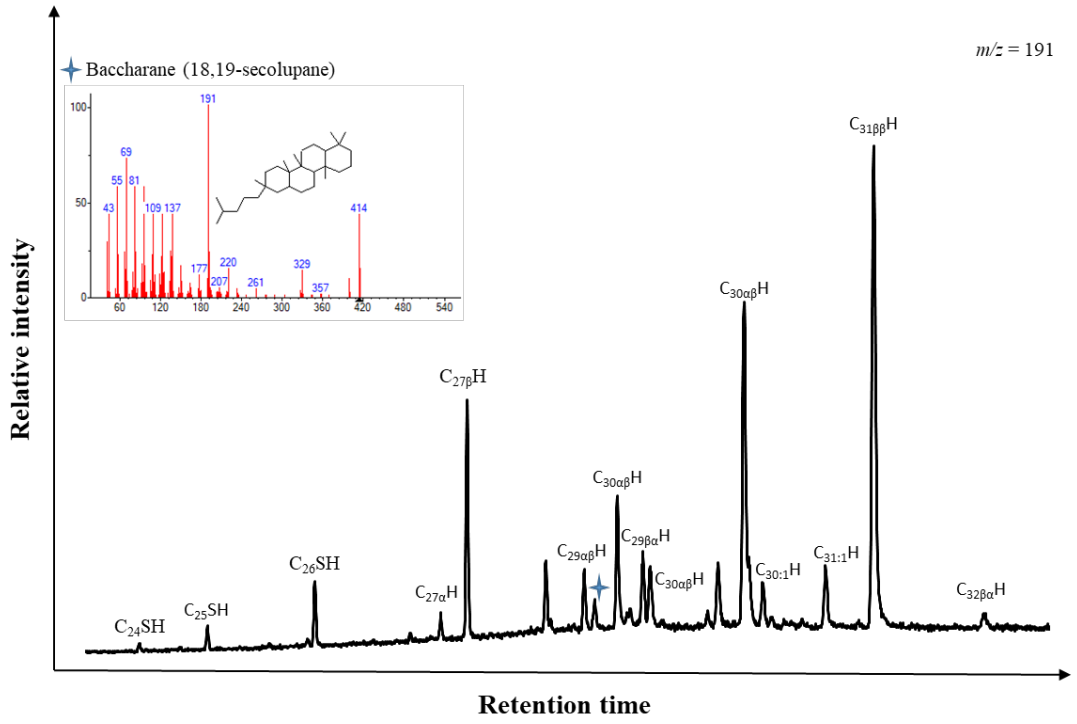

Figure 4.11 Mass fragmentogram (*m/z* = 191) of aliphatic hydrocarbons from the smooth mat. SH = secohopanes, H = hop-anes/enes. Blue star indicating the peak associated to baccharane (18,19-*seco*lupane).

The total relative abundance of hopanes varied from 16-47%, Group 1 containing high abundances between 38-47%, whereas Group 2 contained a relatively lower abundance between 16-24%. C_{24}-C_{26} tetracyclic terpanes (17,21-*seco*hopanes), baccharane (18,19-*seco*lupane), $C_{27\text{-}31}$ hopanes as well as $C_{30\text{-}31}$ hopenes were abundant in Group 1 samples. However, the 17α(H),21β(H)-hopane and 17β(H),21β(H)-homohopane were abundant in all the samples. An example of the hopane distribution can be seen in Figure 4.11. The $\delta^{13}C$ values of 17β(H),21β(H)-homohopane ranged from -19.9 ‰ to -22.4 ‰.

4.3.4.4 Raney nickel desulfurization

Desulfurization of the inner cobble sections' polar fraction released high amounts 6,10,14-trimethyl-2-pentadecanone (182.35 ng/mg TLE), pristane (71.78 ng/mg TLE) and phytane (61.27 ng/mg TLE) (Figure 4.12). The *m/z* = 191 chromatogram showed a release of hopanes (C_{27}-C_{35}), with 17α(H),21β(H)-30-*nor*hopane (3.12 ng/mg TLE), 17β(H),21β(H)-hopane (1.86 ng/mg TLE), 17β(H),21β(H)-homohopane (1.26 ng/mg TLE) and 17α(H),21β(H)-pentakishomohopane (5.49 ng/mg TLE) being the most abundantly released hopanoid products (Supplementary Figure 4.5). Additionally, trace amounts of two aromatized hopanoids were also present, these have been tentatively identified as C_{33} and C_{34} benzohopanes due to the key *m/z* ions at 225 and 239 Daltons being characteristic of structures containing a benzene ring.

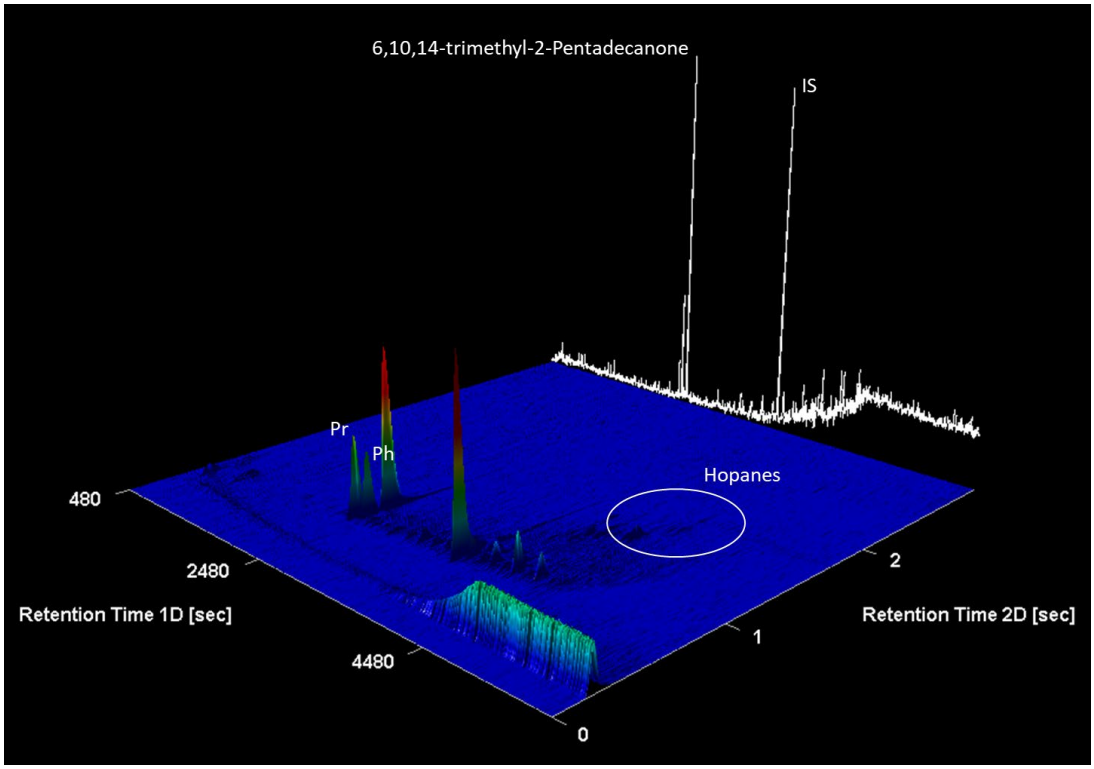

Figure 4.12 Total Ion Chromatogram of the sulfur-bound aliphatic hydrocarbons from the inner cobble section measured by GCxGC-TOFMS. Pr = pristane, Ph = phytane and IS = internal standard: squalene.

4.4 Discussion

4.4.1 Community structure of microbial mats vs black sludge derived materials

Comparison of the active and resident microbial communities indicated that phototrophic Chloroflexi and Cyanobacteria, as well as UV tolerant Deinococcus-Thermus were more abundant in the microbial mats and post cyclone deposit. Cyanobacteria and Deinococcus-Thermus have previously been found to be the dominant phylum in the oxic zones of stratified microbial mats (Toneatti et al., 2017); with Deinococcus-Thermus providing a photoprotective layer on photosynthetic organisms (Tian and Hua, 2010; Farci et al., 2016). Black sludge derived materials had higher levels of heterotrophic and chemoautotrophic bacteria (e.g. Bacteroidetes, Deltaproteobacteria, Acidobacteria and Spirochaetes), as well as more recently characterised groups (Calditrichaeota, Kiritimatiellaeota, Synergistetes and Zixibacteria) that have been associated with organic matter degradation in marine sediments (Scherr et al., 2012; Marshall et al., 2017; Van Vliet et al., 2019; Zinke et al., 2019). Notably, members from the Cytophaga–Flavobacteria cluster were found to be the most active in the outer oxidised layer of the cobble formation. These heterotrophic bacteria are known to have a specialized role in dissolved organic matter (DOM) uptake and degradation in aquatic systems. Several studies have demonstrated that Cytophaga–Flavobacteria are enriched on particulate organic detritus in marine habitats and became more abundant over time on organic aggregates made from marine DOM (DeLong et al., 1993; Ying wu, 1998; Crump et al., 1999; Kirchman, 2006). This is attributed to their ability to survive on high-molecular-weight (HMW) organic material. Therefore, the presence of these heterotrophic bacteria is enhanced by the transportation of detritus-associated materials generated by the cyclone from microbial mats and anoxic sediments; their prevalence over a year later can be attributed to their ability to survive off HMW organic material.

4.4.2 Biogeochemical cycling

Expression of genes involved in nitrogen fixation and ammonia assimilation were elevated in the microbial mats and post cyclone deposit, these samples contained significantly higher proportions of cyanobacteria, suggesting a direct link between phototrophy and nitrogen assimalation in these systems (Stal and Krumbein, 1985;

Forchhammer and Selim, 2019) . Moreover, the transcription of *nif*A was found to be more expressed in the black sludge derived materials, this particular nitrogenase regulator is found in heterotrophic diazotrophs (e.g. Proteobacteria) (Batista and Dixon, 2019). Recent studies have suggested that heterotrophic diazotrophs are more widely distributed than previously thought, fixing nitrogen in "unfavorable" aquatic environments within bioaggregates (Geisler et al., 2019). Furthermore, shifts in active diazotrophic communities have been suggested to reflect changes in environmental conditions (Severin et al., 2010); therefore, cyclonic events in Shark Bay may increase the activity of heterotrophic diazotrophs due to increased anoxic conditions, formation of bioaggregates (e.g. mucilaginous cobbles and sludge) and ultimately result in eutrophication where these materials accumulate in the bay.

Genes associated with inorganic sulfur assimilation, such as sulfate adenylyltransferase and sulfite reductase (ferredoxin), were higher in the microbial mats and post cyclone deposit. Apart from commonly being expressed by Deltaproteobacteria, these genes have previously been shown to be up-regulated by cyanobacteria when there is a lack of sulfur (Kumaresan et al., 2017). Furthermore, sulfur shortages in *Anabaena* species indicated decreases in photopigments and photochemical efficiency, increased oxidative stress and lowering of cyanobacterial biomass (Kharwar and Mishra, 2020). Therefore, with the relatively higher amount of active cyanobacteria conducting sulfur metabolism in the microbial mats and post cyclone deposit suggests that sulfur is being assimilated preferentially for growth and physiological functioning (Mendoza-Cózatl et al., 2005; Mobberley et al., 2013). Whereas the prominace of deltaproteopbacteria and genes encoding sulfate reduction-associated complexes (e.g. *dsr*K, *dsr*P, *dsr*O) in the cyclone-derived materials indicates that the dissimilatory reduction of sulfate is a major pathway for which sulfur is cycled within these ecostsyems (Wong et al., 2018). Lastly, the elevated expression of arylsulfatase (*asl*A) in the inner cobble section indicates a possible increase in the hydrolysis of sulfonated polysaccharides as a source for sulfur, this activity may be brought on by a decrease in free sulfate concretrations occuring within the mucilaginous cobble (Oshrain and Wiebe, 1979; Visscher et al., 1999; Helbert, 2017).

4.4.3 Stress response and defence mechanisms

Genes associated with sigmaB modulation, which is known to play an important role in antibiotic resistance, pathogenesis and cellular differentiation processes such as biofilm formation (Van Schaik and Abee, 2005), were abundantly expressed in the microbial mats. A recent investigation of environmental stress response mechanisms in Gram-positive bacteria found that the activation of R*sb*U leads to the dephosphorylation of the anti-sigmaB factor R*sb*V; R*sb*V targets the anti-sigma factor R*sb*W that releases SigB, allowing transcription of adaptive functions (Bonilla, 2020). Additionally, genes encoding bacterial hemoglobins and phytochrome two-component sensor histidine kinase involved in oxygen regulation were found to be more abundantly expressed in the microbial mats (Frey and Kallio, 2003; Möglich, 2019). The expression of these genes is known to be induced by environmental stress conditions such as oxygen deprivation or oxidative stress (Demple, 1991). Moreover, nitrogen-fixing organisms face the problem of protecting their nitrogenase from inactivation by oxygen (Gallon, 1981), therefore close regulation of reactive oxygen species is required. Additionally, in the black sludge derived materials, rubrerythrin and superoxide reductase were more abundantly expressed. These are thought to be involved in a sulfate reducing bacteria specific response to superoxide (superoxide reductase) and peroxide (rubrerythrin) that avoids the production of O_2 occurring as a by-product of catalase and superoxide dismutase function (Lumppio et al., 2001). The expression of these genes may be a sign of preparation for the high levels of O_2 that would be produced hours later after dawn and the onset of oxygenic photosynthesis, or for protection against the small amount of oxidant possibly present in the dark anoxic conditions (Burow et al., 2014).

Genes associated with copper homeostasis, resistance to fluoroquinolones multidrug resistance efflux pumps, as well as cobalt-zinc-cadmium and arsenic resistance were expressed across all the metatranscriptomes. Copper is an important micronutrient required as a redox co-factor in the catalytic centers of enzymes. However, free copper is a potential hazard because of its high chemical reactivity. Consequently, organisms exert a tight control on Cu^+ transport and traffic through different compartments, ensuring the homeostasis required for cuproprotein synthesis and prevention of toxic effects (Argüello et al., 2013). The elevated expression of genes affiliated with copper homeostasis corroborates with a previous metagenomic

study of Shark Bay smooth mats finding high levels of copper in surrounding water as well as an abundant amount of genes involved in maintaining copper homeostasis (Wong et al., 2018). The arsenical-resistance protein Acr3 is known to mediate the tolerance to As(III) in cyanobacterium *Synechocystis* (Páez-Espino et al., 2009), as well as Actinobacteria and Alphaproteobacteria in response to increased environmental arsenic levels (López-Maury et al., 2003). Multidrug resistance efflux pumps, resistance to fluoroquinolones and cobalt-zinc-cadmium resistance have a broad distribution in environmental samples indicating that these mechanisms of antibiotic resistance are functionally important in many habitats (Durso et al., 2012).

4.4.4 Biomarker and $\delta^{13}C$ distributions

The most abundant *n*-alkanes ranged from odd chain lengths of C_{23-33}, this distribution is distinctive to terrestrial plant input and has been attributed to epicuticular leaf waxes supplied by aeolian transport in coastal settings (e.g. Pancost and Boot, 2004). Similar *n*-alkane distributions have previously been described in Shark Bay microbial mats where it has been noted that *n*-alkanes with odd-carbon-number-predominance may also be derived from coastal seagrass beds, which are [highly] abundant in Shark Bay (Allen et al., 2010; Pagès et al., 2015). The $\delta^{13}C$ values of the long-chain *n*-alkanes were more depleted in ^{13}C, which indicates that they are more likely sourced from terrestrial C_3 plants (Schreuder et al., 2018), whereas the short to mid-chain *n*-alkanes showed more enriched $\delta^{13}C$ values, which potentially indicates a macrophyte source (Jones et al., 2003; Tulipani et al., 2014). These observations are consistent with observed terrestrial and marine plant debris in the beach face and outwash channel recorded immediately after the event (Morris et al in prep).

Straight chain C_{17} and C_{19} alkanes were found to be more abundant in the black sludge derived materials. The *n*-C_{17} alkane is known to be a marker for algae in aquatic environments, but has also been interpreted as a marker of cyanobacteria in microbial mats from hot springs, freshwater or hypersaline environments (Robinson and Eglinton, 1990; Thiel et al., 1997; Allen et al., 2010). The *n*-C_{19} alkane has previously been shown to be a major constituent in Shark Bay stromatolites (Allen et al., 2010) and coniform *Phormidium* mats form Yellowstone (Jahnke et al., 2004). The $\delta^{13}C$ values of the *n*-C_{17} supported a cyanobacterial source (Pagès et al., 2015), whereas the heavier *n*-C_{19} may reflect lower availability of dissolved inoganic carbon in the

environment (Jahnke et al., 2004). $C_{22:1}$-$C_{27:1}$ alkenes were generally higher in abundance within the microbial mats and post cyclone deposit. These alkenes could originate from the diagenetic reduction of monounsaturated fatty acids or from microbial transformation of previously sedimented allochthonous *n*-alkanes (Haddad et al., 1992). The C_{25} and C_{27} alkenes are recognized as biomarkers of cyanobacteria, however these compounds can also be produced by diatoms (Volkman et al., 1998).

HBIs have previously been identified in Shark Bay biomarker studies as markers for diatoms occurring in microbial mats, subtidal sediment material collected from an ocean-to-hypersaline embayment transect and from diatomaceous ooze sampled from the centre of Hamelin Pool (Dunlop and Jefferies, 1985; Summons et al., 1993; Allen et al., 2010; Pagès et al., 2015). These studies showed that there is significant variability within HBI-producing diatom communities colonising intertidal and subtidal regions of Hamelin Pool, possibly due to difference in ecological niches. This study showed that HBIs were a major influence on the grouping of the samples, as shown in Figure 4.10. Group 1 contained relatively higher amounts of the C_{25} HBI alkadienes and the C_{25} HBI alkane whereas Group 2 contained significantly higher amounts of the C_{25} HBI alkenes. As the samples in Group 2 are all derived from material generated by the cyclone (based on mapping immeadiately after the event) it can then be assumed that the abundant signal of the C_{25} HBI alkenes in this group is due to the relocation of subtidal materials from consequent HBI-producing diatoms communities into the intertidal zone. It has been noted that diatoms are likely to be more important in the subtidal communities of Hamelin Pool and their HBI signature preferentially survives in the sedimentary layers of the subtidal environments (Dunlop and Jefferies, 1985). The $\delta^{13}C$ values of the combined $C_{25:1}$ HBI alkene and C_{25} HBI alkane had relatively heavy $\delta^{13}C$ values compared to the other hydrocarbon products. The detection of C_{25} HBIs with relatively heavy $\delta^{13}C$ values has been previously shown in microbial mats (Pagès et al., 2015) and diatomaceous ooze from Hamelin Pool ranging from -12.0 ‰ to -16.9 ‰ (Summons et al., 1993) . Diatoms usually grow in blooms that lead to localised depletions in $^{12}CO_2$, which explains why their biomass is enriched in ^{13}C compared to other primary producers (Gu and Schelske, 1996).

A higher relative abundance of phytane, phytene and pristane were present in the black sludge derived materials. Phytane and phytene were more abundant than pristane indicating reducing conditions and the presence of active anaerobic bacteria

(Rontani and Bonin, 2011). These compounds are known to form by anaerobic microbial processes that can either degrade free phytol or archaeal ether lipids into sedimentary phytene intermediates (Rontani et al., 2013). The $\delta^{13}C$ values of phytane had relatively heavy δ-values compared to the other hydrocarbon products. Phytane that is derived from photoautotrophs that use the Calvin-Benson cycle typically produced $\delta^{13}C$ values between -25 and -30 ‰, here the phytane is roughly 5‰ lower, suggesting that phytane was primarlily derived from lipids of either methylotrophic methanogens (Schouten et al., 2001) or halophilic archaea (Grice et al., 1998a) that are known to give rise to isotopically heavy isoprenoids in marine and saline lacustrine environments.

The microbial mats and post cyclone deposit had the highest overall abundance of hopanes (ranging from C_{27} to C_{31}), however C_{30} αβ hopane and C_{31}ββ hopane were the most abundant hopanoids in all the samples studied. A high abundances of ββ hopanes, as well as C_{29} αβ and βα hopanes, and C_{30} αβ hopanes have been previously reported in Shark Bay from established epibenthic mats not recently disturbed by cyclonic activity (Allen et al., 2010; Pagès et al., 2015). C_{31} ββ hopane usually indicates the presence of cyanobacteria (Talbot et al., 2008). C_{24}-C_{26} tetracyclic terpanes (17,21-*seco*hopanes) have been identified in sediments, petroleums and fossilized bacterial ecosystems; these compounds have been attributed to microbial opening of the ring E of hopanoids during early diagenesis caused by the oxidation of 17(21)-hopenes followed by reduction to the 17,21-*seco*hopane (Trendel et al., 1982; Burhan et al., 2002). Reports of baccharane-derived triterpenoids in the field of natural products are limited and up to now restricted to terrestrial plants. However, sedimentary baccharane derivatives may also represent a contribution of as yet undetermined marine microorganisms, and could be a biogeochemical transformation products (Poinsot et al., 1993). As these compounds have yet to be identifed in Shark Bay microbial mats it can be proposed that they have occurred due to the cyclonic activity, either from the out flushing of terrestral organic matter or from the mixing of marine sediment and outwashed materials within water column during the flocking process.

4.4.5 Cyclone derived cobble formations in Shark Bay and their geological significance

The mucilaginous cobble in its entirety resembled a potentially oncoidal form of microbial mat development with an outer oxic layer (outer cobble section) supporting active phototrophy and an inner anoxic layer (inner cobble section) with a higher amount of chemoorganotrophic activity (van Gemerden, 1993; Prieto-Barajas et al., 2018). Apart from physical processes (e.g. tidal and wave movements), the structure of the cobble is likely a result of microbially produced EPS, which binds sediments and provides an ideal environment for chemical reactions, nutrient entrapment, and protection against environmental stresses such as salinity and dehydration (Dupraz et al., 2013; Costa et al., 2018). EPS also plays an important role in microbial calcification (Decho, 2000; Reid et al., 2000; Visscher et al., 2000; Tourney and Ngwenya, 2014), either inhibiting or promoting carbonate precipitation (Dupraz et al., 2009). EPS can remove free cations from solution by binding them to negatively charged groups, this consequently reduces the saturation of calcium ions and inhibits carbonate precipitation (Dupraz et al., 2009). However, after EPS is degraded; calcium ions may locally reach high concentrations and thus favour precipitation of calcium carbonate (Reid et al., 2000; Dupraz and Visscher, 2005).

Investigating the expressed pathways associated with capsular and extracellular polysaccharides indicated that sialic acid metabolism and aTMP-rhamnose synthesis were the two most abundantly expressed pathways in the mucilaginous cobble along with genes associated with rhamnose containing glycans being highly represented in the inner cobble section. The elevated transcription of these pathways could be attributed the production and protection of EPS in response to increased heterotrophic activity, as rhamnose is an deoxy sugar monomer known for improving the cohesive properties of the EPS and their ability to form aggregates (Decho, 2000), and sialic acids for protecting EPS molecules from attack by proteases or glycosidases (de Graaff et al., 2019). Therefore, these two different types of EPS may be essential for the cobbles (or cobble communities) growth and maintenance. Sulfate reduction has also been suggested to play a significant role in the lithification of microbial mats (Visscher et al., 1998; 2000). This is mainly based on the increase of the calcium carbonate saturation index (SI) during growth of sulfate-reducers with

hydrogen or formate (Gallagher et al., 2012), increased alkalinity driven by sulfate reduction (Braissant et al., 2007), and indirect asscoiation of elevated sulfate reduction rates in zones of active calcium mineral precipitation (Visscher et al., 2000; Dupraz et al., 2004). Sulfur metabolism was highly expressed in the cobble formation with many sulfate reduction-associated complexes being transcribed. Therefore, the abundance of active heterotrophic bacteria degrading OM (e.g Bacteroidetes, Cytophaga and Flavobacteria) and sulfate reducing bacteria increasing the alkalinity and carbonate SI (e.g. Deltaproteobacteria) will likely drive calcium carbonate preciptition in the mucilaginous cobble and aid in its structural preservation.

Sulfate reduction in microbial ecosystems can also lead to the incorporation of reduced inorganic sulfur species into sedimentary OM (Jørgensen et al., 2019). This is an important mechanism for the preservation of functionalized organic compounds during early diagenesis (Grice et al., 1998b; Werne et al., 2000). Early diagenetic sulfurization occurs eithers by intra- and intermolecular incorporation of various reduced sulfur species (e.g., HS^-, polysulfides) into functionalized lipids (Amrani, 2014). Intramolecular incorporation of sulfur, which leads to low-molecular-weight cyclic sulfur compounds such as thianes, thiolanes, and thiophenes were not detected in the mucilaginous cobble. However, the intermolecular sulfur incorporation, which binds organic compounds into macromolecular material through (poly)sulfide linkages, was detected via desulfurization, releasing compounds such as isoprenoids (e.g. pristane, phytane), regular hopanes (C_{27}-C_{35}) and benzohopanes (C_{33}-C_{34}). The absence of intramolecularly bound molecules maybe due to unfavourable reaction kinetics and double bond positions in the precursor molecules (Werne et al., 2000).

The release of isoprenoids such as phytane is likely due to the action of Raney Nickel on the esterified side chain of chlorophyll *a* (Prahl et al., 1996). The hopanes obtained are probably the result of the released S-bound hopanoids due to how their distribution differs from the free hydrocarbons. However, it cannot be excluded that part results may come from the hydrolysis of polyfunctionalized (oxygenated, unsaturated) hopanoids occurring in the immature sample (Burhan et al., 2002). Benzohopanes have previously been reported to be released via desulfurization from S-bound substrates (Van Kaam-Peters et al., 1995; Grice et al., 1996; Van Kaam-Peters and Sinninghe Damsté, 1997). They have not been reported in living organisms, but are thought to be secondary transformation products of C_{35} bacteriohopanepolyol

derivatives (Hussler et al., 1984a, 1984b). It was previously found that benzohopanes and hopanes had similar $\delta^{13}C$ values suggesting a common origin, consistent with a source from phototrophic organisms (Grice et al., 1998b). The formation of benzohopanes by cyclisation and aromatisation reactions requires precursors with the 17α-hopanoid carbon skeleton since 17β-benzohopanes are very strained molecules (Hussler et al., 1984a). It has been suggested that they are only present if ββ-hopanes have isomerised to αβ-epimers, suggesting that this conformation is essential for their formation (Sinninghe Damsté et al., 1995). This corroborates with the abundant release of S-bound 17α(H),21β(H)-pentakishomohopane from the mucilaginous cobble and provides more evidence for the selective preservation of the C_{35} hopane skeleton by sulfur sequestration. This may potentially provide an additional application of the homohopane index with benzohopanes as an indicator of anoxia brought on by episodic events in past coastal settings harbouring extensive microbial mats.

4.5 Conclusions

The combination of metatranscriptomic and organic geochemical techniques proved to be advantageous in understanding the effects of TC activity on microbial communities. We conclude that: 1) the biomarker and taxonomic compositions of the black sludge derived materials were distinct from that of the microbial mats; 2) cyclonic events in Shark Bay may increase the activity of heterotrophic diazotrophs leading to potential localized increases in eutrophication; 3) black sludge derived materials had significantly higher abundances of C_{25} HBI alkenes, that could be attributed to the relocation of subtidal sediments from consequent HBI-producing diatom communities; 4) abundances of active heterotrophic bacteria degrading OM and sulfate-reducing bacteria increasing the alkalinity and carbonate SI will likely drive calcium carbonate precipitation in the mucilaginous cobble; 5) the presence of S-bound hopanes with benzohopanes within mucilaginous cobble could be indicative of microbial matter that has been influenced by the TC, which may reflect the increase of epibenthic anoxia; 6) the retention of the biomarker evidence of storm reworking depends on the physical energy of the depositional setting.

4.6 References

Allen, M.A., Neilan, B.A., Burns, B.P., Jahnke, L.L., Summons, R.E., 2010. Lipid biomarkers in Hamelin Pool microbial mats and stromatolites. Org. Geochem. 41, 1207–1218.

Amrani, A., 2014. Organosulfur Compounds: Molecular and Isotopic Evolution from Biota to Oil and Gas. Annu. Rev. Earth Planet. Sci. 42, 733–768.

Argüello, J.M., Raimunda, D., Padilla-Benavides, T., 2013. Mechanisms of copper homeostasis in bacteria. Front. Cell. Infect. Microbiol. 4, 73.

Azam, F., Malfatti, F., 2007. Microbial structuring of marine ecosystems. Nat. Rev. Microbiol.

Batista, M.B., Dixon, R., 2019. Manipulating nitrogen regulation in diazotrophic bacteria for agronomic benefit. Biochem. Soc. Trans.

Bonilla, C.Y., 2020. Generally stressed out bacteria: environmental stress response mechanisms in Gram-positive bacteria. Integr. Comp. Biol.

Braissant, O., Decho, A.W., Dupraz, C., Glunk, C., Przekop, K.M., Visscher, P.T., 2007. Exopolymeric substances of sulfate-reducing bacteria: Interactions with calcium at alkaline pH and implication for formation of carbonate minerals. Geobiology 5, 401–411.

Brian W. Logan, D.E.C., 1970. Sedimentary Environments of Shark Bay, Western Australia 40, 1–37.

Burhan, R.Y.P., Trendel, J.M., Adam, P., Wehrung, P., Albrecht, P., Nissenbaum, A., 2002. Fossil bacterial ecosystem at methane seeps: Origin of organic matter from Be'eri sulfur deposit, Israel. Geochim. Cosmochim. Acta 66, 4085–4101.

Burow, L.C., Woebken, D., Marshall, I.P.G., Singer, S.W., Pett-Ridge, J., Prufert-Bebout, L., Spormann, A.M., Bebout, B.M., Weber, P.K., Hoehler, T.M., 2014. Identification of *Desulfobacterales* as primary hydrogenotrophs in a complex microbial mat community. Geobiology 12, 221–230.

Chuanmao, L., Friedman, G.M., Zhaochang, Z., 1993. Carbonate storm deposits (Tempestites) of Middle to Upper Cambrian age in the Helan Mountains, northwest China. Carbonates and Evaporites 8, 181–190.

Costa, O.Y.A., Raaijmakers, J.M., Kuramae, E.E., 2018. Microbial Extracellular Polymeric Substances: Ecological Function and Impact on Soil Aggregation.

Front. Microbiol. 9, 1636.

Crump, B.C., Armbrust, E.V., Baross, J.A., 1999. Phylogenetic analysis of particle-attached and free-living bacterial communities in the Columbia River, its estuary, and the adjacent coastal ocean. Appl. Environ. Microbiol. 65, 3192–3204.

de Graaff, D.R., Felz, S., Neu, T.R., Pronk, M., van Loosdrecht, M.C.M., Lin, Y., 2019. Sialic acids in the extracellular polymeric substances of seawater-adapted aerobic granular sludge. Water Res. 155, 343–351.

Decho, A.W., 2000. Microbial biofilms in intertidal systems: An overview. Cont. Shelf Res. 20, 1257–1273.

DeLong, E.F., Franks, D.G., Alldredge, A.L., 1993. Phylogenetic diversity of aggregate-attached vs. free-living marine bacterial assemblages. Limnol. Oceanogr. 38, 924–934.

Demple, B., 1991. Regulation of Bacterial Oxidative Stress Genes. Annu. Rev. Genet. 25, 315–337.

Dunlop, R.W., Jefferies, P.R., 1985. Hydrocarbons of the hypersaline basins of Shark Bay, Western Australia. Org. Geochem. 8, 313–320.

Dupraz, C., Fowler, A., Tobias, C., Visscher, P.T., 2013. Stromatolitic knobs in Storr's Lake (San Salvador, Bahamas): a model system for formation and alteration of laminae. Geobiology 11, 527–548.

Dupraz, C., Reid, R.P., Braissant, O., Decho, A.W., Norman, R.S., Visscher, P.T., 2009. Processes of carbonate precipitation in modern microbial mats. Earth-Science Rev.

Dupraz, C., Visscher, P.T., 2005. Microbial lithification in marine stromatolites and hypersaline mats. Trends Microbiol.

Dupraz, C., Visscher, P.T., Baumgartner, L.K., Reid, R.P., 2004. Microbe-mineral interactions: early carbonate precipitation in a hypersaline lake (Eleuthera Island, Bahamas). Sedimentology 51, 745–765.

Durso, L.M., Miller, D.N., Wienhold, B.J., 2012. Distribution and Quantification of Antibiotic Resistant Genes and Bacteria across Agricultural and Non-Agricultural Metagenomes. PLoS One 7.

Fairchild, I.J., Herrington, P.M., 1989. A tempestite-stromatolite-evaporite association (late Vendian, East Greenland): a shoreface-lagoon model.

Precambrian Res. 43, 101–127.

Fan, D., Liu, K., 2008. Perspectives on the linkage between typhoon activity and global warming from recent research advances in paleotempestology. Sci. Bull. 53, 2907–2922.

Farci, D., Slavov, C., Tramontano, E., Piano, D., 2016. The S-layer Protein DR_2577 Binds Deinoxanthin and under Desiccation Conditions Protects against UV-Radiation in Deinococcus radiodurans. Front. Microbiol. 7.

Forchhammer, K., Selim, K.A., 2019. Carbon/nitrogen homeostasis control in cyanobacteria. FEMS Microbiol. Rev.

Frey, A.D., Kallio, P.T., 2003. Bacterial hemoglobins and flavohemoglobins: Versatile proteins and their impact on microbiology and biotechnology. FEMS Microbiol. Rev.

Gallagher, K.L., Kading, T.J., Braissant, O., Dupraz, C., Visscher, P.T., 2012. Inside the alkalinity engine: The role of electron donors in the organomineralization potential of sulfate-reducing bacteria. Geobiology 10, 518–530.

Gallon, J.R., 1981. The oxygen sensitivity of nitrogenase: a problem for biochemists and micro-organisms. Trends Biochem. Sci.

Geisler, E., Bogler, A., Rahav, E., Bar-Zeev, E., 2019. Direct Detection of Heterotrophic Diazotrophs Associated with Planktonic Aggregates. Sci. Rep. 9, 1–9.

Grice, K., Schaeffer, P., Schwark, L., Maxwell, J.R., 1996. Molecular indicators of palaeoenvironmental conditions in an immature Permian shale (Kupferschiefer, Lower Rhine Basin, north-west Germany) from free and S-bound lipids. Org. Geochem. 25, 131–147.

Grice, K., Schouten, S., Nissenbaum, A., Charrach, J., Sinninghe Damsté, J.S., 1998a. Isotopically heavy carbon in the C21 to C25 regular isoprenoids in halite-rich deposits from the Sdom Formation, Dead Sea Basin, Israel. Org. Geochem. 28, 349–359.

Grice, K., Schouten, S., Nissenbaum, A., Charrach, J., Sinninghe Damsté, J.S., 1998b. A remarkable paradox: Sulfurised freshwater algal (Botryococcus braunii) lipids in an ancient hypersaline euxinic ecosystem. Org. Geochem. 28, 195–216.

Gu, B., Schelske, L., 1996. Temporal and spatial variations in phytoplankton carbon

isotopes in a polymictic subtropical lake. J. Plankton Res. 18, 2081–2092.

Haddad, R.I., Martens, C.S., Farrington, J.W., 1992. Quantifying early diagenesis of fatty acids in a rapidly accumulating coastal marine sediment. Org. Geochem. 19, 205–216.

Helbert, W., 2017. Marine polysaccharide sulfatases. Front. Mar. Sci.

Hussler, G., Albrecht, P., Ourisson, G., Cesario, M., Guilhem, J., Pascard, C., 1984a. Benzohopanes, a novel family of hexacyclic geomarkers in sediments and petroleums. Tetrahedron Lett. 25, 1179–1182.

Hussler, G., Connan, J., Albrecht, P., 1984b. Novel families of tetra- and hexacyclic aromatic hopanoids predominant in carbonate rocks and crude oils. Org. Geochem. 6, 39–49.

Jahnert, R., de Paula, O., Collins, L., Strobach, E., Pevzner, R., 2012. Evolution of a coquina barrier in Shark Bay, Australia by GPR imaging: Architecture of a Holocene reservoir analog. Sediment. Geol. 281, 59–74.

Jahnke, L.L., Embaye, T., Hope, J., Turk, K.A., Van Zuilen, M., Des Marais, D.J., Farmer, J.D., Summons, R.E., 2004. Lipid biomarker and carbon isotopic signatures for stromatolite-forming, microbial mat communities and Phormidium cultures from Yellowstone National Park. Geobiology 2, 31–47.

Jones, W., Cifuentes, L., Kaldy, J., 2003. Stable carbon isotope evidence for coupling between sedimentary bacteria and seagrasses in a sub-tropical lagoon. Mar. Ecol. Prog. Ser. 255, 15–25.

Jørgensen, B.B., Findlay, A.J., Pellerin, A., 2019. The biogeochemical sulfur cycle of marine sediments. Front. Microbiol. 10, 849.

Kharwar, S., Mishra, A.K., 2020. Unraveling the complexities underlying sulfur deficiency and starvation in the cyanobacterium Anabaena sp. PCC 7120. Environ. Exp. Bot. 172, 103966.

Kirchman, D.L., 2006. The ecology of Cytophaga-“Flavobacteria in aquatic environments. FEMS Microbiol. Ecol. 39, 91–100.

Koleva-Rekalova, E., Dobrev, N., 2019. Доклади на Българската академия на науките SARMATIAN CARBONATE TEMPESTITES FROM KALIAKRA CAPE (NE BULGARIA): EVIDENCE FOR THE EXISTENCE OF MICROBIALITES Selection of optimum loess-cement mixture for construction of a compacted soil-cement cushion View project Geodynamics View project.

Kumaresan, V., Nizam, F., Ravichandran, G., Viswanathan, K., Palanisamy, R., Bhatt, P., Arasu, M.V., Al-Dhabi, N.A., Mala, K., Arockiaraj, J., 2017. Transcriptome changes of blue-green algae, Arthrospira sp. in response to sulfate stress. Algal Res. 23, 96–103.

Laajoki, K., 1996. Precambrian tempestite sequences in Finland. GFF 118, 106–106.

Logan, B., Hoffman, P., Gebelein, C., 1974. Algal mats, cryptalgal fabrics, and structures, Hamelin Pool, Western Australia.

López-Maury, L., Florencio, F.J., Reyes, J.C., 2003. Arsenic sensing and resistance system in the cyanobacterium Synechocystis sp. Strain PCC 6803. J. Bacteriol. 185, 5363–5371.

Lumppio, H.L., Shenvi, N. V., Summers, A.O., Voordouw, G., Kurtz, J., 2001. Rubrerythrin and rubredoxin oxidoreductase in Desulfovibrio vulgaris: A novel oxidative stress protection system. J. Bacteriol. 183, 101–108.

Marshall, I.P.G., Starnawski, P., Cupit, C., Fernández Cáceres, E., Ettema, T.J.G., Schramm, A., Kjeldsen, K.U., 2017. The novel bacterial phylum Calditrichaeota is diverse, widespread and abundant in marine sediments and has the capacity to degrade detrital proteins. Environ. Microbiol. Rep. 9, 397–403.

Mendoza-Cózatl, D., Loza-Tavera, H., Hernández-Navarro, A., Moreno-Sánchez, R., 2005. Sulfur assimilation and glutathione metabolism under cadmium stress in yeast, protists and plants. FEMS Microbiol. Rev.

Mobberley, J.M., Khodadad, C.L.M., Foster, J.S., 2013. Metabolic potential of lithifying cyanobacteria-dominated thrombolitic mats. Photosynth. Res. 118, 125–140.

Möglich, A., 2019. Signal transduction in photoreceptor histidine kinases. Protein Sci. 28, 1923–1946.

Morris, T.E., Visscher, P.T., O'Leary, M.J., Fearns, P.R.C.S., Collins, L.B., 2020. The biogeomorphology of Shark Bay's microbialite coasts. Earth-Science Rev.

Oshrain, R.L., Wiebe, W.J., 1979. Arylsulfatase activity in salt marsh soils. Appl. Environ. Microbiol. 38, 337–340.

Páez-Espino, D., Tamames, J., De Lorenzo, V., Cánovas, D., 2009. Microbial responses to environmental arsenic, in: BioMetals. Springer, pp. 117–130.

Pagès, A., Grice, K., Welsh, D.T., Teasdale, P.T., Van Kranendonk, M.J., Greenwood, P., 2015. Lipid Biomarker and Isotopic Study of Community

Distribution and Biomarker Preservation in a Laminated Microbial Mat from Shark Bay, Western Australia. Microb. Ecol. 70, 459–472.

Pancost, R.D., Boot, C.S., 2004. The palaeoclimatic utility of terrestrial biomarkers in marine sediments. Mar. Chem. 92, 239–261.

Poinsot, J., Adam, P., Trendel, J.M., Albrecht, P., Riva, A., 1993. Baccharane (18,19-secolupane): A rare triterpenoid skeleton widespread in Triassic sediments and petroleum from the Adriatic Basin. Geochim. Cosmochim. Acta 57, 3201–3205.

Prahl, F.G., Pinto, L.A., Sparrow, M.A., 1996. Phytane from chemolytic analysis of modern marine sediments: A product of desulfurization or not? Geochim. Cosmochim. Acta 60, 1065–1073.

Preisner, E.C., Fichot, E.B., Norman, R.S., 2016. Microbial mat compositional and functional sensitivity to environmental disturbance. Front. Microbiol. 7.

Prieto-Barajas, C.M., Valencia-Cantero, E., Santoyo, G., 2018. Microbial mat ecosystems: Structure types, functional diversity, and biotechnological application. Electron. J. Biotechnol. 31, 48–56.

Reid, R.P., Visscher, P.T., Decho, A.W., Stolz, J.F., Bebout, B.M., Dupraz, C., Macintyre, I.G., Paerl, H.W., Pinckney, J.L., Prufert-Bebout, L., Steppe, T.F., DesMarais, D.J., 2000. The role of microbes in accretion, lamination and early lithification of modern marine stromatolites. Nature 406, 989–992.

Robinson, N., Eglinton, G., 1990. Lipid chemistry of Icelandic hot spring microbial mats. Org. Geochem. 15, 291–298.

Rontani, J.F., Bonin, P., 2011. Production of pristane and phytane in the marine environment: Role of prokaryotes. Res. Microbiol. 162, 923–933.

Rontani, J.F., Bonin, P., Vaultier, F., Guasco, S., Volkman, J.K., 2013. Anaerobic bacterial degradation of pristenes and phytenes in marine sediments does not lead to pristane and phytane during early diagenesis. Org. Geochem. 58, 43–55.

Scherr, K.E., Lundaa, T., Klose, V., Bochmann, G., Loibner, A.P., 2012. Changes in bacterial communities from anaerobic digesters during petroleum hydrocarbon degradation. J. Biotechnol. 157, 564–572.

Schouten, S., Rijpstra, W.I.C., Kok, M., Hopmans, E.C., Summons, R.E., Volkman, J.K., Sinninghe Damsté, J.S., 2001. Molecular organic tracers of biogeochemical process in a saline meromictic lake. Geochim. Cosmochim.

Acta 65, 1629–1640.

Schreuder, L.T., Stuut, J.-B.W., Korte, L.F., Sinninghe Damsté, J.S., Schouten, S., 2018. Aeolian transport and deposition of plant wax n-alkanes across the tropical North Atlantic Ocean. Org. Geochem. 115, 113–123.

Severin, I., Acinas, S.G., Stal, L.J., 2010. Diversity of nitrogen-fixing bacteria in cyanobacterial mats. FEMS Microbiol. Ecol. 73, no-no.

Sinninghe Damsté, J.S., Van Duin, A.C.T., Hollander, D., Kohnen, M.E.L., De Leeuw, J.W., 1995. Early diagenesis of bacteriohopanepolyol derivatives: Formation of fossil homohopanoids. Geochim. Cosmochim. Acta 59, 5141–5157.

Stal, L.J., Krumbein, W.E., 1985. Nitrogenase activity in the non-heterocystous cyanobacterium Oscillatoria sp. grown under alternating light-dark cycles. Arch. Microbiol. 143, 67–71.

Summons, R.E., Capon, R.J., Stranger, C., Barrow, R.A., 1993. The structure of a new c25 isoprenoid alkene biomarker from diatomaceous microbial communities. Aust. J. Chem. 46, 907–915.

Talbot, H.M., Summons, R.E., Jahnke, L.L., Cockell, C.S., Rohmer, M., Farrimond, P., 2008. Cyanobacterial bacteriohopanepolyol signatures from cultures and natural environmental settings. Org. Geochem. 39, 232–263.

Thiel, V., Merz-Preiß, M., Reitner, J., Michaelis, W., 1997. Biomarker studies on microbial carbonates: Extractable lipids of a Calcifying Cyanobacterial mat (Everglades, USA). Facies 36, 163–172.

Tian, B., Hua, Y., 2010. Carotenoid biosynthesis in extremophilic Deinococcus-Thermus bacteria. Trends Microbiol.

Toneatti, D.M., Albarracín, V.H., Flores, M.R., Polerecky, L., Farías, M.E., 2017. Stratified Bacterial Diversity along Physico-chemical Gradients in High-Altitude Modern Stromatolites. Front. Microbiol. 8.

Tourney, J., Ngwenya, B.T., 2014. The role of bacterial extracellular polymeric substances in geomicrobiology. Chem. Geol.

Trendel, J.M., Restle, A., Connan, J., Albrecht, P., 1982. Identification of a novel series of tetracyclic terpene hydrocarbons (C24 - C27) in sediments and petroleums. J. Chem. Soc. Chem. Commun. 304–306.

Tulipani, S., Grice, K., Krull, E., Greenwood, P., Revill, A.T., 2014. Salinity

variations in the northern Coorong Lagoon, South Australia: Significant changes in the ecosystem following human alteration to the natural water regime. Org. Geochem. 75, 74–86.

van Gemerden, H., 1993. Microbial mats: A joint venture. Mar. Geol. 113, 3–25.

Van Kaam-Peters, H.M.E., Köster, J., De Leeuw, J.W., Damsté, J.S.S., 1995. Occurrence of two novel benzothiophene hopanoid families in sediments. Org. Geochem. 23, 607–616.

Van Kaam-Peters, H.M.E., Sinninghe Damsté, J.S., 1997. Characterisation of an extremely organic sulphur-rich, 150 Ma old carbonaceous rock: Palaeoenvironmental implications. Org. Geochem. 27, 371–397.

Van Schaik, W., Abee, T., 2005. The role of σB in the stress response of Gram-positive bacteria - Targets for food preservation and safety. Curr. Opin. Biotechnol.

Van Vliet, D.M., Ayudthaya, S.P.N., Diop, S., Villanueva, L., Stams, A.J.M., Sánchez-Andrea, I., 2019. Anaerobic degradation of sulfated polysaccharides by two novel Kiritimatiellales strains isolated from black sea sediment. Front. Microbiol. 10.

Visscher, P.T., Gritzer, R.F., Leadbetter, E.R., 1999. Low-molecular-weight sulfonates, a major substrate for sulfate reducers in marine microbial mats. Appl. Environ. Microbiol. 65, 3272–3278.

Visscher, P.T., Pamela Reid, R., Bebout, B.M., Hoeft, S.E., Macintyre, L.G., Thompson, J.A., 1998. Formation of lithified micritic laminae in modem marine stromatolites (Bahamas): The role of sulfur cycling. Am. Mineral. 83, 1482–1493.

Visscher, P.T., Reid, R.P., Bebout, B.M., 2000. Microscale observations of sulfate reduction: Correlation of microbial activity with lithified micritic laminae in modern marine stromatolites. Geology 28, 919–922.

Volkman, J.K., Barrett, S.M., Blackburn, S.I., Mansour, M.P., Sikes, E.L., Gelin, F., 1998. Microalgal biomarkers: A review of recent research developments, in: Organic Geochemistry. pp. 1163–1179.

Werne, J.P., Hollander, D.J., Behrens, A., Schaeffer, P., Albrecht, P., Sinninghe Damsté, J.S., 2000. Timing of early diagenetic sulfurization of organic matter: A precursor-product relationship in Holocene sediments of the anoxic Cariaco

Basin, Venezuela. Geochim. Cosmochim. Acta 64, 1741–1751.

Williams, H.F.L., 2011. Shell bed tempestites in the Chenier Plain of Louisiana: late Holocene example and modern analogue. J. Quat. Sci. 26, 199–206.

Wong, H.L., White, R.A., Visscher, P.T., Charlesworth, J.C., Vázquez-Campos, X., Burns, B.P., 2018. Disentangling the drivers of functional complexity at the metagenomic level in Shark Bay microbial mat microbiomes. ISME J. 12, 2619–2639.

Ying wu, K., 1998. High phylogenetic diversity in a marine-snow--associated bacterial assemblaae, AQUATIC MICROBIAL ECOLOGY Aquat Microb Ecol.

Zinke, L.A., Glombitza, C., Bird, J.T., Røy, H., Jørgensen, B.B., Lloyd, K.G., Amend, J.P., Reese, B.K., 2019. Microbial organic matter degradation potential in Baltic Sea Sediments is influenced by depositional conditions and in situ geochemistry. Appl. Environ. Microbiol. 85.

4.7 Supplementary material

Supplementary Table 4.1 Summary of sampling times, biogeomorphological units, and physical properties of the surrounding water.

Sample	Date	Sampling time	Subsampling time	Biogeomorphic unit	Geomorphic setting	Morphological feature	Water Temp (°C)	pH	Salinity (‰)
Tufted mat	7/07/2016	12:12 PM	4:35 PM	Mat platform unit	Intertidal terrace	Mat sheet	15	7.91	69
Sludge between columns	7/07/2016	1:00 PM	4:20 PM	Transitional microbial mosaic	Intertidal terrace front	Mucilage on sandy substrate between columns	15	7.9	69
Cobble	7/07/2016	1:10 PM	5:15 PM	Breccia platform unit	Base beach face	Mucilage on sand between rock	15	7.9	66
Smooth mat	7/07/2016	1:25 PM	4:45 PM	Outwash channel subunit within mat platform unit	Outwash channel delta sand sheet	Mat sheet patch	15	7.9	68
Ooze over sand	7/07/2016	1:35 PM	5:00 PM			New sand sheet	15	7.92	66
Black Sludge									

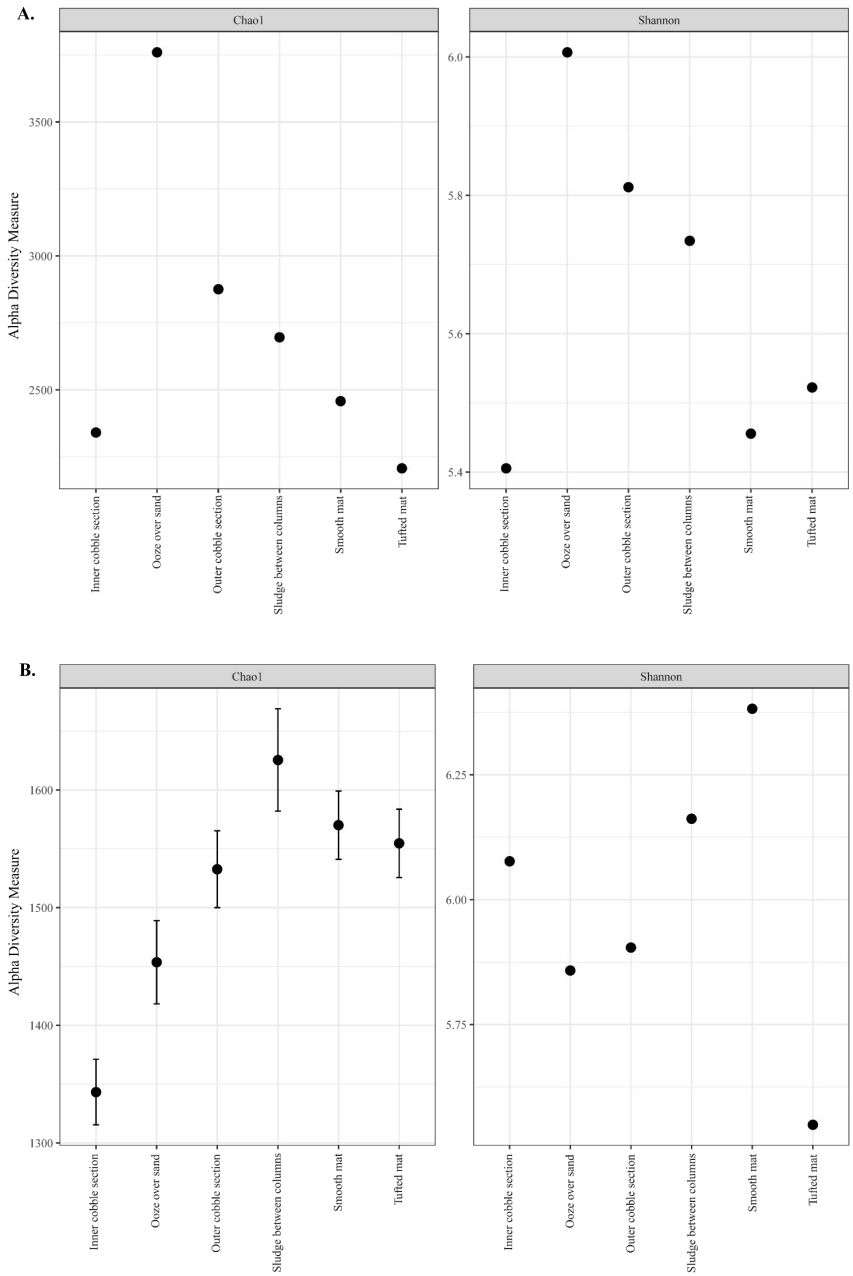

Supplementary Figure 4.1 Alpha diversity represented by the Choa1 and Shannon's diversity indices of RRBS samples. A. SSU rRNA (SILVA) and B. Transcripts (RefSeq).

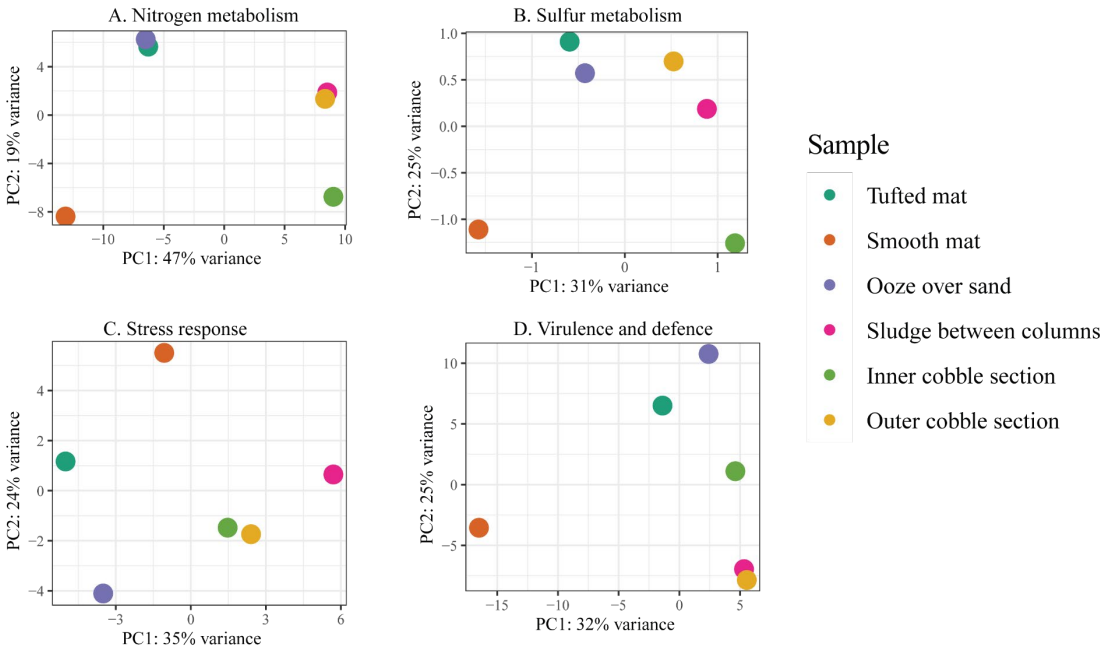

Supplementary Figure 4.2 Principle component analysis (PCA) showing relationships between RRBS samples based on differential analysis of the transcribed genes from A. nitrogen metabolism, B. sulfur metabolism, C. stress response and D. virulence and defence. Differential analysis of the transcribed genes was calculated from the variance stabilising transformation of SEED subsystem count data using the DESeq2 package in R.

A.

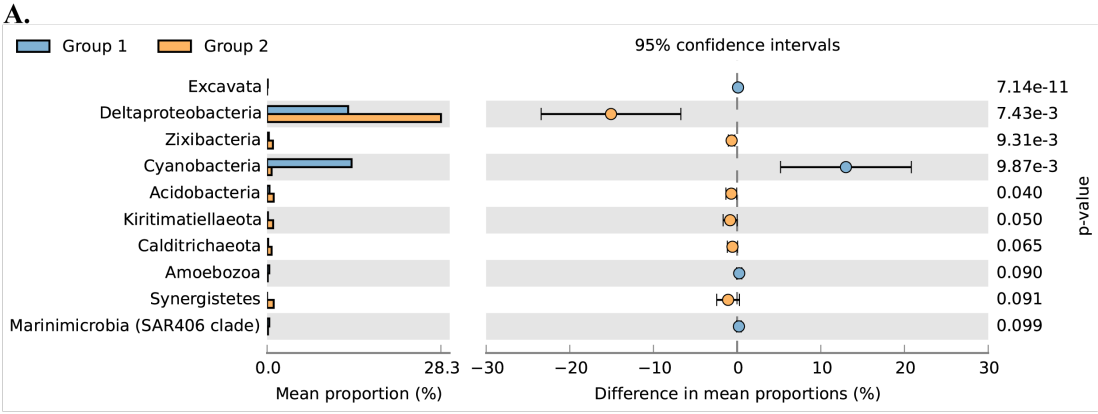

B.

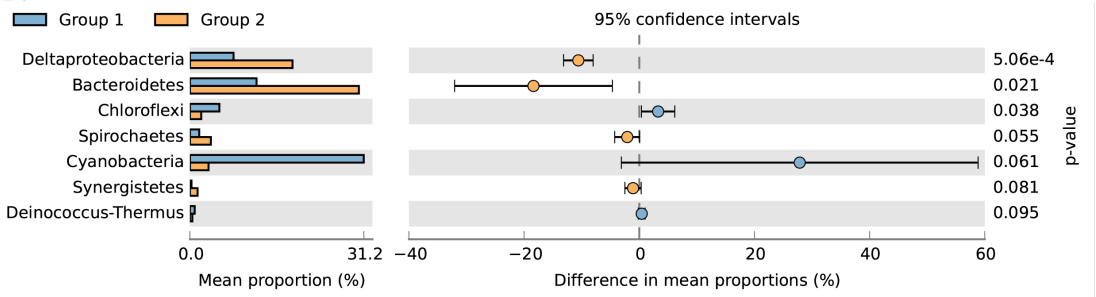

Supplementary Figure 4.3 Extended error bar plots identifying significant differences ($p < 0.1$) between mean proportions of microbial taxa in Groups 1 and 2 (ANOVA, Tukey's t-test). A. SSU rRNA (SILVA) and B. Transcripts (RefSeq).

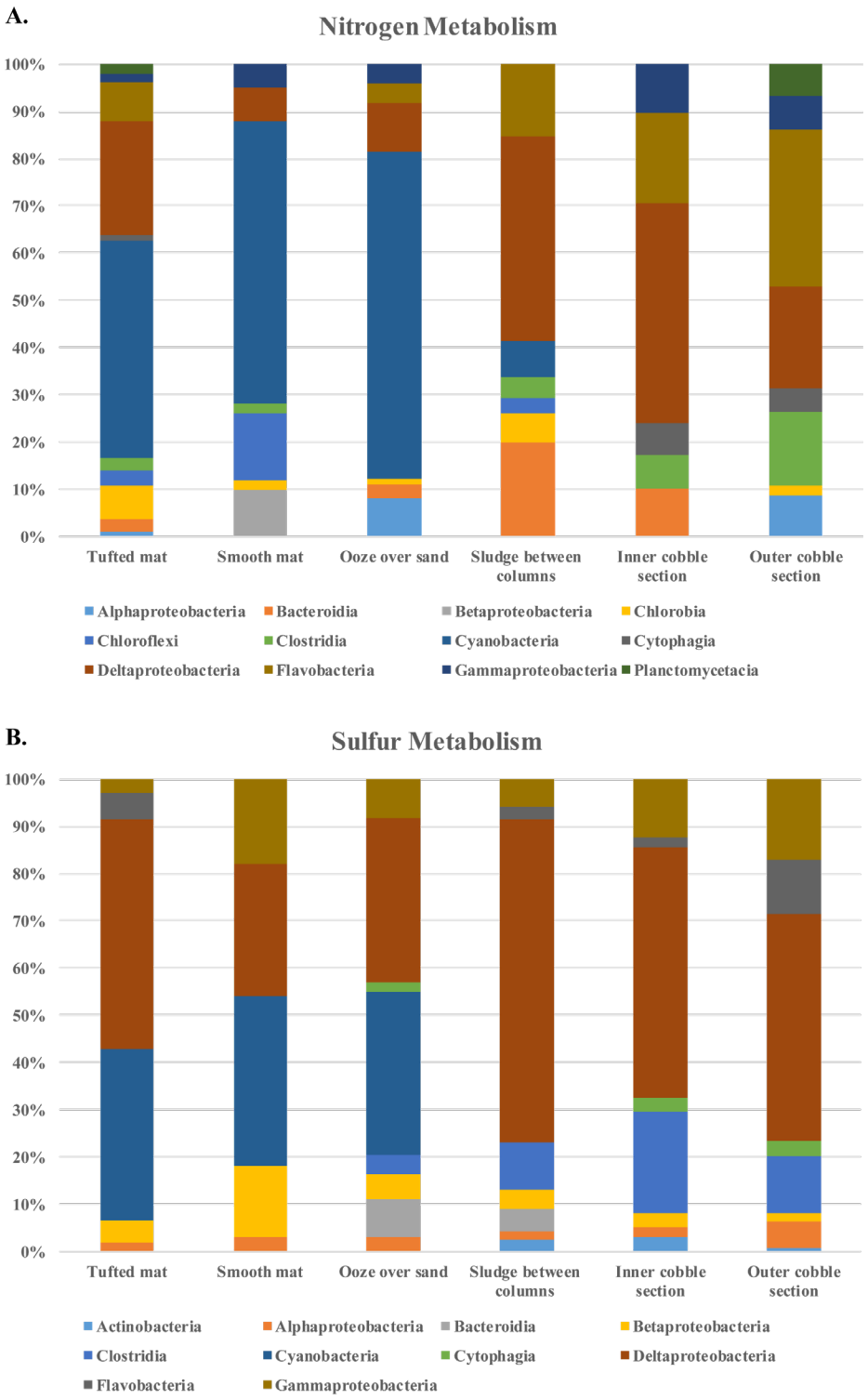

Supplementary Figure 4.4 Stacked bar charts displaying the relative abundances of active taxa (Order level) involved in A. Nitrogen and B. Sulfur metabolisms derived from SEED subsystem and NCBI RefSeq annotations.

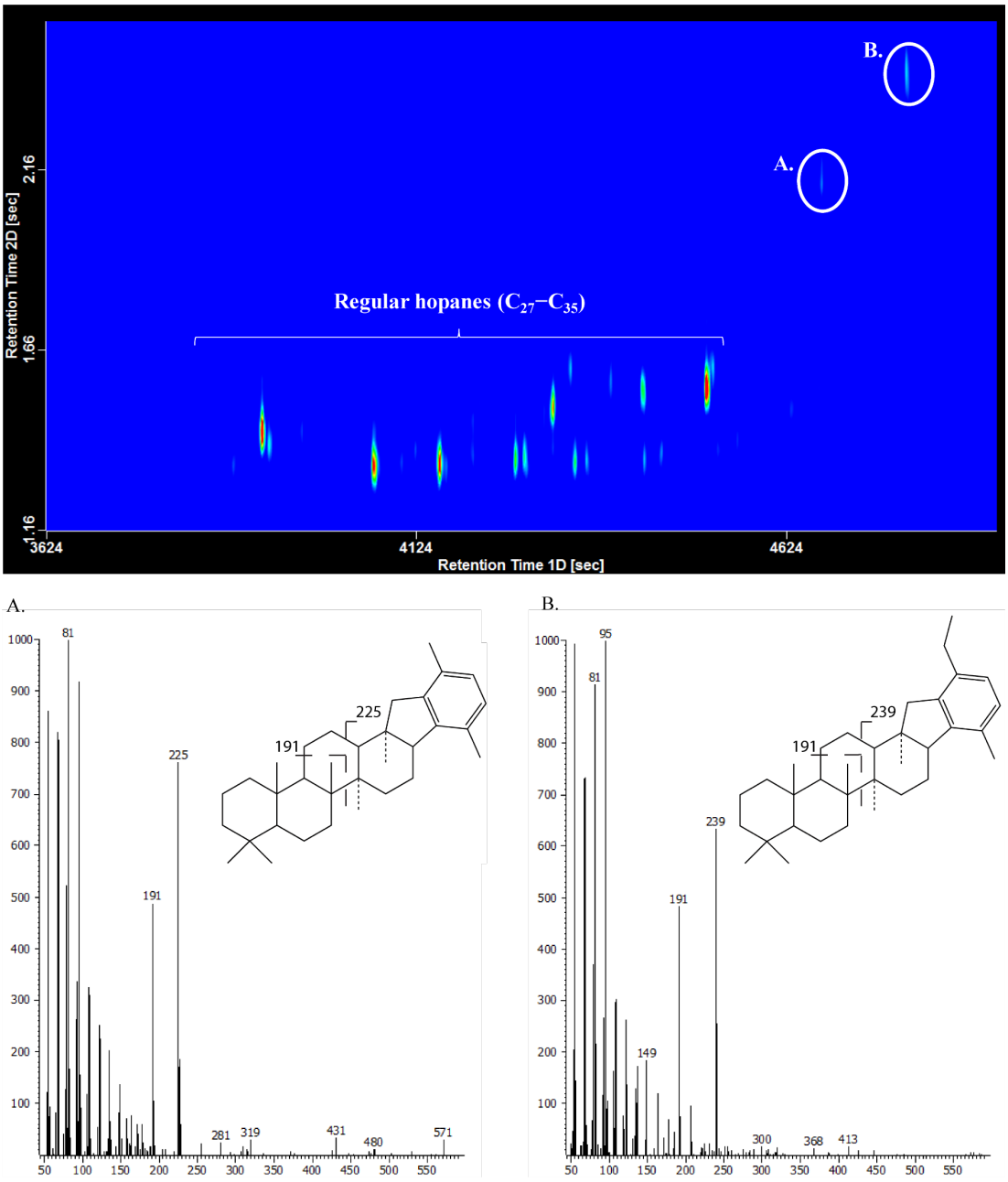

Supplementary Figure 4.5 Mass fragmentogram (*m/z* = 191) of the sulfur-bound aliphatic hydrocarbons from the inner cobble section measured by GCxGC-TOFMS displaying regular hopanes series (C_{27}-C_{35}) and two tentatively identified aromatized hopanoids. A. C_{33} benzohopane (ion fragment 225) and B. C_{34} benzohopane (ion fragment 239).

Chapter 5

Prevalence of heterocytous cyanophytes in elevated salinity environments

This Chapter is in preparation to be submitted to The ISME Journal: Multidisciplinary Journal of Microbial Ecology.

5.1 Background

Microbial mats are complex ecosystems that can be found globally in a wide range of environments, such as hypersaline ponds, hot springs, hot- and cold dry deserts, and coastal intertidal settings (Stal, 2012). Microbial mats typically have an upper green layer where Cyanobacteria predominantly act as primary producers (Ley et al., 2006; Stal, 2012; Kirk Harris et al., 2013) and atmospheric nitrogen fixers (Díez et al., 2007; Bauersachs et al., 2011), while also being responsible for the production of exopolymeric substances (EPSs) that provide physical protection and resistance to desiccation for the microbial community (Dupraz et al., 2009). Salinity is known to be a key factor in determining which Cyanobacteria are able to inhabit and develop in hypersaline lake and marine environments and some studies have listed taxa commonly occurring from low to high salt concentrations (Oren, 2008; Srivastava et al., 2009; Canfora et al., 2014). However, due to taxonomy-related issues, obtaining an accurate and comprehensive list of cyanobacterial species is challenging (Dvořák et al., 2015; Ramos et al., 2017). Traditional systems of classification and identification key genera of Cyanobacteria are based mainly on morphological criteria, which lacks taxonomic resolution. Molecular analyses on the contrary showed that genetically very diverse Cyanobacteria are often morphologically indistinguishable and do not share a common evolutionary history (Komárek, 2016). Public databases (e.g., GenBank, Greengenes) feature a large number of poorly annotated cyanobacterial sequences (Komárek, 2016) and sequences from reference strains are still missing in such databases (Garcia-Etxebarria et al., 2014; Tuzhikov et al., 2014). Moreover, certain groups of lipids (*e.g.* hopanoids, branched alkanes, have been put

forward as useful chemotaxonomic markers and are indicators of environmental factors for Cyanobacteria (Volkman et al., 1998; Bauersachs et al., 2017).

Cyanobacteria are currently divided into five morphological groups, two of which, *i.e.* the orders Nostocales and Stigonematales, are capable of differentiating vegetative cells into heterocytes under nitrogen-depleted conditions (Castenholz et al., 2001). These specialised cells contain nitrogenase, the enzyme required for the conversion of dinitrogen gas (N_2) to ammonia (Kumar et al., 2010). As nitrogenase is readily inactivated by even low amounts of oxygen, the thick heterocyte cell wall, consisting of an distinct outer polysaccharide and an inner glycolipid layers, limits gas diffusion into the cell interior (Meeks and Elhai, 2002). The inner layer contains a suite of unique glycolipid structures commonly referred to as heterocyte glycolipids (HGs; previously also known as heterocyst glycolipids), comprising either various modifications of hexose or pentose head groups, which are bound to long-chain diols, triols, or hydroxyketones (Bauersachs et al., 2009; Wörmer et al., 2012) (Supplementary Figure 5.1A). Their distribution in heterocytous Cyanobacteria suggests a chemotaxonomic relevance that might allow for identification between different genera (Bauersachs et al., 2009) and as biomarkers (molecular fossils) of N_2 fixation in both ecological and paleoenvironmental settings (Wörmer et al., 2012).

Studies of different cultured cyanobacterial species have expanded the range of known HGs. Based on the head group and chain length, number, and type of functional moieties, a diverse range of HGs have now been described in genera of Nostocales and Stigonematales (Supplementary Figure 5.1B). Currently, known lengths of the *n*-alkyl chains range from 26 to 32 carbon-atoms, and appear to be limited to even-carbon-atom numbers (Wörmer et al., 2012). Analysis of HGs has mainly focused on cyanobacterial isolates and has allowed a systematic description of the most common HG classes (Bauersachs et al., 2009). Still, the number of species tested is low compared to the large diversity of heterocytous Cyanobacteria in nature, and further work is needed to provide evidence for taxonomic heterogeneity concerning HG synthesis (Wörmer et al., 2012). Biomarker applications of HGs in microbial mats were recently reported: Microbial mats from the North Sea (Bauersachs et al., 2011) and revealed a relatively simple HG profile that consisted of only hexose HG_{26} diol, HG_{26} keto-ol and/or HG_{28} triol. The presence of these compounds was consistent with the species composition of the mats, which demonstrated the

taxonomic specificity of HGs. Analysis of HGs in microbial mats from Livingston Island and South Shetland Islands, Antarctica (Wörmer et al., 2012) revealed a larger diversity and increased abundance of certain HGs that were minor components in cultured strains, which could be applied to support taxonomic characterization of the community of heterocytous Cyanobacteria and to detect changes in the cyanobacterial consortia mediating N_2 fixation.

With recent advances in microbial transcriptomic profiling, the ability to assess microbiome-wide gene expression profiles with high-throughput RNA sequencing (metatranscriptomics) has become possible (Shakya et al., 2019). It has been used to investigate complex microbial communities occurring in a variety of environments, such as marine habits (e.g. Louyakis et al., 2018; Campbell et al., 2020) and soils (Redfield et al., 2002; Rippin et al., 2018), to unravel the role that particular organisms (e.g. cyanobacteria) play in regulating the flow of nutrients and energy. In this study, we aimed to establish the origin of HGs in microbial mat communities from a range of salinities (e.g. Shark Bay, Western Australia and Giblin River, Tasmania) to determine the diversity and ecological role (*e.g.* nitrogen and carbon fixation) of biologically active heterocytous cyanobacteria.

5.2 Materials and methods

5.2.1 Site and sample descriptions

Microbial mats were sampled from four locations in Shark Bay, Western Australia: Nilemah, Ron's Running Beach South (RRBS), Linke Lake and Garden Point (see Chapter 1, Figure 1.8). Pustular mats (PM) were sampled from Nilemah and Garden Point; these mats had a dark pigmented surface layer with a crenulated or pustular surface (Figure 5.1.1). The surface layer of these mats had a thickness of 1 to 8 mm through an individual pustule. No clear lamination was visible beneath the surface layer, although patches of green (cyanobacteria), pink (purple sulfur bacteria) and black (e.g. sulfate reducers) colouration indicates that vertical zonation of microorganisms occurs within the medium-grain irregular fenestral fabric of this mat (Logan et al., 1974). Smooth mats (SM) were sampled from Nilemah, RRBS and Garden Point; these mats had a light brown visible band of Cyanobacteria present 1-2 mm beneath the surface (Figure 5.1.2). This mat type had distinct lamination of

subsurface sediments with purple/pink (3–6 mm deep) and black (7–10 mm deep) zones visible in the fine to medium laminoid fenestral fabric (Logan et al., 1974; Pagès et al., 2014; Plet et al., 2018). Tufted mats (TM) were collected from RRBS and Garden Point and consisted of a greenish-brown to black colour (1-5 mm thick), and characterized by corrugated surfaces of sharp-crested ridges and low, broad depressions (Figure 5.1.3). The ridges are formed by vertically oriented tufts composed of large filaments of *Lyngbya aestuarii* (Logan et al., 1974; Flannery and Walter, 2012). The sample described as "ooze over sand" (OVS) was collected from RRBS, initially described as a thin mucilaginous sheet deposited as floc/ooze on a newly formed sand sheet that occurred after TC Owlyn; a year later this material was found to be transitioning into a microbial mat and was sampled for this study. The Birrida mat (BM) sampled from Linke Lake was a ~12 mm thick gelatinous mat with a smooth slimy yellow-brown surface layer (1-4 mm deep), covering laminated subsurface layers with green (5-8 mm deep), purple/pink (9-11 mm deep) and black (12 mm deep) zones (Figure 5.1.4). Green (GM) and yellow (YM) mats were sampled from Giblin River (Figures 5.1.5 and 5.1.6). These mats were ~20-30 mm thick with a smooth surface layer and contained either greenish or yellowish globular structures with calcite laminations (Proemse et al., 2017).

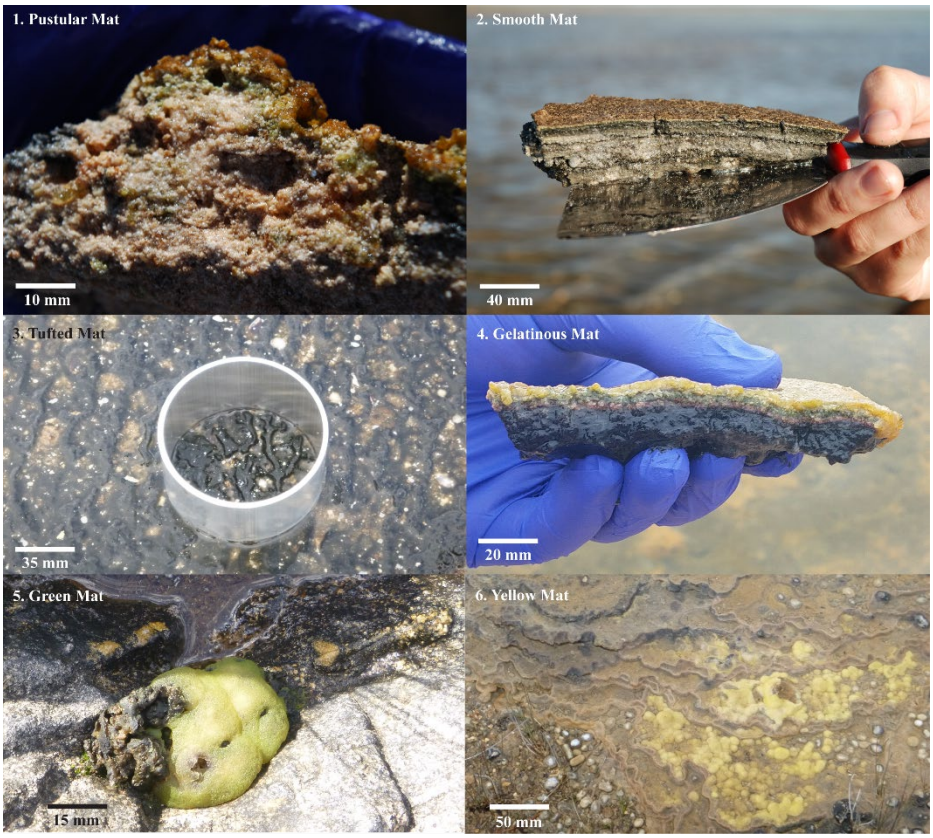

Figure 5.1 Field images of 1. Pustular and 2. Smooth mats from Nilemah; 3. Tufted mat from Garden Point; 4. Gelatinous mat from Linke Lake; and 5. Green and 6. Yellow mats from Giblin River. Photography credits to Alex Sessions (1 and 2) and Yalimay Jiménez (4).

5.2.2 Genomic and lipid biomarker analysis

Metatranscriptomic analysis is detailed in Section 2.2 – Chapter 2. RNA isolation, library preparation and sequencing (2.2.1), and bioinformatics (2.2.2). Illumina HiSeq 2500 pair-end sequencing read output with percentage summaries of trimmed and aligned sequences, number of assembled transcripts and number of annotations for Phyloflash and MG-RAST can be found in Supplementary Table 2.1 and Supplementary Table 5.2. Lipid biomarker analysis is detailed in Section 2.3 – Chapter 2. Lipid extraction and lipid fractionation (2.3.2), and HPLC–ESI/MS^2 (2.3.8). Statistical analysis and visualisation are detailed in Section 2.4 – Chapter 2.

5.3 Results

5.3.1 Distribution of Cyanobacteria

Cyanobacterial 16S rRNA transcripts accounted for an average 13.2 ± 9.3 % of total reads in hypersaline mats, 8.6 ± 3.5 % in metahaline mats and 11.8 ± 5.7 % in freshwater mats (Supplementary Table 5.3). In contrast, cyanobacterial transcripts (mRNA transcripts) accounted for a larger proportion with an average 29.2 ± 9.5 % of total reads in hypersaline mats, 21.0 ± 6.5 % in metahaline mats and 22.1 ± 13.3 % in freshwater mats (Supplementary Table 5.4). 16S rRNA transcripts of non-heterocytous Cyanobacteria were on average 9 times more abundant in hypersaline mats and 21 times in metahaline mats than 16S rRNA transcripts of heterocytous cyanobacteria; whereas in freshwater mats, heterocytous cyanobacterial 16S rRNA was on average twice as abundant. Interestingly in the cyanobacterial mRNA transcripts, heterocytous Cyanobacteria accounted for a larger proportion of the reads with non-heterocytous Cyanobacteria being on average only 3 times more abundant in hypersaline mats, 2 times in metahaline mats and in freshwater mats, the heterocytous Cyanobacteria were on average 4 times as abundant as non-heterocytous Cyanobacteria. Oscillatoriales and Synechococcales were the prominent non-heterocytous Cyanobacteria in 16S rRNA transcripts from mats occurring in the saline environments of Shark Bay. Synechococcales, however, were not annotated in the cyanobacterial mRNA transcripts rather Chroococcales and Oscillatoriales were the most annotated non-heterocytous Cyanobacteria. Nostocales and Stigonematales accounted for >1 % 16S rRNA transcripts in both the hypersaline and metahaline mats with the exception of Nil PM1 2016 having a higher relative abundance of Nostocales (2.3 %). In freshwater mats, 16S rRNA transcripts of heterocytous Cyanobacteria represented 3.1-5.9 % of the reads. Nostocales accounted for 2.5-9.5 % of the cyanobacterial mRNA transcripts in both the hypersaline and metahaline mats and 1.1-25.6 % in the freshwater mats.

5.3.2 Functional role of Cyanobacteria

Nostocales accounted for 9-16% of the photosynthesis gene transcripts in saline mats, but were highly varied in the freshwater mats, accounting for 66 % in GR GM1 2016, 14% in GR GM2 2016 and 5 % in GR YM 2016 (Supplementary Table 5.5). Overall, large proportions of the photosynthesis related gene transcripts were associated to the

Chroococcales (10-70 %) and Oscillatoriales (7-15%). Similarly, Nostocales accounted for 3-15% of the CO_2 fixation gene transcripts, but were also found to be highly varied in the freshwater mats accounting for 44 % in GR GM1 2016, 22 % in GR GM2 2016 and 3 % in GR YM 2016 (Supplementary Table 5.6). Overall, large proportions of the CO_2 fixation gene transcripts were related to the Chroococcales (22-58 %) and Oscillatoriales (4-44 %). Cyanobacteria also accounted for a large proportion of the gene transcripts involved in biofilm (EPSs) formation with Nostocales accounting for 7-35 % and Chroococcales for 8-31 % in saline mats (Supplementary Table 5.7). In freshwater mats, Nostocales accounted for a large fraction of the gene transcripts involved in biofilm (EPSs) formation in the green mats with 42% in GR GM1 2016 and 38% in GR GM2 2016, but only 2 % in GR YM 2016. Bacterial phyla, such as Actinobacteria, Bacteroidetes, Chloroflexi, Firmicutes and Proteobacteria, also accounted for a substantial fraction of the transcripts involved in biofilm (EPSs) formation in some of the mats.

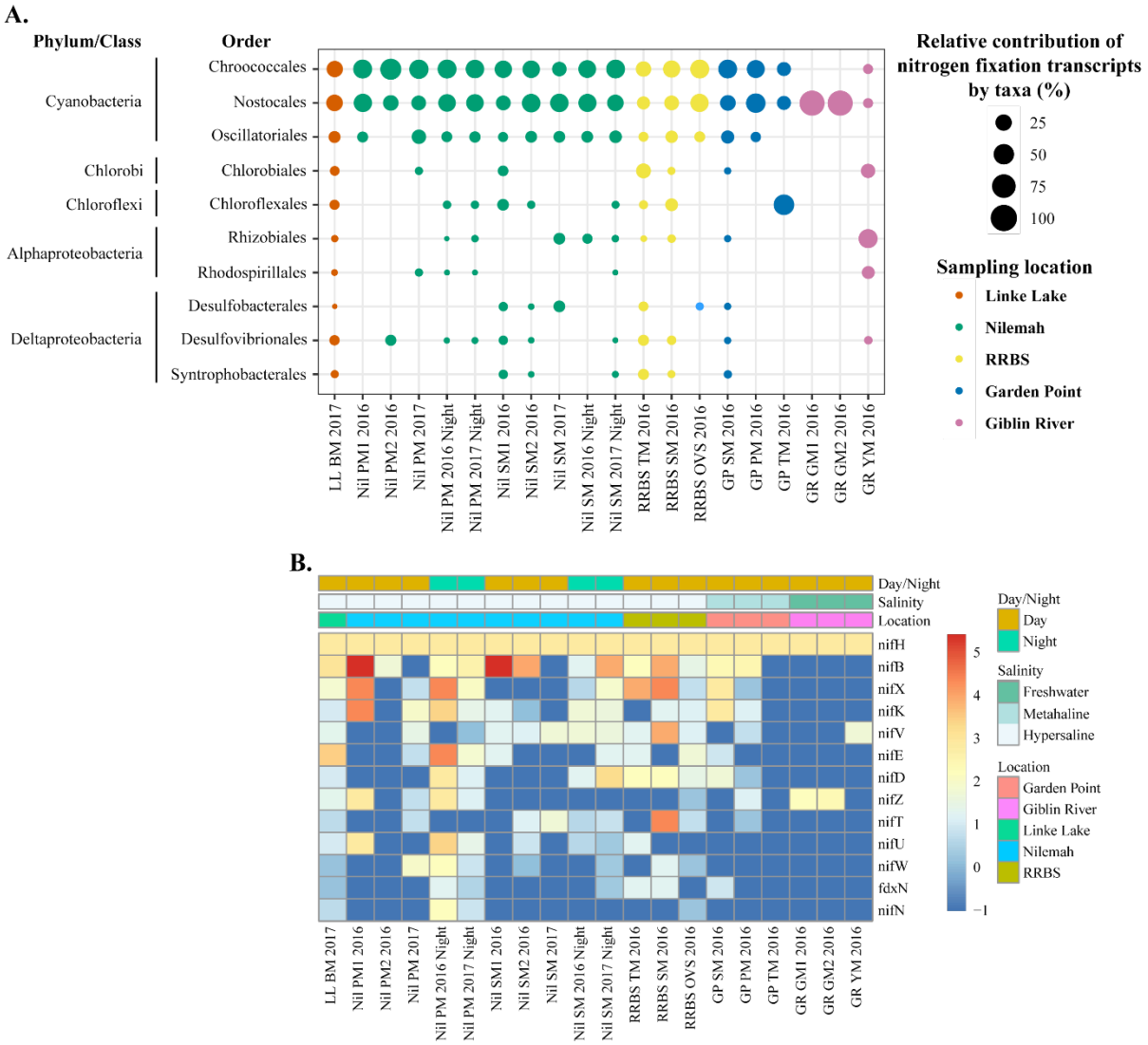

Figure 5.2 Metatranscriptomic profiling of nitrogen fixation in microbial mats during the daytime. **A.** Relative transcript abundances from taxa transcribing genes involved in nitrogen fixation. **B.** Heatmap showing 13 nitrogen fixation genes (>10) abundantly transcribed in Nostocales transcriptomes. The nif genes encode enzymes involved in the fixation of atmospheric nitrogen and fdx genes encode ferredoxin-like proteins in the nif region. Differential analysis of the transcribed genes was calculated from the variance stabilising transformation of KO count data using the DESeq2 package in R. A gradient from red to blue indicates gene abundance across samples with red representing genes that are highly transcribed and blue indicating genes that have lower relative transcription.

In saline mats, Cyanobacteria accounted for the largest proportion of the gene transcripts involved in nitrogen fixation with Nostocales accounting for 16-52 %, Chroococcales for 20-64 % and Oscillatoriales for 6-22% (Figure 5.2A; Supplementary Table 5.8). Nostocales were the only taxa found to be transcribing nitrogen fixation genes in the green freshwater mats. In the yellow freshwater mat,

however, they only accounted for 7 % of the nitrogen fixation genes. Rhizobiales (57 %) and Chlorobiales (25 %) were the largest contributors to nitrogen fixation in the yellow mat. Comparison of mats sampled during the day and night from Nilemah indicated no relative change in transcription by cyanobacterial groups. 13 nitrogen fixing genes were found to be transcribed by Nostocales with the nitrogenase iron protein (*nif*H) being abundantly transcribed in all of the mats studied (Figure 5.2B). Transcription of nitrogen fixing genes was much higher and diverse in Nostocales occurring in saline environments; Nostocales occurring in the freshwater mats were found to only transcribe *nif*HVZ genes. Abundantly transcribed nitrogen fixing genes by Nostocales in saline mats included nitrogenase *nif*BDEHKNTUVWXZ genes and *fdx*N (ferredoxin-like protein in the *nif* region).

5.3.3 Distribution of heterocytous Cyanobacteria

A highly diverse and active community of heterocytous cyanobacteria consisting of non-branching families *Aphanizomenonaceae*, *Calotrichaceae*, *Cyanomargaritaceae*, *Fortieaceae*, *Gleotrichiaceae*, *Nostocaceae*, *Rivulariaceae*, *Scytonemataceae*, *Symphyonemataceaea* and *Tolypothrichaceae*, and true-branching families *Chlorogloeopsidaceae*, *Hapalosiphonaceae* and *Stigonemataceae* were found in microbial mats from all sampling sites based on 16S rRNA analysis (Figure 5.3). Cyanobacterial genera were found to significantly differ between sampling locations (ANOSIM, R= 0.61; p = .0001). Microbial mats from Nilemah and Garden Point appear to contain abundant *Anabaena* (p = .003) and *Gloeotrichia* (p = .01), while *Chakia* was exclusively present in Giblin River (p = .01) (Supplementary Table 9). *k*-means cluster analysis indicated that microbial mats from Nilemah had greater inputs from *Anabaena*, *Stigonema*, *Nostoc, Rivularia* and *Calothrix*; RRBS and Garden Point had greater inputs from *Calothrix*, *Fischerella* and *Chlorogloeopsis*; Linke Lake had greater inputs from *Fischerella* and *Chlorogloeopsis*; and Giblin River had greater inputs from *Scytonema* and *Ewamiania* (both belonging to the Scytonemataceae; Figure 5.4). PCA of cyanobacterial genera revealed that the microbial mats typically grouped within their sampling locations, although especially low amounts variance was observed between Nilemah and Garden Point mats (Supplementary Figure 5.2). Furthermore, tufted mats from RRBS and Garden Point grouped together, as well as

the OVS from RRBS and the gelatinous mat from Linke Lake grouping together with the Giblin River microbial mats.

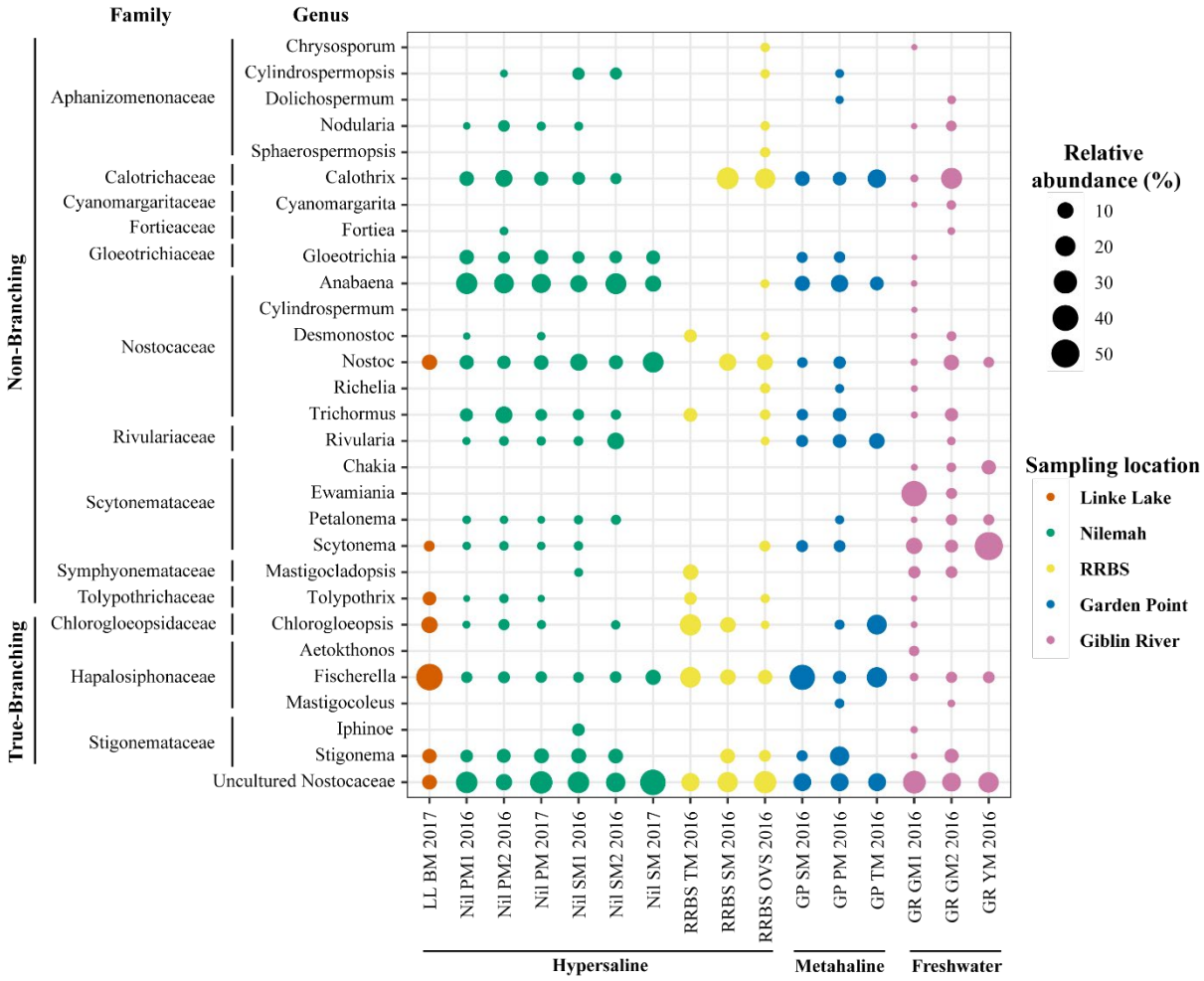

Figure 5.3 Dot plot displaying the composition and relative abundance of the cyanobacterial non-branching (Order Nostocales) and true-branching (Order Stigonematales) families and genera in microbial mats from Shark Bay, Western Australia (Linke Lake (LL)), Nilemah (Nil), RRBS and Garden Point (GP), and Tasmania (Giblin River (GR)). BM = birrida mat (gelatinous mat), PM = pustular mat, SM = smooth mat, TM = tufted mat, OVS= ooze over sand, GM = green mat and YM = yellow mat.

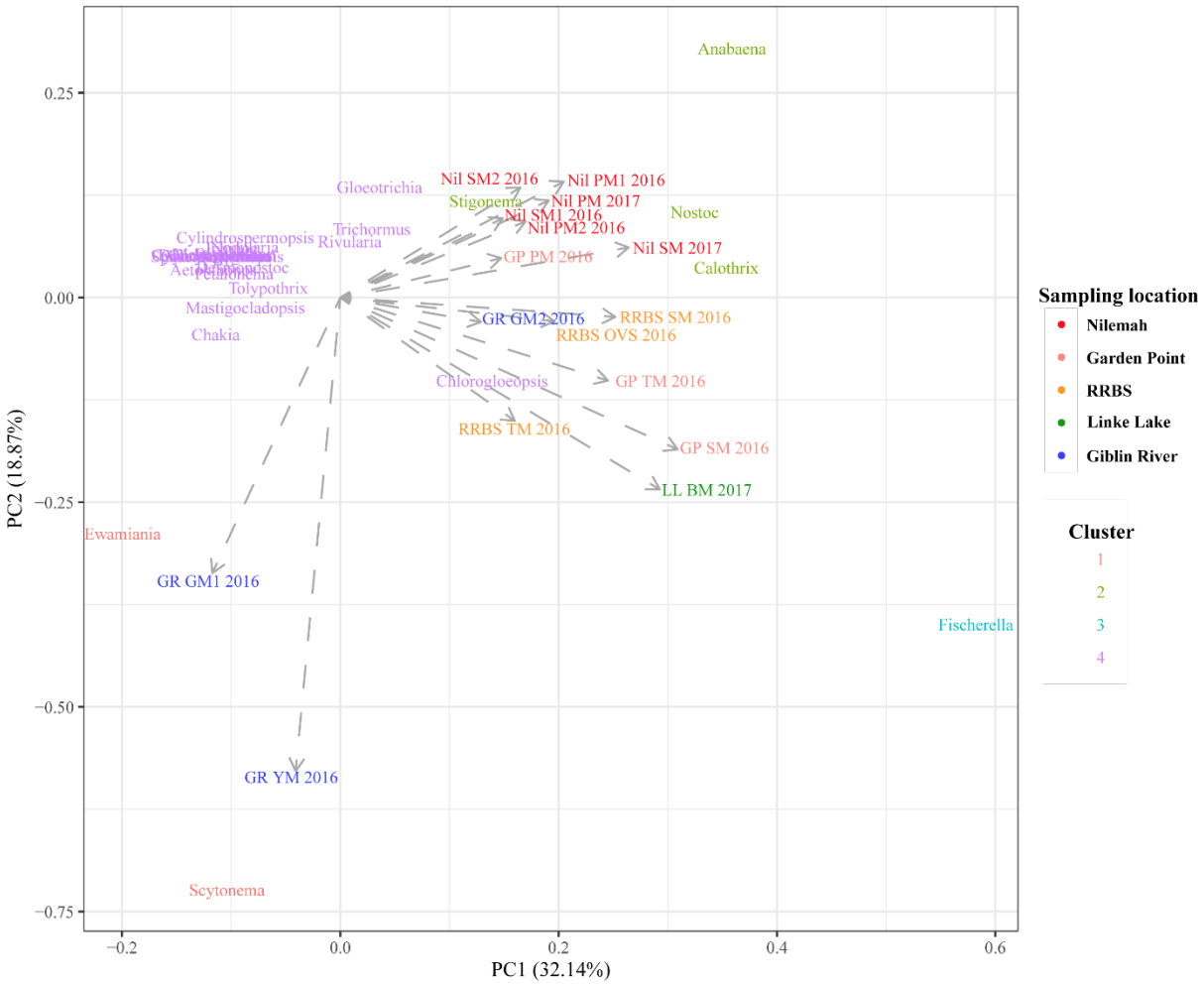

Figure 5.4 PCA plot constructed from k-means cluster analysis of active heterocytous genera within microbial mats from Shark Bay, Western Australia (Nilemah, RRBS, Garden Point and Linke Lake) and Tasmania (Giblin River). PM = pustular mat, SM = smooth mat, TM = tufted mat, OVS= ooze over sand, BM = birrida mat (gelatinous mat).

5.3.4 Distribution of heterocyte glycolipids

We detected a total of 20 different HG structures in the Shark Bay and Giblin River microbial mats (Figure 5.5). Pentose HGs (P HGs) were generally abundant in the saline microbial mats and ranged from P HG_{26} to P HG_{30} diols and P HG_{30} to P HG_{32} triols. In addition, a suite of previously undescribed HGs with pentose headgroup and exceptionally long carbon chains ranging from 32 to 36 carbon atoms has tentatively been identified. In contrast, HGs with a pentose headgroup occurred only in minor proportions in the Giblin River samples. A diverse suite of hexose HGs, which have been reported previously mainly from freshwater taxa, were found at all sites. These HGs included HG_{26} to HG_{30} diols and keto-ols as well as HG_{28} to HG_{32} triols and keto-

diols (see Supplementary Figure 5.1 for structures). The Me-hexose (Me-H) HG_{28} triol was ubiquitously present at all locations irrespective of the salinity. HGs differed significantly between sampling locations (ANOSIM, R= 0.92; P= 0.0001). In microbial mats from Nilemah, Garden Point and RRBS P HG_{30} diol (p = .047) was present exclusively. The tentatively identified P HG_{32} to P HG_{36} triols (p = .009) were detected only at the Shark Bay locations. Microbial mats from Giblin River exclusively contained HG_{30} diol and HG_{32} triol (p = .009), albeit only in low relative abundances (Supplementary Table 10). *k*-means cluster analysis indicated that microbial mats from Nilemah generally received greater inputs of the P HG_{32} and HG_{34} triols; Garden Point, RRBS, Linke Lake and Giblin River microbial mats had greater inputs from Me-H HG_{28} triol; and RRBS, Linke Lake and Giblin River microbial mats also had greater inputs from HG_{26} diol, HG_{28} triol and HG_{30} triol (Figure 5.6). PCA of HGs revealed that microbial mats generally grouped within their sampling locations, however a discrepancy was observed with the smooth mat from RRBS and the Birrida (gelatinous) mat from Linke Lake grouping together with the Giblin River microbial mats (Supplementary Figure 5.3).

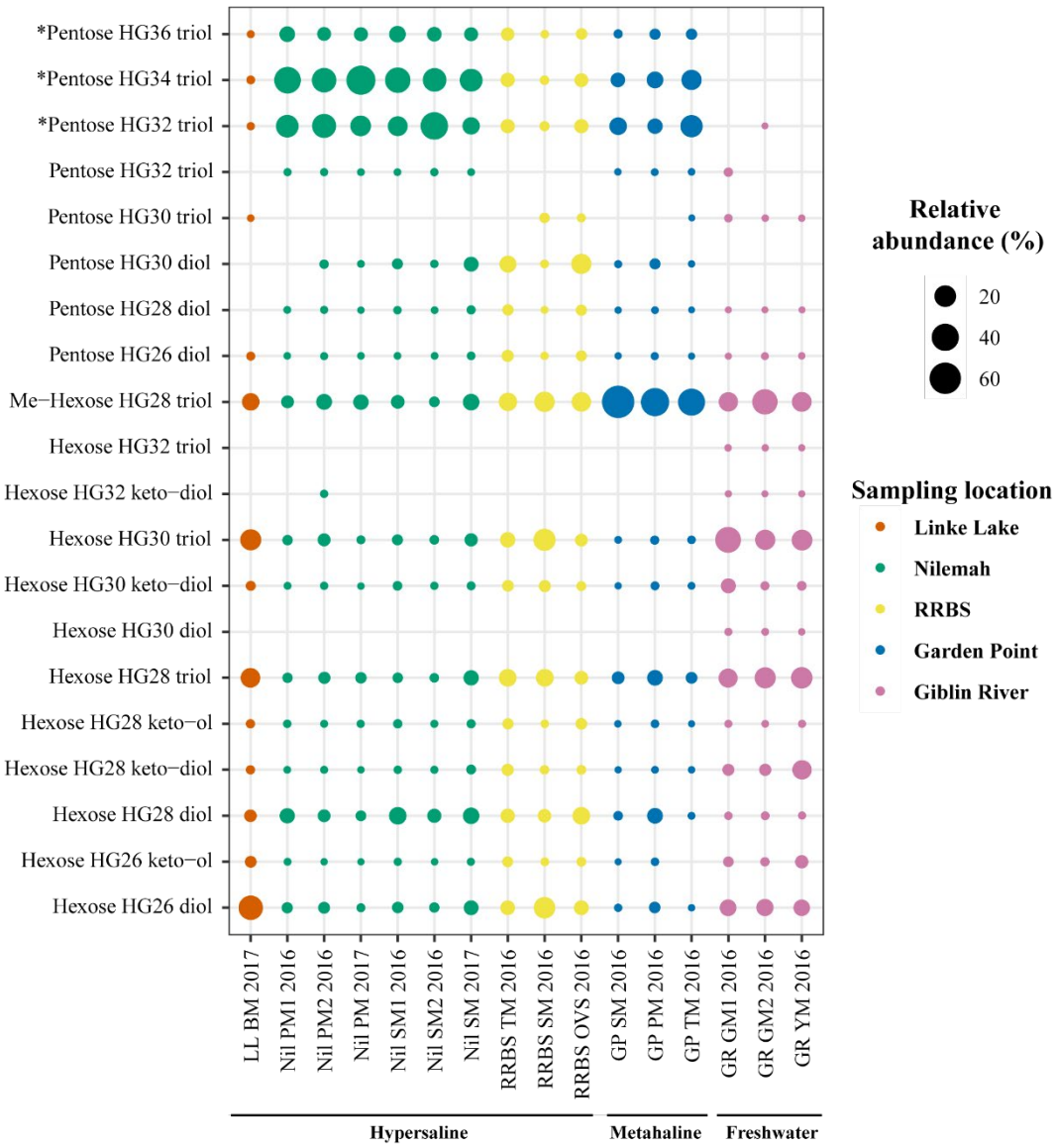

Figure 5.5 Dot plot displaying the composition and relative abundance of heterocyte glycolipids (HGs) in microbial mats from Shark Bay, Western Australia (Linke Lake (LL)), Nilemah (Nil), RRBS and Garden Point (GP), and Tasmania (Giblin River (GR)). BM = BM = birrida mat (gelatinous mat), PM = pustular mat, SM = smooth mat, TM = tufted mat, OVS= ooze over sand, GM = green mat and YM = yellow mat. *tentatively identified novel HG isomers.

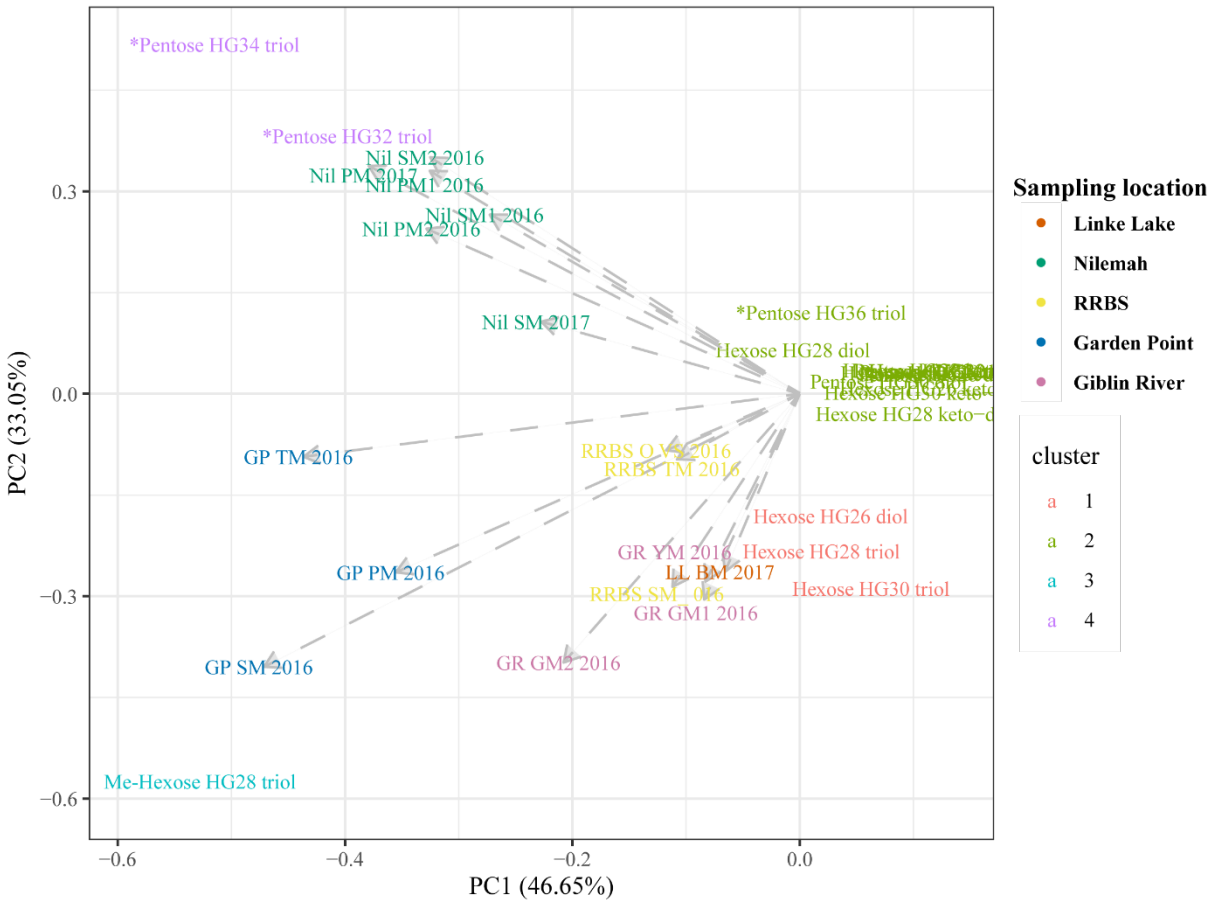

Figure 5.6 PCA plot constructed from *k*-means cluster analysis of heterocyte glycolipids (HGs) within microbial mats and microbially derived materials from Shark Bay, Western Australia (Nilemah, RRBS, Garden Point and Linke Lake) and Tasmania (Giblin River). PM = pustular mat, SM = smooth mat, TM = tufted mat, OVS= ooze over sand, BM = birrida mat (gelatinous mat), GM = green mat and YM = yellow mat. *tentative identification of novel HGs.

5.3.5 Lipidomic and taxonomic integration

The regularized canonical correlation analysis (rCCA) revealed that a majority of the HGs had positive correlations with a number of active cyanobacterial genera, which exceeded a similarity score higher than 0.4 (Figure 5.7). A strong positive relationship with the P HG_{32} to HG_{36} triols, HG_{28} diol and HG_{32} keto-diol was observed for *Gloeotrichia* and *Anabaena*. Positive relationships of these lipids were also observed for *Calothrix*, *Cylindrospermopsis*, *Nostoc*, *Trichormus* and *Stigonema*. A strong positive relationship with pentose HG_{32} triol, pentose HG_{32} triol, hexose HG_{30} triol, hexose HG_{30} keto-diol, hexose HG_{30} diol and hexose HG_{32} triol was observed for *Ewaniana*, *Cylindrospermum*, *Aekothonos* and *Mastigocladopsis*. *Chakia*, *Scytonema* and *Petalonema* had strong positive relationships with hexose HG_{28} keto-diol and

hexose HG_{26} keto-ol. *Chakia* and *Scytonema* also had positive relationships observed with hexose HG_{30} triol, and hexose HG_{32} triol. Hexose HG_{28} triol had positive relationships with *Chakia*, *Scytonema, Ewaniana*, *Cylindrospermum*, *Aekothonos*, *Mastigocladopsis*, *Fischerella* and *Tolypothrix*. A positive relationship with P HG_{26} diol, me-hexose HG_{28} triol and hexose HG_{26} diol was observed for *Mastigocladopsis*, *Desmonostoc*, *Fischerella*, *Tolypothrix* and *Chlorogloeopsis*.

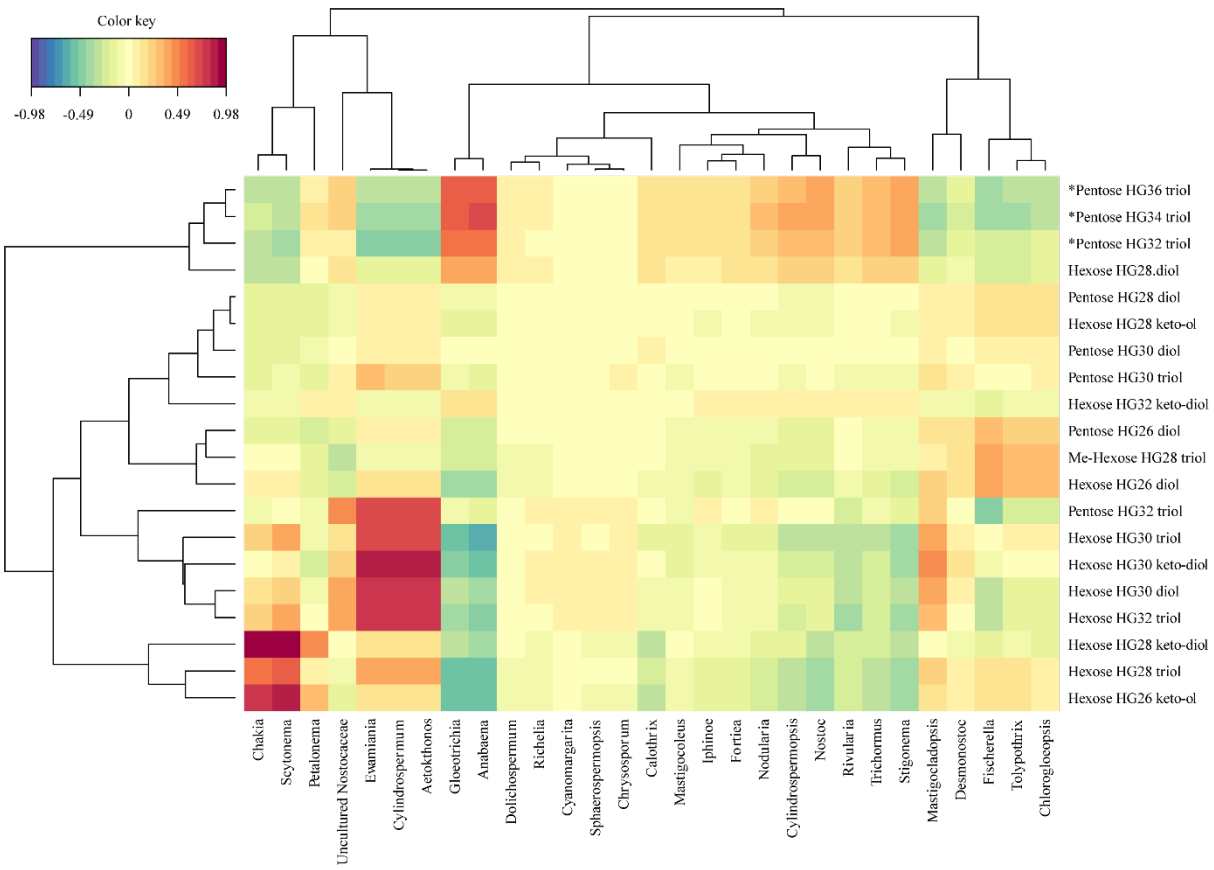

Figure 5.7 Heatmap analysis performed by using regularized canonical correlations analysis showing the relation between taxonomic and lipidomic datasets. Correlation strengths are indicated by the colour key. * indicates tentatively identified novel HG isomers found in the mats studied herein.

5.4 Discussion

In this work, we have identified an unexpected large variety of heterocytous Cyanobacteria in the marine setting of Shark Bay, Western Australia and freshwater setting of Giblin River, Tasmania using two independent approaches, molecular genetics and molecular lipid analysis.

5.4.1 Distribution of active heterocytous Cyanobacteria in microbial mats

Low salinity favoured the presence of heterocytous Cyanobacteria in freshwater mats of Giblin River, while mats occurring in higher salinities mainly supported the presence of non-heterocytous genera. This corroborates with previous findings indicating that the taxonomic distribution of Cyanobacteria is affected by salinity (Kirkwood et al., 2008; Oren, 2015). Previous analyses of Shark Bay microbial ecosystems based on rDNA (Goh et al., 2009) and microscopy (Jahnert and Collins, 2013) have detected the cyanobacterial orders Oscillatoriales, Chroococcales and Pleurocapsales, with many of the top species belonging to the Chroococcales and Oscillatoriales (i.e. *Lyngbya* in tufted mats). In contrast, heterocytous Cyanobacteria have been only infrequently encountered in hypersaline environments so far with instances of *Calothrix* (Oren, 2015), *Scytonema* (Roney et al., 2009) and *Nodularia* (Paerl et al., 2000) reported in hypersaline lakes. A previous study of Shark Bay microbial mats did not observe heterocytous Cyanobacteria during microscopic examination and universal bacterial 16S rDNA gene analysis (Allen et al., 2009). However, more recent metagenomic and cyanobacterial 16S rDNA focused studies of this ecosystem have indicated the presence of Nostocales (Garby et al., 2013; Babilonia et al., 2018).. The 16S rRNA analysis done in this study indeed revealed a large diversity of heterocytous Cyanobacteria in the metahaline and hypersaline microbial mats, including representatives of the genera *Anabaena*, *Gloeotrichia*, *Stigonema*, *Nostoc*, *Fischerella,* and *Chlorogloeopsis*. These genera have previously been found to occur in saline environments (e.g. Ali and Sandhu, 1972; Sheridan, 1992; Hindák, 2008; Srivastava et al., 2009b; Pfeffer and Brown, 2016). However, there are limited reports of these Cyanobacteria in Shark Bay. So far, *Gloeotrichia*, *Stigonema, Fischerella* and *Chlorogloeopsi* have yet to be identified in Shark Bay. Whereas, *Anabaena* have not directly been identified, their presence has been proposed *via* non-ribosomal peptide synthetases present in stromatolite communities (Burns et al., 2005) and a culture based study of the actively growing microbial layer from a Shark Bay stromatolite characterized by *Nostoc* in the Cyanobacteria community (Burns et al., 2004).

In contrast, our study found that *Scytonemataceae*, *Chakia, Scytonema* and *Ewamiania,* were prominent active heterocytous Cyanobacteria in Giblin River. A previous study of freshwater mats from Giblin River indicated that the cyanobacterial diversity (26.4% of reads) was extensive (113 OTUs), with the main phylotypes most similar to Cyanobacteria from soil crust, freshwater lakes and biofilms (Proemse et al., 2017). *Scytonema* mats have been recognised in a karstic freshwater lake on the Yucatan Peninsula, Mexico (Gischler et al., 2011). These mats show morphological similarities to the green mats sampled from Giblin River, forming firmly lithified hemispheroid structures 4–6 cm in diameter, densely covered by a cyanobacterial biofilm which was internally permeated throughout by calcified sheaths. *Chakia* and *Ewamiania* were recently characterised genera from *Scytonemataceae*; *Chakia* was isolated from mats occurring in alkaline marshes from Belize, Central America (Komárková et al., 2013) and *Ewamiania* was isolated from a mat occurring in a thermal spring complex in tropical, north-eastern Australia (McGregor and Sendall, 2017).

5.4.2 Physiological activities of heterocytous Cyanobacteria in microbial mats

Heterocytous Cyanobacteria made up relatively small proportions of the overall active microbial communities in mats. Yet, they were found to contribute to the majority of gene transcripts associated with nitrogen fixation and biofilm production. Cyanobacteria occurring in the upper aerobic layer of the mat (2–3 mm) are considered as some of the most important primary producers of all phototrophic mat types (Stal, 1995). We found abundant contributions of photosynthetic and carbon fixation gene transcripts from Chroococcales in the saline mats, with smaller contributions from Oscillatoriales and Nostocales. Nostocales made greater contributions to these autotrophic pathways in freshwater green mats. Chroococcales have previously been shown to make the largest contribution to photosynthesis related gene transcripts in coastal mats (Hörnlein et al., 2018), whereas in freshwater microbial mats from Antarctica, Nostocales were reported to be the major primary producers (Almela et al., 2019). Or study suggests that heterocytous Cyanobacteria are likely to be the main primary producers in the freshwater microbial mats of Giblin River. Heterocytous Cyanobacteria were also found to be prominent biofilm producers in all the

investigated microbial mat types. *Nostoc* and *Anabaena* are known to be the major producer of EPSs (De Philippis and Vincenzini, 1998; Singh et al., 2016; Cruz et al., 2020). Cyanobacteria yield EPSs as a direct response to selective pressures from their natural environment (Rossi and De Philippis, 2015). Bacterial EPSs play a role in providing anchorage to substrate(s), to allow protection against desiccation, predation, masking of antibody recognition, and prevention of lysis by other bacteria and viruses (Li et al., 2001). Therefore, biofilm forming heterocytous Cyanobacteria are likely to play an essential role in the formation and ongoing protection of microbial mats.

A previous study assessing *nif*H transcripts indicative of active diazotrophic communities in microbial mats found that Oscillatoriales were dominant under freshwater conditions, whereas Chroococcales were abundant under marine conditions (Severin et al., 2012). Under elevated salinities, both orders as well as Nostocales were found, but the contribution of Cyanobacteria to the *nif*H transcript libraries decreased noticeably with rising salinity. Another study detecting *nif*H transcripts found that communities dominated by heterocytous Cyanobacteria exhibited light-independent nitrogen fixation at total salinity up to 60‰; whereas, communities dominated by non-heteroctous Cyanobacteria exhibited nitrogen fixation at total salinity up to 100‰ (Namsaraev et al., 2018). The use of metatranscriptomics in our study has enabled for a larger group of *nif* transcripts to be observed, with many other *nif* transcripts (i.e. *nif*B or *nif*X) other than *nif*H being highly transcribed by Nostocales in the mats, putting into question the reliability of the *nif*H transcript as an indicator for overall diazotrophic activity. A majority of the *nif* genes observed in this study are a part of large gene cluster including *nif*B-*fdx*N-*nif*S-*nif*U-*nif*H-*nif*D-*nif*K-*nif*E-*nif*N-*nif*X found within the *Anabaena* genome (Haselkorn, 1986). Therefore, abundance of these *nif* gene transcripts in the Nostocolean transcriptomes from Shark Bay microbial mats further implies the presence of *Anabaena* genera. Furthermore, a study of nitrogenase gene expression in *Anabaena variabilis* indicated that *nif*B appeared to be the primary promoter for the entire *nif* cluster and that structural genes *nif*HDK were the most abundant transcripts; however, their abundance was not controlled by an independent *nif*H promoter (Pratte and Thiel, 2014). Therefore, due to the abundance of the *nif*B transcript in Nostocolean transcriptomes from Shark Bay, the *nif*B transcript may pose as a more reliable indicator of diazotrophic activity of heterocytous Cyanobacteria occurring in enhanced saline environments.

Additionally, our study showed that either Nostocales and/or Chroococcales transcribed the greatest extent of nitrogenase genes in metahaline and hypersaline environments with similar amounts of these genes being transcribed during the day and night by both orders. This suggests that both orders are playing a similar role in nitrogen acquisition within saline mats from Shark Bay. In the freshwater environment of Giblin River, Nostocales were found to be the only bacteria fixing nitrogen in the green mat type, whereas Rhizobiales (Alphaproteobacteria) made major contributions in nitrogen fixing transcripts in the yellow mat type. Rhizobiales have been found to be the second highest diazotroph group in soils, forming symbiotic relationships with plants (Che et al., 2018), therefore considerations must be taken when studying nitrogen inputs in terrestrial mats harbouring both cyanobacterial and alphaproteobacterial genera capable of fixing nitrogen. The abundance and range of nitrogen fixing gene transcription was higher in the saline mats when compared to the freshwater mats, suggesting that the marine environment of Shark Bay is more depleted in available nitrogen than that of Giblin River.

5.4.3 Sources and environmental controls on HG distributions

PCA of taxonomic and HG data showed that our microbial mats mainly grouped together based on sampling location but not based on the type of mat nor time of sampling. Nilemah and Garden Point mats grouped together based on the taxonomic data but were separated based on their HG distributions, suggesting salinity could be the controlling factor in the HG synthesis in heterocytous Cyanobacteria in intertidal/subtidal zones. HGs with pentose moieties and the tentatively identified P HG_{32} to P HG_{36} triols in the mats were dominant in saline environments. The latter were found to correlate with mats containing high proportions of non-branching Nostocales (e.g. *Anabaena* and *Nostoc*), as well as the true-branching *Stigonema*. HG_{26} diol has previously been described from cultures of *Anabaena* and *Nostoc* (Bauersachs et al., 2009), whereas the HG_{32} keto-diol has been described in stigonematalean Cyanobacteria (Bauersachs et al., 2019a). Mats from RRBS, Linke Lake and Giblin River were rich in HGs containing mainly diols and triols. PCA of taxonomic and HG data indicated that mats from these locations were similar and with their proximity to the land suggests that terrestrial runoff may be a contributing factor. Linke Lake (Shark

Bay) had the highest salinity (>80) but contained the lowest diversity of heterocytous cyanobacteria, mainly comprising of true-branching *Fischerella*, *Chlorogloeopsis* and *Stigonema* with smaller amounts of non-branching *Nostoc*, *Tolypthrix* and *Scyotnema*. Therefore, salinities above 70 are affecting the diversity of heterocytous cyanobacteria, especially for non-branching Nostocales. Abundances of hexose HG_{30} diol and hexose HG_{32} triol were observed in the freshwater environment of Giblin River, which contained mainly non-branching Nostocales with abundances of *Scytonema, Chakia, Ewamiania* and *Calothrix*. Hexose HG_{30} diol has been identified in *Scytonema* and hexose HG_{32} triol has previously reported to be unique for stigonematalean Cyanobacteria (i.e *Fischerella*) (Bauersachs et al., 2019).Our study found that hexose HG_{32} triol had strong correlations with non-branching *Ewaniana*, *Cylindrospermum*, and *Mastigocladopsis*, as well as true-branching *Aekothonos.* Me-hexose HG_{28} triol was abundantly present in Garden Point, RRBS, Linke Lake and Giblin River mats, this HG has been identified in *Calothrix* (Bale et al., 2018).

5.5 Conclusions

Taxonomic and functional analysis showed that the diversity and physiological activity of heterocytous cyanophytes in enhanced salinity environments is much greater than previously thought. Analysis of microbial mats occurring in a diverse range of environmental settings revealed a high diversity of HGs; this further corroborates with the taxonomic diversity indicating potentially serval cyanobacterial sources. The diverse distributions of both heterocytous cyanophytes and HGs provides valuable taxonomic information that offers an insight into the effect of salinity on N_2-fixing Cyanobacteria and may have application in paleoenvironment reconstruction providing insights into past nutrient cycling within lagoonal environments harbouring microbial mats. Future work combining molecular genetics and lipid analyses from environmental samples with cultivations of heterocytous cyanophytes under varying salinities will be needed to further our understanding of who is synthesizing particular HGs under certain saline conditions.

5.6 References

Ali, S., Sandhu, G.R., 1972. Blue-Green Algae of the Saline Soils of the Punjab. Oikos 23, 268.

Allen, M.A., Goh, F., Burns, B.P., Neilan, B.A., 2009. Bacterial, archaeal and eukaryotic diversity of smooth and pustular microbial mat communities in the hypersaline lagoon of Shark Bay. Geobiology 7, 82–96.

Allen, M.A., Neilan, B.A., Burns, B.P., Jahnke, L.L., Summons, R.E., 2010. Lipid biomarkers in Hamelin Pool microbial mats and stromatolites. Org. Geochem. 41, 1207–1218.

Almela, P., Velázquez, D., Rico, E., Justel, A., Quesada, A., 2019. Carbon pathways through the food web of a microbial mat from byers peninsula, antarctica. Front. Microbiol. 10.

Babilonia, J., Conesa, A., Casaburi, G., Pereira, C., Louyakis, A.S., Reid, R.P., Foster, J.S., 2018. Comparative metagenomics provides insight into the ecosystem functioning of the Shark Bay Stromatolites, Western Australia. Front. Microbiol. 9, 1359.

Bale, N.J., Hopmans, E.C., Dorhout, D., Stal, L.J., Grego, M., van Bleijswijk, J., Sinninghe Damsté, J.S., Schouten, S., 2018. A novel heterocyst glycolipid detected in a pelagic N2-fixing cyanobacterium of the genus Calothrix. Org. Geochem. 123, 44–47.

Bauersachs, T., Compaoré, J., Hopmans, E.C., Stal, L.J., Schouten, S., Sinninghe Damsté, J.S., 2009. Distribution of heterocyst glycolipids in cyanobacteria. Phytochemistry 70, 2034–2039.

Bauersachs, T., Compaoré, J., Severin, I., Hopmans, E.C., Schouten, S., Stal, L.J., Sinninghe Damsté, J.S., 2011. Diazotrophic microbial community of coastal microbial mats of the southern North Sea. Geobiology 9, 349–359.

Bauersachs, T., Miller, S.R., Gugger, M., Mudimu, O., Friedl, T., Schwark, L., 2019a. Heterocyte glycolipids indicate polyphyly of stigonematalean cyanobacteria. Phytochemistry 166, 112059.

Bauersachs, T., Miller, S.R., Gugger, M., Mudimu, O., Friedl, T., Schwark, L., 2019b.

Heterocyte glycolipids indicate polyphyly of stigonematalean cyanobacteria. Phytochemistry 166.

Bauersachs, T., Rochelmeier, J., Schwark, L., 2015. Seasonal lake surface water temperature trends reflected by heterocyst glycolipid Seasonal lake surface water temperature trends reflected by heterocyst glycolipid based molecular thermometers Seasonal lake surface water temperature trends reflected by heterocyst glycolipid. Biogeosciences Discuss 12, 751–778.

Bauersachs, T., Talbot, H.M., Sidgwick, F., Sivonen, K., Schwark, L., 2017. Lipid biomarker signatures as tracers for harmful cyanobacterial blooms in the Baltic Sea. PLoS One 12, e0186360.

Bligh, E.G., Dyer, W.J., 1959. A rapid method of total lipid extraction and purification. Can. J. Biochem. Physiol. 37, 911–917.

Bufarale, G., Collins, L.B., 2015. Stratigraphic architecture and evolution of a barrier seagrass bank in the mid-late Holocene, Shark Bay, Australia. Mar. Geol. 359, 1–21.

Burns, B.P., Goh, F., Allen, M., Neilan, B.A., 2004. Microbial diversity of extant stromatolites in the hypersaline marine environment of Shark Bay, Australia. Environ. Microbiol. 6, 1096–1101.

Burns, B.P., Seifert, A., Goh, F., Pomati, F., Jungblut, A.-D., Serhat, A., Neilan, B.A., 2005. Genetic potential for secondary metabolite production in stromatolite communities. FEMS Microbiol. Lett. 243, 293–301.

Bushmanova, E., Antipov, D., Lapidus, A., Prjibelski, A.D., 2019. RnaSPAdes: A de novo transcriptome assembler and its application to RNA-Seq data. Gigascience 8.

Bushnell, B., 2014. BBMap: a fast, accurate, splice-aware aligner.

Canfora, L., Bacci, G., Pinzari, F., Lo Papa, G., Dazzi, C., Benedetti, A., 2014. Salinity and bacterial diversity: To what extent does the concentration of salt affect the bacterial community in a saline soil? PLoS One 9.

Castenholz, R.W., Wilmotte, A., Herdman, M., Rippka, R., Waterbury, J.B., Iteman, I., Hoffmann, L., 2001. Phylum BX. Cyanobacteria, in: Bergey's Manual® of

Systematic Bacteriology. Springer New York, pp. 473–599.

Che, R., Deng, Y., Wang, F., Wang, W., Xu, Z., Hao, Y., Xue, K., Zhang, B., Tang, L., Zhou, H., Cui, X., 2018. Autotrophic and symbiotic diazotrophs dominate nitrogen-fixing communities in Tibetan grassland soils. Sci. Total Environ. 639, 997–1006.

Cruz, D., Vasconcelos, V., Pierre, G., Michaud, P., Delattre, C., 2020. Exopolysaccharides from Cyanobacteria: Strategies for Bioprocess Development. Appl. Sci. 10, 3763.

De Cáceres, M., Jansen, F., 2016. 'indicspecies' R Package - Functions to assess the strength and significance of relationship of species site group associations.

De Philippis, R., Vincenzini, M., 1998. Exocellular polysaccharides from cyanobacteria and their possible applications. FEMS Microbiol. Rev. 22, 151–175.

Díez, B., Bauer, K., Bergman, B., 2007. Epilithic cyanobacterial communities of a marine tropical beach rock (Heron Island, Great Barrier Reef): Diversity and diazotrophy. Appl. Environ. Microbiol. 73, 3656–3668.

Dixon, P., 2003. VEGAN, a package of R functions for community ecology. J. Veg. Sci.

Dupraz, C., Reid, R.P., Braissant, O., Decho, A.W., Norman, R.S., Visscher, P.T., 2009. Processes of carbonate precipitation in modern microbial mats. Earth-Science Rev.

Dvořák, P., Poulíčková, A., Hašler, P., Belli, M., Casamatta, D.A., Papini, A., 2015. Species concepts and speciation factors in cyanobacteria, with connection to the problems of diversity and classification. Biodivers. Conserv.

Edwards, R., Edwards, J.A., 2019. fastq-pair: efficient synchronization of paired-end fastq files. bioRxiv 552885.

Federhen, S., 2012. The NCBI Taxonomy database. Nucleic Acids Res. 40.

Flannery, D.T., Walter, M.R., 2012. Archean tufted microbial mats and the Great Oxidation Event: new insights into an ancient problem. Aust. J. Earth Sci. 59, 1–

11.

Garby, T.J., Walter, M.R., Larkum, A.W.D., Neilan, B.A., 2013. Diversity of cyanobacterial biomarker genes from the stromatolites of Shark Bay, Western Australia. Environ. Microbiol. 15, 1464–1475.

Garcia-Etxebarria, K., Garcia-Garcerà, M., Calafell, F., 2014. Consistency of metagenomic assignment programs in simulated and real data. BMC Bioinformatics 15, 90.

Gischler, E., Golubic, S., Gibson, M.A., Oschmann, W., Hudson, J.H., 2011. Microbial mats and microbialites in the freshwater Laguna Bacalar, Yucatan Peninsula, Mexico. Lect. Notes Earth Sci. 131, 187–205.

Goh, F., Allen, M.A., Leuko, S., Kawaguchi, T., Decho, A.W., Burns, B.P., Neilan, B.A., 2009. Determining the specific microbial populations and their spatial distribution within the stromatolite ecosystem of Shark Bay. ISME J. 3, 383–396.

Goslee, S.C., Urban, D.L., 2007. The ecodist package for dissimilarity-based analysis of ecological data. J. Stat. Softw. 22, 1–19.

Gruber-Vodicka, H.R., Seah, B.K., Pruesse, E., 2019. phyloFlash — Rapid SSU rRNA profiling and targeted assembly from metagenomes. bioRxiv 521922.

Hallmann, C., Schwark, L., Grice, K., 2008. Community dynamics of anaerobic bacteria in deep petroleum reservoirs. Nat. Geosci. 1, 588–591.

Haselkorn, R., 1986. Organization of the Genes for Nitrogen Fixation in Photosynthetic Bacteria and Cyanobacteria. Annu. Rev. Microbiol. 40, 525–547.

Heinzelmann, S.M., Bale, N.J., Hopmans, E.C., Sinninghe Damsté, J.S., Schouten, S., van der Meer, M.T.J., 2014. Critical assessment of glyco- and phospholipid separation by using silica chromatography. Appl. Environ. Microbiol. 80, 360–5.

Hindák, F., 2008. On Chlorogloeopsis fritschii (Cyanophyta/Cyanobacteria) from thermal springs in Slovakia and from a saline lake in Tunisia. Arch. Hydrobiol. Suppl. Algol. Stud. 126, 47–64.

Hörnlein, C., Confurius-Guns, V., Stal, L.J., Bolhuis, H., 2018. Daily rhythmicity in coastal microbial mats. npj Biofilms Microbiomes 4.

Jahnert, R.J., Collins, L.B., 2013. Controls on microbial activity and tidal flat evolution in Shark Bay, Western Australia. Sedimentology 60, 1071–1099.

Kirk Harris, J., Gregory Caporaso, J., Walker, J.J., Spear, J.R., Gold, N.J., Robertson, C.E., Hugenholtz, P., Goodrich, J., McDonald, D., Knights, D., Marshall, P., Tufo, H., Knight, R., Pace, N.R., 2013. Phylogenetic stratigraphy in the Guerrero Negro hypersaline microbial mat. ISME J. 7, 50–60.

Kirkwood, A.E., Buchheim, J.A., Buchheim, M.A., Henley, W.J., 2008. Cyanobacterial diversity and halotolerance in a variable hypersaline environment. Microb. Ecol. 55, 453–465.

Komárek, J., 2016. A polyphasic approach for the taxonomy of cyanobacteria: principles and applications. Eur. J. Phycol. 51, 346–353.

Komárek, J., Kaštovský, J., Mareš, J., Johansen, J.R., 2014. Taxonomic classification of cyanoprokaryotes (cyanobacterial genera) 2014, using a polyphasic approach, Preslia.

Komárková, J., Zapomělová, E., Komárek, J., 2013. Chakia (cyanobacteria), a new heterocytous genus from Belizean marshes identified on the basis of the 16S rRNA gene.

Kumar, K., Mella-Herrera, R.A., Golden, J.W., 2010. Cyanobacterial heterocysts. Cold Spring Harb. Perspect. Biol. 2.

Langmead, B., Salzberg, S.L., 2012. Fast gapped-read alignment with Bowtie 2. Nat. Methods 9, 357–359.

Ley, R.E., Harris, J.K., Wilcox, J., Spear, J.R., Miller, S.R., Bebout, B.M., Maresca, J.A., Bryant, D.A., Sogin, M.L., Pace, N.R., 2006. Unexpected diversity and complexity of the Guerrero Negro hypersaline microbial mat. Appl. Environ. Microbiol. 72, 3685–3695.

Li, H., Handsaker, B., Wysoker, A., Fennell, T., Ruan, J., Homer, N., Marth, G., Abecasis, G., Durbin, R., 2009. The Sequence Alignment/Map format and SAMtools. Bioinformatics 25, 2078–2079.

Li, P., Harding, S.E., Liu, Z., Lp, P., Harding2, S.E., Liu', Z., 2001. Cyanobacterial Exopolysaccharides: Their Nature and Potential Biotechnological Applications.

Biotechnol. Genet. Eng. Rev. 18, 375–404.

Logan, B., Hoffman, P., Gebelein, C., 1974. Algal mats, cryptalgal fabrics, and structures, Hamelin Pool, Western Australia.

Logan, B.W., Cebulski, D.E., 1970. Sedimentary environments of Shark Bay, Western Australia. _In_: B.W. Logan, G.R. Davies, J.F. Read and D.E. Cebulski (Eds). Carbonate sedimentation and environments in Shark Bay, Western Australia. Am. Assoc. Pet. Geol. Mem. 13, 1–37.

Louyakis, A.S., Gourlé, H., Casaburi, G., Bonjawo, R.M.E., Duscher, A.A., Foster, J.S., 2018. A year in the life of a thrombolite: comparative metatranscriptomics reveals dynamic metabolic changes over diel and seasonal cycles. Environ. Microbiol. 20, 842–861.

Love, M.I., Huber, W., Anders, S., 2014. Moderated estimation of fold change and dispersion for RNA-seq data with DESeq2. Genome Biol. 15, 550.

McGregor, G.B., Sendall, B.C., 2017. Ewamiania thermalis gen. et sp. nov. (Cyanobacteria, Scytonemataceae), a new cyanobacterium from Talaroo thermal springs, north-eastern Australia. Aust. Syst. Bot. 30, 38–47.

Meeks, J.C., Elhai, J., 2002. Regulation of Cellular Differentiation in Filamentous Cyanobacteria in Free-Living and Plant-Associated Symbiotic Growth States. Microbiol. Mol. Biol. Rev. 66, 94–121.

More, K.D., Giosan, L., Grice, K., Coolen, M.J.L., 2019. Holocene paleodepositional changes reflected in the sedimentary microbiome of the Black Sea. Geobiology 17, 436–448.

Morris, T.E., Visscher, P.T., O'Leary, M.J., Fearns, P.R.C.S., Collins, L.B., 2020. The biogeomorphology of Shark Bay's microbialite coasts. Earth-Science Rev.

Namsaraev, Z., Samylina, O., Sukhacheva, M., Borisenko, G., Sorokin, D.Y., Tourova, T., 2018. Effect of salinity on diazotrophic activity and microbial composition of phototrophic communities from Bitter-1 soda lake (Kulunda Steppe, Russia). Extremophiles 22, 651–663.

Oren, A., 2008. Microbial life at high salt concentrations: Phylogenetic and metabolic diversity. Saline Systems 4, 2.

Oren, A., 2015. Cyanobacteria in hypersaline environments: biodiversity and physiological properties. Biodivers Conserv 24, 781–798.

Paerl, H.W., Pinckney, J.L., Steppe, T.F., 2000. Cyanobacterial-bacterial mat consortia: Examining the functional unit of microbial survival and growth in extreme environments. Environ. Microbiol.

Pagès, A., Grice, K., Ertefai, T., Skrzypek, G., Jahnert, R., Greenwood, P., 2014. Organic geochemical studies of modern microbial mats from Shark Bay: Part I: Influence of depth and salinity on lipid biomarkers and their isotopic signatures. Geobiology 12, 469–487.

Pfeffer, S., Brown, R.M., 2016. Complete genome sequence of the cyanobacterium Anabaena sp. 33047. Genome Announc. 4, 809–825.

Plet, C., Pagès, A., Holman, A.I., Madden, R.H.C., Grice, K., 2018. From supratidal to subtidal, an integrated characterisation of Carbla Beach shallow microbial mats (Hamelin Pool, Shark Bay, WA): Lipid biomarkers, stable carbon isotopes and microfabrics. Chem. Geol. 493, 338–352.

Pratte, B.S., Thiel, T., 2014. Regulation of nitrogenase gene expression by transcript stability in the cyanobacterium Anabaena variabilis. J. Bacteriol. 196, 3609–3621.

Proemse, B.C., Eberhard, R.S., Sharples, C., Bowman, J.P., Richards, K., Comfort, M., Barmuta, L.A., 2017. Stromatolites on the rise in peat-bound karstic wetlands. Sci. Rep. 7, 15384.

R Core Team, 2017. R: A Language and Environment for Statistical Computing.

Ramos, V.M.C., Castelo-Branco, R., Leão, P.N., Martins, J., Carvalhal-Gomes, S., Sobrinho da Silva, F., Mendonça Filho, J.G., Vasconcelos, V.M., 2017. Cyanobacterial Diversity in Microbial Mats from the Hypersaline Lagoon System of Araruama, Brazil: An In-depth Polyphasic Study. Front. Microbiol. 8, 1233.

Redfield, E., Barns, S.M., Belnap, J., Daane, L.L., Kuske, C.R., 2002. Comparative diversity and composition of cyanobacteria in three predominant soil crusts of the Colorado Plateau. FEMS Microbiol. Ecol. 40, 55–63.

Rippin, M., Borchhardt, N., Williams, L., Colesie, C., Jung, P., Büdel, B., Karsten, U.,

Becker, B., 2018. Genus richness of microalgae and Cyanobacteria in biological soil crusts from Svalbard and Livingston Island: morphological versus molecular approaches. Polar Biol. 41, 909–923.

Rohart, F., Gautier, B., Singh, A., Lê Cao, K.-A., 2017. mixOmics: An R package for 'omics feature selection and multiple data integration. PLOS Comput. Biol. 13, e1005752.

Roney, H.C., Booth, G.M., Cox, P.A., 2009. Competitive exclusion of Cyanobacterial species in the Great Salt Lake. Extremophiles 13, 355–361.

Rossi, F., De Philippis, R., 2015. Role of cyanobacterial exopolysaccharides in phototrophic biofilms and in complex microbial mats. Life.

Schaefer, B., Grice, K., Coolen, M.J.L., Summons, R.E., Cui, X., Bauersachs, T., Schwark, L., Böttcher, M.E., Bralower, T.J., Lyons, S.L., Freeman, K.H., Cockell, C.S., Gulick, S.P.S., Morgan, J. V., Whalen, M.T., Lowery, C.M., Vajda, V., 2020. Microbial life in the nascent Chicxulub crater. Geology 48, 328–332.

Severin, I., Confurius-Guns, V., Stal, L.J., 2012. Effect of salinity on nitrogenase activity and composition of the active diazotrophic community in intertidal microbial mats. Arch. Microbiol. 194, 483–491.

Shakya, M., Lo, C.C., Chain, P.S.G., 2019. Advances and challenges in metatranscriptomic analysis. Front. Genet.

Sheridan, R.P., 1992. Nitrogen Fixation by Epicaulous Cyanobacteria in the Pointe de la Saline Mangrove Community, Guadeloupe, French West Indies. Biotropica 24, 571.

Singh, S., Verma, E., Niveshika, Tiwari, B., Mishra, A.K., 2016. Exopolysaccharide production in Anabaena sp. PCC 7120 under different CaCl2 regimes. Physiol. Mol. Biol. Plants 22, 557–566.

Srivastava, A.K., Bhargava, P., Kumar, A., Rai, L.C., Neilan, B.A., 2009a. Molecular characterization and the effect of salinity on cyanobacterial diversity in the rice fields of Eastern Uttar Pradesh, India. Saline Systems 5, 4.

Srivastava, A.K., Bhargava, P., Kumar, A., Rai, L.C., Neilan, B.A., 2009b. Molecular characterization and the effect of salinity on cyanobacterial diversity in the rice

fields of Eastern Uttar Pradesh, India. Saline Systems 5, 4.

Stal, L.J., 2012. Cyanobacterial mats and stromatolites, in: Ecology of Cyanobacteria II: Their Diversity in Space and Time. Springer Netherlands, pp. 65–125.

Stal, L.J., 1995. Physiological ecology of cyanobacteria in microbial mats and other communities. New Phytol. 131, 1–32.

Suosaari, E.P., Reid, R.P.R., Araujo, T.A.A., Playford, P.E., Holley, D.K., McNamara, K.J., Eberli, G.P., 2016. Environmental Pressures Influencing Living Stromatolites in Hamelin Pool, Shark Bay, Western Australia. Palaios 31, 483–496.

Suzuki, R., Shimodaira, H., 2006. Pvclust: An R package for assessing the uncertainty in hierarchical clustering. Bioinformatics 22, 1540–1542.

Tang, Y., Horikoshi, M., Li, W., 2016. Ggfortify: Unified interface to visualize statistical results of popular r packages. R J. 8, 478–489.

Tuzhikov, A., Panchin, A., Shestopalov, V.I., 2014. TUIT, a BLAST-based tool for taxonomic classification of nucleotide sequences. Biotechniques 56, 78–84.

Volkman, J.K., Barrett, S.M., Blackburn, S.I., Mansour, M.P., Sikes, E.L., Gelin, F., 1998. Microalgal biomarkers: A review of recent research developments, in: Organic Geochemistry. Pergamon, pp. 1163–1179.

Wickham, H., Chang, W., 2009. ggplot2: An implementation of the Grammar of Graphics. R package version 0.8. 3.

Wörmer, L., CirÉs, S., VelÁzquez, D., Quesada, A., Hinrichs, K.-U., 2012. Cyanobacterial heterocyst glycolipids in cultures and environmental samples: Diversity and biomarker potential. Limnol. Oceanogr. 57, 1775–1788.

5.7 Supplementary information

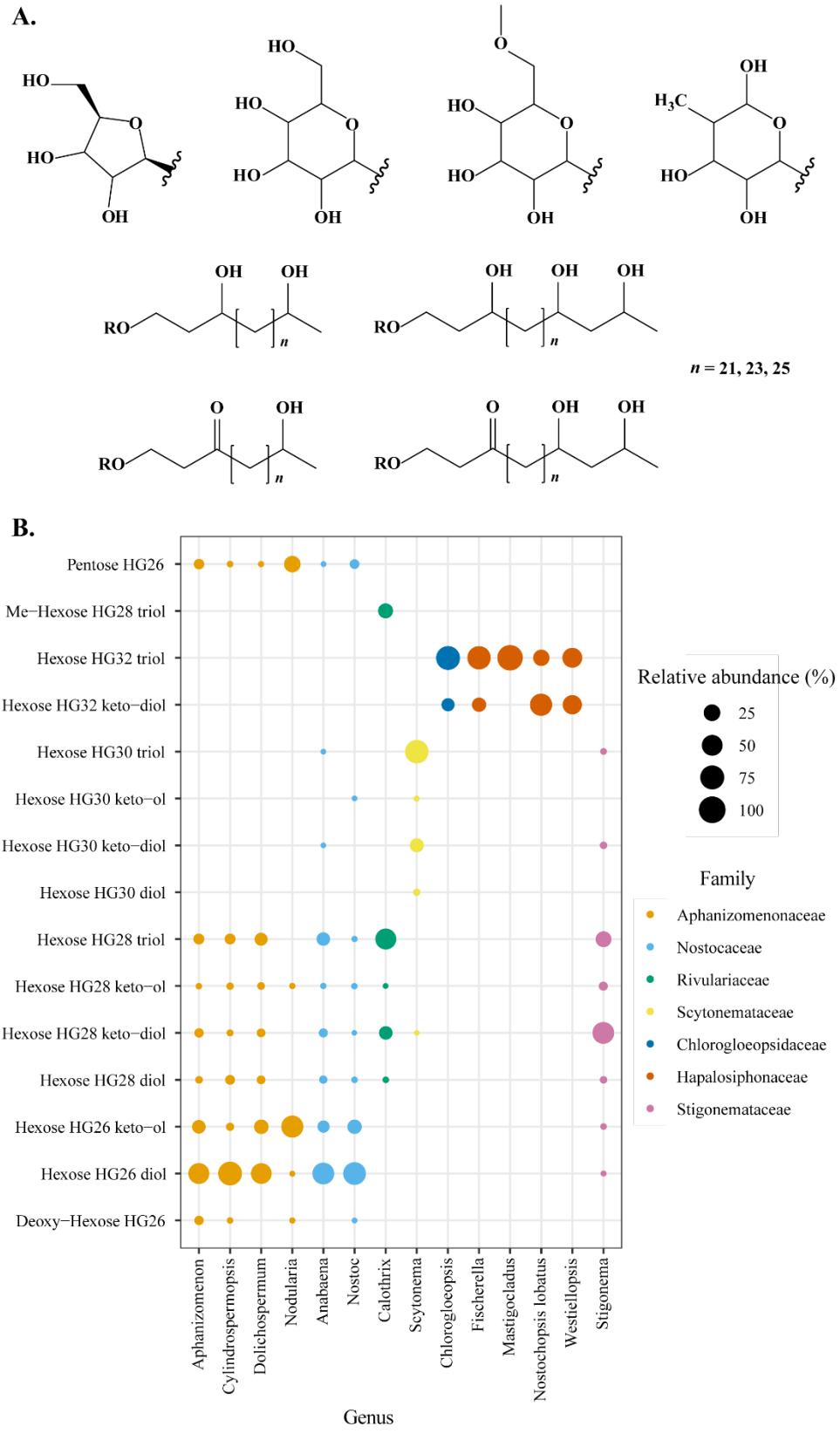

Supplementary Figure 5.1 HG structures and their distribution in cultured cyanobacteria (e.g. Bauersachs et al., 2009, 2019; Bale et al., 2015, 2018). A. sugar head groups (pentose-, hexose-, methyl-hexose and deoxy-hexose),

functional moieties (diol, triol, keto-ol, and keto-diol) and chain lengths. B. Relative abundance of HGs described in cultured cyanobacteria.

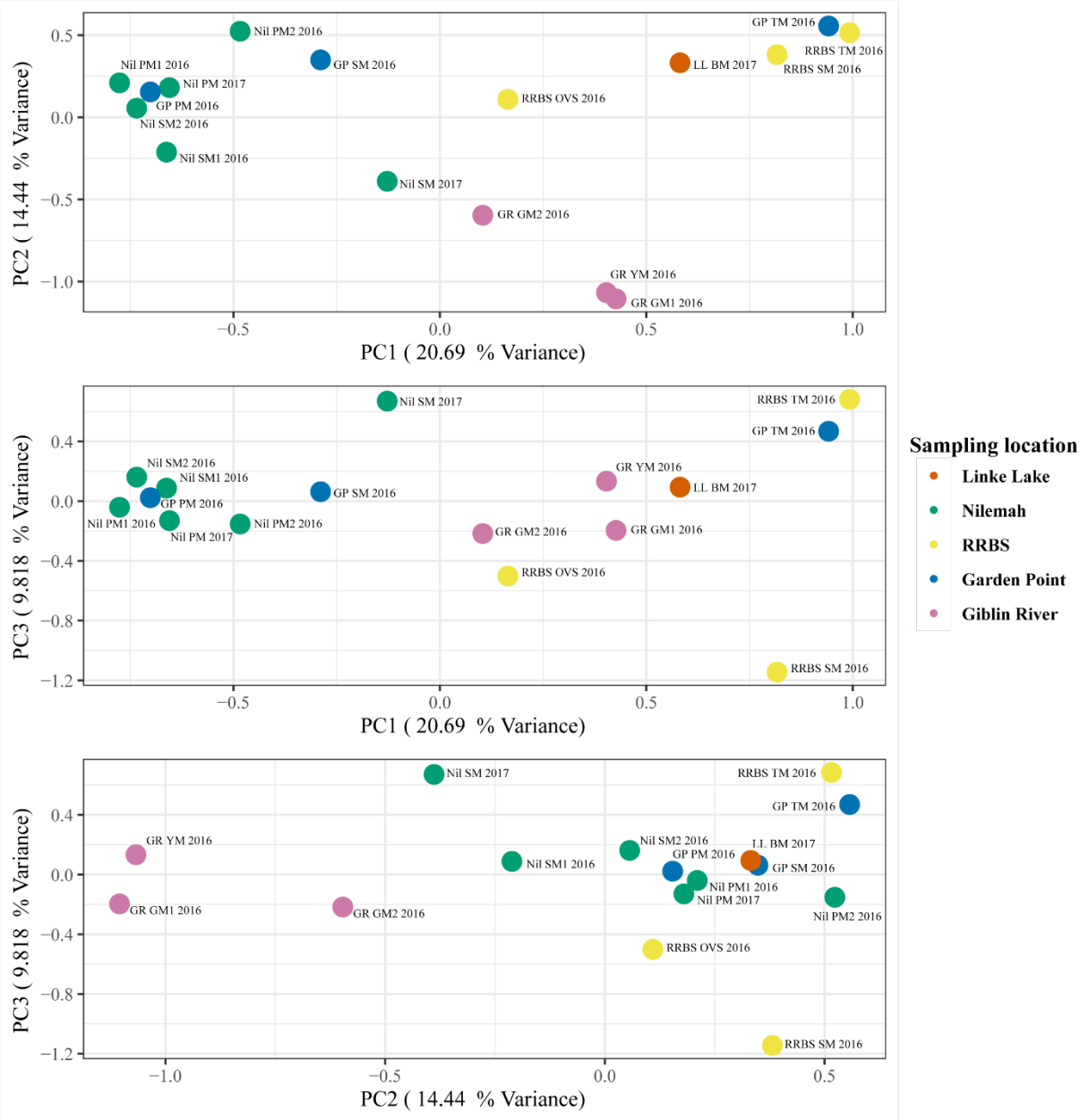

Supplementary Figure 5.2 PCA plot constructed from similarity matrices utilising 16S rRNA gene recruitment of non-branching (Order Nostocales) and true-branching (Order Stigonematales) genera in microbial mats from Shark Bay, Western Australia (Linke Lake (LL)), Nilemah (Nil), RRBS and Garden Point (GP), and Tasmania (Giblin River (GR)). BM = BM = birrida mat (gelatinous mat), PM = pustular mat, SM = smooth mat, TM = tufted mat, OVS= ooze over sand, GM = green mat and YM = yellow mat.

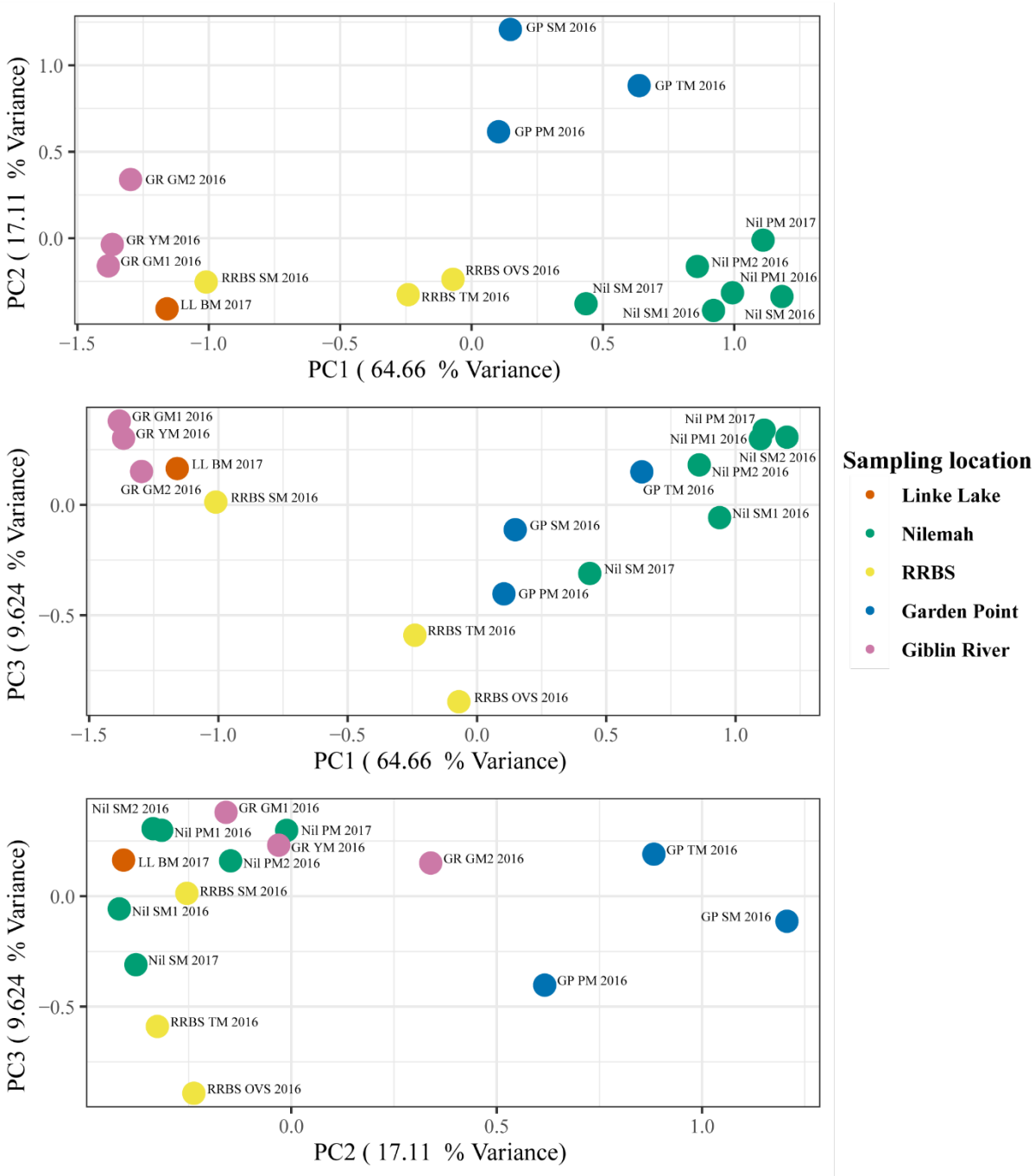

Supplementary Figure 5.3 PCA plot constructed from similarity matrices utilising fractional abundances of heterocyte glycolipids (HGs) within microbial mats from Shark Bay, Western Australia (Linke Lake (LL)), Nilemah (Nil), RRBS and Garden Point (GP), and Tasmania (Giblin River (GR)). BM = birrida mat (gelatinous mat), PM = pustular mat, SM = smooth mat, TM = tufted mat, OVS= ooze over sand, GM = green mat and YM = yellow mat.

Supplementary Table 5.1 Summary of the mat types collected with locations, sampling dates and times, field measurements of salinity, pH and water temperature, geomorphic settings and morphological features.

Sample ID	Location	Mat type	Sampling date	Sampling time	Salinity (‰)	pH	Water temperature (°C)	Geomorphic setting	Morphological feature
Nil PM1 2016	Nilemah	Pustular mat	5/07/2016	12:40 PM	67	7.94	13.2	intertidal terrace front	microbialite ridge crest
Nil PM2 2016	Nilemah	Pustular mat	5/07/2016	12:10 PM	66	8.06	13.2		continuous mat sheet
Nil PM 2017	Nilemah	Pustular mat	########	8:30 AM	70	7.51	18		microbialite ridge crest
Nil SM1 2016	Nilemah	Smooth mat	5/07/2016	12:00 PM	66	7.99	13.2		swale between microbialite ridges
Nil SM2 2016	Nilemah	Smooth mat	5/07/2016	12:30 PM	67	7.93	13.2		swale between microbialite ridges
Nil SM 2017	Nilemah	Smooth mat	########	8:45 PM	70	7.51	18		swale between microbialite ridges
LL BM 2017	Linke Lake	Gelatenous mat	########	3:30 PM	80	7.75	15.2	birrida - moat-like depression	evaporative pool
GP PM 2016	Garden Point	Pustular mat	6/07/2016	12:00 PM	51	7.85	14	intertidal	mat sheet
GP SM 2016	Garden Point	Smooth mat	6/07/2016	11:00 AM	51	7.85	14	subtidal	sand sheet
GP TM 2016	Garden Point	Tufted mat	6/07/2016	11:30 AM	51	7.85	14	intertidal	continuous mat sheet
RRBS TM 2016	RRBS	Tufted mat	7/07/2016	12:12 PM	69	7.6	15	intertidal terrace within outwash channel delta sand sheet	mat sheet
RRBS SM 2016	RRBS	Smooth mat	7/07/2016	1:25 PM	68	7.17	15		mat sheet patch
RRBS OVS 2016	RRBS	Transitioning mat	7/07/2016	1:35 PM	66	7.21	-		new sand sheet
GR GM1 2016	Giblin River	Green mat	18/8/2016	10:45 AM	0.24	7.68	14.3	karstic wetland	calcareous mud and tufa
GR YM 2016	Giblin River	Yellow mat	18/8/2016	1:30 AM	0.16	7.08	16.1		calcareous mud and tufa
GR GM2 2016	Giblin River	Green mat	18/8/2016	3:15 PM	0.06	7.96	13		creek bank

Supplementary Table 5.2 Illumina HiSeq 2500 pair-end sequencing read output with percentage summaries of trimmed and aligned sequences, number of assembled transcripts and number of annotations for Phyloflash and MG-RAST.

							# annotations	
	Percentage of trimmed and aligned sequences						PhyloFlash (SSU rRNA SILVA)	MG-RAST RefSeq
Sample Name	**Paired Reads**	**Quality trimming**	**Remaining reads**	**aligned 0 times**	**aligned >1 times**	**# transcripts assembled**	**Total**	**Total**
Nil PM1 2016	1.10E+07	8.87	91.13	7.1	92.9	26890	1474649	102200
Nil PM2 2016	9066195	7.71	92.29	7.57	92.43	9393	1652757	42492
Nil PM 2017	9184291	9.86	90.14	9.39	90.61	29423	1827324	121125
Nil SM1 2016	9621836	8.49	91.51	8.41	91.59	25348	1707460	121088
Nil SM2 2016	9771353	9.38	90.62	15.57	84.43	63494	905558	137750
Nil SM 2017	9214600	8.74	91.26	9.47	90.53	24822	1293097	151598
LL BM 2017	9810574	8.85	91.15	6.59	93.41	16412	1453025	64193
GP PM 2016	8509997	8.39	91.61	10.1	89.9	27442	1850380	92066
GP SM 2016	8966989	8.63	91.37	8.52	91.48	14554	1206356	123465
GP TM 2016	8890215	14.87	85.13	58.27	41.73	14284	751314	238791
RRBS TM 2016	9189088	8.73	91.27	9.55	90.45	28538	778082	114382
RRBS SM 2016	8084891	16.74	83.26	31.44	68.56	48288	1040348	217075
RRBS OVS 2016	9975457	8.47	91.53	7.12	92.88	19737	1683164	92373
GR GM1 2016	8674558	9.39	90.61	7.19	92.81	8192	2322053	49295
GR YM 2016	9232190	10.9	89.1	95.29	4.71	447678	45821	2013150
GR GM2 2016	8732656	9.14	90.86	4.66	95.34	13725	1595651	42926

Supplementary Table 5.3 Relative abundance (%) of cyanobacterial 16S rRNA transcripts from microbial mats occurring in hypersaline, metahaline and freshwater environments.

		Hypersaline												Metahaline					Freshwater				
		LL BM 2017	Nil PM1 2016	Nil PM2 2016	Nil PM 2017	Nil SM1 2016	Nil SM2 2016	Nil SM 2017	RRBS TM 2016	RRBS SM 2016	RRBS OVS 2016	Average	Std.dev	GP SM 2016	GP PM 2016	GP TM 2016	Average	Std.dev	GR GM1 2016	GR GM2 2016	GR YM 2016	Average	Std.dev
	Cyanobacteria	36.7	15.2	11.0	9.9	4.0	4.6	6.0	20.3	8.5	16.0	13.2	9.3	3.7	10.7	11.4	8.6	3.5	9.1	19.7	6.6	11.8	5.7
Non-heterocystous	**Chroococcales**	0.3	2.4	1.9	1.4	0.5	0.5	0.2	0.2	0.2	0.4	0.8	0.8	0.2	1.5	0.1	0.6	0.7	0.2	2.9	0.7	1.3	1.2
	Oscillatoriales	29.6	3.3	3.0	3.3	0.6	0.7	0.7	18.6	3.9	9.5	7.3	9.1	0.3	0.9	9.9	3.7	4.4	0.7	4.8	0.1	1.9	2.1
	Pleurocapsales	0.3	1.5	0.9	0.7	0.4	0.5	0.2	0.1	0.3	0.4	0.5	0.4	0.8	2.2	0.3	1.1	0.8	0.0	1.3	0.2	0.5	0.6
	Synechococcales	4.1	0.8	0.7	1.3	1.0	1.8	4.4	0.03	2.9	3.5	2.1	1.5	1.6	2.8	0.1	1.5	1.1	0.0	0.4	0.2	0.2	0.1
Heterocystous	**Nostocales**	0.02	2.3	1.0	0.8	0.3	0.3	0.1	0.05	0.1	0.1	0.5	0.7	0.04	0.2	0.02	0.1	0.1	5.9	3.1	3.5	4.2	1.3
	Stignomatales	0.03	0.2	0.2	0.1	0.1	0.1	0.002	0.02	0.01	0.02	0.1	0.1	0.04	0.1	0.01	0.05	0.04	0.2	0.3	0.1	0.2	0.1
	Unclassified Cyanobacteria	2.3	4.6	3.2	2.4	1.2	0.8	0.5	1.3	1.2	1.9	2.0	1.2	0.8	2.9	1.0	1.6	1.0	2.0	7.0	1.8	3.6	2.4

Supplementary Table 5.4 Relative abundance (%) of cyanobacterial mRNA transcripts from microbial mats occurring in hypersaline, metahaline and freshwater environments.

		Hypersaline												Metahaline					Freshwater				
		LL BM 2017	Nil PM1 2016	Nil PM2 2016	Nil PM 2017	Nil SM1 2016	Nil SM2 2016	Nil SM 2017	RRBS TM 2016	RRBS SM 2016	RRBS OVS 2016	Average	Std.dev	GP SM 2016	GP PM 2016	GP TM 2016	Average	Std.dev	GR GM1 2016	GR GM2 2016	GR YM 2016	Average	Std.dev
	Cyanobacteria	40.4	35.9	38.5	28.6	15.1	18.9	23.9	39.9	15.6	34.5	29.1	9.6	13.5	20.1	29.4	21.0	6.5	36.5	25.2	4.4	22.0	13.3
Non-heterocystous	**Chroococcales**	17.0	16.4	18.6	13.8	7.8	9.9	13.4	10.5	8.0	15.9	13.1	3.7	7.3	10.9	7.4	8.5	1.7	6.5	10.5	1.9	6.3	3.5
	Gloeobacterales	0.4	0.6	0.6	0.4	0.3	0.3	0.3	0.3	0.2	0.3	0.4	0.1	0.3	0.3	0.3	0.3	0.0	0.4	0.8	0.5	0.6	0.2
	Oscillatoriales	14.5	7.9	8.8	6.6	3.4	4.1	4.9	21.1	3.3	10.1	8.5	5.3	2.8	3.8	16.5	7.7	6.2	3.6	4.9	0.6	3.0	1.8
	Prochlorales	0.1	0.2	0.2	0.2	0.1	0.1	0.1	0.1	0.2	0.1	0.1	0.04	0.2	0.1	0.1	0.1	0.0	0.1	0.1	0.1	0.1	0.0
Heterocystous	**Nostocales**	7.6	9.5	8.9	6.5	3.1	3.9	4.6	7.3	3.6	6.9	6.2	2.2	2.5	4.5	4.4	3.8	0.9	25.6	8.1	1.1	11.6	10.3
	Unclassified Cyanobacteria	0.8	1.3	1.3	1.1	0.4	0.5	0.5	0.7	0.4	1.1	0.8	0.3	0.4	0.5	0.6	0.5	0.1	0.3	0.7	0.1	0.4	0.2

Supplementary Table 5.5 Relative transcript abundances (%) from taxa (Domain/Phylum and Order levels) transcribing genes involved in photosynthesis in microbial mats occurring in hypersaline, metahaline and freshwater environments.

		Hypersaline										Metahaline			Freshwtaer		
Domain/Phylum	**Order**	**LL BM 2017**	**Nil PM1 2016**	**Nil PM2 2016**	**Nil PM 2017**	**Nil SM1 2016**	**Nil SM2 2016**	**Nil SM 2017**	**RRBS TM 2016**	**RRBS SM 2016**	**RRBS OVS 2016**	**GP SM 2016**	**GP PM 2016**	**GP TM 2016**	**GR GM1 2016**	**GR GM2 2016**	**GR YM 2016**
Cyanobacteria	Chroococcales	53.3	60.9	62.7	56.2	60.8	58.8	45.6	45.2	59.6	57.4	54.5	70.3	52.6	32.1	63.6	9.5
Cyanobacteria	Nostocales	9.8	12.4	15.2	10.3	10.4	16.2	11.5	11.5	14.1	11.7	15.3	12.0	9.0	66.0	13.9	5.0
Cyanobacteria	Oscillatoriales	6.6	13.4	14.3	10.9	12.6	10.4	7.5	14.7	12.2	8.8	11.0	8.1	17.9	1.9	6.6	0.0
Chloroflexi	Chloroflexales	10.9	6.4	4.6	9.7	11.5	4.3	14.8	20.2	5.1	13.5	6.7	1.5	17.9	0.0	0.0	9.1
Proteobacteria	Rhizobiales	5.5	0.2	0.5	2.4	0.7	0.8	5.8	0.8	0.0	1.6	4.8	3.9	0.0	0.0	0.0	36.4
Bacillariophyta	Eupodiscales	3.2	2.1	0.0	6.6	1.4	5.1	7.3	6.0	6.4	3.2	1.4	1.2	0.0	0.0	2.6	0.4
Proteobacteria	Rhodospirillales	1.6	0.2	0.0	0.6	0.4	0.0	1.9	0.0	0.0	1.1	0.0	0.0	0.0	0.0	0.0	17.8
Proteobacteria	Chromatiales	2.7	0.2	0.0	0.6	0.4	0.3	0.8	0.4	0.6	0.5	1.0	0.4	0.0	0.0	0.0	7.9
Proteobacteria	Rhodobacterales	3.9	0.0	0.5	0.5	0.4	0.3	0.2	0.0	0.0	0.0	1.4	0.0	1.3	0.0	1.3	4.5
Cyanobacteria	Gloeobacterales	0.0	1.2	0.9	0.3	0.4	0.5	0.4	0.0	0.0	0.2	0.5	0.4	0.0	0.0	4.0	4.5
Eukaryota	Cyanidiales	0.2	0.7	0.0	1.5	0.4	0.8	1.3	0.4	0.6	0.7	0.5	0.4	0.0	0.0	2.0	0.0
Bacteroidetes	Sphingobacteriales	0.2	0.2	0.5	0.0	0.0	0.0	0.6	0.0	0.0	0.7	0.5	0.0	1.3	0.0	0.7	2.5
Chlorophyta	Chlamydomonadales	0.0	0.5	0.5	0.0	0.4	0.8	0.4	0.0	0.0	0.0	0.5	0.8	0.0	0.0	2.6	0.0
Chlorophyta	Chlorellales	0.5	0.5	0.0	0.0	0.0	0.3	1.0	0.0	0.0	0.0	0.5	0.0	0.0	0.0	2.6	0.4
Eukaryota	Bangiales	0.5	0.2	0.0	0.0	0.4	0.5	0.2	0.4	1.3	0.2	0.5	0.4	0.0	0.0	0.0	0.0
Proteobacteria	Unclassified Gammaproteobacteria	0.7	0.5	0.0	0.3	0.0	0.0	0.4	0.0	0.0	0.2	0.0	0.4	0.0	0.0	0.0	2.1
Eukaryota	Unclassified Glaucocystophyceae	0.5	0.2	0.5	0.2	0.0	1.1	0.2	0.4	0.0	0.2	1.0	0.4	0.0	0.0	0.0	0.0

Supplementary Table 5.6 Relative transcript abundances (%) from taxa (Phylum and Order levels) transcribing genes involved in carbon fixation in microbial mats occurring in hypersaline, metahaline and freshwater environments.

		Hypersaline										Metahaline			Freshwtaer		
Phylum	**Order**	**LL BM 2017**	**Nil PM1 2016**	**Nil PM2 2016**	**Nil PM 2017**	**Nil SM1 2016**	**Nil SM2 2016**	**Nil SM 2017**	**RRBS TM 2016**	**RRBS SM 2016**	**RRBS OVS 2016**	**GP SM 2016**	**GP PM 2016**	**GP TM 2016**	**GR GM1 2016**	**GR GM2 2016**	**GR YM 2016**
Cyanobacteria	Chroococcales	50.0	51.1	56.5	43.6	32.9	47.6	50.9	33.6	45.7	40.7	33.7	57.5	22.2	18.5	43.5	6.0
Cyanobacteria	Nostocales	11.8	14.8	15.2	13.4	17.1	8.1	5.5	15.5	10.9	14.8	3.1	5.0	11.1	44.4	21.7	2.9
Cyanobacteria	Oscillatoriales	12.5	11.1	10.9	11.4	5.7	4.8	3.6	14.5	0.0	13.9	7.1	5.0	44.4	3.7	0.0	0.4
Proteobacteria	Burkholderiales	0.7	1.5	0.0	1.3	1.4	4.8	0.0	1.8	10.9	0.0	3.1	10.0	5.6	11.1	0.0	16.2
Proteobacteria	Rhizobiales	1.5	3.0	2.2	3.4	4.3	2.4	0.0	1.8	6.5	0.0	3.1	0.0	5.6	0.0	8.7	20.9
Chloroflexi	Chloroflexales	1.5	0.7	0.0	0.0	7.1	0.8	1.8	0.0	2.2	2.8	2.0	2.5	0.0	0.0	13.0	6.7
Cyanobacteria	Gloeobacterales	1.5	1.5	6.5	4.0	1.4	1.6	1.8	1.8	4.3	4.6	0.0	5.0	5.6	0.0	0.0	0.6
Firmicutes	Bacillales	2.9	0.7	2.2	0.0	7.1	1.6	6.1	1.8	2.2	1.9	3.1	2.5	0.0	0.0	0.0	5.0
Bacteroidetes	Flavobacteriales	0.7	0.0	2.2	2.0	1.4	2.4	3.6	1.8	0.0	2.8	3.1	2.5	0.0	11.1	0.0	0.7
Actinobacteria	Actinomycetales	1.5	0.7	0.0	1.3	0.0	1.6	1.8	1.8	0.0	0.0	0.0	0.0	0.0	3.7	8.7	12.1
Bacteroidetes	Sphingobacteriales	0.7	1.5	2.2	1.3	1.4	3.2	3.6	3.6	2.2	2.8	2.0	5.0	0.0	0.0	0.0	1.3
Bacteroidetes	Bacteroidales	3.7	0.7	0.0	2.0	0.0	4.8	1.8	1.8	0.0	1.9	3.1	2.5	0.0	3.7	0.0	0.9
Chlorobi	Chlorobiales	0.7	3.0	0.0	1.3	1.4	3.2	1.2	7.3	2.2	0.9	4.1	0.0	0.0	0.0	0.0	1.4
Firmicutes	Clostridiales	0.7	0.0	0.0	0.0	1.4	4.0	2.4	1.8	4.3	2.8	4.1	0.0	0.0	0.0	0.0	2.4
Proteobacteria	Myxococcales	0.7	0.0	0.0	2.0	1.4	1.6	0.0	0.0	0.0	1.9	2.0	0.0	5.6	0.0	4.3	4.2
Proteobacteria	Chromatiales	0.0	0.0	0.0	2.7	0.0	0.8	3.6	0.9	0.0	2.8	9.2	0.0	0.0	0.0	0.0	2.7
Proteobacteria	Alteromonadales	1.5	0.0	0.0	2.7	2.9	0.8	0.6	2.7	4.3	0.9	3.1	0.0	0.0	0.0	0.0	2.3
Bacteroidetes	Cytophagales	0.0	2.2	2.2	0.7	0.0	1.6	1.2	0.9	0.0	0.0	4.1	0.0	0.0	3.7	0.0	1.1
Firmicutes	Thermoanaerobacterales	1.5	0.0	0.0	2.0	1.4	1.6	2.4	0.9	0.0	0.0	4.1	0.0	0.0	0.0	0.0	3.7
Proteobacteria	Desulfobacterales	0.7	0.7	0.0	0.7	4.3	0.0	0.6	0.9	0.0	3.7	2.0	2.5	0.0	0.0	0.0	1.3
Planctomycetes	Planctomycetales	0.7	3.0	0.0	1.3	1.4	0.8	0.0	0.0	2.2	0.9	0.0	0.0	0.0	0.0	0.0	3.7
Verrucomicrobia	Methylacidiphilales	2.2	1.5	0.0	0.0	2.9	0.0	3.0	0.0	0.0	0.0	0.0	0.0	0.0	0.0	0.0	1.0
Deinococcus-Thermus	Thermales	0.7	1.5	0.0	2.7	0.0	0.8	0.6	0.9	0.0	0.0	1.0	0.0	0.0	0.0	0.0	2.0
Proteobacteria	Oceanospirillales	0.0	0.7	0.0	0.0	1.4	0.8	0.6	2.7	0.0	0.0	3.1	0.0	0.0	0.0	0.0	0.0
Spirochaetes	Spirochaetales	1.5	0.0	0.0	0.0	1.4	0.0	3.0	0.9	2.2	0.0	0.0	0.0	0.0	0.0	0.0	0.3

Supplementary Table 5.7 Relative transcript abundances (%) from taxa (Phylum and Order levels) transcribing genes involved in exopolysaccharides (EPS) and capsular polysaccharides (biofilm formation) in microbial mats occurring in hypersaline, metahaline and freshwater environments.

		Hypersaline										Metahaline			Freshwtaer		
Phylum	**Order**	**LL BM 2017**	**Nil PM1 2016**	**Nil PM2 2016**	**Nil PM 2017**	**Nil SM1 2016**	**Nil SM2 2016**	**Nil SM 2017**	**RRBS TM 2016**	**RRBS SM 2016**	**RRBS OVS 2016**	**GP SM 2016**	**GP PM 2016**	**GP TM 2016**	**GR GM1 2016**	**GR GM2 2016**	**GR YM 2016**
Cyanobacteria	Nostocales	12.5	34.9	16.7	16.7	10.5	7.1	12.8	25.5	9.7	24.0	12.9	15.4	23.1	41.7	38.5	2.3
Chloroflexi	Chloroflexales	12.5	11.6	0.0	12.5	28.9	14.3	12.8	21.8	6.5	4.0	25.8	15.4	15.4	8.3	7.7	20.7
Cyanobacteria	Chroococcales	31.3	16.3	0.0	18.8	0.0	8.9	28.2	21.8	12.9	8.0	0.0	15.4	23.1	0.0	0.0	3.5
Proteobacteria	Burkholderiales	6.3	9.3	0.0	4.2	10.5	8.9	7.7	0.0	32.3	0.0	3.2	38.5	7.7	16.7	0.0	13.8
Actinobacteria	Actinomycetales	0.0	0.0	33.3	6.3	2.6	8.9	5.1	0.0	6.5	8.0	3.2	0.0	15.4	8.3	23.1	8.4
Bacteroidetes	Cytophagales	3.1	4.7	33.3	4.2	2.6	12.5	0.0	0.0	3.2	8.0	0.0	0.0	0.0	0.0	7.7	2.1
Bacteroidetes	Flavobacteriales	6.3	2.3	0.0	8.3	7.9	5.4	5.1	1.8	0.0	4.0	6.5	7.7	0.0	0.0	15.4	1.5
Bacteroidetes	Sphingobacteriales	6.3	2.3	16.7	0.0	0.0	0.0	2.6	5.5	9.7	0.0	3.2	7.7	7.7	0.0	0.0	2.3
Firmicutes	Clostridiales	6.3	2.3	0.0	8.3	7.9	8.9	5.1	3.6	3.2	4.0	9.7	0.0	0.0	0.0	0.0	4.3
Proteobacteria	Rhizobiales	0.0	2.3	0.0	4.2	0.0	1.8	7.7	0.0	0.0	4.0	9.7	0.0	0.0	0.0	0.0	18.1
Firmicutes	Bacillales	6.3	0.0	0.0	2.1	0.0	7.1	0.0	5.5	3.2	0.0	3.2	0.0	0.0	16.7	0.0	3.1
Bacteroidetes	Bacteroidales	6.3	2.3	0.0	2.1	2.6	5.4	0.0	0.0	3.2	0.0	6.5	0.0	0.0	8.3	7.7	1.2
Proteobacteria	Desulfuromonadales	0.0	0.0	0.0	2.1	7.9	3.6	0.0	5.5	3.2	8.0	6.5	0.0	0.0	0.0	0.0	7.2
Cyanobacteria	Oscillatoriales	0.0	4.7	0.0	4.2	2.6	5.4	5.1	1.8	3.2	0.0	3.2	0.0	7.7	0.0	0.0	1.2
Chlorobi	Chlorobiales	3.1	2.3	0.0	0.0	2.6	1.8	0.0	1.8	3.2	16.0	0.0	0.0	0.0	0.0	0.0	2.9
Proteobacteria	Syntrophobacterales	0.0	0.0	0.0	2.1	5.3	0.0	5.1	3.6	0.0	8.0	6.5	0.0	0.0	0.0	0.0	2.1
Proteobacteria	Rhodobacterales	0.0	4.7	0.0	4.2	7.9	0.0	2.6	1.8	0.0	4.0	0.0	0.0	0.0	0.0	0.0	5.2

Supplementary Table 5.8 Relative transcript abundances (%) from taxa (Phylum and Order levels) transcribing genes involved in nitrogen fixation in microbial mats occurring in hypersaline, metahaline and freshwater environments.

		Hypersaline										Metahaline			Freshwtaer		
Phylum	**Order**	**LL BM 2017**	**Nil PM1 2016**	**Nil PM2 2016**	**Nil PM 2017**	**Nil SM1 2016**	**Nil SM2 2016**	**Nil SM 2017**	**RRBS TM 2016**	**RRBS SM 2016**	**RRBS OVS 2016**	**GP SM 2016**	**GP PM 2016**	**GP TM 2016**	**GR GM1 2016**	**GR GM2 2016**	**GR YM 2016**
Cyanobacteria	Nostocales	33.2	43.5	27.3	23.6	23.4	44.9	44.4	15.7	23.3	42.9	27.9	51.8	20.0	100.0	100.0	7.1
Cyanobacteria	Chroococcales	31.7	47.8	63.6	51.4	37.5	38.3	22.2	26.5	36.4	47.6	47.1	41.1	20.0	0.0	0.0	7.1
Cyanobacteria	Oscillatoriales	11.9	8.7	0.0	22.2	6.3	11.2	11.1	5.9	13.2	8.3	16.2	7.1	0.0	0.0	0.0	0.0
Chloroflexi	Chloroflexales	6.4	0.0	0.0	0.0	10.9	2.8	0.0	3.9	14.7	0.0	0.0	0.0	60.0	0.0	0.0	0.0
Proteobacteria	Rhizobiales	1.5	0.0	0.0	0.0	0.0	0.0	11.1	1.0	3.1	0.0	1.5	0.0	0.0	0.0	0.0	57.1
Chlorobi	Chlorobiales	5.4	0.0	0.0	2.8	7.8	0.0	0.0	23.5	2.3	0.0	1.5	0.0	0.0	0.0	0.0	25.0
Proteobacteria	Desulfovibrionales	6.9	0.0	9.1	0.0	4.7	0.9	0.0	8.8	4.7	0.0	1.5	0.0	0.0	0.0	0.0	3.6
Proteobacteria	Desulfobacterales	0.5	0.0	0.0	0.0	4.7	0.9	11.1	5.9	0.0	1.2	1.5	0.0	0.0	0.0	0.0	0.0
Proteobacteria	Syntrophobacterales	2.5	0.0	0.0	0.0	4.7	0.9	0.0	8.8	2.3	0.0	2.9	0.0	0.0	0.0	0.0	0.0

Supplementary Table 5.9 Multilevel pattern analysis of Nostocales genera.

Genera	Nilemah	Garden Point	RRBS	Linke Lake	Giblin River	Index	Stat	P.Value
Gloeotrichia	1	1	0	0	0	6	0.942	0.01
Anabaena	1	1	0	0	0	6	0.992	0.003
Rivularia	1	1	0	0	0	6	0.914	0.065
Chakia	0	0	0	0	1	5	1	0.011
Petalonema	1	0	0	0	1	9	0.891	0.062

Supplementary Table 5.10 Multilevel pattern analysis of heterocyte glycolipids. *tentatively identified novel HG isomers.

HG	Nilemah	Garden Point	RRBS	Linke Lake	Giblin River	Index	Stat	P.Value
Pentose HG30 diol	1	1	1	0	0	16	0.968	0.047
Pentose HG30 triol	0	0	1	1	1	25	0.925	0.063
Pentose HG32 triol	0	0	1	1	1	25	0.918	0.069
***Pentose HG32 triol**	1	1	1	1	0	26	0.999	0.009
***Pentose HG34 triol**	1	1	1	1	0	26	1	0.009
***Pentose HG36 triol**	1	1	1	1	0	26	1	0.009
Pentose HG28 diol	1	1	1	0	1	27	1	0.070
Hexose HG26 keto-ol	1	0	1	1	1	15	0.991	0.151
Hexose HG30 diol	0	0	0	0	1	5	1	0.009
Hexose HG32 keto-diol	1	0	0	0	1	5	0.666	0.563
Hexose HG32 triol	0	0	0	0	1	5	1	0.009

5.7.1 References

Bale, N.J., Hopmans, E.C., Dorhout, D., Stal, L.J., Grego, M., van Bleijswijk, J., Sinninghe Damsté, J.S., Schouten, S., 2018. A novel heterocyst glycolipid detected in a pelagic N2-fixing cyanobacterium of the genus Calothrix. Org. Geochem. 123, 44–47.

Bale, N.J., Hopmans, E.C., Zell, C., Sobrinho, R.L., Kim, J.H., Sinninghe Damsté, J.S., Villareal, T.A., Schouten, S., 2015. Long chain glycolipids with pentose head groups as biomarkers for marine endosymbiotic heterocystous cyanobacteria. Org. Geochem. 81, 1–7.

Bauersachs, T., Compaoré, J., Hopmans, E.C., Stal, L.J., Schouten, S., Sinninghe Damsté, J.S., 2009. Distribution of heterocyst glycolipids in cyanobacteria. Phytochemistry 70, 2034–

2039.

Bauersachs, T., Miller, S.R., Gugger, M., Mudimu, O., Friedl, T., Schwark, L., 2019. Heterocyte glycolipids indicate polyphyly of stigonematalean cyanobacteria. Phytochemistry 166, 112059.

6 Conclusions and outlook

This PhD project provided a comprehensive characterisation of active microbial communities and their chemotaxonomic signatures from extant microbial mats living under a range of different environmental settings. Integration of a metatranscriptomic and organic geochemical approach provided insights into the complexity of biogeochemical cycles and microbial community structures. The influence of environmental conditions and community structure was crucial when deciphering the whole microbial communities' activity in different types of microbial mats and in mats from different locations.

6.1 Active microbial communities

Currently, our knowledge about the community structure of smooth and pustular mats occurring within Nilemah tidal flat has been based on DNA based techniques (e.g. Burns et al., 2004; Goh et al., 2009). The present study (Chapter 3) based on RNA based techniques provided new insights into the abundances of active prokaryotes within these ecosystems, illustrating that Proteobacteria, Bacteroidetes, Planctomycetes, Cyanobacteria, Spirochaetes, Firmicutes and Chloroflexi are the prominent active taxa in both mat types. Comparing the active taxa between mat types indicated that Cyanobacteria, Planctomycetes, Alphaproteobacteria, Gemmatimonadetes, Thaumarchaeota, Nitrospirae, Omnitrophicaeota and Actinobacteria were significantly more active in pustular mats (P-value < 0.05). Whereas, smooth mats contained significantly more active Spirochaetes, Deltaproteobacteria, Asgardeota, Dependentiae, Modulibacteria and Nanoarcheaeota. The difference in the active microbial communities between the mats is due to the microbe's preference for oxic and/or anoxic conditions. This study showed that sulfur and methane metabolising prokaryotes were much more active in the smooth mats that occur in lower water depths where anoxic conditions prevail. This study was the first to examine the effect that cyclonic activity has on active microbial communities in Shark Bay (Chapter 4). Cyclone affected microbial assemblages from 'RRBS' contained a variety of other prominent bacterial taxa, such as Acidobacteria,

Calditrichaeota, Kiritimatiellaeota, Synergistetes and Zixibacteria. The presence of these active bacterial taxa was attributed to their ability to survive on high-molecular-weight organic material generated by the cyclone (e.g. Crump et al., 1999; Kirchman, 2006). Investigation of cyanobacteria occurring in mats from freshwater, metahaline and hypersaline environments (Chapter 5) indicated that the variety of active heterocytous cyanophytes in elevated salinities is much more diverse than previously thought (Oren, 2015). It was concluded that the use of high throughput sequencing, newly developed bioinformatics packages (e.g. rnaSPAdes, Phyloflash) and an updated taxonomic database allowed for an enhanced phylogenetic resolution of heterocytous cyanobacteria.

6.2 Adaptive responses

Many microbial ecosystems are under a continuous state of change due to fluctuations in abiotic factors caused by diel and seasonal cycles, as well as pressures from biotic influences (Bolhuis et al., 2014). Metatranscriptomic analysis (Chapter 3) of smooth and pustular mats found elevated transcription of genes associated with their resistance to hypersalinity and low nutrient conditions such as biofilm formation, nutrient uptake and osmoadaptation. Increased transcription of peptide/nickel ABC transporters suggests that prokaryotes utilising nickel in Shark Bay need to highly regulate their intracellular concentrations of nickel to ensure adequate levels for metalloenzyme activities while not inhibiting quorum sensing (Rutherford and Bassler, 2012; Papenfort and Bassler, 2016). Transcription of genes involved in the uptake and regulation of iron, phosphorus and long chain fatty acids were also abundantly transcribed in the Nilemah mat metatranscriptomes. This response is due to the limited supply of nutrients in Shark Bay ecosystems (i.e. phosphorus) with their distribution known to fluctuate in accordance to oxic and anoxic conditions (Pagès et al., 2014; Wong et al., 2018). Transcription of genes enhancing a microbe's ability to sense chemical gradients was observed in the smooth mat's metatranscriptomes. The elevated transcription of these genes in the laminated smooth mats is likely a result of the heterotrophic bacteria needing to adjust their position within these stratified systems during diel fluctuations that change the oxic and anoxic conditions (Salah Ud-Din and Roujeinikova, 2017). Combating osmotic stress is common in hypersaline

environments, previous functional annotations of Shark Bay metagenomes have identified clusters of osmoadaptive traits such as the uptake of the osmoprotectant (Wong et al., 2018). According to the results presented in Chapter 3, elevated transcription of genes encoding osmoprotectants, glutamine and glutamate, as well as the gene encoding H^+/Na^+ dependent F_1F_0-ATP synthase to which maybe a significant osmoadaptation for photosynthetic organisms living in the hypersaline mats of Shark Bay (von Ballmoos et al., 2009).

6.3 Biogeochemical cycles

Photosynthesis is one of the primary driving forces of various nutrient cycles in microbial mats (Mobberley et al., 2013). The present study (Chapter 3) found that phototrophy-related genes involved in anoxygenic photosystem II were highly transcribed in all the metatranscriptomes. It was concluded that the higher transcription of genes associated with anoxygenic photosystem II could be attributed to the presence of green non-sulfur bacteria (Chloroflexi) that utilise the 3-hydroxypropionate bi-cycle. This finding indicates that anoxygenic photoautrophs are playing a greater role in providing carbon compared to cyanobacteria and diatoms, which are typically thought to be the key providers of fixed carbon in these ecosystems.

Transcription of genes associated with the Wood–Ljungdahl pathway along with methanogenic pathways (i.e. CO_2 to methane and acetate to methane) were over-represented in the smooth mats' metatranscriptomes. It was concluded that the abundance of active methane producing and consuming bacteria in smooth mats suggests a symbiotic relationship, which completes the cycling of methane. Furthermore, the enrichment of these anaerobic pathways in smooth mats corroborates previous metagenomic studies (Wong et al., 2018) and further advocates the potential of these communities as modern analogues of ancient microbialites that are believed to have initially evolved in elevated salinity and anoxic conditions (Wong et al., 2016). Moreover, the primary gene for methane production, *mcr*A, encoding methyl-coenzyme M reductase, was absent in all of the metatranscriptomes (Chapter 3). This may be due to degradation of mRNA, or there may be another novel gene responsible for methanogenesis in Shark Bay smooth mats. Genes involved in sulfur metabolism were also found to be highly transcribed within smooth mat metatranscriptomes. In

2018, Wong et al (2018) found that the majority of the draft genomes constructed from Nilemah smooth mats encode partial and complete assimilatory sulfate reduction pathways, indicating the potential importance of sulfur respiration in the Shark Bay ecosystems. The use of metatranscriptomics in this study found elevated transcription of sulfur reduction pathways, thus proving elevated sulfur respiration in smooth mats (Chapter 3).

Nitrogen metabolising pathways showed no clear transcription pattern between mat types from the Nilemah tidal flat (Chapter 3), however the transcription of genes involved in nitrogen fixation were abundantly expressed as well as other reduction pathways such as assimilatory and dissimilatory nitrate reduction. Recent taxonomic studies of Shark Bay microbial mats revealed a low relative abundance of nitrifiers, leading to a potential incomplete cycling of nitrogen (Wong et al., 2015, 2018; Ruvindy et al., 2016). Examination of nitrogen metabolising genes in 'RRBS' samples (Chapter 4) found that the transcription of *nif*A was higher in cyclone derived materials. This particular nitrogenase regulator is found in heterotrophic diazotrophs (e.g. Proteobacteria) (Batista and Dixon, 2019). Shifts in active diazotrophic communities have been suggested to reflect changes in environmental conditions (Severin et al., 2010) and therefore, ongoing cyclonic events in Shark Bay may increase the activity of heterotrophic diazotrophs and ultimately result in eutrophication in the bay. Additionally, the investigation of the nitrogen fixation within freshwater, metahaline and hypersaline mats (Chapter 5) found that cyanobacteria accounted for the largest proportion of the gene transcripts involved in nitrogen fixation with heterocytous cyanobacteria accounting for a large proportion of the transcripts. Interestingly, heterocytous cyanophytes made up a small portion of the active microbial community, but they transcribed large portions of genes involved in nitrogen fixation indicating that they key nutrient providers for the microbial mats.

6.4 Lipid biomarkers

In the present study (Chapter 4), biomarker profiles were successfully used to decipher cyclone derived materials from microbial mats. A major difference, to which has not been previously observed in biomarker studies of Shark Bay microbial mats (Allen et al., 2010; Pagès et al., 2015), was high abundances of C_{25} HBI alkenes within the

cyclone derived materials. The abundance of these biomarkers was attributed to the relocation of subtidal sediments from consequent HBI-producing diatom communities.

The release of sulfurised lipids indicated the early preservation in microbially-derived lipids and possible indication that cyclonic activity may influence with the release of S-bound benzohopanes from within the mucilaginous cobble (Chapter 4). Furthermore, our study (Chapter 5) is the first to identify HGs in microbial mats from Shark Bay (WA) and Giblin River (Tasmania). Our study identified 8 HGs with a pentose moiety (including currently uncharacterised pentose HG_{32} to HG_{36} triol isomers), 11 HGs with a hexose moiety and 1 HG_{28} triol with a methyl-hexose moiety, The large diversity of HGs found in our study greatly extends our knowledge of HG distributions within microbial mats from elevated saline and freshwater environments, and illustrates the potential of HGs as chemotaxonomic markers for heterocytous cyanophytes in both ecological and paleoenvironmental studies.

6.5 Future perspectives

The combination of metatranscriptomic and organic geochemical techniques proved to be significant in providing an understanding microbial community structure and function in modern microbial mats. The combination of these disciplines in the future will allow for further advancements in ecological and paleoenvironmental studies of other microbial ecosystems. However, considerations are needed whilst applying the methodologies. Metatranscriptomics does not capture the entire metatranscriptome due in part to the complexity of some microbial communities, the large dynamic range of transcript expression, the short half-life of RNA, abundances of extracted rRNA (> 80% of total extracted RNA) and a number of technology-specific limitations (Shakya et al., 2019). It is thus recommended that metatranscriptomes are to be additionally ribo-depleted and sequenced in a paired-end format of at least 100 bp with a minimum of 40 million reads per sample to increase the amount of available mRNA transcripts (Westreich et al., 2018). Furthermore, future work should focus on coupling metatranscriptomic data with metagenomic information to greatly extend our knowledge of metabolic functions and gene expression patterns in complex microbial assemblages (Wang et al., 2020). This is achieved by mapping transcripts to assembled draft metagenome-assembled genomes. Future work combing molecular genetics and

lipid analyses from environmental samples along with cultivations of specific bacteria (i.e. heterocytous cyanophytes) under varying salinities will be needed to further our understanding of who is synthesizing certain HGs under particular saline conditions.

References

Allen, M.A., Neilan, B.A., Burns, B.P., Jahnke, L.L., Summons, R.E., 2010. Lipid biomarkers in Hamelin Pool microbial mats and stromatolites. Org. Geochem. 41, 1207–1218.

Batista, M.B., Dixon, R., 2019. Manipulating nitrogen regulation in diazotrophic bacteria for agronomic benefit. Biochem. Soc. Trans.

Bolhuis, H., Cretoiu, M.S., Stal, L.J., 2014. Molecular ecology of microbial mats. FEMS Microbiol. Ecol.

Burns, B.P., Goh, F., Allen, M., Neilan, B.A., 2004. Microbial diversity of extant stromatolites in the hypersaline marine environment of Shark Bay, Australia. Environ. Microbiol. 6, 1096–1101.

Crump, B.C., Armbrust, E.V., Baross, J.A., 1999. Phylogenetic analysis of particle-attached and free-living bacterial communities in the Columbia River, its estuary, and the adjacent coastal ocean. Appl. Environ. Microbiol. 65, 3192–3204.

DeLong, E.F., Franks, D.G., Alldredge, A.L., 1993. Phylogenetic diversity of aggregate-attached vs. free-living marine bacterial assemblages. Limnol. Oceanogr. 38, 924–934.

Goh, F., Allen, M.A., Leuko, S., Kawaguchi, T., Decho, A.W., Burns, B.P., Neilan, B.A., 2009. Determining the specific microbial populations and their spatial distribution within the stromatolite ecosystem of Shark Bay. ISME J. 3, 383–396.

Kirchman, D.L., 2006. The ecology of Cytophaga-□Flavobacteria in aquatic environments. FEMS Microbiol. Ecol. 39, 91–100.

Mobberley, J.M., Khodadad, C.L.M., Foster, J.S., 2013. Metabolic potential of lithifying cyanobacteria-dominated thrombolitic mats. Photosynth. Res. 118, 125–140.

Oren, A., 2015. Cyanobacteria in hypersaline environments: biodiversity and physiological properties. Biodivers Conserv 24, 781–798.

Pagès, A., Grice, K., Ertefai, T., Skrzypek, G., Jahnert, R., Greenwood, P., 2014. Organic geochemical studies of modern microbial mats from Shark Bay: Part I: Influence of depth and salinity on lipid biomarkers and their isotopic signatures. Geobiology 12, 469–487.

Pagès, A., Grice, K., Welsh, D.T., Teasdale, P.T., Van Kranendonk, M.J., Greenwood, P., 2015. Lipid Biomarker and Isotopic Study of Community Distribution and Biomarker Preservation in a Laminated Microbial Mat from Shark Bay, Western Australia. Microb. Ecol. 70, 459–472.

Papenfort, K., Bassler, B.L., 2016. Quorum sensing signal-response systems in Gram-negative bacteria. Nat. Rev. Microbiol.

Rutherford, S.T., Bassler, B.L., 2012. Bacterial quorum sensing: Its role in virulence and possibilities for its control. Cold Spring Harb. Perspect. Med.

Ruvindy, R., White, R.A., Neilan, B.A., Burns, B.P., 2016. Unravelling core microbial metabolisms in the hypersaline microbial mats of Shark Bay using high-throughput metagenomics. ISME J. 10, 183–196.

Salah Ud-Din, A.I.M., Roujeinikova, A., 2017. Methyl-accepting chemotaxis proteins: a core sensing element in prokaryotes and archaea. Cell. Mol. Life Sci.

Severin, I., Acinas, S.G., Stal, L.J., 2010. Diversity of nitrogen-fixing bacteria in cyanobacterial mats. FEMS Microbiol. Ecol. 73, no-no.

Shakya, M., Lo, C.C., Chain, P.S.G., 2019. Advances and challenges in metatranscriptomic analysis. Front. Genet.

von Ballmoos, C., Wiedenmann, A., Dimroth, P., 2009. Essentials for ATP Synthesis by F 1 F 0 ATP Synthases. Annu. Rev. Biochem. 78, 649–672.

Wang, D., Zheng, Q., Huang, K., Springael, D., Zhang, X.X., 2020. Metagenomic and metatranscriptomic insights into the complex nitrogen metabolic pathways in a single-stage bioreactor coupling partial denitrification with anammox. Chem. Eng. J. 398, 125653.

Westreich, S.T., Treiber, M.L., Mills, D.A., Korf, I., Lemay, D.G., 2018. SAMSA2: A standalone metatranscriptome analysis pipeline. BMC Bioinformatics 19, 175.

Wong, H., Ahmed-Cox, A., Burns, B., 2016. Molecular Ecology of Hypersaline Microbial Mats: Current Insights and New Directions. Microorganisms 4, 6.

Wong, H.L., Smith, D.L., Visscher, P.T., Burns, B.P., 2015. Niche differentiation of bacterial communities at a millimeter scale in Shark Bay microbial mats. Sci. Rep. 5, 15607.

Wong, H.L., White, R.A., Visscher, P.T., Charlesworth, J.C., Vázquez-Campos, X., Burns, B.P., 2018. Disentangling the drivers of functional complexity at the metagenomic level in Shark Bay microbial mat microbiomes. ISME J. 12, 2619–2639.

Ying wu, K., 1998. High phylogenetic diversity in a marine-snow--associated bacterial assemblaae, AQUATIC MICROBIAL ECOLOGY Aquat Microb Ecol.

Appendix

Following pages contain documents stating the rights, granted by publishing groups to the first author of the publications that forms the chapter 1 of this thesis respectively, to reproduce their articles in full or in part, for a wide range of scholarly, non-commercial purposes, including in a thesis (provided that this is not to be published commercially).

MINERALOGICAL SOCIETY OF AMERICA
3635 Concorde Pkwy Ste 500 • Chantilly VA 20151-1110 • USA
Tel: 1 (703) 652-9950 • Fax: 1 (703) 652-9951 • Internet: www.minsocam.org

22 July 2020

Mr. Matthew Campbell
Curtin University
Kent street
Perth WA 6102
Australia

Email 15164810@student.curtin.edu.au

Dear Mr. Campbell:

I received your e-mail message requesting permission to reproduce the following figure from *Elements* magazine*:*

Figure 1 from Druschel, Gregory K. and Kappler, Andreas., (2015). *Geomicrobiology and Microbial Geochemistry*, Volume 11, 289-394.

It is with pleasure that we grant you permission to reproduce this figure for inclusion without cost and all subsequent editions of the work, its ancillaries, and other derivative works, in any form or medium, whether now known or hereafter developed, in all languages, for distribution throughout the world on the conditions that reference is given to the original publication of the Mineralogical Society of America.

Sincerely,

[redacted]

Ann E. Benbow, Ph.D.

Executive Director, MSA

JOHN WILEY AND SONS LICENSE
TERMS AND CONDITIONS

Jul 23, 2020

This Agreement between Curtin University -- Matthew Campbell ("You") and John Wiley and Sons ("John Wiley and Sons") consists of your license details and the terms and conditions provided by John Wiley and Sons and Copyright Clearance Center.

License Number	4874290140094
License date	Jul 22, 2020
Licensed Content Publisher	John Wiley and Sons
Licensed Content Publication	Environmental Microbiology Reports
Licensed Content Title	Issue Information
Licensed Content Date	Jul 20, 2017
Licensed Content Pages	10
Type of use	Dissertation/Thesis
Requestor type	University/Academic
Format	Print and electronic
Portion	Figure/table
Number of figures/tables	1

Will you be translating?	No
Title	Functional diversity of active microbial mat communities inferred from lipid biomarkers and metatranscriptomics
Institution name	Curtin University
Expected presentation date	Jul 2020
Portions	Figure 1
Requestor Location	Curtin University Kent street Bentley, 6102 Australia Attn: Curtin University
Publisher Tax ID	EU826007151
Total	0.00 AUD

Terms and Conditions

TERMS AND CONDITIONS

This copyrighted material is owned by or exclusively licensed to John Wiley & Sons, Inc. or one of its group companies (each a"Wiley Company") or handled on behalf of a society with which a Wiley Company has exclusive publishing rights in relation to a particular work (collectively "WILEY"). By clicking "accept" in connection with completing this licensing transaction, you agree that the following terms and conditions apply to this transaction (along with the billing and payment terms and conditions established by the Copyright Clearance Center Inc., ("CCC's Billing and Payment terms and conditions"), at the time that you opened your RightsLink account (these are available at any time at http://myaccount.copyright.com).

Terms and Conditions

- The materials you have requested permission to reproduce or reuse (the "Wiley Materials") are protected by copyright.
- You are hereby granted a personal, non-exclusive, non-sub licensable (on a stand-alone basis), non-transferable, worldwide, limited license to reproduce the Wiley Materials for the purpose specified in the licensing process. This license, **and any CONTENT (PDF or image file) purchased as part of your order,** is for a one-time

ELSEVIER LICENSE
TERMS AND CONDITIONS

Jul 23, 2020

This Agreement between Curtin University -- Matthew Campbell ("You") and Elsevier ("Elsevier") consists of your license details and the terms and conditions provided by Elsevier and Copyright Clearance Center.

License Number	4757081122531
License date	Jan 27, 2020
Licensed Content Publisher	Elsevier
Licensed Content Publication	Earth-Science Reviews
Licensed Content Title	Lipid biomarkers for the reconstruction of deep-time environmental conditions
Licensed Content Author	Genming Luo,Huan Yang,Thomas J. Algeo,Christian Hallmann,Shucheng Xie
Licensed Content Date	Feb 1, 2019
Licensed Content Volume	189
Licensed Content Issue	n/a
Licensed Content Pages	26
Start Page	99
End Page	124
Type of Use	reuse in a thesis/dissertation

Portion	figures/tables/illustrations
Number of figures/tables/illustrations	1
Format	both print and electronic
Are you the author of this Elsevier article?	No
Will you be translating?	No
Title	Functional diversity of active microbial mat communities inferred from lipid biomarkers and metatranscriptomics
Institution name	Curtin University
Expected presentation date	Jan 2020
Portions	Figure 1
Requestor Location	Curtin University Kent street Bentley, 6102 Australia Attn: Curtin University
Publisher Tax ID	GB 494 6272 12
Total	0.00 AUD

Terms and Conditions

INTRODUCTION

1. The publisher for this copyrighted material is Elsevier. By clicking "accept" in connection with completing this licensing transaction, you agree that the following terms and conditions apply to this transaction (along with the Billing and Payment terms and conditions established by Copyright Clearance Center, Inc. ("CCC"), at the time that you opened your Rightslink account and that are available at any time at http://myaccount.copyright.com).

GENERAL TERMS

2. Elsevier hereby grants you permission to reproduce the aforementioned material subject to the terms and conditions indicated.

3. Acknowledgement: If any part of the material to be used (for example, figures) has appeared in our publication with credit or acknowledgement to another source, permission must also be sought from that source. If such permission is not obtained then that material may not be included in your publication/copies. Suitable acknowledgement to the source must be made, either as a footnote or in a reference list at the end of your publication, as follows:

"Reprinted from Publication title, Vol /edition number, Author(s), Title of article / title of chapter, Pages No., Copyright (Year), with permission from Elsevier [OR APPLICABLE SOCIETY COPYRIGHT OWNER]." Also Lancet special credit - "Reprinted from The Lancet, Vol. number, Author(s), Title of article, Pages No., Copyright (Year), with permission from Elsevier."

4. Reproduction of this material is confined to the purpose and/or media for which permission is hereby given.

5. Altering/Modifying Material: Not Permitted. However figures and illustrations may be altered/adapted minimally to serve your work. Any other abbreviations, additions, deletions and/or any other alterations shall be made only with prior written authorization of Elsevier Ltd. (Please contact Elsevier at permissions@elsevier.com). No modifications can be made to any Lancet figures/tables and they must be reproduced in full.

6. If the permission fee for the requested use of our material is waived in this instance, please be advised that your future requests for Elsevier materials may attract a fee.

7. Reservation of Rights: Publisher reserves all rights not specifically granted in the combination of (i) the license details provided by you and accepted in the course of this licensing transaction, (ii) these terms and conditions and (iii) CCC's Billing and Payment terms and conditions.

8. License Contingent Upon Payment: While you may exercise the rights licensed immediately upon issuance of the license at the end of the licensing process for the transaction, provided that you have disclosed complete and accurate details of your proposed use, no license is finally effective unless and until full payment is received from you (either by publisher or by CCC) as provided in CCC's Billing and Payment terms and conditions. If full payment is not received on a timely basis, then any license preliminarily granted shall be deemed automatically revoked and shall be void as if never granted. Further, in the event that you breach any of these terms and conditions or any of CCC's Billing and Payment terms and conditions, the license is automatically revoked and shall be void as if never granted. Use of materials as described in a revoked license, as well as any use of the materials beyond the scope of an unrevoked license, may constitute copyright infringement and publisher reserves the right to take any and all action to protect its copyright in the materials.

9. Warranties: Publisher makes no representations or warranties with respect to the licensed material.

10. Indemnity: You hereby indemnify and agree to hold harmless publisher and CCC, and their respective officers, directors, employees and agents, from and against any and all claims arising out of your use of the licensed material other than as specifically authorized pursuant to this license.

11. No Transfer of License: This license is personal to you and may not be sublicensed, assigned, or transferred by you to any other person without publisher's written permission.

Gold Open Access Articles: May be shared according to the author-selected end-user license and should contain a CrossMark logo, the end user license, and a DOI link to the formal publication on ScienceDirect.

Please refer to Elsevier's posting policy for further information.

18. **For book authors** the following clauses are applicable in addition to the above: Authors are permitted to place a brief summary of their work online only. You are not allowed to download and post the published electronic version of your chapter, nor may you scan the printed edition to create an electronic version. **Posting to a repository:** Authors are permitted to post a summary of their chapter only in their institution's repository.

19. **Thesis/Dissertation**: If your license is for use in a thesis/dissertation your thesis may be submitted to your institution in either print or electronic form. Should your thesis be published commercially, please reapply for permission. These requirements include permission for the Library and Archives of Canada to supply single copies, on demand, of the complete thesis and include permission for Proquest/UMI to supply single copies, on demand, of the complete thesis. Should your thesis be published commercially, please reapply for permission. Theses and dissertations which contain embedded PJAs as part of the formal submission can be posted publicly by the awarding institution with DOI links back to the formal publications on ScienceDirect.

Elsevier Open Access Terms and Conditions

You can publish open access with Elsevier in hundreds of open access journals or in nearly 2000 established subscription journals that support open access publishing. Permitted third party re-use of these open access articles is defined by the author's choice of Creative Commons user license. See our open access license policy for more information.

Terms & Conditions applicable to all Open Access articles published with Elsevier:

Any reuse of the article must not represent the author as endorsing the adaptation of the article nor should the article be modified in such a way as to damage the author's honour or reputation. If any changes have been made, such changes must be clearly indicated.

The author(s) must be appropriately credited and we ask that you include the end user license and a DOI link to the formal publication on ScienceDirect.

If any part of the material to be used (for example, figures) has appeared in our publication with credit or acknowledgement to another source it is the responsibility of the user to ensure their reuse complies with the terms and conditions determined by the rights holder.

Additional Terms & Conditions applicable to each Creative Commons user license:

CC BY: The CC-BY license allows users to copy, to create extracts, abstracts and new works from the Article, to alter and revise the Article and to make commercial use of the Article (including reuse and/or resale of the Article by commercial entities), provided the user gives appropriate credit (with a link to the formal publication through the relevant DOI), provides a link to the license, indicates if changes were made and the licensor is not represented as endorsing the use made of the work. The full details of the license are available at http://creativecommons.org/licenses/by/4.0.

CC BY NC SA: The CC BY-NC-SA license allows users to copy, to create extracts, abstracts and new works from the Article, to alter and revise the Article, provided this is not done for commercial purposes, and that the user gives appropriate credit (with a link to the formal publication through the relevant DOI), provides a link to the license, indicates if changes were made and the licensor is not represented as endorsing the use made of the

work. Further, any new works must be made available on the same conditions. The full details of the license are available at http://creativecommons.org/licenses/by-nc-sa/4.0.

CC BY NC ND: The CC BY-NC-ND license allows users to copy and distribute the Article, provided this is not done for commercial purposes and further does not permit distribution of the Article if it is changed or edited in any way, and provided the user gives appropriate credit (with a link to the formal publication through the relevant DOI), provides a link to the license, and that the licensor is not represented as endorsing the use made of the work. The full details of the license are available at http://creativecommons.org/licenses/by-nc-nd/4.0. Any commercial reuse of Open Access articles published with a CC BY NC SA or CC BY NC ND license requires permission from Elsevier and will be subject to a fee.

Commercial reuse includes:

- Associating advertising with the full text of the Article
- Charging fees for document delivery or access
- Article aggregation
- Systematic distribution via e-mail lists or share buttons

Posting or linking by commercial companies for use by customers of those companies.

20. **Other Conditions**:

v1.9

Questions? customercare@copyright.com or +1-855-239-3415 (toll free in the US) or +1-978-646-2777.